27610

NATIONAL LIBRARY
OTTAWA

CANADA

BIBLIOTHÈQUE NATIONALE
OTTAWA

NAME OF AUTHOR..JOHANNES HENDRIK DE BEER.....

TITLE OF THESIS..MAGNETOMETER ARRAY STUDIES
AND ELECTRICAL CONDUCTIVITY
IN SOUTHERN AFRICA.....

UNIVERSITY....ALBERTA.....

DEGREE FOR WHICH THESIS WAS PRESENTED..PH.D.....

YEAR THIS DEGREE GRANTED.....1976.....

Permission is hereby granted to THE NATIONAL LIBRARY OF CANADA to microfilm this thesis and to lend or sell copies of the film.

The author reserves other publication rights, and neither the thesis nor extensive extracts from it may be printed or otherwise reproduced without the author's written permission.

(Signed)..J.H. de Beer.....

PERMANENT ADDRESS:

GEOPHYSICS DIVISION
NPRL of the CSIR
P.O. BOX 395
PRETORIA
SOUTH AFRICA

DATED..February 9.....1976

NL-91 (10-68)

INFORMATION TO USERS

THIS DISSERTATION HAS BEEN
MICROFILMED EXACTLY AS RECEIVED

This copy was produced from a microfiche copy of the original document. The quality of the copy is heavily dependent upon the quality of the original thesis submitted for microfilming. Every effort has been made to ensure the highest quality of reproduction possible.

PLEASE NOTE: Some pages may have indistinct print. Filmed as received.

Canadian Theses Division
Cataloguing Branch
National Library of Canada
Ottawa, Canada K1A 0N4

AVIS AUX USAGERS

LA THESE A ETE MICROFILMEE
TELLE QUE NOUS L'AVONS RECUE

Cette copie a été faite à partir d'une microfiche du document original. La qualité de la copie dépend grandement de la qualité de la thèse soumise pour le microfimage. Nous avons tout fait pour assurer une qualité supérieure de reproduction.

NOTA BENE: La qualité d'impression de certaines pages peut laisser à désirer. Microfilmée telle que nous l'avons reçue.

Division des thèses canadiennes
Direction du catalogage
Bibliothèque nationale du Canada
Ottawa, Canada K1A 0N4

THE UNIVERSITY OF ALBERTA

MAGNETOMETER ARRAY STUDIES AND ELECTRICAL CONDUCTIVITY IN SOUTHERN AFRICA

by

© JOHANNES HENDRIK DE BEER

A THESIS

SUBMITTED TO THE FACULTY OF GRADUATE STUDIES AND RESEARCH

IN PARTIAL FULFILMENT OF THE REQUIREMENTS FOR THE DEGREE

OF DOCTOR OF PHILOSOPHY IN GEOPHYSICS

DEPARTMENT OF PHYSICS

EDMONTON, ALBERTA

SPRING, 1976

THE UNIVERSITY OF ALBERTA

FACULTY OF GRADUATE STUDIES AND RESEARCH

The undersigned certify that they have read, and recommend to the Faculty of Graduate Studies and Research, for acceptance, a thesis entitled MAGNETOMETER ARRAY STUDIES AND ELECTRICAL CONDUCTIVITY IN SOUTHERN AFRICA submitted by JOHANNES HENDRIK DE BEER in partial fulfilment of the requirements for the degree of Doctor of Philosophy in Geophysics.

D. J. Gough
Supervisor

C. M. Swift

M. E. Evans

E. D. Gaulard
External Examiner

Date 26th. January, 1976

ABSTRACT

Two arrays of magnetometers were operated in southern Africa in 1971 and 1972 to supplement deep Schlumberger resistivity studies. The first two-dimensional array of 24 three-component magnetometers was operated in central South Africa during September and October, 1971. Three substorm sequences have been analysed. Magnetograms and maps of Fourier transform amplitudes and phases show a large anomaly in the vertical and northward horizontal variation fields over the period range 24-293 minutes. The vertical field has a maximum near Beaufort West and the horizontal field increases southward to a presumed maximum just south of the array. The principal result is the discovery of a major conductive structure under the Cape Fold Belt and deep Karroo basin. Transfer functions between mean horizontal field components and the vertical component show that induction is principally in phase with the normal field. The effect of the Karroo sediments is seen in the quadrature phase induction anomaly. For this and other reasons the conductive body under the Cape Fold Belt and southernmost Karroo is provisionally placed in the upper mantle. A review of other geophysical parameters in the area indicates that the induction anomaly can be associated with either a

transition from ~600 to ~2,600 Myr old lithosphere or a ridge on the more conductive mantle. More quantitative interpretation is not possible without further observations south of the 1971 array.

Since the variation fields at the northernmost stations in this array contain only small anomalous components, these data were used for one-dimensional modelling. Although the data have some properties that indicate a deviation from a one-dimensional situation, the results suggest a slower increase in conductivity with depth in the range 200-800 km in the Kaapvaal shield than in the global model of Banks (1972).

The second array of magnetometers was operated in South-West Africa, Botswana and north-western Rhodesia from December 1971 to February 1972. Results from three periods of geomagnetic disturbance are presented. Magnetograms and maps of Fourier transform amplitudes and phases show an anomaly in the vertical and horizontal variation fields over the period range 21-171 minutes. A well-defined reversal in the vertical field is observed between Outjo and Sukses on the western edge of the array. Transfer functions and vertical field phase maps show a zone of induced currents that continues the south-westward trend of the Luangwa-middle Zambezi Rift, an extension of the East African Rift system. The conductor bends south of

the Okavango Delta to run in line with the Walvis Ridge nearly due west across South-West Africa. A study of the induction vectors and the half-widths of normalized anomalous profiles indicates a lithospheric conductor. The eastern branch of the conductor parallels the known faults in that area. Seismicity suggests that the Luangwa-middle Zambezi Rift continues to the south-west into Botswana along the conductivity anomaly. The westward arm of the conductor is associated with seismic activity. The zone of induced currents coincides with linear positive Bouguer anomalies. Overall geophysical and geological evidence indicates that the high conductivity may be associated with a fracture zone in the lithosphere and may trace an extension of the African Rift system along old weak zones in the continent.

ACKNOWLEDGEMENTS

I am indebted first and foremost to Professor D. I. Gough for introducing me to magnetometer array studies and for his guidance and encouragement during all stages of the project. I greatly value the friendship he has given me and I am especially grateful for his initiative in arranging my return to Edmonton to enroll in a Ph.D. programme at the University of Alberta.

I owe many thanks to Dr. Jan van Zijl, Head of the Geophysics Division of the N.P.R.L. in Pretoria, South Africa, who introduced me to the Schlumberger sounding technique and who conceived and organized the magnetometer array studies discussed in this thesis. I appreciate the opportunity he gave me to come to the University of Alberta in 1972 to work on the 1971 array data and his willingness to grant me leave of absence from the Geophysics Division to return to Edmonton. I also would like to thank Dr. A. Strasheim, Director of the N.P.R.L., for granting me study leave for the final phase of the work. His interest in and support of the project is highly appreciated.

My colleagues at the Geophysics Division of the N.P.R.L., Dr. Jan van Zijl, Dr. Reinhard Huyssen, Mr. Sarel Joubert, Mr. Philip Hugo and Mr. Reinhard Meyer are thanked for the field work they did during these

experiments. The interesting and formative discussions that I had with these gentlemen are highly appreciated. In this respect I would also like to mention my colleagues at the Institute of Earth and Planetary Physics and in the Department of Physics at the University of Alberta and in particular, Mr. John Bannister, Mr. Robert Withers and Dr. Doug Oldenburg. I am obliged to Mr. John Davis for his assistance in the task of data reduction.

Mr. A. M. van Wijk of the Magnetic Observatory of the C.S.I.R. is thanked for the use of data from the Tsumeb station.

I owe thanks to Dr. F. K. Bahnemann for providing me with the aeromagnetic map of the Cape Province (Fig. 6.3), Mr. C. Reeves for making available to me a first draft of the Bouguer gravity map of Botswana and Dr. K. D. Töpfer for sending me the gravity map of Zambia (these gravity maps are incorporated in Fig. 6.7). I also wish to thank Dr. F. K. Bahnemann, Professor G. Bond and Mr. D. Hutchins for information regarding some related geophysical and geological problems in the study areas.

I am most grateful to Mrs. Lee Cech for the care and patience she showed in producing such a finely typed thesis.

The work was supported by the National Research Council of Canada, the National Physical Research Laboratory (N.P.R.L.) of the South African Council for Scientific and

Industrial Research (C.S.I.R.) and the Bernard Price Institute of Geophysical Research, University of the Witwatersrand, Johannesburg. Thanks are due to the C.S.I.R. and the University of Alberta for supporting me financially (the latter through a Graduate Teaching assistantship).

My wife Trienette has been a constant source of encouragement through the many years of my studies. I thank her for that and the many things she sacrificed to my studies. I also wish to apologize to my daughter, Thearina for all the nights I have been studying when she wanted to play with me.

TABLE OF CONTENTS

CHAPTER		PAGE
I.	BACKGROUND TO THE INVESTIGATION	1
1.1	Induction theory for geomagnetic induction studies	1
1.2	Conductivity distribution in the earth	5
1.2.1	Global geomagnetic sounding: a study of the radial distribution of electrical conductivity	5
1.2.2	Direct-current sounding methods	13
1.2.3	The magnetotelluric method	16
1.2.4	Geomagnetic deep sounding: linear array method and large two-dimensional arrays	18
1.2.5	Conductivity distribution in the crust and uppermost mantle in areas away from major lateral inhomogeneities	22
1.2.6	Results of some magnetometer array studies	24
1.3	Geological background to the investigation	29
1.4	Results of ultra deep Schlumberger soundings in southern Africa	36
II.	DATA ANALYSIS AND INTERPRETATION TECHNIQUES	42
2.1	The data	42
2.2	Spectral analysis and maps of Fourier spectral components	43
2.3	Errors in Fourier spectral components	47

CHAPTER			PAGE
II.		2.3.1 Calibration errors	48
		2.3.2 Timing errors	48
		2.3.3 Digitizing errors	49
	2.4	Polarization of the horizontal field	52
	2.5	Transfer functions and induction vectors	54
	2.6	Numerical modelling	61
III.		THE 1971 ARRAY STUDY IN SOUTH AFRICA	66
	3.1	Introduction	66
	3.2	Magnetograms	68
	3.3	Maps of Fourier-spectral components	81
	3.4	Transfer functions	91
	3.5	Normalized anomalous fields	97
	3.6	Two-dimensional numerical modelling	105
	3.7	Discussion	109
IV.		THE 1972 ARRAY STUDY IN SOUTH-WEST AFRICA BOTSWANA AND RHODESIA	111
	4.1	Introduction	111
	4.2	Magnetograms	116
	4.3	Maps of Fourier spectral components	130
	4.4	Transfer functions	145
	4.5	Normalized anomalous fields	151
	4.6	Discussion	158

CHAPTER		PAGE
V.	A STUDY OF THE ELECTRIC CONDUCTIVITY STRUCTURE IN THE KAAPVAAL CRATON	162
	5.1 Electromagnetic induction in a plane-layered Earth	162
	5.2 Considerations for interpreting observed data	172
	5.3 Conductivity structure in the Kaapvaal craton as compared to a global model	178
VI.	THE CONDUCTIVITY ANOMALIES IN SOUTHERN AFRICA IN RELATION TO LOCAL GEOLOGY AND GEOPHYSICAL PARAMETERS AND THEIR POSSIBLE CAUSES	198
	6.1 The Southern Cape induction anomaly	198
	6.1.1 Heat flow data	198
	6.1.2 Gravity data	200
	6.1.3 Aeromagnetic data	203
	6.1.4 The Cape Fold Belt and its origin	206
	6.1.5 Proposed causes of induction anomaly	211
	6.1.6 Conclusion	214
	6.2 The conductive zone in South-West Africa and Botswana	216
	6.2.1 Seismological evidence	223
	6.2.2 Gravity data	227
	6.2.3 Geomagnetic depth sounding and heat flow	236
	6.2.4 Origin of the conductive zone	237

CHAPTER PAGE

VI. 6.3 Concluding remarks 240

REFERENCES 241

LIST OF TABLES

Table		Page
1.1	Tectonic provinces in which centres of Schlumberger soundings were situated, maximum current electrode spacing and transverse resistance of second unit	37
3.1	Coordinates and magnetic declination of stations in the 1971 array	69
3.2	Phase differences between Z and X at BEA and OLI for different periods for three events	90
4.1	Coordinates and magnetic declination of stations in the 1972 array	113
4.2	Phase differences in Z for stations to the north and south of conductor	144
4.3	Two-hour events used in calculating transfer functions	148

LIST OF FIGURES

Figure		Page
1.1a	Classical models for radial electrical conductivity of the Earth	10
1.1b	The models of Banks (1969, 1972) and Parker (1970) for the radial electrical conductivity of the Earth	10
1.2	Sketch map of shields and mobile belts in southern Africa showing localities of deep Schlumberger soundings	30
1.3	Experimental Schlumberger sounding data and best fitting models for soundings on the Namaqualand-Natal Belt, Rhodesian craton and Kaapvaal craton	40
3.1	The location of the stations in the 1971 array study in relation to tectonic provinces and continental edge of southern Africa	67
3.2	Magnetograms for the substorm of August 31, 1971	71
3.3	Magnetograms for the disturbance event of September 17 and 18, 1971	73
3.4	Magnetograms for the disturbance event of September 26 and 27, 1971	75
3.5	Amplitude spectra for the event of August 31, 1971, for the stations BEA and VEN	83
3.6	Amplitude spectra for the event of September 17 and 18, 1971, for the stations BEA and VRY	84
3.7	Amplitude spectra for the event of September 26 and 27, 1971, for the stations BEA and VRY	85
3.8	Fourier amplitudes and phases for 18.30-22.30 G.M.T., August 31, 1971, at period 24 min	87

Figure		Page
3.9	Fourier amplitudes and phases for 18.30-22.30 G.M.T., September 26, 1971, at period 51 min	88
3.10	Fourier amplitudes and phases for 18.30-22.30 G.M.T., August 31, 1971, at period 120 min	89
3.11	Induction vectors at four different periods	95
3.12	Normalized anomalous profiles for the horizontal field polarized approximately north-south	99
3.13	Normalized anomalous profiles for the horizontal field polarized in a NW-SE direction	101
3.14	Normalized anomalous profiles at periods of 24 min and 102 min in relation to geological section showing resistivity structure	104
3.15	Results of two-dimensional model calculations for a crustal structure	106
3.16	Results of two-dimensional model calculations for a subcrustal structure	107
4.1	The location of the magnetometer array in South-West Africa, Botswana and Rhodesia	112
4.2	The array in relation to the main tectonic features in the study area	114
4.3	Magnetograms for the event of January 16, 1972	118
4.4	Magnetograms for the event of January 21 and 22, 1972	120
4.5	Magnetograms for the event of January 28, 1972	128

Figure		Page
4.6	Amplitude spectra for the event of January 16, 1972 for the stations EIS, OKA and DET	132
4.7	Amplitude spectra for the event of January 28, 1972 for the stations ARA, OKA and DET	134
4.8	Fourier amplitudes and phases for 14.30-22.30 G.M.T., January 28, 1972, at period 21 min	136
4.9	Fourier amplitudes and phases for 17.30-22.30 G.M.T., January 28, 1972, at period 28 min	137
4.10	Fourier amplitudes and phases for 17.30-22.30 G.M.T., January 28, 1972, at period 35 min	138
4.11	Fourier amplitudes and phases for 17.30-22.30 G.M.T., January 28, 1972, at period 54 min	139
4.12	Fourier amplitudes and phases for 14.30-22.30 G.M.T., January 28, 1972, at period 79 min	140
4.13	Fourier amplitudes and phases for 14.30-22.30 G.M.T., January 28, 1972, at period 120 min	141
4.14	Induction vectors at four different periods	150
4.15	Normalized anomalous profiles along section AB for the horizontal field polarized west of north	154
4.16	Normalized anomalous profiles along section AB for the horizontal field polarized east of north	155
4.17	Normalized anomalous profiles along section CD	157

Figure		Page
5.1	Earth model with N-1 conductive plane layers above a conductive halfspace	163
5.2	Conductivity models investigated in one-dimensional model studies	181
5.3	Observed $\left\|\frac{H_z}{F}\right\|$ values for stations on the Kaapvaal shield in relation to computed values for Model 1 and Model 2	186
5.4	Observed $\left\|\frac{H_z}{F}\right\|$ values for stations on the Kaapvaal shield in relation to computed values for Model 3	189
5.5	Observed $\left\|\frac{H_z}{F}\right\|$ ratios at the stations CHR and VRY in relation to computed values for Model 1 and Model 2	191
5.6	Frequency-band averaged values of Mod[C(ω,0)] in relation to computed values for Model 1 and Model 3	196
6.1	Heat-flow data in relation to tectonic provinces in southern Africa	199
6.2	Magnetic, gravity and conductivity anomalies in southernmost Africa in relation to the Cape Fold Belt	202
6.3	Aeromagnetic map of central and south-eastern Cape Province, South Africa	204
6.4	The conductor in relation to seismicity and tectonics of southern central Africa	218
6.5	The zone of induced currents in relation to shields and rift structures	220
6.6a	Simplified Bouguer anomaly map of Africa	230
6.6b	Simplified relief map of Africa	230
6.7	Simplified Bouguer anomaly map of South-West Africa, Botswana and Zambia	232
6.8	Simplified isostatic anomaly map for South-West Africa	235

CHAPTER I

BACKGROUND TO THE INVESTIGATION

1.1 Induction theory for geomagnetic induction studies

The time varying magnetic fields used in geomagnetic induction studies such as magnetotelluric sounding, geomagnetic deep sounding and magnetometer array studies, have their origin outside the earth and diffuse through the earth to induce currents and produce secondary fields.

The mathematical formulation of the necessary induction theory begins with Maxwell's equations. In MKSA units these are:

$$\nabla \times \vec{E} = - \frac{\partial \vec{B}}{\partial t} \qquad (1.1)$$

$$\nabla \times \vec{H} = \vec{J} + \frac{\partial \vec{D}}{\partial t} \qquad (1.2)$$

$$\nabla \cdot \vec{B} = 0 \qquad (1.3)$$

$$\nabla \cdot \vec{D} = \rho \qquad (1.4)$$

In an isotropic medium:

$$\vec{J} = \frac{1}{\rho} \vec{E} \qquad (1.5)$$

$$\vec{B} = \mu \vec{H} \qquad (1.6)$$

$$\vec{D} = \varepsilon \vec{E} \qquad (1.7)$$

With $\vec{B}$ the magnetic flux density (Wb/m^2, Tesla)

$\vec{H}$ the magnetic field intensity (A/m)

$\vec{E}$ the electric field strength (V/m)

$\vec{D}$ the electric displacement (C/m^2)

$\rho = \frac{1}{\sigma}$ the resistivity (ohm.m, Ω-m)

σ the electrical conductivity (Siemens/m)

$\vec{J}$ the current density (A/m^2)

ϵ the permittivity (F/m)

μ the magnetic permeability (H/m)

For the period range and conductivities of interest in magnetometer array studies the displacement current $\frac{\partial \vec{D}}{\partial t}$ is negligible compared with $\vec{J}$ (Price, 1967). When the curl of eq. 1.2 is taken and eq. 1.1 and the relations of eqs 1.5, 1.6 and 1.7 used, $\vec{E}$ can be eliminated to reduce Maxwell's equations to the induction (or diffusion) equation

$$\nabla^2 \vec{H} = \frac{\mu}{\rho} \frac{\partial \vec{H}}{\partial t} \qquad (1.8)$$

Similarly, by eliminating $\vec{H}$ the diffusion equation in $\vec{E}$ can be written as

$$\nabla^2 \vec{E} = \frac{\mu}{\rho} \frac{\partial \vec{E}}{\partial t} \qquad (1.9)$$

Tozer (1959) showed that deep in the earth μ is close to μ_o (i.e. $4\pi \cdot 10^{-7}$ H/m), which means the diffusion equation

depends only on the period of the field and the resistivity. The atmosphere is assumed non-conducting, with ρ thus infinite so that

$$\nabla^2 \vec{H} = 0 \tag{1.10}$$

above the surface of the earth. Above the ground the magnetic field intensity $\vec{H}$ can therefore be expressed as

$$\vec{H} = - \nabla U \tag{1.11}$$

where U is a scalar potential function obeying Laplace's equation

$$\nabla^2 U = 0 \tag{1.12}$$

Within the earth, where $\rho \neq 0$, the propagation of the field is controlled by another equation. Assuming a time dependence of $\exp(i\omega t)$ with ω the angular frequency of the inducing field and neglecting displacement currents, eqs 1.1, 1.2, 1.5, 1.6 can be combined to give

$$\nabla^2 \vec{H} = \frac{i\omega\mu\vec{H}}{\rho} - (\rho\nabla(\frac{1}{\rho}) \cdot \nabla \times \vec{H}) \tag{1.13}$$

This represents the basic equation for the variation field within the earth.

Schmucker (1970a) separates eq. 1.13 into two parts, the first being the "normal" solution for variations above a horizontally stratified medium, and the second being the "anomalous" variation field superimposed on the

normal field due to lateral variations of conductivity in the substratum. The two solutions are additive since eq. 1.13 is a linear equation. By writing H_a, ρ_a for the anomalous parts and H_n and ρ_n for the normal parts where $H = H_n + H_a$, $\rho = \rho_n + \rho_a$ and bearing in mind that $\rho_n = \rho_n(z)$ only, the normal equation becomes

$$\nabla^2 \vec{H}_n = \frac{i\omega\mu \vec{H}_n}{\rho_n} \tag{1.14}$$

The equation for the anomalous parts becomes

$$\nabla^2 \vec{H}_a + (\frac{1}{\rho}\nabla\frac{1}{\rho} \cdot \nabla \times \vec{H}) = i\omega\mu(\frac{1}{\rho_n}\vec{H}_a + \frac{1}{\rho_a}\vec{H}) \tag{1.15}$$

The normal equation is generally soluble in cartesian and polar coordinates, as will be shown in Chapter 5. The anomalous equation is, however, only readily soluble for configurations of high symmetry or for two-dimensional cases (Hobbs, 1975).

The diffusion of the primary field into the Earth is related to the skin depth given by the equation

$$\delta = \sqrt{\frac{2\rho}{\omega \mu_0}} \tag{1.16}$$

This defines the depth beneath the plane surface of a uniform conducting half-space where the amplitude of the primary field falls to 1/e of its surface value. The skin

depth decreases as the resistivity and/or period decreases. Skin depths of interest in array studies vary from just more than 6 km for a field of period 10 min incident on seawater with a resistivity of .25 ohm.m, to more than 4,000 km for period 24 hours and resistivity 1,000 ohm.m (e.g. resistivity of lower crust and uppermost mantle in stable continental areas).

1.2 Conductivity distribution in the earth

1.2.1 Global geomagnetic sounding: a study of the radial distribution of electrical conductivity

Time-varying magnetic fields arising outside the earth which acts like a conducting body, induce electric currents in the earth so that magnetic fields with an internal origin are produced. The theory of electromagnetic induction incorporated in the relationship between the parts of transient geomagnetic variations of external and internal origins, as obtained by analyses of world-wide data, provides a means of inferring the electrical conductivity within the earth.

The theories involved in global electromagnetic induction are from Lahiri and Price (1939) and Eckhardt (1968) and have been reviewed by Bailey (1970). In the air above the earth, the magnetic field can be represented as $-\nabla W$ where W is a magnetic scalar potential satisfying

Laplace's equation. The magnetic scalar potential can be represented in terms of spherical harmonics which are solutions of Laplace's equation. Any solution for W can thus be expanded as

$$W(r,\theta,\phi,t) = \sum_{n=1}^{\infty} \sum_{m=-n}^{+n} a\left[e_n^m(t)\left(\frac{r}{a}\right)^n + i_n^m(t)\left(\frac{r}{a}\right)^{-n-1}\right] P_n^m(\cos\theta)\, e^{im\phi} \tag{1.17}$$

With n the harmonic degree, m the order, θ the colatitude, ϕ the longitude, a the earth's radius and e_n^m and i_n^m are the amplitudes of the external and internal parts of the field respectively. $P_n^m(\cos\theta)$ is the associated Legendre function of degree n and order m.

In the conductive earth use can be made of the magnetic vector potential such that

$$\vec{B} = \nabla \times \vec{A} \tag{1.18}$$

Lahiri and Price (1939) have shown that where the conductivity is a function of radius only, $\vec{A}$ must be of the form

$$\vec{A} = \vec{r} \times \nabla U \tag{1.19}$$

with U a scalar potential.

Taking the curl of eq. 1.8 and using the relations $\vec{B} = \mu\vec{H}$, $\nabla \cdot \vec{A} = 0$ and $\vec{E} = -\frac{\partial \vec{A}}{\partial t}$ together with the assumption

that free charges are not present within the conductor one finds that

$$\nabla^2 \vec{A} = i\omega\mu\sigma(r)\vec{A} \tag{1.20}$$

This induction equation which is also satisfied by U is the central equation of geomagnetic deep sounding.

Inside the conductor, solution of eq. 1.20 for U yields

$$U = \sum_{n=1}^{\infty} \sum_{m=-n}^{+n} f_n^m(r)\, P_n^m(\cos\theta) e^{im\phi} \tag{1.21}$$

where f_n^m satisfies the radial induction equation

$$\frac{\partial}{\partial r}\left(r^2 \frac{\partial}{\partial r} f_n^m\right) = [n(n+1) + i\omega\mu_o\sigma(r)r^2] f_n^m \tag{1.22}$$

Under the boundary conditions that the tangential components of $\vec{E}$ and $\vec{H}$ and the normal component of $\vec{B}$ are continuous at the surface of the sphere, the potential and its radial derivatives above and below the surface of the sphere are fitted smoothly together. The resulting ratio of the induced amplitude i_n^m to the inducing field amplitude e_n^m is $S_n^m(\omega)$ the geomagnetic response of the earth in the spherical harmonic mode P_n^m. It is a function of frequency and the conductivity and is used to model observational data by comparison to the internal and external field ratios.

Lahiri and Price (1939) obtained an analytic solution for eq. 1.22 for a model whose conductivity varied as an arbitrary power of the radius. They fitted a five-parameter model to both Sq- and Dst-variations. Sq contains important harmonics at periods 6, 8, 12 and 24 hr and Dst is a transient with useful amplitudes in the Fourier transform with periods up to several days. In the Lahiri-Price model the major features are the following:

(1) The resistivity varies slowly from a value of 100 ohm.m near the earth's surface to about 5 ohm.m at a depth of about 400 km.

(2) Between 400 and 800 km the conductivity increases rapidly with depth.

Rikitake (1966) reporting work done around 1950, determined uniform core models which were compatible with available analyses of Sq, Dst, the geomagnetic bay (typical period 1 hour), solar flare effect (period of about 30 min) and the 27-day period variation. He modelled the induction by means of a rapid fall of resistivity to about 10 ohm.m at a depth of about 400 km. All the models obtained in the classical studies (Fig. 1.1a) show a steep rise in conductivity in the depth range 400 to 700 km, but it was not possible to say confidently if, or where, the conductivity leveled off. Estimates of the deep conductivity have been made by studying the transmission through the mantle of the secular variation of the main

Figure 1.1a Examples of conductivity models of the Earth obtained in classical studies (McDonald, 1957; Rikitake, 1960). The Price-McDonald curve published by McDonald (1957) combines his estimate of the lower mantle conductivity with one of the Lahiri and Price (1939) models.

Figure 1.1b The models of Banks (1969, 1972) and Parker (1970) for the radial conductivity of the Earth.

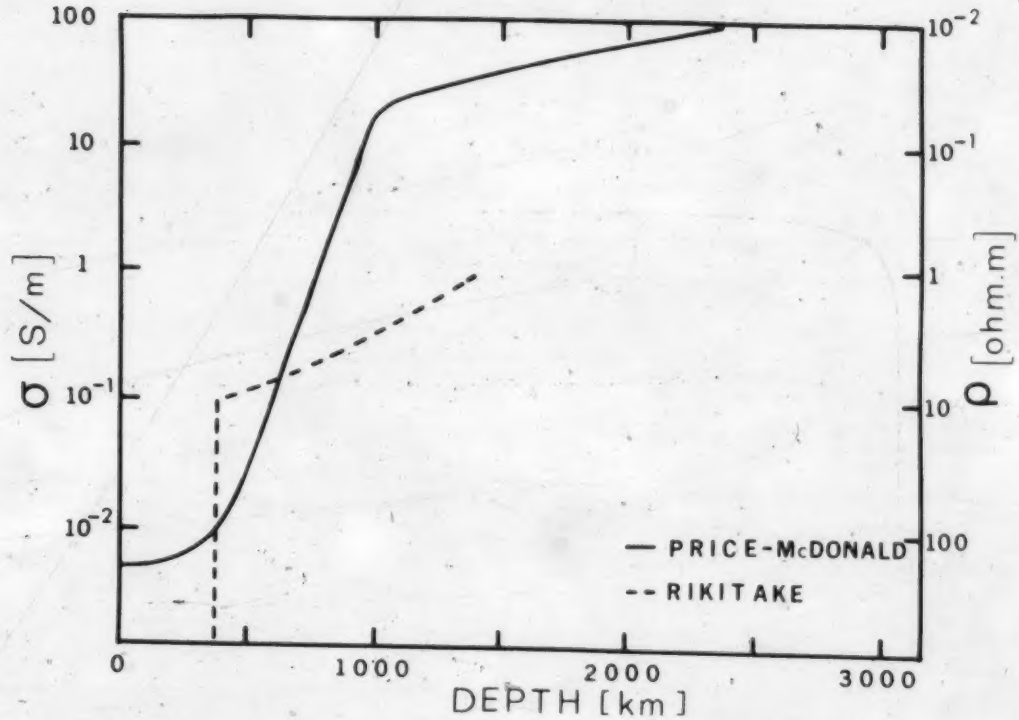
100
10
1
10^{-1}
10^{-2}
σ [S/m]
10^{-2}
10^{-1}
1
10
100
ρ [ohm.m]
— PRICE-McDONALD
-- RIKITAKE
0
1000
2000
3000
DEPTH [km]

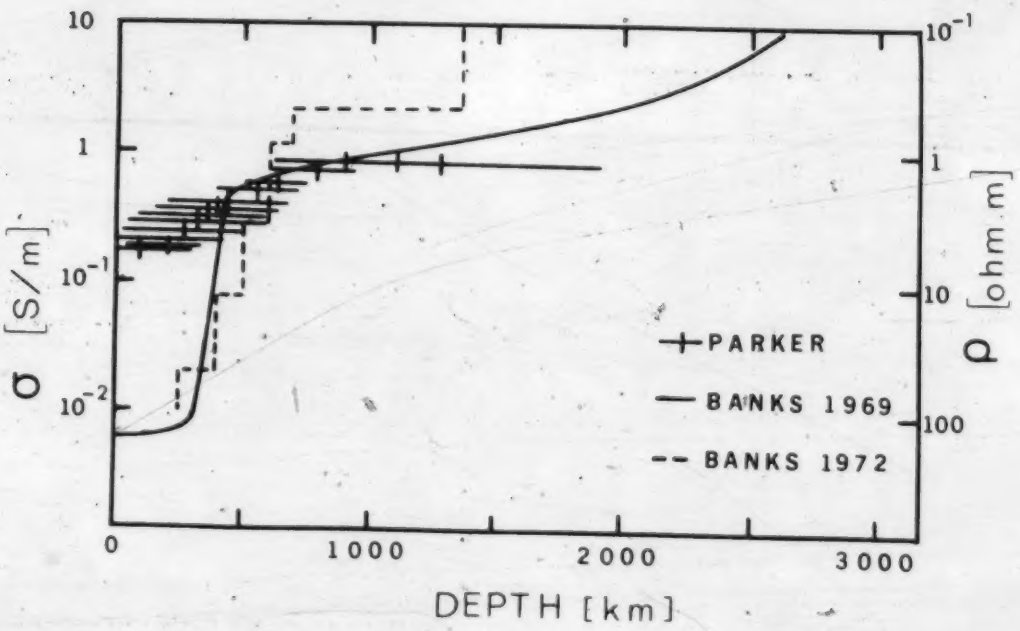
10
1
10^{-1}
10^{-2}
σ [S/m]
10^{-1}
1
10
100
ρ [ohm.m]
+PARKER
— BANKS 1969
-- BANKS 1972
0
1000
2000
3000
DEPTH [km]

geomagnetic field, which is generated in the outer core. Assuming that the cut-off frequency of the secular variation (0.25 yr^{-1} as determined by Currie (1968)) is not an intrinsic property, but due to the filtering properties of the mantle, a number of investigators (e.g. McDonald, 1957; Smylie, 1965) estimated the conductivity of the lower mantle to be 100 $S.m^{-1}$.

It was only about 1960 with the advent of high-speed computers capable of handling large data sets, that detailed analysis of the conductivity distribution in the earth became possible. Outstanding among the recent work is that of Banks (1969, 1972) and Parker (1970, 1972). Banks examined the nature of the geomagnetic spectrum, the peaks as well as the continuum between them and found that the single spherical harmonic P_1^0 described the variations quite well. An estimate of the response of the earth in the P_1^0 mode over the frequency range 0.1 to .25 day^{-1} was obtained. A multi-layered model was fitted to these response data and produced a conductivity estimate as shown in Fig. 1.1b (Banks, 1969). Also shown in this figure is an improved model obtained by taking into account a better fit of the phase relations (Banks, 1972).

Parker (1970) applied the Backus-Gilbert linear inverse technique (Backus and Gilbert, 1967, 1968), to the geomagnetic induction problem. He used as observables

(from the Banks (1969) data) the moduli of the geomagnetic response of the earth in the P_1^0 mode at 35 frequencies between .01 and .2 day^{-1}. The final model fitted to the data is shown in Fig. 1.1b. Parker's model differs from that of Banks in that it gives a conductivity for the top 400 km of the earth about one order of magnitude higher. The cause of this discrepancy could be the fact that Banks' data contain negative (nonphysical) phases at periods less than 5 days, or that Parker did not incorporate the phase information in his inversion, or an inherent ambiguity of the modelling method Banks used, or more than one of these (Banks, 1972; Jady, 1974a,b).

Bailey (1970) and Weidelt (1972) described exact inverse methods, which unfortunately require as input precise data over a broad frequency range. Data of that quality are not yet available.

In all studies discussed in this section, spherical symmetry has to be assumed to make the theoretical problem tractable. The short period limit for these studies is determined by induction effects caused by lateral variations in electrical conductivity in the crust and upper mantle. In practise this means that only data with a period longer than about five days could be used in these studies. The outcome of this limitation at the high frequency end of the spectrum is

that the conductivity structure in the upper 400 km of the earth is poorly resolved (Rikitake, 1973). Studies of the top few hundred kilometres of the earth is thus best left to other methods like the direct current sounding methods, magnetotelluric soundings and short-period geomagnetic deep sounding techniques not depending on the radial symmetry requirement.

Since the resistivity decreases to values less than 1 ohm.m in the depth range 400-800 km (Fig. 1.1b) even storm-time fields with periods of several days have highly reduced amplitudes at a depth of 1000 km. This limits geomagnetic induction studies by means of external fields effectively to depths less than 1000 km. The power of the geomagnetic variation spectrum indicates a steep rise at frequencies less than 10^{-3} day^{-1} due to the geomagnetic secular variation (Rikitake, 1973; Banks, 1969) which originates entirely within the earth. Even if very low-frequency external fields were available, the secular variation fields would mask them and would make it very difficult to use such very low-frequency external fields for study of the lower mantle.

1.2.2 Direct-current sounding methods

The two most widely used direct-current sounding methods as far as crustal-scale investigations are concerned are the Schlumberger and dipole techniques.

The Schlumberger electrode array consists of four colinear electrodes (Kunetz, 1966). To make a sounding the two outer electrodes, the contacts for current emission, are moved progressively away from the centre of the spread. The inner two electrodes, arranged symmetrically with respect to the centre of the array measure the voltage drop due to the current flowing through the ground between the current electrodes. In the Schlumberger array the distance between the current electrodes is always more than five times that between the potential electrodes and in deep crustal to upper mantle studies it can exceed 200 times the potential electrode distance. The ratio of the voltage drop to potential electrode separation thus approximates the electric field.

In the dipole array the four electrodes are arranged in two pairs, one pair supplying current and the other measuring a potential difference, and the relative arrangement of the pairs determines the type of dipole array (Al'pin et al., 1966). The current electrode pair is usually fixed in location, while a component of the electric field is mapped as a function of distance from this current source with the potential-difference pair of electrodes. Normally the electric field is mapped away from the dipole source along one of the principal

directions. In an equatorial dipole sounding, the component of electric field parallel to the source axis is mapped outwards on the equatorial axis. For a horizontally layered earth - but only for this configuration - the resulting apparent resistivity curve as a function of separation is the same as one obtained from a Schlumberger sounding. When the electric field is measured at locations along the axis of the source the sounding is called a polar dipole sounding.

In the direct-current sounding method the apparent resistivity ρ_a in onm.m is given by

$$\rho_a = K \frac{\Delta V}{I} \qquad (1.23)$$

with ΔV the potential drop in Volts, I the current in Ampere and K a constant dependent on the electrode configuration and given by

$$K = \frac{2\pi}{(\frac{1}{AM} - \frac{1}{AN}) - (\frac{1}{BM} - \frac{1}{BN})}$$

where A and B denotes current electrode positions and M and N potential electrode positions. The distances AM, AN, BM and BN are measured in metres.

The classical method of interpreting dc soundings is by comparison of a field curve with a precalculated catalogue of reference curves (e.g. Orellana and Mooney,

1966). The curve-matching technique is, however, rapidly being replaced by computer-assisted interpretation techniques which permit more reliable results to be obtained with less effort (Kunetz and Rocroi, 1970; Inman, Ryu and Ward, 1973).

1.2.3 The magnetotelluric method

The magnetotelluric sounding method makes use of the natural electromagnetic field of the earth as power source. The technique requires that simultaneous observations be made of orthogonal electric and magnetic variations in the electromagnetic field. Cagniard (1953) and Keller and Frischknecht (1966) provide excellent introductions to the theory of magnetotelluric fields over a plane-layered earth.

With a coordinate system at the earth's surface having the axes aligned x north, y east and z down we have for plane waves generated by sources in the ionosphere

$$Z = \frac{E_x}{H_y} \tag{1.24}$$

where Z is the characteristic impedance in ohms, E_x the electric field intensity (north) in V/m and H_y is the magnetic field intensity (east) in A/m. In this section capital letters signify frequency-domain representations of the field quantities.

In a homogeneous and isotropic earth the true resistivity is related to the characteristic impedance through the relation:

$$\rho = \frac{T}{2\pi\mu} |Z|^2 = \frac{T}{2\pi\mu} \left|\frac{E_x}{H_y}\right|^2 \qquad (1.25)$$

where ρ is the resistivity in ohm.m, T the period in seconds and μ the magnetic permeability of the medium. In the case of a horizontally layered earth (one-dimensional earth) eq. 1.25 becomes that for the apparent resistivity

$$\rho_a = \frac{T}{2\pi\mu} \left|\frac{E_x}{H_y}\right|^2 \qquad (1.26)$$

which is frequency dependent.

In the presence of lateral changes in the electrical properties of the earth, however, each electric field component couples to both magnetic field components through a relationship of the form:

$$E_x = Z_{xx}H_x + Z_{xy}H_y$$
$$E_y = Z_{yx}H_x + Z_{yy}H_y \qquad (1.27)$$

where the matrix

$$\begin{pmatrix} Z_{xx} & Z_{xy} \\ Z_{yx} & Z_{yy} \end{pmatrix}$$

is called the impedance tensor (Word, Smith and Bostick, 1970; Hermance, 1973).

1.2.4 Geomagnetic deep sounding: linear array method and large two-dimensional arrays

Classical geomagnetic deep sounding (G.D.S.) methods were developed mainly by Schmucker (1964, 1970a). In G.D.S. studies use is made of observations from a small number of three-component variometers, usually less than ten, recording simultaneously. Since the best arrangement of such a small number of instruments is often along a straight line, G.D.S. methods are usually associated with small linear arrays. In regions removed from local anomalies the smoothness of the observed field indicates that the electrical conductivity varies approximately with depth alone, and is thus one-dimensional. In this case it is the practise to compute the ratio Z/H of vertical to horizontal components for an incident field of given period T and spatial wave number k, at the surface of a layered conductive half-space (Schmucker; 1970a). The computed Z/H ratio is compared with the observed ratio for several periods at which data are available. These models are highly non-unique and the estimation of k is a major difficulty. This problem will be discussed in Chapter 5.

In regions with lateral conductivity changes, the station-to-station changes in amplitude and phase of

the field components indicate the presence and configuration of internal conductive structure. To map the conductive structure through the use of different variation events, several events are recorded with the magnetometers in each of a number of positions successively. A measure of the response of the earth to the incident field is required, normalized to that field. Parkinson (1959, 1962) and Wiese (1962) took a first step with their arrow representations of response. Schmucker (1970a) introduced the use of a matrix of transfer functions, each of which gives the response of the earth in one component of the anomalous field to one component of the normal field. This method preserves the phase information. The estimation of transfer functions, however, requires computation of powers and cross-products between normal and anomalous field components. Unique separation of normal and anomalous fields is commonly impossible with a small array, and usually the field at one station is arbitrarily designated as representing the "normal" field.

Large two-dimensional arrays of magnetometers came into use as a result of the development of an inexpensive portable three-component magnetometer by Gough and Reitzel (1967). An advantage of an array is that it allows mapping of a single variation event over the whole array which may cover 10^5-10^6 km^2. This proves important

when dealing with specially polarization-sensitive anomalies. A Fourier transform refers to a precise period and sums the energy of the whole event at that period and for this reason the Fourier transform amplitudes and phases of variation components have proven good parameters to map (Reitzel et al., 1970). The data analyses involved in array studies will be discussed in Chapter 2.

Magnetic fields observed over part of the earth may be separable into external and internal parts by use of surface integrals. Porath, Oldenburg and Gough (1970) used surface integrals to separate fields obtained with a two-dimensional magnetometer array. The separation can be done for instantaneous fields in the time domain or for a given frequency in the frequency domain.

Separation of variation fields over a limited portion of the earth, however, has some short-comings. Fields whose dimensions are larger than the dimensions of the array are not separable by the method. In the middle latitudes the source fields have dimensions that are larger than the array dimensions and cannot be separated. These limitations led Gough (1973b) to state: "The separation exercise described by Porath et al. (1970) was valuable, but it may be doubted whether it should be repeated."

Quantitative interpretation of conductivity anomalies involves fitting models of conductive structures

to the anomalous fields, normalized with respect to the normal (inducing) fields. Analytic methods of modelling deal only with conductors of a few simple geometrical shapes. d'Erceville and Kunetz (1962) obtained exact solutions for a semi-infinite conductor with a vertical plane of discontinuity. Rankin (1962) solved the problem of a dyke model exactly. Weaver (1963) and Weaver and Thomson (1972) produced analytic approximate solutions for a non-uniform earth with an overhead line current.

Analogue scaled models have been used to study conductivity structure (Dosso, 1966; Dosso and Jacobs, 1968; Hermance, 1968).

The most successful approach to the problem was through numerical methods. In two-dimensional cases it is useful to consider anomalous fields which are E-polarized or H-polarized. In the E-polarized field, the induced currents flow parallel to the infinitely long dimension of the structure. The induced field is also E-polarized. The induced currents of the H-polarized field flow at right angles to the long dimension of the structure and their magnetic fields are not observable at the earth's surface.

Of the numerical methods used for modelling of arbitrary shapes three have been widely used, viz. the transmission line analogy method (Madden and Swift, 1969;

Wright, 1969), the finite difference method (Jones and Price, 1970; Jones and Pascoe, 1971; Pascoe and Jones, 1972) and the finite element method (Coggon, 1971; Reddy and Rankin, 1973).

Geomagnetic deep sounding techniques proved to be especially well suited to detect lateral changes in conductivity in the crust and uppermost mantle (Porath, 1971; Gough, 1974).

1.2.5 Conductivity distribution in the crust and uppermost mantle in areas away from major lateral inhomogeneities

Many attempts have been made in recent years to determine quantitative electrical resistivity profiles for the crust and uppermost mantle by means of surface measurements (e.g. Keller, 1971). The vast majority of these investigations were conducted by studying variations in the natural electromagnetic field of the earth, the magnetotelluric method being the most widely used technique.

It is widely recognised that the stable continental crust can be divided into three broad units as far as its electrical conductivity is concerned (e.g. Keller et al., 1966; Dvořák, 1975). The uppermost of these units is the conductive surface layer which consists of sedimentary or decomposed igneous and metamorphic rocks sometimes containing water. The underlying second unit is highly resistant (of the order of 10^4 ohm.m in stable continental regions (Keller

et al., 1966) and is made up of fresh igneous and metamorphic rocks which although buried, are still at low temperatures but extend to depths where pressures are high enough to close cracks and exclude water. As the temperature increases with depth, the resistivity decreases and the third unit, which is distinctly more conductive than the second, is reached. This unit has a resistivity of about 1,000 ohm.m for the stable continental model (Dvořák, 1975). Another interesting feature in the conductivity profile is that there is no decrease in resistivity associated with the Mohorovičić discontinuity (Dvořák, 1975). It is worthy of note that resistivity ranges through at least 6 orders of magnitude in the earth, whereas seismic wave velocities, for instance, do not cover a factor of 10.

In a conductor-resistor-conductor sequence of units as in an idealized crust, the magnetotelluric method is sensitive mainly to the thickness of the resistant zone and gives a poor indication of its resistivity (Madden, 1971). Direct current sounding methods which use a controlled artificial source of electrical energy, however, are sensitive to the transverse resistance T_2 (thickness-resistivity product) of the resistant zone, especially if the surface layer has a large longitudinal conductance S_1 (thickness-resistivity ratio). If, however, areas can be

found where the conductive first zone is absent or where S_1 is small it should be possible to determine the true resistivity and thus the thickness of the resistant zone or at least to approach the true value. The direct current-resistivity methods are thus from a theoretical point of view the most suitable methods to study the resistivity distribution in the resistant portion of the crust (Madden, 1971).

The dc and MT methods are probably comparable as regards the investigation of the third unit because the response of both methods depends on the longitudinal conductance S_3.

Both the dc and MT methods should ideally be used in areas where the conductivity distribution approximates a horizontally stratified case. Although local geomagnetic deep sounding studies can be, and have been, used for studying horizontally stratified situations (Schmucker, 1970a; Porath et al., 1971; Kuckes, 1973a; Camfield and Gough, 1975) it is more suitable for mapping lateral conductivity changes.

1.2.6 Results of some magnetometer array studies

Linear magnetometer array work discovered several important conductivity anomalies. Examples are: the Rio Grande anomaly near the Mexican border in the

Midwestern United States (Schmucker, 1964, 1970a), the extensively studied Japanese anomaly (Rikitake, 1966; Rikitake and Honkura, 1973) and the conductivity anomaly under the Peruvian Andes (Schmucker et al., 1967).

The first two-dimensional array studies were carried out in western North America by the University of Texas at Dallas and the University of Alberta (Reitzel, Gough, Porath and Anderson, 1970; Porath, Oldenburg and Gough, 1970; Porath and Gough, 1971; Camfield, Gough and Porath, 1971; Porath, Gough and Camfield, 1971; Camfield and Gough, 1975). These initial studies were followed by studies with arrays from either of the above institutions (e.g. Porath and Dziewonski, 1971a; Alabi, 1974; Alabi, Camfield and Gough, 1975).

Large arrays were also operated in Australia (Gough, McElhinny and Lilley, 1974; Bennett and Lilley, 1973), Scotland (Sik et al., 1974), Ethiopia (Berktold et al., 1974), Kenya (Banks and Beamish, 1974) as well as South Africa and South-West Africa, Botswana and Rhodesia (the present study, Gough, De Beer and Van Zijl, 1973; De Beer et al., in press).

Comprehensive reviews of magnetometer array studies have been published by Porath and Dziewonski (1971b), Gough (1973a,b), Frazer (1974) and Lilley (1975). In this section I will therefore only summarize some of the more

important results from the above two-dimensional array studies and indicate the correlations between the electrical conductivity anomalies and other geophysical anomalies.

The complicated conductivity structure of western North America has been studied in great detail by the arrays that operated in that area. Gough (1974) gave a comprehensive review of the results. It was found that highly conductive mantle material which has to be at least 100 km thick for a resistivity of 5 ohm.m underlies the Basin and Range Province and ridges of still lower resistivity (or greater thickness for a given resistivity) underlie the Wasatch Fault Belt and the southern Rockies. The upper mantle under the Great Plains proved to be more resistive and may approximate a sub-shield type. The conductivity under the Colorado Plateau is of the Great Plains type or intermediate between this and that beneath the Basin and Range. Gough emphasizes in his review the ambiguity of interpretation of depths of structures associated with the models for the section through the two belts of high conductivity on either side of the Colorado Plateau. The array results could be satisfied equally well by undulations in the depth to the highly-conducting mantle (giving depths of between 100 and 400 km) or by variations in thickness of a conducting layer in the upper mantle separated from the deep mantle. The second

interpretation is more attractive because it allows a comparison with the low-velocity zone. The seismic velocity models for western and eastern North America show a striking difference in thickness and intensity between the two portions of the continent. In the west the depth extent of the zone corresponds well with the required thickness of conducting material, while the much smaller low-velocity zone in the east is compatible with the fact that conductivity anomalies in eastern North America appear to be controlled by crustal rather than mantle conditions (Garland, 1975). High heat flow in the western United States also shows a good correlation with the distribution of structures with high conductivity. Gough (1974) points out that there can be no serious doubt that the highly-conductive regions of western North America are conductive because they are hot.

The North American Central Plains magnetic variation anomaly is one of the most striking elongated anomalies (Gough and Camfield, 1972; Alabi, 1974). The conductive body underlies an area where the basement rocks are poorly exposed and its presence was indicated for the first time by magnetometer array measurements. The above methods have shown that there is supporting evidence for a metamorphic belt (graphite schist belt) in the crust and faulting in the basement under the Palaeozoic sediments.

This anomaly, first detected near the Black Hills, is also of the current concentration type which means the anomalous fields are those of currents concentrated in a body of high conductivity which joins large undefined regions of the Earth in which the induction occurs. This effect precludes two-dimensional modelling of the anomaly.

The first array study in Africa was over the Afar Depression and Main Ethiopian Rift in Ethiopia (Berktold et al., 1974). Analysis of the spatial inhomogeneity of the magnetic variations near the magnetic dip equator which crosses the southern part of the Afar Depression indicates a resistivity of less than 10 ohm.m at a depth of 100-300 km in this area. Higher electrical conductivities are also indicated under the Afar Depression than beneath the adjacent plateaus. South of 12°N, however, Parkinson arrows suggest higher conductivity beneath the southern part of the Western Plateau than beneath the Afar Depression. The above authors suggest that the low resistivities are temperature related.

Banks and Ottey (1974) found a similar situation from a linear array study across the eastern branch of the East African Rift Valley near the Equator. They concluded that the type of model that fits the experimental data involves a strip of high conductivity material at a depth of no more than 20 km beneath the floor of the rift with, in addition, a 100 km thick slab of material of more

moderate conductivity at a depth of 50 km beneath the eastern flank of the rift. The two regions of high conductivity are interpreted as zones of partial melting in the upper mantle. An associated low velocity, low density zone is indicated by the gravity and seismic experiments which support the interpretation of partial melting in the upper mantle. Additional strong evidence in favour of such an interpretation is the recent volcanic activity in and around the rift valley and the associated geothermal activity. A two-dimensional array was operated in the same region during 1972 (Banks and Beamish, 1974). Data from the east-west line of instruments roughly along the equator appear to confirm the linear array results and indicate a two-dimensional conductive structure beneath and to the east of the Rift Valley. The results from this array also indicate a three-dimensional structure underneath the area to the south-east of the 1971 line.

1.3 Geological background to the investigation

The tectonic pattern within the Precambrian continental basement in southern Africa is characterized by a network of intersecting mobile belts (Fig. 1.2). These mobile belts surround and separate from one another cratonic areas which have remained undeformed for at least the last 2,500 Myr (Anhaeusser et al., 1969).

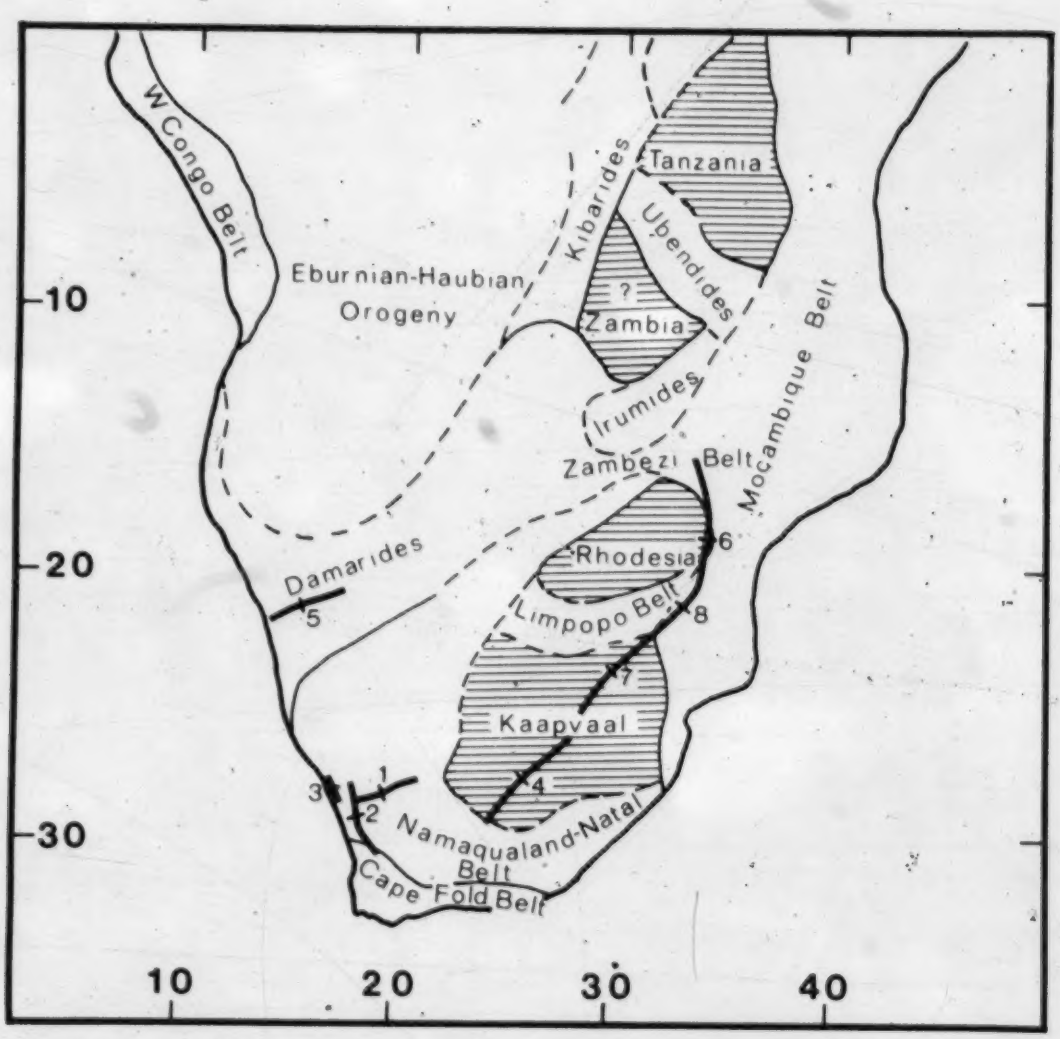

Figure 1.2 Sketch map of shields older than 2,500 Myr (shaded areas) and mobile belts in southern Africa. The numbers from 1 to 8 indicate the centres of deep Schlumberger soundings listed in Table 1.1 and the heavy lines indicate telephone and power lines used as current emission lines in these soundings.

Clifford (1972) argued on the basis of available geologic and geochronologic data that the major part of the African continent is a segment of primeval crust more than 3,000 Myr old, which has been affected by several major orogenies. At least two of these orogenic events are older than 2,500 Myr and the best evidence for their occurrence is preserved in the cratonic nuclei. The major younger orogenic events in southern Africa occurred as a sequence of polyepisodic orogenies 1,850 $\pm$ 250 Myr ago (Eburnian and Huabian orogenic episodes), 1,100 $\pm$ 200 Myr ago (Kibaran orogeny), 600 $\pm$ 100 Myr ago (Damaran-Katangan or Pan-African orogeny) and during middle Palaeozoic - early Mesozoic time when the Cape Fold belt was formed (Clifford, 1974).

The recognition, delineation and structural analysis of these tectonic units have been the topics of many studies. Outstanding in the early work in southern Africa is the interpretation of Holmes (1951) who combined tectonic studies and the then new study of geochronology to discern internal features within the Precambrian terrains. Similar studies by Cahen (1961), Nicolaysen (1962), Cahen and Snelling (1966) and Clifford (1968) followed. Detailed analyses on limited areas have been made by, among others, Nicolaysen and Burger (1965), Vail (1965), Clifford (1967), Vail et al. (1968), Allsopp et al. (1969), Vail and

Snelling (1971), Van Breemen and Dodson (1972), Wilson and Harrison (1973) and Clifford et al. (1975).

These studies established the present knowledge about the distribution and interrelationship of the different structural units as depicted in Fig. 1.2.

A brief description of the structural units as shown in Fig. 1.2 will facilitate later discussion. The Kaapvaal and Rhodesian cratons consist largely of a granite and gneiss terrain incorporating early Precambrian greenstone belts. The whole suite is older than about 2,600 Myr, the age of the last major granitic and pegmatitic intrusion (Nicolaysen and Burger, 1965; Martin, 1969). The ancient nuclei within these 2,600 Myr old terrains consists of intrusive suites of granitic rocks and schist belts of metasedimentary and volcanic rocks with ages up to 3,400 Myr (Van Niekerk and Burger, 1969; Allsopp et al., 1969; Vail and Dodson, 1969).

The Limpopo Belt consists of reworked Archean granite-greenstone terrain with an early Proterozoic cover sequence infolded and metamorphosed with the basement (Mason, 1973). Van Breemen and Dodson (1972) found that although the main folding and metamorphism dates back to 2,700 Myr, a strong thermal event affected the Limpopo Belt about 2,000 Myr ago.

The Namaqualand-Natal Belt is constituted of granite gneiss, together with remnants of the metavolcanic

and metasedimentary rocks of the Kheis System that are older than 2,600 Myr. The near-equality of ages of 900 to 1100 Myr yielded by a wide range of minerals is believed to reflect a period of intense reconstruction of older basement (Nicolaysen and Burger, 1965).

The Zambezi Belt comprises a zone of high-grade metamorphism around the north-western and northern margins of Rhodesia. Down-faulted Karroo (Permo-Triassic) rocks in the Zambezi Rift Valley cover the metamorphic rocks of the belt for the largest part. Geochronological results indicate an age of about 500 Myr for the latest thermal event in the belt (Vail and Snelling, 1971). In the west the Zambezi Belt disappears under the Cainozoic Kalahari cover and in the east it joins the north-south trending Moçambique Belt. The Moçambique Belt consists of high-grade metamorphic rocks with associated granites and pegmatites. This belt is also characterized by ages between 400 and 700 Myr (Clifford, 1967). The Damara geosynclinal belt consists of a miogeosynclinal facies in which dolomitic limestone predominates and an eugeosynclinal facies containing mafic volcanics and consisting of predominantly pelitic sediments. The most recent orogenic event in the eugeosyncline is indicated by consistent radiometric ages in the general range 450-550 Myr (Clifford, 1967). The similarity in the age patterns between the Damara geosyn-

cline, Zambezi Belt and Moçambique Belt suggests a tectono-thermal kinship of the zones. The exact structural relationship between the Damara geosyncline and the Zambezi Belt is, however, obscured by the Kalahari sediments in Botswana, southern Angola and western Zambia.

The youngest of the major tectonic events observable in South Africa is represented by the Cape Fold Belt. This fold belt consists of the less severe north-south trending Cedarberg folds in the west and the main east-west trending fold system in the south. The folded sedimentary strata range in age from Late Ordovician (Cramer et al., 1974) to Late Permian (Haughton, 1969), but the main phase of folding occurred in Triassic times. Several authors suggested a continental collision origin for the formation of this fold belt (De Swardt et al., 1974; De Beer et al., 1974: Martini, 1974; Rhodes, 1974).

Clifford (1972) concluded that these mobile zones are floored by older crystalline basement and that no geosynclinal sequences were deposited on extensive areas of oceanic crust. In large segments of almost all these orogenic zones, the orogenic event is entirely recorded as rejuvenated floor rocks. Shackleton (1973) makes the important point that there are no large offsets of earlier structures across these belts. This implies that where two mobile belts cross, there has been little, if any, crustal

shortening in the younger orogenic belt and thus little, if any, relative motions of the stable cratons on either side of this belt.

Despite all the geochronologic-tectonic studies, the information regarding both extent and age of the units is still ambiguous. The difficulty of interpreting isotopic age measurements as dating either tectono-thermal events, or merely regional cooling through uplift without orogenesis, inhibits the correlation and recognition of many of the active belts (Vail, 1968). The overprinting of isotopic events on stable cratonic blocks or earlier orogenic belts without the apparent accompanying metamorphism may also mask the aerial extent of the units. Undisturbed younger sedimentary cover further obscures vast areas of the Precambrian of Africa, especially since the cratons have provided basins for considerable sedimentation during Upper Palaeozoic and Mesozoic times (Kennedy, 1965; Haughton, 1969). The Palaeozoic-Mesozoic Karroo strata obscure in this way the transition from the Kaapvaal shield to the Namaqualand-Natal Belt. The Cainozoic Kalahari beds in central southern Africa similarly impede a definitive structural correlation between the Damara geosynclinal belt and the Zambezi Belt.

1.4 Results of ultra deep Schlumberger soundings in southern Africa

During 1967 the National Physical Research Laboratory (N.P.R.L.) of the C.S.I.R., South Africa embarked on a programme of ultra deep Schlumberger soundings to investigate the electrical conductivity structure of the crust and uppermost mantle in southern Africa (Van Zijl, 1969; Van Zijl et al., 1970; Van Zijl and Joubert, 1975). The positions of the eight soundings carried out since the start of the programme are indicated in Fig. 1.2. Table 1.1 gives the tectonic province on which the centre of each of the soundings was situated, the maximum current electrode spacing and the transverse resistance of the resistive part of the crust. In these soundings telephone lines and power lines were used as current emission lines.

The programme proved to be very successful in establishing a resistivity profile for the major structural units in the country. Table 1.1 shows that the transverse resistance of the resistant part of the crust in the Kaapvaal and Rhodesian cratons is from a half to two-thirds that in the Namaqualand-Natal Belt. This is most probably due to a more complex metamorphic history in the latter region (Van Zijl et al., 1970). It

Table 1.1

Tectonic provinces on which centres of Schlumberger soundings were situated, maximum current electrode spacing and transverse resistance of second unit

Sounding No. (Fig. 1.2)	Tectonic Province	Maximum current electrode spacing (km)	Transverse Resistance of second unit, T_2 (ohm.m^2)
1	Namaqualand-Natal Belt	270	11×10^8
2	Namaqualand-Natal Belt	330	$.8 \times 10^8$
3	Namaqualand-Natal Belt	130	not determined
4	Kaapvaal craton	600	5×10^8
5	Damara Eugeosyncline	300	1×10^8
6	Rhodesian craton	450	5.6×10^8
7	Kaapvaal craton	450	5.6×10^8
8	Moçambique Belt	1200	not determined yet

also shows that the transverse resistance of the resistant unit in the Damara eugeosyncline is in turn about five times less than that of the cratons. Figure 1.3 depicts three of the latest sounding curves on the cratons and the Namaqualand-Natal Belt together with the best fitting models. The conductor-resistor-conductor structure for the stable continental crust is very clear. The models show that the crust has a maximum resistivity not exceeding 10^5 ohm.m at a depth of less than 10 km. Below this highly resistive layer the resistivity then decreases progressively to reach a value of 700-1300 ohm.m at a depth of 16-20 km, after which the resistivity does not decrease appreciably until a depth of at least 200 km is reached. No obvious change in resistivity thus exists at depths comparable to the Mohorovičić discontinuity which is at a depth of 35 to 37 km in the Kaapvaal shield (Green and Bloch, 1969).

Despite the good results obtained, the deep Schlumberger sounding technique has the big disadvantage that the availability of long emission lines dictates the study area. The investigator thus has very little control over the siting of a sounding with respect to the geological province, and can only make studies where the necessary long lines can be obtained.

Figure 1.3 Experimental Schlumberger sounding data (discrete symbols) and curves for best fitting models for soundings on the Namaqualand-Natal Belt (curve 1), Rhodesian craton (curve 2) and Kaapvaal craton (curve 3) are shown in the upper diagram. These soundings correspond respectively to soundings numbered 2, 6 and 7 in Table 1.1. The lower figure depicts the best fitting resistivity models for the three cases. The thin weathered surface layer is omitted.

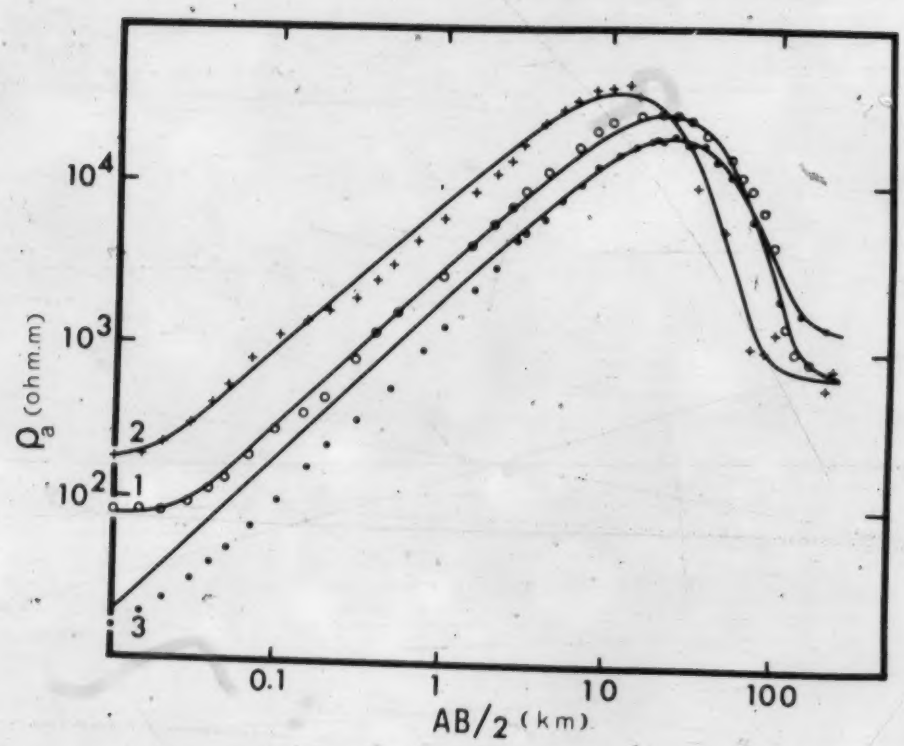
10^4
10^3
10^2
ρ_a (ohm.m)
2
1
3
0.1
1
10
100
AB/2 (km)

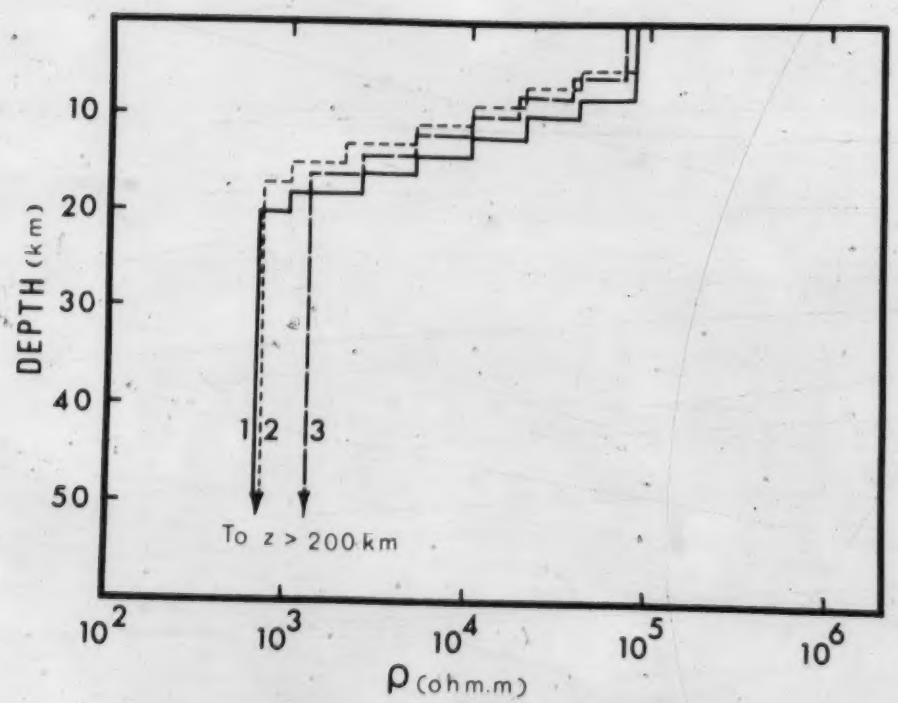
10
20
30
40
50
DEPTH (km)
1
2
3
To z > 200 km
10^2
10^3
10^4
10^5
10^6
ρ (ohm.m)

In order to expand the information obtained by the Schlumberger soundings the N.P.R.L. thus introduced a programme of magnetometer array studies to investigate lateral changes in conductivity in the crust and upper mantle in southern Africa. The analysis of the magnetometer array data and the interpretation of the results obtained form the basis of this thesis.

CHAPTER II

DATA ANALYSIS AND INTERPRETATION TECHNIQUES

2.1 The data

The analysis of magnetometer array data has been described in great detail by Anderson (1970) and Camfield (1973) and has been discussed by Gough (1973b).

The Gough-Reitzel magnetometers record the H (magnetic north), D (magnetic east) and Z (vertical down) components, in the period range 2 min $\leq$ T $\leq$ 1 day, on 35 mm film. These films are examined and sections of record showing clear magnetic disturbance events are chosen for analysis. In the present study the sections of 35 mm film recordings of the selected events were printed electrostatically at ten times magnification, edited and all deflections with a period of less than two minutes smoothed by hand. The smoothing was carried out to prevent aliasing during the commercial digitizing at one minute intervals from the prints. Full-scale plots of the digital values were superposed on the prints and carefully checked to ensure that the digital values were within one tracewidth from the recorded curve. Values with larger deviations were corrected and in some cases the entire record was redigitized. The digitized trace ordinates were converted to nanotesla (gammas) using the scale factors

derived from the field calibration of the magnetometers. A first order correction for a small interaction between the H and Z magnets in the magnetometer was also made at this stage (Camfield, 1973). The H and D (local magnetic) co-ordinates were also rotated to X and Y (geographic) co-ordinates.

With the data in this form stacks of magnetograms were prepared and the first qualitative interpretation of anomalous variation fields carried out. This type of interpretation will be discussed in Chapters 3 and 4 for actual array studies.

2.2 Spectral analysis and maps of Fourier spectral components

Quantitative analysis of magnetic variation data is best performed in the frequency domain, because the depth of penetration of the magnetic field over a given structure is controlled by its frequency and spatial wavenumber. In this work simple magnetic disturbance events such as geomagnetic bays are considered as complete transient events with definite onset and finish times. If that is the case Fourier transformation of the transient gives the complete and exact representation of the set of infinite waves of which the event is composed. The spectral density function at any frequency can then be considered to reveal the response of the system at that frequency. This allows examination of simultaneous frequency responses over a whole array area.

The definition of the Fourier transform used is

$$F(\omega) = \int_{-T/2}^{T/2} f(t)\, e^{-i\omega t} dt \qquad (2.1)$$

$$= \int_{-T/2}^{T/2} f(t)\, e^{-i2\pi ft}\, dt$$

with $-T/2 < t < T/2$. (See e.g. Otnes and Enochson, 1972, p.12).

In the digital case we have the data series X_j, $j=0,1,2,\ldots,2N-1$, with $t = j\Delta t$, $\omega = \frac{2\pi k}{2N\Delta t}$ and $f = \frac{k}{2N\Delta t}$. Therefore

$$F_k = \Delta t \sum_{j=0}^{2N-1} X_j\, e^{-\frac{i2\pi jk\Delta t}{2N\Delta t}} \qquad (2.2)$$

$$= \Delta t \sum_{j=0}^{2N-1} X_j \{\cos \frac{2\pi jk\Delta t}{2N\Delta t} + i \sin \frac{2\pi jk\Delta t}{2N\Delta t}\}$$

The actual Fourier analyses of the data were performed with the aid of the IBM SSP subroutine RHARM. This subroutine calculates cosine and sine coefficients A_k and B_k for an input X_j of data points as

$$X_j = \frac{1}{2}A_o + \sum_{k=1}^{N-1} \{A_k \cos \frac{\pi jk}{N} + B_k \sin \frac{\pi jk}{N} +$$

$$\frac{1}{2} A_N(-1)^j \} \qquad (2.3)$$

where $j = 0,1,\ldots,2N-1$,

$$A_k = \frac{1}{N} \sum_{j=0}^{2N-1} X_j \cos \frac{\pi jk}{N} \qquad (2.4)$$

and $$B_k = \frac{1}{N} \sum_{j=0}^{2N-1} X_j \sin \frac{\pi jk}{N}$$

(See e.g. Jenkins and Watts, 1968, p. 19).

If the real part of F_k in eq. 2.2 is denoted as F_k^r it is clear that

$$F_k^r = \frac{A_k \cdot 2N\Delta t}{2} = \frac{A_k T}{2} \qquad (2.5)$$

and similarly for the imaginary part

$$F_k^i = \frac{B_k T}{2} \qquad (2.6)$$

To relate the coefficients of RHARM to the Fourier transform as defined by eqs 2.1 and 2.2 the A_k and B_k of eqs 2.4 are thus multiplied by T/2 (Bennett, 1972).

The Cooley-Tukey (1965) fast Fourier transform algorithm on which the RHARM subroutine is based requires a work vector of 2^M points (M integer) for maximum computing efficiency (Gentleman and Sande, 1966) and for this study 2^M was taken as 2048. The data lengths analysed were much shorter than this, but the remaining points of the work vector were filled with zeros. Oldenburg (1969) showed

that the addition of zeros in the work vector has no effect on the frequency spectra. A base line and a linear trend were removed from every event analysed and a $\sin^2$ taper varying from zero to one was applied to the first and last ten minutes of data to remove fictitious high frequency components due to abrupt truncations at the beginning and end of the event. In the cases where the entire event was Fourier analysed, this taper was probably an unnecessary precaution, because every event was selected so as to include a smooth interval before and after it.

The Fourier amplitudes as used for contouring are calculated as the square root of the sum of the real (cosine) term squared and imaginary (sine) term squared. These amplitudes are quoted in nT/c/ min since the digitizing interval Δt was in all cases one minute. The phase is the arctangent of the sine term divided by the cosine term. As pointed out by Bennett and Lilley (1972) this gives phase lag since if the input is a frequency component $\cos(\omega t-\phi)$ then

$$\cos(\omega t-\phi) = \cos \omega t \cos \phi + \sin \omega t \sin \phi$$

giving $\arctan\left(\frac{\text{Fourier sine term}}{\text{Fourier cosine term}}\right) = \arctan\left(\frac{\sin \phi}{\cos \phi}\right) = \phi$ (2.7)

The phases are given in minutes.

A representation of a variation event at a selected period requires six maps, which may show amplitude and phase for the three orthogonal components X, Y, Z or cosine and sine coefficients for the three components. These maps of Fourier transform amplitudes and phases were introduced in the first array study by the Alberta and Dallas groups (Reitzel et al., 1970; Gough, 1973b) and serve two main purposes. Firstly they give a great deal of qualitative and some first order quantitative information and secondly form the basis of any further quantitative interpretation.

A very important point is that contour maps of Fourier spectral components show both source and response functions and in this way differ drastically from more familiar maps such as gravity anomaly maps. If local anomalies appear consistently with approximately unchanged positions for different variation events, one can with some confidence assign them to internal conductive structure, unless the array is under either the equatorial or auroral electrojet.

The use and value of these contour maps will be demonstrated in Chapters 3 and 4.

2.3 Errors in Fourier spectral components

The sources of error in the spectral components which are used in constructing the contour maps and which

also form the input to all other interpretation in the frequency domain are the following.

2.3.1 Calibration errors

At least two and sometimes three estimates of the calibration factors were obtained for each magnetic component from the calibration marks at the start of every film. Two estimates were used in the cases where the first two factors obtained differed by less than 1%. For the first array 43% and for the second 76% of the calibrations fell into this group. If the first two differed by more than 1% a third estimate was obtained. The differences were, however, always less than 3% which can be taken as a 95% confidence limit or two standard deviations. An estimate of the standard deviation of the calibration factors is thus 1.5% with corresponding errors in the amplitudes of spectral values.

2.3.2 Timing errors

With the aid of the time calibration marks at the beginning and end of every film the drift rates of the Accutron timers were determined. This gave relative times between instruments to within a minute. An additional check on the timing and linearity of the drift rate was made within every selected event by examining Pi2 micropulsations which should occur simultaneously (within a

minute) over the whole array (Rostoker, 1972). The relative starting times of the magnetic disturbance events are thus known to within a minute and in most cases within 30 seconds.

The errors in spectral phases due to timing are given by

$$\Delta\phi = f\Delta t \cdot 360 \text{ degrees} \qquad (2.8)$$

where Δt is timing error (taken as timing interval, one minute) and f = frequency (cycles/min). With the timing error one minute the corresponding phase errors are thus 18° for a period of 20 min; 6° for a period of one hour and 2° for a period of three hours.

2.3.3 Digitizing errors

By far the most important contribution to the errors in the Fourier sine and cosine coefficients is the part due to digitizing errors.

With d_j, $j=0,1,\ldots,2N-1$, the differences between the true values and the digital values and under the assumption that $\{d_j\}$ is Gaussian with zero mean, is uncorrelated and has standard deviation σ_o, the expected value of d_k

$$E[d_k] = E\left[\sum_{j=0}^{2N-1} d_j \, e^{-\frac{i\pi jk}{N}}\right]$$

$$= \sum_{j=0}^{2N-1} E[d_j] \, e^{-\frac{i\pi jk}{N}}$$

$$= 0 \qquad (2.9)$$

and $$\text{Variance}\,[d_k] = E[d_k^* d_k]$$

$$= 2N\,\sigma_o^2 \qquad (2.10)$$

where d_k^* is the complex conjugate of d_k (Otnes and Enochson, 1972, p. 213). This will also give the digital errors in individual sine and cosine coefficients. The corresponding errors in amplitude and phase at a specific frequency can be calculated from these errors by normal propagation of errors formulae (e.g. Bevington, 1969).

An estimate for σ_o can be obtained in the following way. As discussed before, the digital values were determined to within one trace width (about 2 mm) on the xerox enlargements. This means that we know with 95% confidence that $|d_j| < 2$ mm or more specifically that σ_o corresponds to 1 mm on the xerox prints. This implies for average sensitivities of 1.001 nT/mm for X, 1.091 nT/mm for Y and .719 nT/mm for Z as used in the

present array studies, that the standard deviation σ_o is 1.001 nT for X, 1.091 nT for Y and .719 nT for Z. From eq. 2.10 it follows that for a four hour long event the standard deviations of the cosine and sine coefficients are 15.5 nT/c/min for X, 16.9 nT/c/min for Y and 11.2 nT/c/min for Z.

Since the longer periods usually contain more power, this constant standard deviation for all periods will have a larger effect on the accuracy of the short-period Fourier spectral values. It is informative to consider examples from the next chapter. Figure 3.8 shows Fourier transform amplitudes and phases at period 24 minutes for a substorm that occurred 18.30 - 22.30 G.M.T. on August 31, 1971. The amplitudes are given in nT/c/min $\times$ 10 and the phases in minutes. The average standard deviations as percentage of the X, Y, and Z amplitudes are respectively 12%, 24% and 25% and 3%, 4% and 16% for the phases. Figure 3.10 shows Fourier transform amplitudes (in nT/c/min $\times 10^2$) and phases (in minutes) at a period of 12 min, again for the event of August 31. In this case the average standard deviations in X, Y and Z amplitudes due to digitizing errors are respectively 1%, 2% and 2% and 1%, 1% and 2% for X, Y, Z phases.

It is clear that at short periods the digitizing error contributes most to the total errors in amplitude

and phase, while at longer periods the magnitude of the digitizing errors is comparable to that of the errors in calibration and timing.

2.4 Polarization of the horizontal field

The polarization of the horizontal field is important in geomagnetic studies, especially when induction in three-dimensional bodies is involved. With the aid of monochromatic wave theory the polarization of the horizontal field can be determined for any frequency component from the frequency spectrum of a transient. The horizontal field polarization is highly relevant to the interpretation of Fourier component contour maps for regions of complicated conductive structure (Gough et al., 1974).

The polarization parameters for the horizontal variation fields were calculated following the monochromatic wave theory discussed by Born and Wolf (1959, p. 34). The adaptation of the formulae for the geomagnetic case (the X-Y axes of geomagnetism are reversed from the conventional 2-D x-y axes) is described by Lilley and Bennett (1972).

If a disturbance has horizontal components

$$X = a_2 \cos(\omega t + \delta)$$
$$Y = a_1 \cos \omega t \qquad (2.11)$$

then the point (X,Y) traces out an ellipse with the passage of time.

The angle α, $(0 \leq \alpha \leq \frac{\pi}{2})$ is defined such that

$$\tan \alpha = \frac{a_2}{a_1} \tag{2.12}$$

The principal semi-axes a and b of the ellipse and the angle ψ $(0 \leq \psi \leq \pi)$, the angle measured clockwise between the major axis of the ellipse and the geographic east are specified by the formulae

$$a^2 + b^2 = a_1^2 + a_2^2$$

$$\tan 2\psi = (\tan 2\alpha) \cos \delta \tag{2.13}$$

$$\sin 2\chi = (\sin 2\alpha) \sin \delta$$

where $0 < \psi < \pi/2$ if $\cos \delta > 0$,

$\pi/2 < \psi < \pi$ if $\cos \delta < 0$,

$\psi = 0$ if $\cos \delta = 0$ and $a_1 > a_2$,

$\psi = \pi/2$ if $\cos \delta = 0$ and $a_1 < a_2$,

and χ, $(-\pi/4 < \chi \leq \pi/4)$ is an auxiliary angle which determines the shape and orientation of the ellipse,

$$\tan \chi = \pm \frac{b}{a} \tag{2.14}$$

If $\sin \delta < 0$, the ellipse is described in a clockwise sense and if $\sin \delta > 0$, the ellipse is described anticlockwise. With $\sin \delta = 0$, or if either a_1 or a_2 is zero, the ellipse degenerates to a straight line. The values a_1, a_2 and δ as functions of the angular frequency ω come from the Fourier transforms of the selected events.

In this study it was found that the horizontal field polarization varied somewhat across an array area, more at the shorter periods than at the longer periods. This is most probably caused by changes in the amplitudes and phases of the horizontal fields due to different induction effects across the array. Another contributing factor may be the errors in the Fourier spectral components. The horizontal polarization ellipses shown on the contour diagrams in Chapters 3 and 4 are ellipses from stations removed from the main anomalous structures. These ellipses will thus show the polarization in the more "normal" regions of the array.

2.5 Transfer functions and induction vectors

Transfer functions between observed components of variation fields preserve amplitude, phase and polarization information and have proved invaluable in the interpretation of linear magnetometer arrays where data from different arrays often have to be combined to define a geomagnetic induction anomaly (Schmucker, 1964 and 1970a; Everett and Hyndman, 1967).

Following Schmucker (1970a), suppose the function $Z(t)$ is linearly related to $X(t)$, both normalized to zero mean value in the interval $-T/2 \leq t \leq T/2$. Their relation shall be independent of time in this interval and thus expressible by a linear transfer function z_X in the frequency domain, assuming $T \to \infty$. If we denote the Fourier transforms of $X(t)$ and $Z(t)$ in eq. 2.1 by $C(X)$ and $C(Z)$ respectively

$$C(Z) = z_X \, C(X) \tag{2.15}$$

Furthermore

$$S(X) = \frac{C(X) \cdot C^*(X)}{T} \tag{2.16}$$

$$S(ZX) = S^*(XZ) = \frac{C(Z) \cdot C^*(X)}{T} \tag{2.17}$$

$$z_X = \frac{S(ZX)}{S(X)} \tag{2.18}$$

Here $C^*(X)$ and $S^*(XZ)$ denote the complex conjugates of $C(X)$ and $S(ZX)$, $S(X)$ is the auto-power of $X(t)$ and $S(ZX)$ the cross-power between $Z(t)$ and $X(t)$. If $Z(t)$ contains some uncorrelated part $\delta Z(t)$, its power is given by

$$S(\delta Z) = \frac{C(\delta Z) \cdot C^*(\delta Z)}{T} \tag{2.19}$$

or

$$S(\delta Z) = S(Z) - \frac{|S(ZX)|^2}{S_X} \tag{2.20}$$

since $|z_X\ C(X)|^2$ is the power of the related part of $Z(t)$.

The anomalous components of the total geomagnetic variation field are related to the normal components of the field and since Maxwell's equations are linear in the field variables, the anomalous parts are expressible as linear functions of the normal parts. These relations can be expressed in matrix form as

$$\begin{bmatrix} C(X_a) \\ C(Y_a) \\ C(Z_a) \end{bmatrix} = \begin{bmatrix} x_X & x_Y & x_Z \\ y_X & y_Y & y_Z \\ z_X & z_Y & z_Z \end{bmatrix} \cdot \begin{bmatrix} C(X_n) \\ C(Y_n) \\ C(Z_n) \end{bmatrix} + \begin{bmatrix} C(\delta X) \\ C(\delta Y) \\ C(\delta Z) \end{bmatrix} \quad (2.21)$$

with X_a and X_n and the like representing the anomalous and normal parts of the fields respectively. The 3×3 matrix is the complex transfer function matrix such that

$$z_X = z_X(u) + i z_X(v) \quad (2.22)$$

for example, with $z_X(u)$ the real part and $z_X(v)$ the imaginary part of z_X. The last vector in eq. 2.21 contains the residuals (uncorrelated parts) of the field components. The matrix of transfer functions must be determined such that the powers of the residuals $S(\delta X)$, $S(\delta Y)$ and $S(\delta Z)$ are minimal.

The third scalar equation in the matrix equation 2.21 can be written as

$$C(\delta Z) = C(Z_a) - z_X C(X_n) - z_Y C(Y_n) - z_Z C(Z_n) \tag{2.23}$$

With the aid of this equation and eq. 2.19 the power spectrum of $C(\delta Z)$ is obtained. On differentiation this yields

$$\frac{\partial S(\delta Z)}{\partial z_X(u)} = - \{C(\delta Z)\cdot C^*(X_n) + C^*(\delta Z)\cdot C(X_n)\} \tag{2.24}$$

$$\frac{\partial S(\delta Z)}{\partial z_X(v)} = i \{C(\delta Z)\ C^* X_n) - C^*(\delta Z)\cdot C(X_n)\}$$

The condition of minimum power in the residuals implies that both derivatives in eq. 2.24 go to zero. This is achieved when the cross spectra between $\delta Z(t)$ and the normal parts X_n, Y_n and Z_n vanish, thus when

$$S(\delta Z X_n) = S(\delta Z Y_n) = S(\delta Z Z_n) = 0 \tag{2.25}$$

If the cross spectra of $C(\delta Z)$ with $C(X_n)$, $C(Y_n)$ and $C(Z_n)$ are formed using this condition and eq. 2.23 we obtain the matrix equation

$$\begin{bmatrix} S(X_n) & S(Y_nX_n) & S(Z_nX_n) \\ S(X_nY_n) & S(Y_n) & S(Z_nY_n) \\ S(X_nZ_n) & S(Y_nZ_n) & S(Z_n) \end{bmatrix} \begin{bmatrix} z_X \\ z_Y \\ z_Z \end{bmatrix} = \begin{bmatrix} S(Z_aX_n) \\ S(Z_aY_n) \\ S(Z_aZ_n) \end{bmatrix} \quad (2.26)$$

and the vertical transfer functions z_X, z_Y, z_Z at a particular frequency can be obtained by matrix inversion. Similarly the horizontal transfer functions x_X, x_Y, x_Z and y_X, y_Y, y_Z can be obtained. Because of the practical problems involved in separating the normal and anomalous fields, a topic discussed in Section 1.2.4, this general form of transfer functions (eq. 2.26) has hardly been used in geomagnetic depth sounding.

Reliable estimates of transfer functions require the use of a number of events of various polarization and if possible due to various current sources, which are combined to obtain average power and cross-power spectra. Schmucker (1970a) showed that when M events are used the residuals should not exceed $\{(M-5)/(M-3)\}^{\frac{1}{2}}$ as upper permissible limit in order to have meaningful conerences. This means power and cross spectra should be obtained from more than five events.

In practice the major problem in computing transfer functions is to obtain fair estimates of the normal and anomalous fields. The 1971 array study in South Africa

discussed in the next chapter was the first large two-dimensional array for which transfer functions were calculated. For that study and also for the subsequent study in 1972 the following approximations were made. Firstly, for each spectral term of each event an estimate of the normal field in X and Y was made by taking mean cosine and sine Fourier coefficients over all stations.

Furthermore, at the magnetic latitude of southern Africa the normal Z component in substorm fields is small. The magnetograms in Chapters 3 and 4 support the view that the Z variations are mainly anomalous. It is thus explicitly assumed that $Z_n = 0$ and $Z_a = Z$ so that the terms in eq. 2.26 that involve Z_n vanish. Consequently we can solve eq. 2.26 explicitly for z_X and z_Y to yield

$$z_X = \frac{S(ZX_n)\,S(Y_n) - S(ZY_n)\,S(Y_nX_n)}{S(X_n)\,S(Y_n) - |S(Y_nX_n)|^2}$$

$$z_Y = \frac{S(ZY_n)\,S(X_n) - S(ZX_n)\,S(X_nY_n)}{S(X_n)\,S(Y_n) - |S(Y_nX_n)|^2} \qquad (2.27)$$

Parkinson (1959, 1962) and Wiese (1962) introduced the use of arrow representations to display the anomalous behaviour of the vertical magnetic field with position. Transfer functions can be used to form similar convenient induction vectors. With $\vec{i}$ and $\vec{j}$ unit vectors in the geographic north and east directions at a particular station,

the induction vectors at any particular frequency are given as

$$\vec{W}_u = z_X(u)\vec{i} + z_Y(u)\vec{j}$$
$$\vec{W}_v = z_X(v)\vec{i} + z_Y(v)\vec{j} \qquad (2.28)$$

The real parts of z_X and z_Y give the in-phase responses of Z to X_n and Y_n and their imaginary parts the quadrature-phase responses. When plotted the in-phase vector points away from a conductor in which the current flows in phase with the normal field. This vector is usually reversed to be in the same sense as a Parkinson arrow so that it points toward a conductor in which the current flows in phase with the normal field. The quadrature-phase vector points away from a conductor in which the induced current leads the normal field in phase. The direction of this vector is also sometimes reversed.

In the Earth induced currents flow at a phase angle between 0 and $\pi/2$ with the normal field and a given conductor will contribute to both induction vectors. As pointed out by Gough et al. (1974), in the extreme case of very high reactance, arising typically when the normal field does not penetrate through the conductor, the in-phase vector will dominate. At the other extreme, when the normal field penetrates easily, as through a thin surface conductive

layer, the inductive reactance will be low compared to the resistance and the quadrature-phase vector will dominate.

2.6 Numerical modelling

One-dimensional modelling of layered structures is discussed in some detail in Chapter 5 and will thus not be dealt with in this section.

It is often possible to consider observed magnetic variation anomalies as approximately two-dimensional on a local scale and also to consider the inducing field to be nearly uniform over the region of anomalous induction, especially in geomagnetic mid latitudes. Under such conditions the modelling of the observed variations by induction in two-dimensional conductivity structures is in most cases adequate. The most prominent exception is when the anomaly is of the current concentration type. However, when no complicating circumstances exist, the general interpretation of induction in the earth is then that of considering the local perturbations (in two dimensions) by local lateral conductivity structure of the pattern of induced currents flowing in the large scale stratified (one dimensional) structures remote from the anomalous region.

For this situation let the Cartesian co-ordinate system (x,y,z) be aligned such that the x-axis is parallel to the strike of the anomaly and $z > 0$ as usual is

directed downwards. Maxwell's equations (eqs 1.1-1.7) can now be rewritten for the two dimensional case where all quantities are independent of x and (X,Y,Z) are the cartesian components of $\vec{B}$. By combining eqs 1.2 and 1.5 and assuming as usual that displacement currents can be neglected one obtains

$$\frac{\partial Z}{\partial y} - \frac{\partial Y}{\partial z} = \mu\sigma E_x \tag{2.29}$$

$$\frac{\partial X}{\partial z} = \mu\sigma E_y \tag{2.30}$$

$$\frac{\partial X}{\partial y} = -\mu\sigma E_z \tag{2.31}$$

By combining eqs 1.1 and 1.6 one obtains

$$\frac{\partial E_z}{\partial y} - \frac{\partial E_y}{\partial z} = -i\omega X \tag{2.32}$$

$$\frac{\partial E_x}{\partial z} = -i\omega Y \tag{2.33}$$

$$\frac{\partial E_x}{\partial y} = i\omega Z \tag{2.34}$$

where all variables have a time dependence of $\exp(i\omega t)$.

The requirement that $\frac{\partial}{\partial x} = 0$ has decoupled the x components of $\vec{E}$ and $\vec{B}$ from the other components of each vector, so that eqs 2.29 to 2.34 separate into two

independent sets of equations. Equations 2.29, 2.33 and 2.34 involve only E_x, Y, Z while eqs 2.30, 2.31 and 2.32 involve only X, E_y and E_z. By combining the first set and eliminating Y and Z one obtains

$$\frac{\partial^2 E_x}{\partial y^2} + \frac{\partial^2 E_x}{\partial z^2} = i\sigma\omega\mu E_x \qquad (2.35)$$

where $\vec{E}$ is parallel to the strike and is termed the E-POLARIZATION case.

Elimination of E_y and E_z from the second set yields

$$\frac{\partial^2 X}{\partial y^2} + \frac{\partial^2 X}{\partial z^2} = i\sigma\omega\mu X \qquad (2.36)$$

which is termed the H-POLARIZATION case.

The problem of adapting these diffusion equations to a numerical solution of observed anomalies has been extensively studied in recent years (e.g. Weaver, 1963; Wright, 1969; Madden and Swift, 1969; Jones and Price, 1970, 1971; Swift, 1971; Jones and Pascoe, 1971; Coggon, 1971; Pascoe and Jones, 1972; Reddy and Rankin, 1973).

Equations 2.35 and 2.36 can be written as

$$\Delta^2 F_m = i\,\eta_m^2 F_m \qquad (2.37)$$

where F_m is either E_x or X, $\eta_m^2 = \sigma_m\omega\mu$ and the subscript m identifies the different units within the model. In

geomagnetic depth sounding only the E-polarization case is of relevance because the H-polarization case does not produce anomalies at the Earth's surface. The relevant boundary conditions have been the subject of some discussion (cf. Weaver, 1963 v. Jones and Price, 1970; Hermance, 1972 v. Price and Jones, 1972). The computer formulation used in this thesis is based on the algorithm of Jones and Price (1970) as programmed by Jones and Pascoe (1971) and Pascoe and Jones (1972). The boundary conditions as given by Pascoe and Jones are used in the computer program.

The Jones and Price (1970) method is a finite difference method and with $F_m = f_m + ig_m$, eq. 2.37 separates into

$$\nabla^2 f_m = - \eta_m^2 g_m$$
$$\nabla^2 g_m = \eta_m^2 f_m \qquad (2.38)$$

These two equations are replaced by their finite difference equivalents which are then solved at a rectangular mesh of grid points under the condition that at the boundaries between meshes, the tangential magnetic and electric field components are continuous. By the use of the Gauss-Seidel iterative method, the solutions at the mesh points are iterated until stable convergence is obtained.

A linearly polarized external field with uniform horizontal component at a large distance from the main conductor is applied to the system as a source field, and the total field is set to zero at the greatest distance into the main conductor reached by the grid.

CHAPTER III

THE 1971 ARRAY STUDY IN SOUTH AFRICA

3.1 Introduction

A triangular array of magnetometers was operated in central South Africa from August 31 to October 27, 1971 by the Geophysics Division of the National Physical Research Laboratory of the C.S.I.R., Pretoria, South Africa. The 24 three-component magnetometers were of the type described by Gough and Reitzel (1967) and were on loan from the University of Alberta, Edmonton, Canada.

The location of the array is shown in Fig. 3.1 in relation to the tectonic provinces and to the continental edge. The study was designed largely to look for a possible contrast in electrical conductivity of the crust and upper mantle between the Kaapvaal craton with a typical basement age of 2600 Myr and the 1000 Myr old Namaqualand-Natal mobile belt (Nicolaysen and Burger, 1965). The distribution and main features of these tectonic provinces were discussed in Section 1.3. In Section 1.4 it was pointed out that the resistive portion of the crust in the Kaapvaal craton as determined by ultra-deep Schlumberger soundings seems to be in general more conductive than the same unit in the Namaqualand-Natal mobile belt. It was realized that the crustal conductivity con-

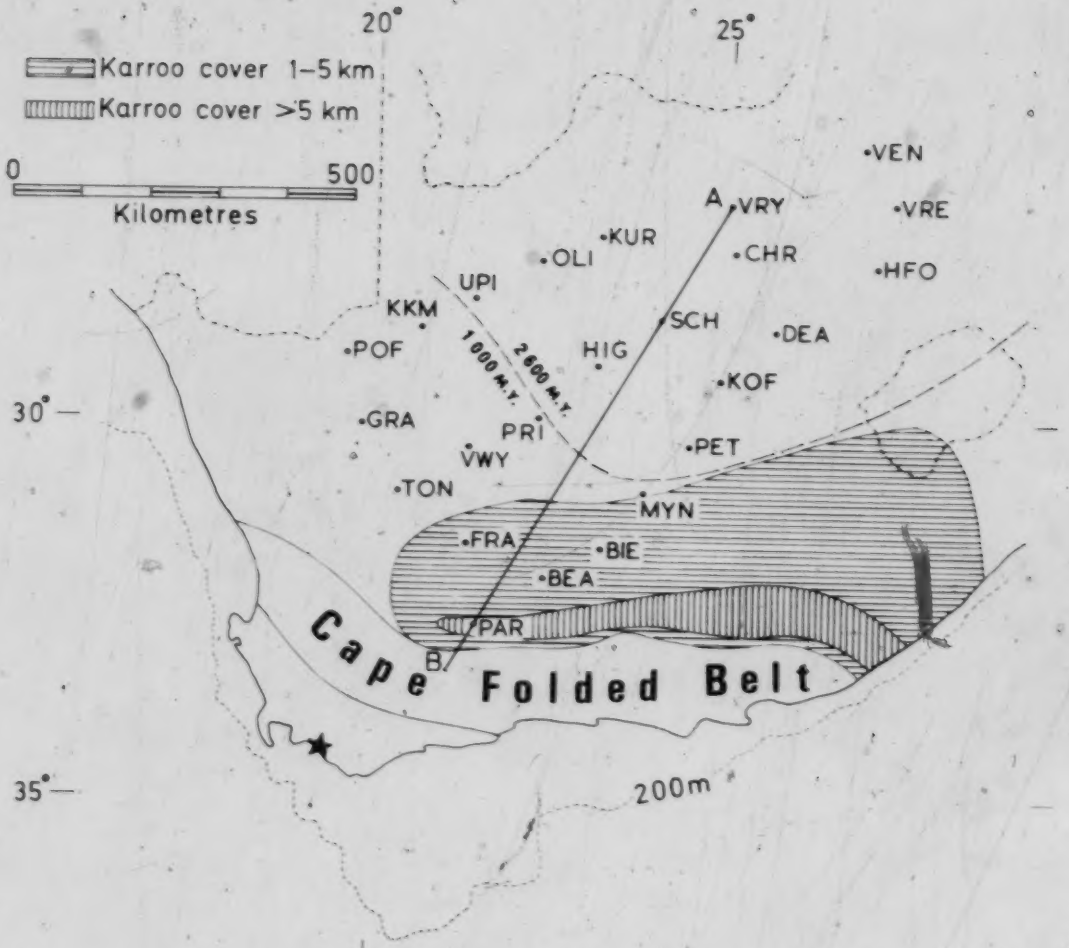

Figure 3.1 The location of the stations in the 1971 array study in relation to tectonic provinces and continental edge of southern Africa. The star indicates the Hermanus Magnetic Observatory of the C.S.I.R.

trast between the two regions, which differ by a factor of about 1.5, was not enough to cause a detectable induction anomaly, but at that stage we had no knowledge about possible conductivity differences in the upper mantle. The boundary between the Kaapvaal craton and the Namaqualand-Natal belt is indicated in Fig. 3.1 and the array straddled it.

The field procedure similar to that described excellently by Camfield (1973) will not be repeated here. The instruments were serviced at about 21 day intervals.

Station code names are given in Fig. 3.1 and the geographic co-ordinates and magnetic declinations at the stations are given in Table 3.1. The work discussed in this chapter has been the subject of a paper by Gough, DeBeer and Van Zijl (1973).

3.2 Magnetograms

Three periods of geomagnetic disturbance were selected for analysis. These periods were August 31, 18.30-22.30 G.M.T., September 17, 20.00-September 18, 06.00 G.M.T. and September 26, 15.30-September 27, 03.30. The recording efficiencies for the three events were respectively 80%, 74% and 79%. The main causes of loss of record lay in poor operation of the stepping motor camera drives and in traces going off scale or becoming

Table 3.1

Coordinates and magnetic declination of stations in the 1971 array

Station Name	Code	Latitude Degrees and min South	Longitude Degrees and min East	Magnetic declination (degrees)
Prince Albert Road	PAR	32°50'	21°36'	-22.5
Fraserburg	FRA	31°40'	21°18'	-21.9
Beaufort West	BEA	32°09'	22°28'	-21.9
Biesiespoort	BIE	31°45'	23°18'	-21.7
Mynfontein	MYN	30°56'	23°57'	-21.1
Petrusburg	PET	30°19'	24°35'	-20.7
Koffiefontein	KOF	29°28'	24°57'	-20.1
Dealesville	DEA	28°45'	25°50'	-19.8
Schmidtsdrift	SCH	28°42'	24°04'	-19.7
Higg's Hope	HIG	29°19'	23°12'	-20.3
Prieska	PRI	29°57'	22°23'	-20.9
Vanwyksvlei	VWY	30°23'	21°22'	-21.0
Tontelbos	TON	30°57'	20°21'	-21.5
Granaatboskolk	GRA	30°02'	19°51'	-21.0
Pofadder	POF	29°04'	19°34'	-20.4
Kakamas	KKM	28°45'	20°39'	-19.5
Ventersdorp	VEN	26°18'	26°54'	-17.8
Christiana	CHR	27°38'	25°06'	-18.9
Vryburg	VRY	27°04'	25°00'	-18.5
Kuruman	KUR	27°34'	23°11'	-19.2
Olifantshoek	OLI	28°07'	22°22'	-19.5
Vredefort	VRE	No data were obtained from these stations due to instrument problems.		
Upington	UPI			

too faint on the film. The selected data sections were digitized and reduced for analysis as described in Section 2.1. The sets of normalized time series representing the three orthogonal components in the geographic coordinate system (X northward, Y eastward, Z downward positive) were plotted in stacks by means of a calcomp plotter. These magnetograms are illustrated in Fig. 3.2 for the substorm event of August 31, in Fig. 3.3 for the disturbance event of September 17 and 18 and in Fig. 3.4 for the event of September 26 and 27. The three 'lines' of stations run from the three stations nearest the north-east corner of the array south-westward, Line 1 being the north-west side and Line 3 the south-east side of the triangle (Fig. 3.1). In each stack of magnetograms the sequence from top to bottom runs from north-east to south-west along the line. The time marks are in Universal time (UT) and the local midnight in the centre of the array is around 2230 UT. Scale bars relate the amplitudes to gammas (1 γ = 10^{-9} tesla = 10^{-5} oersted). Note the different scales for the vertical and horizontal components.

Visual inspection of the sets of magnetograms in Figs 3.2, 3.3 and 3.4 indicates that the three events have the following common features due to local anomalous variation fields superimposed on the normal part. The

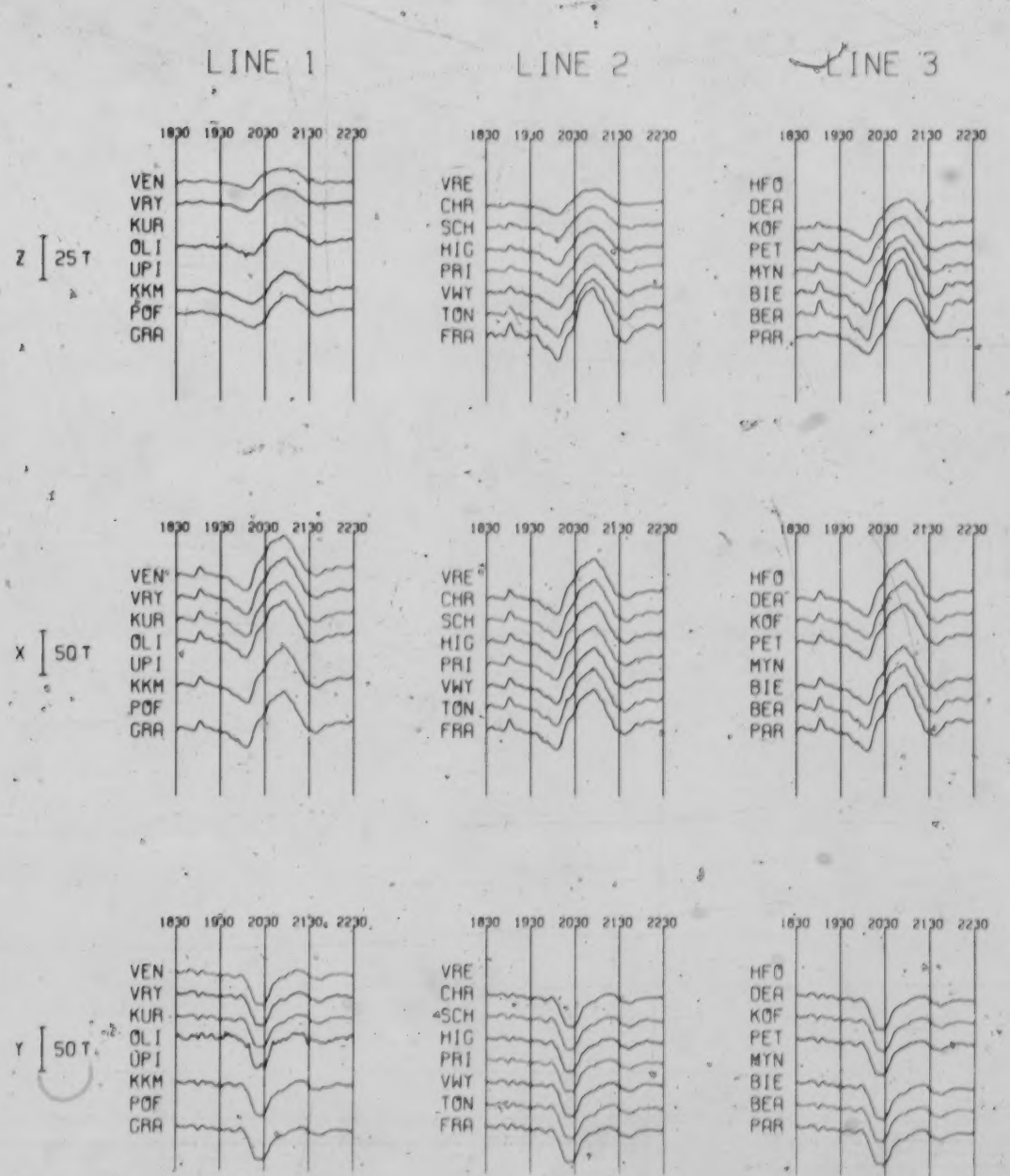

Figure 3.2 Magnetograms of a substorm 18.30-22.30 G.M.T. on August 31, 1971. In each line the stations run north-east to south-west down the stack. Components are X northward, Y eastward and Z downward. The unit is the nanotesla (gamma).

Figure 3.3 Magnetograms of a magnetic disturbance event September 17, 20.00-September 18, 06.00 G.M.T.

SEPTEMBER 17 AND 18, 1971

LINE 1

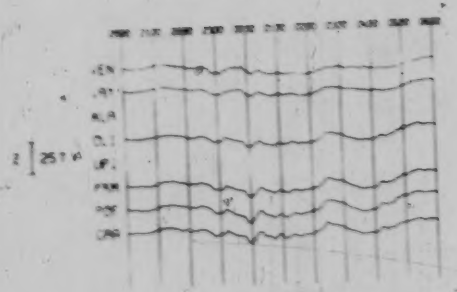

LINE 2

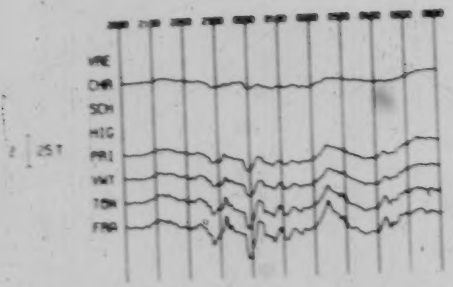

LINE 3

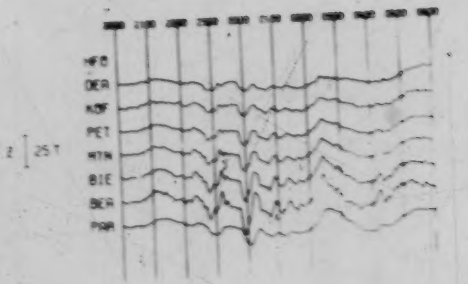

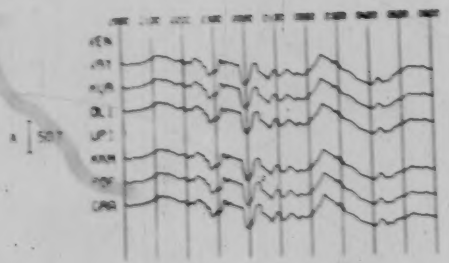

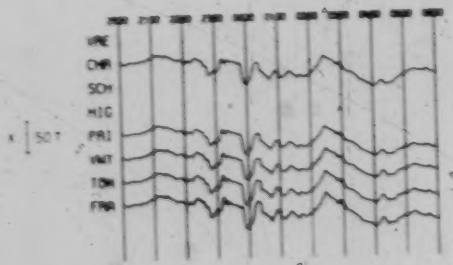

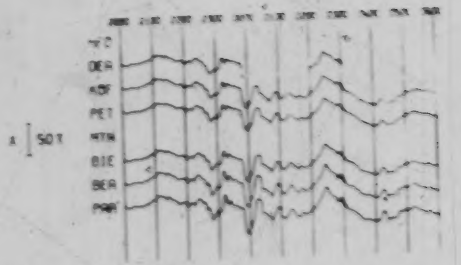

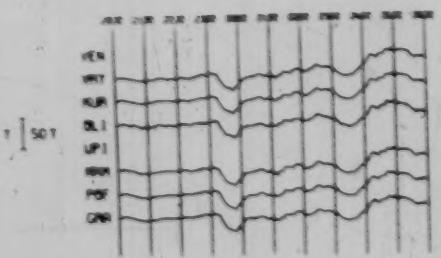

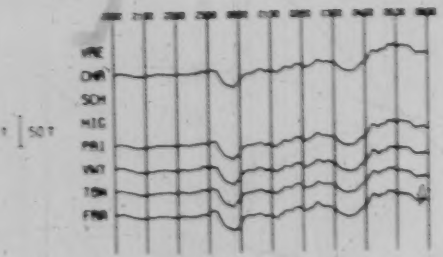

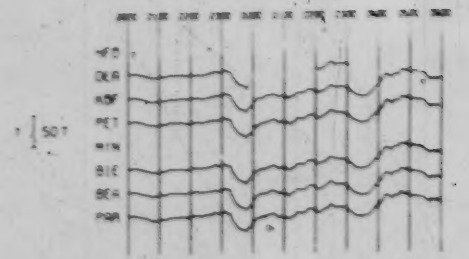

Figure 3.4a Magnetograms of a magnetic disturbance event September 26, 15.30-September 27, 03.30 G.M.T., Line 1.

SEPTEMBER 26 AND 27, 1971

LINE 1°

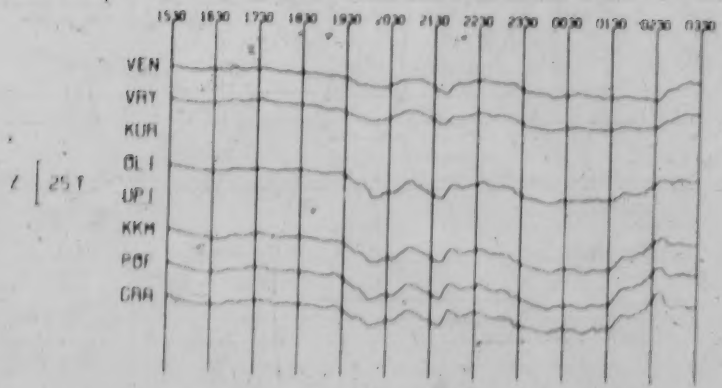

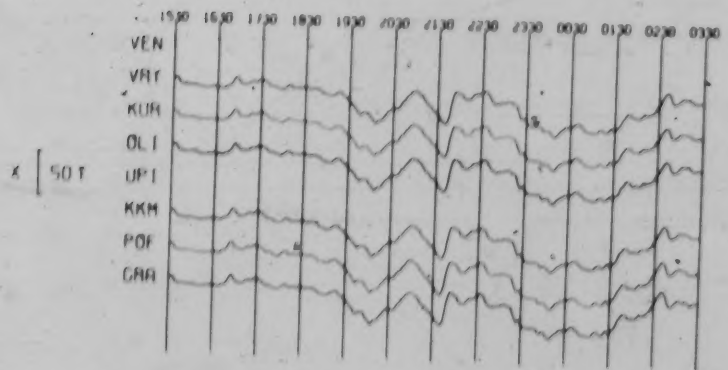

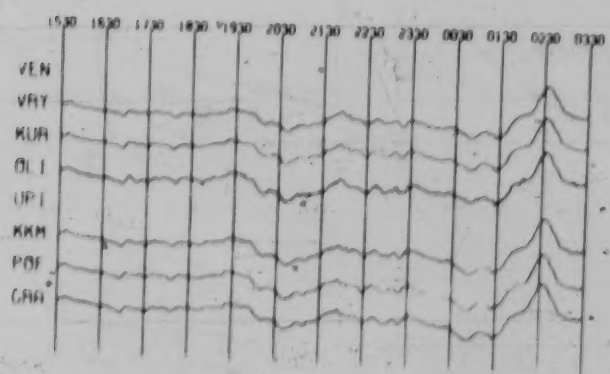

Figure 3.4b Magnetograms of a magnetic disturbance event September 26, 15.30-September 27, 03.30 G.M.T., Line 2.

SEPTEMBER 26 ANU 27, 1971

LINE 2

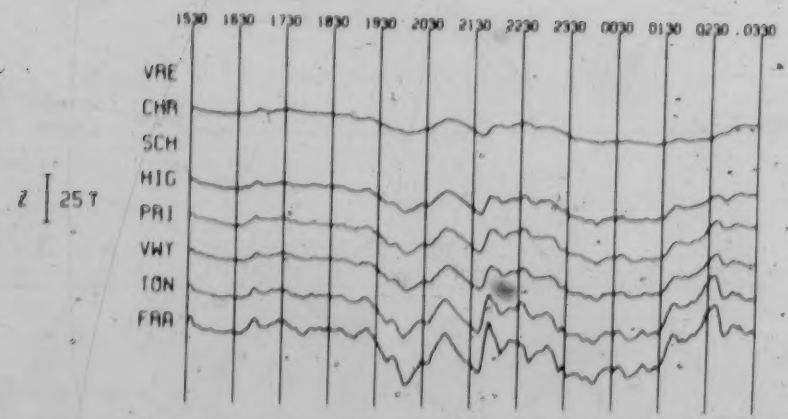

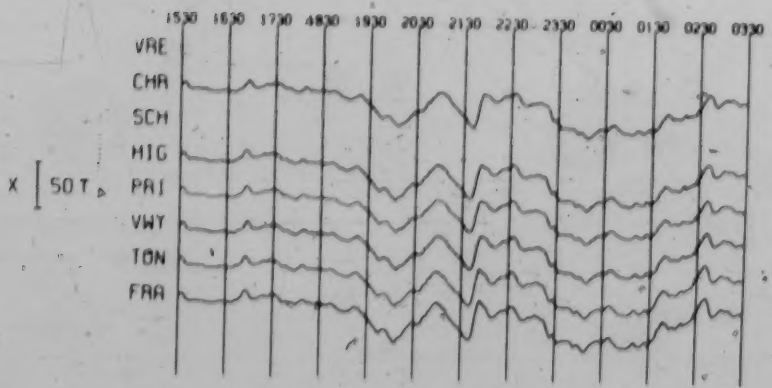

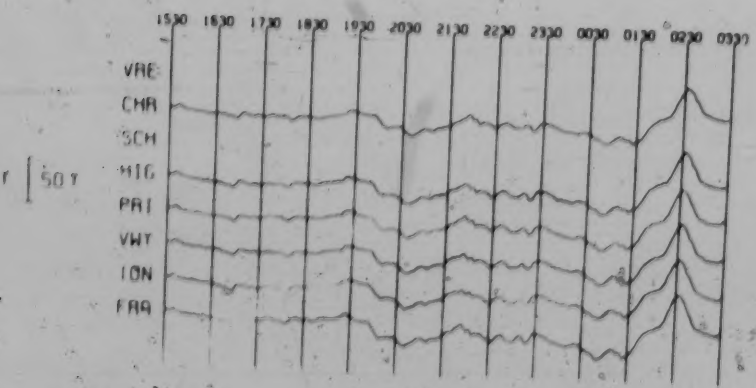

Figure 3.4c Magnetograms of a magnetic disturbance event September 26; 15.30-September 27, 03.30 G.M.T., Line 3.

SEPTEMBER 26 AND 27, 1971

LINE 3

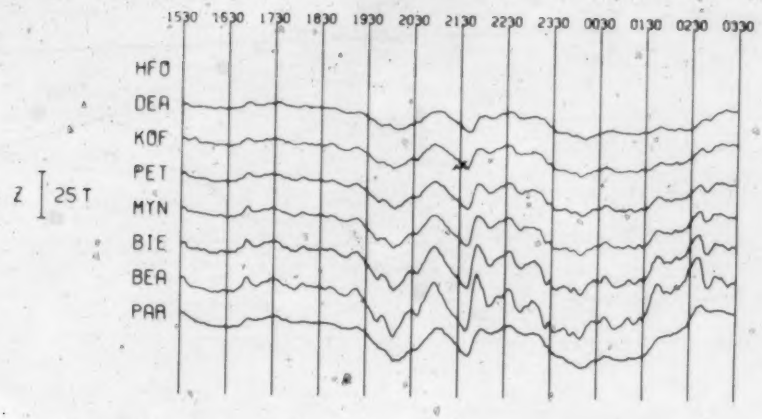

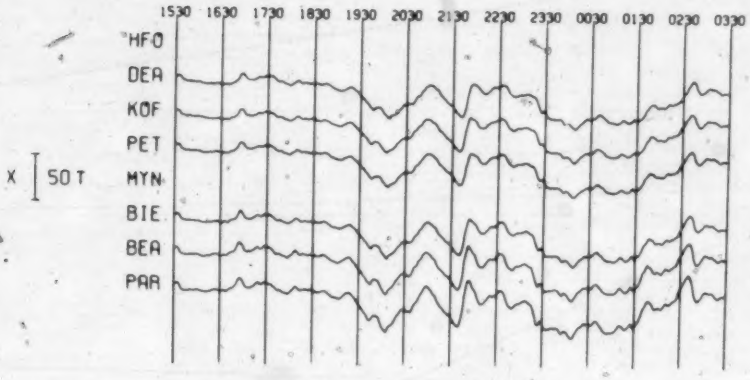

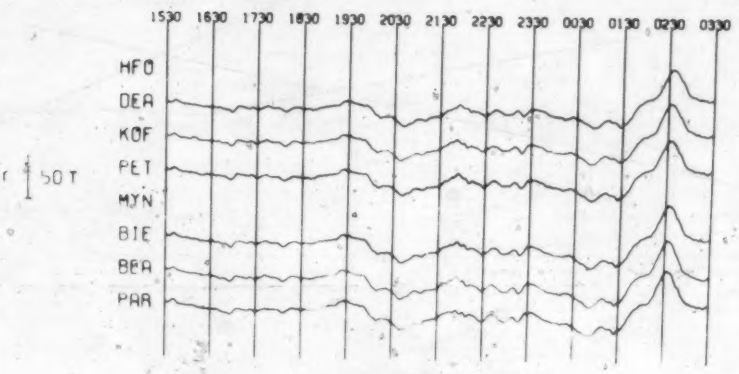

magnetograms for each component are rather constant along Line 1, except for a slight increase in the amplitude of Z to the south-west. In Line 2 there is a marked increase in Z and a smaller increase in X south-westward. Line 3 has the same trend, except that the Z component shows a large enhancement at Beaufort West (BEA) and is greatly reduced at Prince Albert Road (PAR). In Fig. 3.2 the Z traces at these two stations show this difference in a striking way for periods of about 30 minutes and 2 hours. The X component increases steadily to PAR at the south-western end of Line 3. Comparison of traces along the rows in Figs 3.2, 3.3 and 3.4 shows that Z and X increase to the south-east, and it is clear that the main effect is a southward increase of X and, except at PAR, of Z.

The waveform Z(t) bears a strong resemblance to X(t) at the more southerly stations, and still resembles X(t), passed through a high-cut filter, even at the north-east of the array. There is no resemblance of Z(t) to Y(t). The amplitude variation of Z and the resemblance of its waveform to X suggests immediately that much of the Z variation field is an anomalous field resulting from induction by X in a conductor near PAR at the south-west corner of the array. This conductor also produces a marked attenuation of high-frequency variations in Z at PAR reminiscent of the attenuation of Z west of the Northern

Rocky Mountains (Camfield et al., 1971). The attenuation suggests that PAR is above the conductor.

3.3 Maps of Fourier spectral components.

Sequences were selected for Fourier transformation from each of the three data sets described in the previous section. These data sets were August 31, 18.30-22.30 G.M.T., September 17, 22.00-September 18, 01.50 G.M.T., September 26, 18.30-22.30 G.M.T. and September 26, 15.30-September 27, 03.30 G.M.T. In each case amplitude spectra like those shown in Figs 3.5, 3.6 and 3.7 for the four-hour long sequences were plotted. The periods used in constructing the contour maps were chosen near spectral peaks for X and Z to get the optimum signal to noise ratio. Contoured maps of amplitudes and phases at the selected periods were prepared; in all ten sets each containing six maps were drawn. The techniques are described by Reitzel et al. (1970) and Camfield et al. (1971). The period range covered is 24 minutes to 293 minutes. The 12 hour long data sets for September 26-27 were transformed to provide the maps at this last period. The polarization of the horizontal field was determined using the theory described in Section 2.4. The polarization ellipses were always elongated and often nearly linear, with major axes ranging from N53°W to N28°E for the ten periods mapped.

Figure 3.5 Fourier amplitude spectra in the period range 20-240 min for 18.30-22.30 G.M.T., August 31 for the stations VEN and BEA.

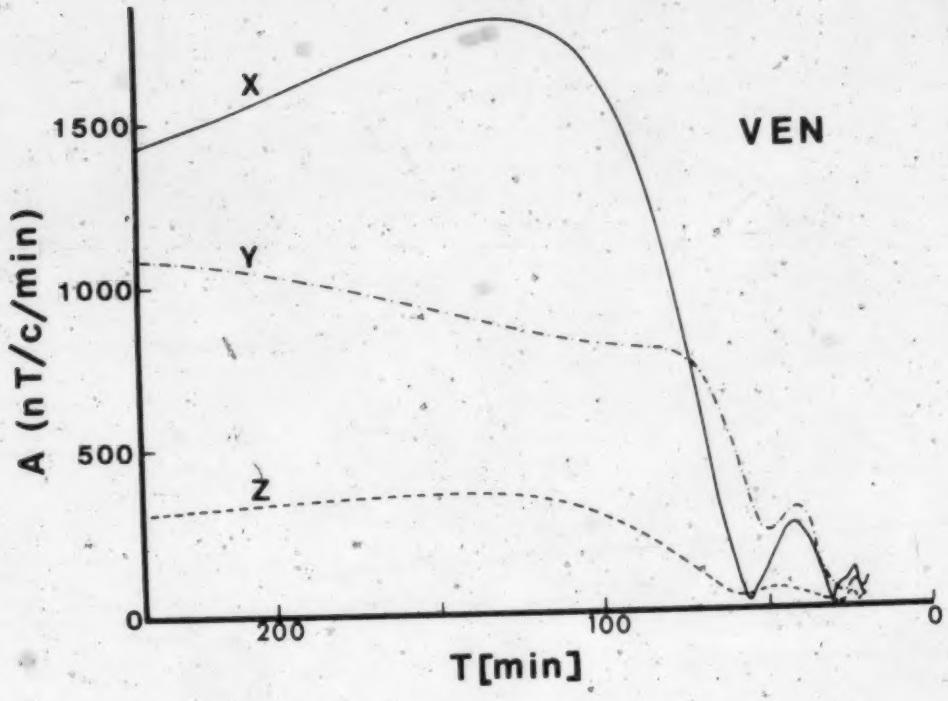
VEN
X
Y
Z
1500
1000
500
0
200
100
0
A (nT/c/min)
T[min]

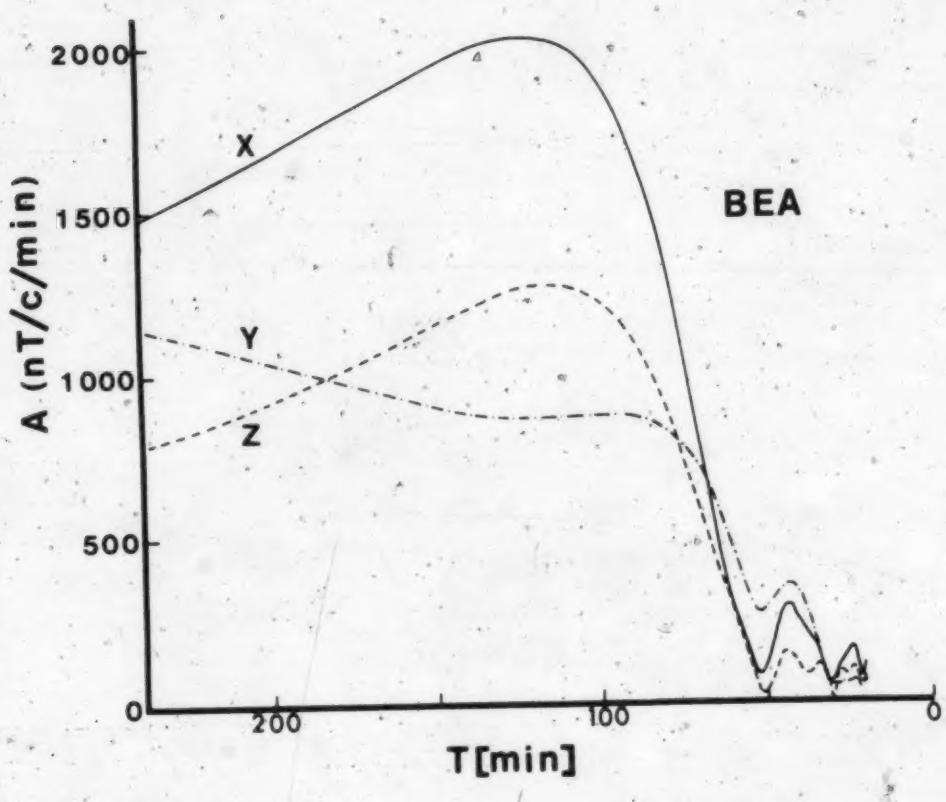
BEA
X
Y
Z
2000
1500
1000
500
0
200
100
0
A (nT/c/min)
T[min]

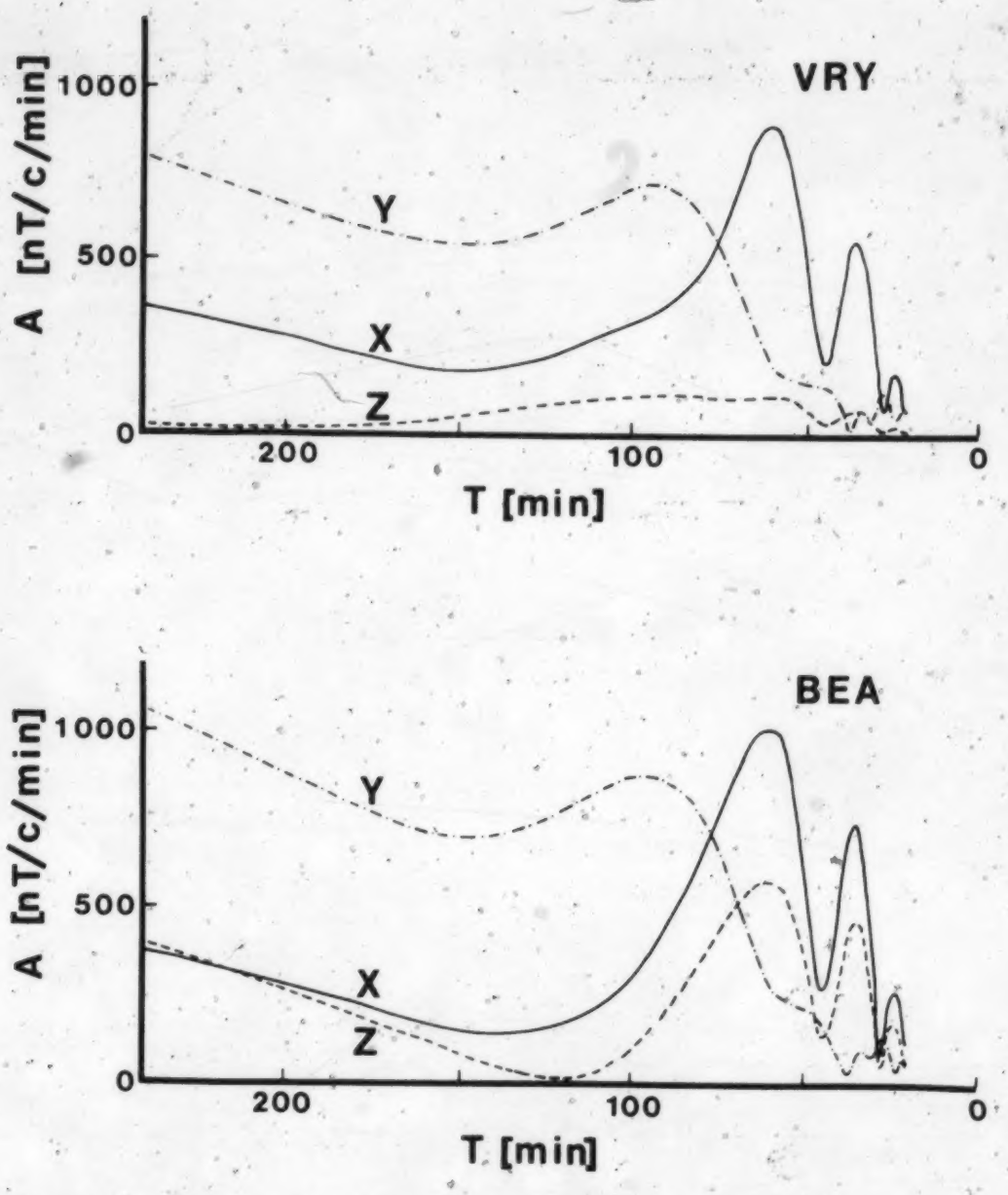

Figure 3.6 Fourier amplitude spectra in the period range 20-240 min for September 17, 22.00-September 18, 01.50 G.M.T. for the stations VRY and BEA.

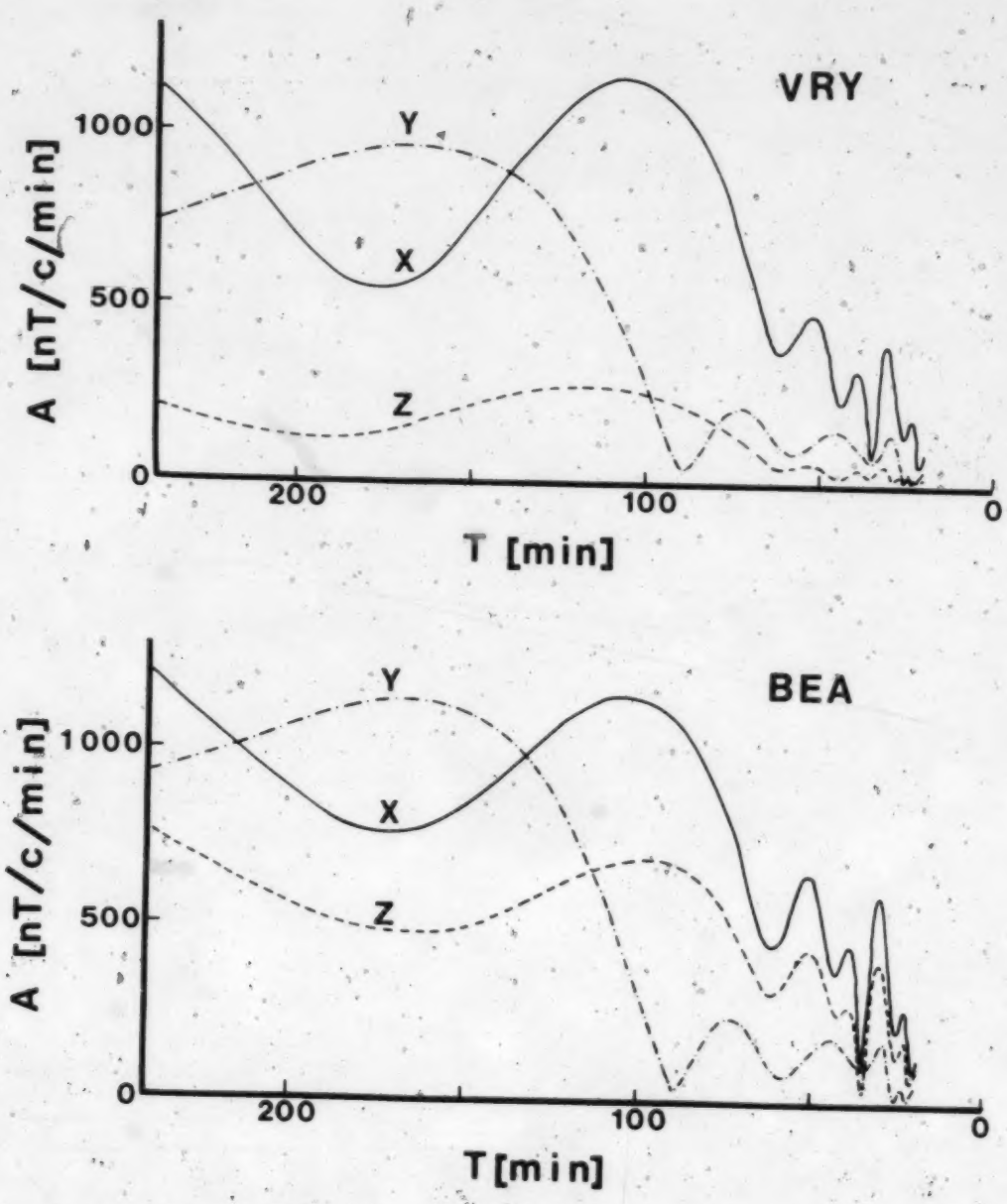

Figure 3.7 Fourier amplitude spectra in the period range 20-240 min for September 26, 18.30-22.30 G.M.T. for the stations VRY and BEA.

Typical sets of Fourier spectral component maps are shown in Figs 3.8, 3.9 and 3.10. These maps cover the period range 24-120 minutes and polarization azimuth range N21°W to N17°E. All of them show a large anomaly in Z with a maximum near BEA and lower values at PAR, as already noted from the magnetograms. All maps also exhibit a southward increase of X suggestive of a maximum in this component a short distance south of PAR. The amplitude maps of X and Z are thus qualitatively consistent with the hypothesis that X induces current in an approximately east-west striking conductor just south of PAR and that Z is mainly an anomalous field produced by this current. This hypothesis is strongly supported by the phase relationships. In all maps the phase of Z is very close to that of X at stations such as BEA, BIE and FRA which are near the amplitude maximum in Z. This phase relation is shown in Figs 3.8-3.10. In Table 3.2 the phase difference (Z-X) is shown at BEA, at the maximum of the Z anomaly, and at OLI far to the north. It is interesting to note that the largest phase differences between Z and X occur for the first two periods at the top of the table; these have the largest content of Y in the horizontal field and north-west polarization.

A small maximum in X lies near the stations OLI, PRI and PET in Fig. 3.8 with an associated maximum in

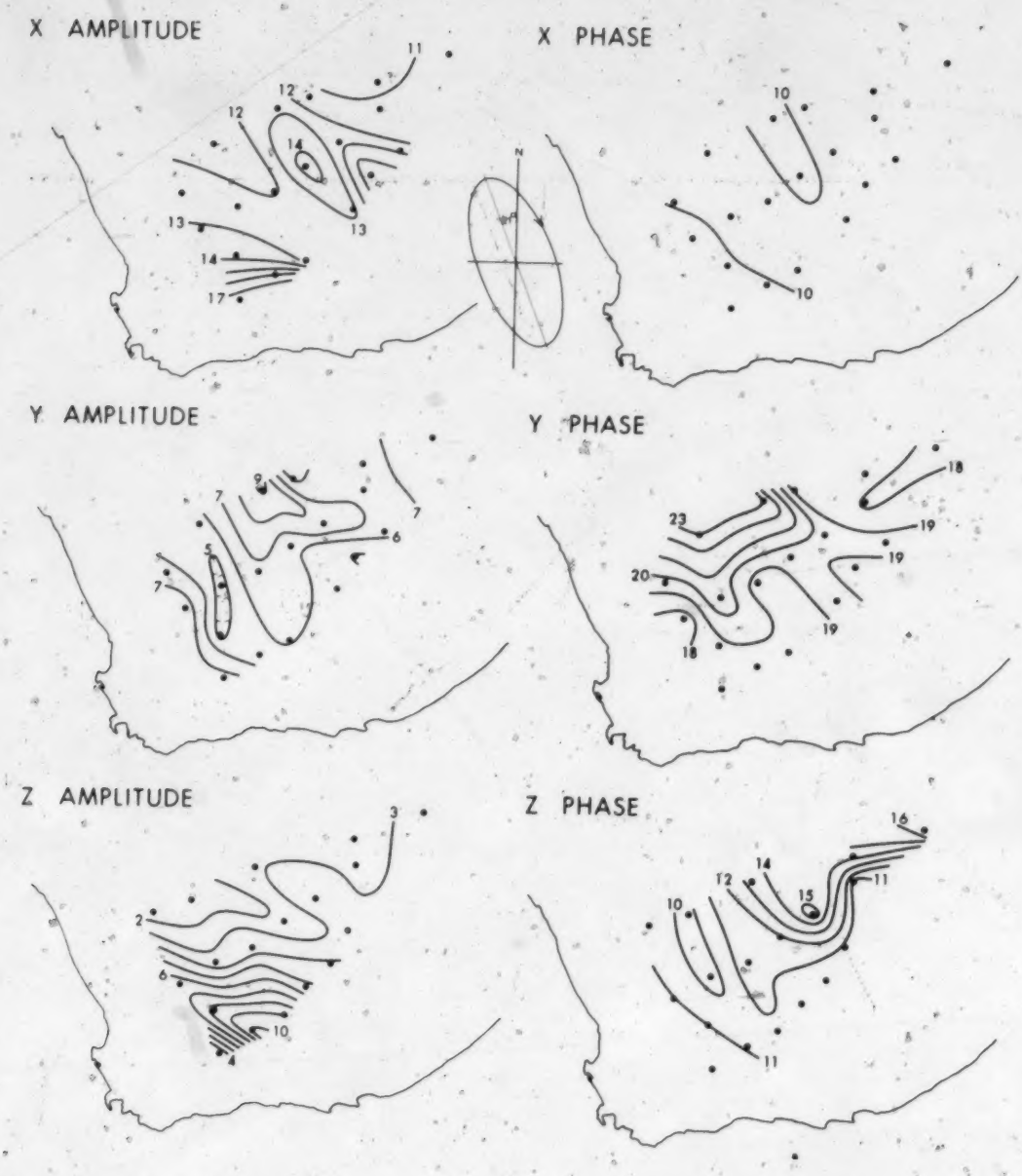

Figure 3.8 Fourier transform amplitudes (nT/c/min × 10) and phases (min) at period 24 min for 18.30-22.30 G.M.T., August 31. Estimates for the standard deviations in the X, Y and Z components are respectively 18, 17 and 14 nT/c/min for the amplitudes and .5, .1 and 1.5 min for the phases. The polarization ellipse for the horizontal field is shown.

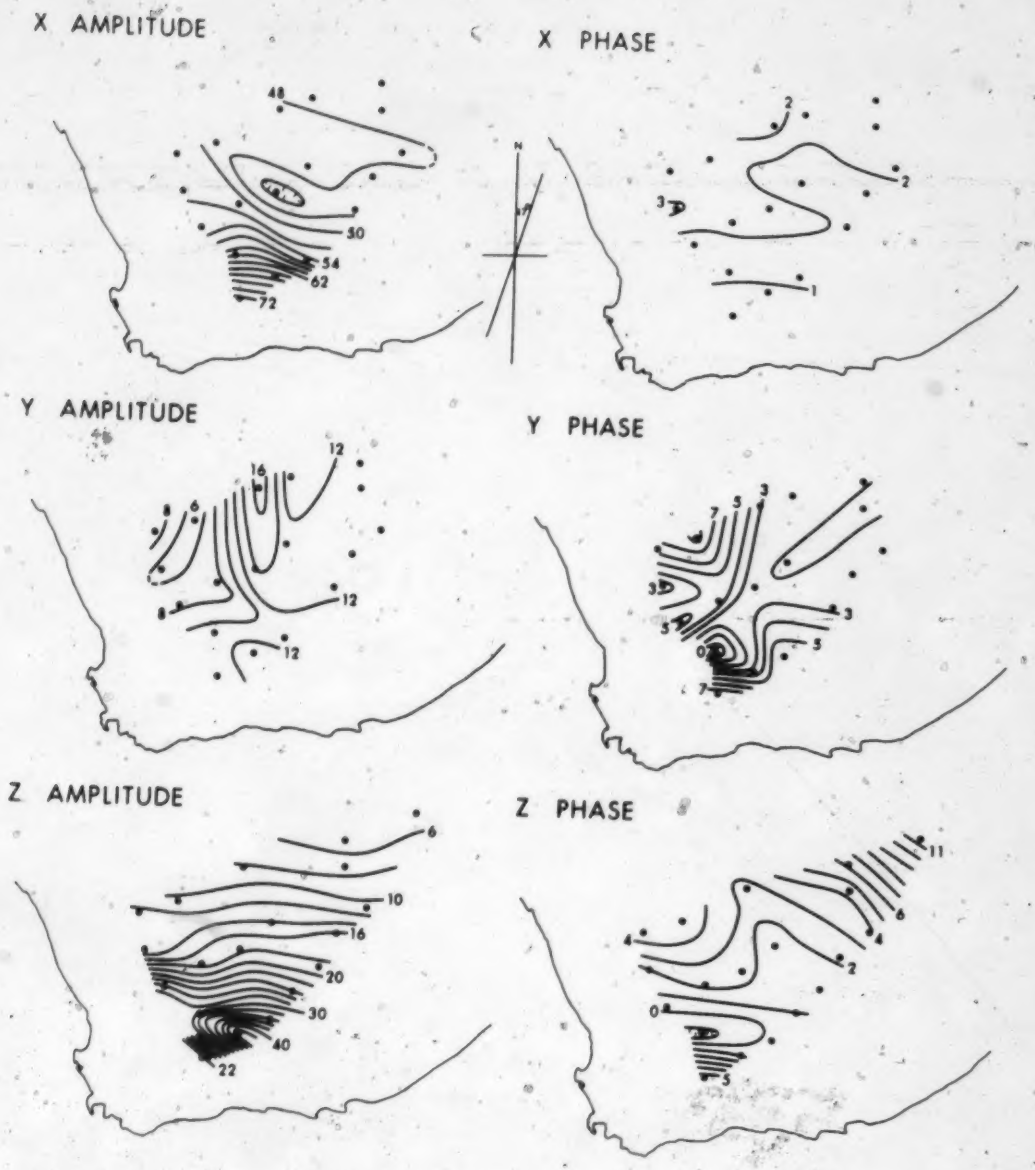

Figure 3.9 Fourier transform amplitudes (nT/c/min × 10) and phases (min) at period 51 min for 18.30-22.30 G.M.T., September 26. Estimates for the standard deviations in the X, Y and Z components are respectively 20, 16 and 15 nT/c/min for the amplitudes and 1, 1 and 1.5 min for the phases. The essentially linear polarization of the horizontal field is indicated.

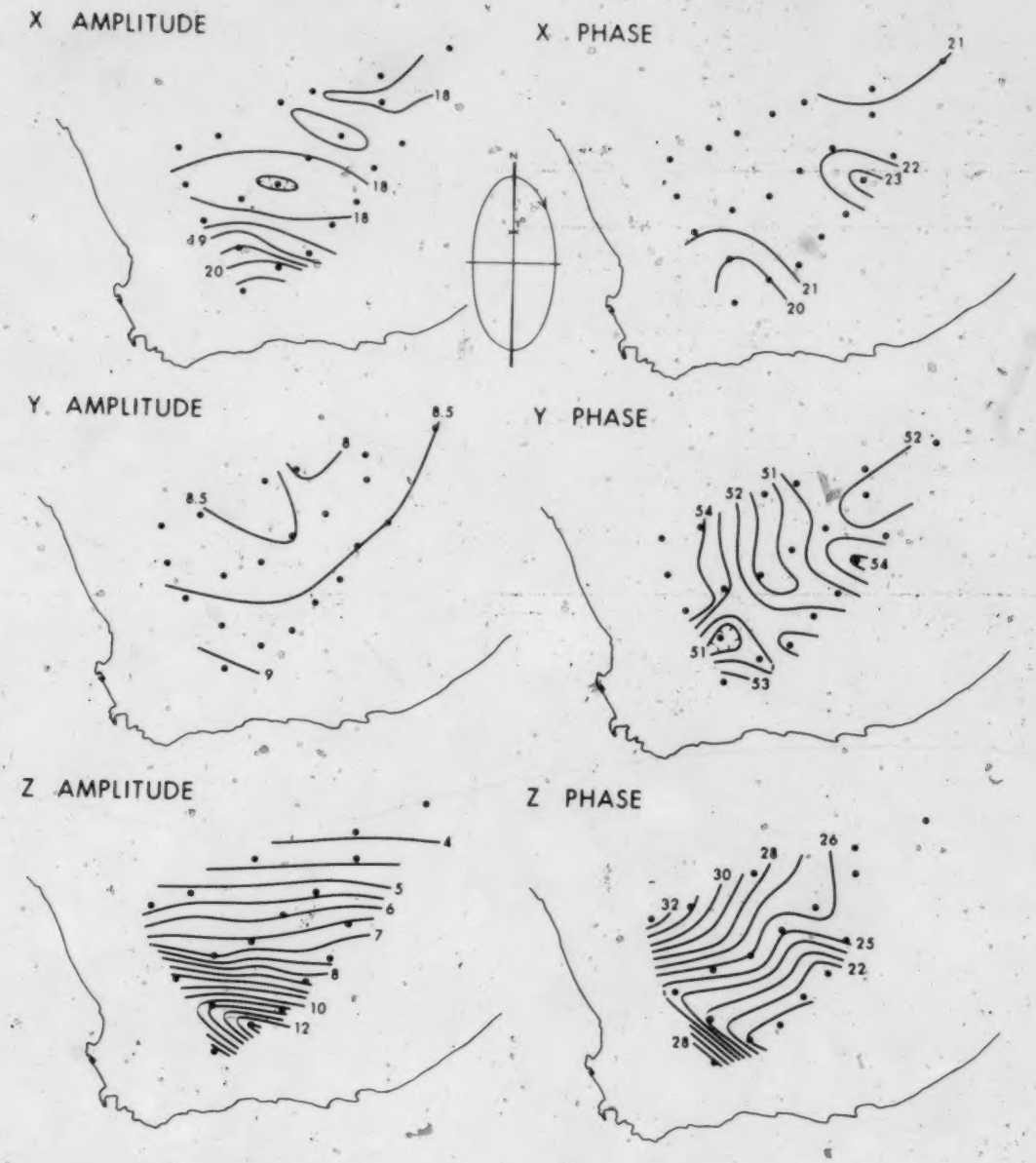

Figure 3.10 Fourier transform amplitudes (nT/c/min $\times 10^2$) and phases (min) at period 120 min for 18.30-22.30 G.M.T., August 31. Estimates for the standard deviations in the X, Y and Z components are respectively 43, 28 and 25 nT/c/min for the amplitudes and 1.5, 1 and 2 min for the phases. The polarization ellipse for the horizontal field is shown.

Table 3.2

Event		$\Delta\phi(\underline{Z}-\underline{X})$ degrees	
Date	Period min.	BEA	OLI
Aug. 31	24	+ 15	+ 56
	43	+ 17	+ 77
	120	+ 3	+ 16
Sept. 17-18	24	+ 3	+ 18
	35	+ 1	+ 11
	60	- 9	+ 2
Sept. 26-27	31	+ 7	+ 28
	51	+ 1	- 3
	102	+ 1	+ 26
	293	- 7	+ 22

Z just north of this. Similar anomalies are found in another map (not shown) at period 43 minutes for August 31, for which the horizontal field is also polarized NW-SE. The X anomaly coincides with the boundary between the Kaapvaal craton and the Namaqualand-Natal mobile belt.

Since the current system giving rise to the large, southern anomaly is beyond the corner of the array, contour maps are of little use in determining the geometry of the current system. Even the question whether the conductor is straight or curved is open. Transfer functions were therefore computed to try to answer this question.

3.4 Transfer functions

The centre of this array was situated at magnetic latitude 40°S. The magnetic latitude (μ) is derived from the magnetic inclination (I) according to $2 \tan\mu = \tan I$. At longitude 22°E which runs through the centre of the array the geomagnetic and magnetic equators differ by about 10°. The magnetic latitude is quoted because the latitudinal variation in geomagnetic activity is determined by the magnetic and not the geomagnetic equator (Rastogi, 1962).

At the magnetic latitudes where this array was situated, the normal Z component in substorm fields is small. The magnetograms of Figs 3.2-3.4, the phase

relations in Table 3.2 and the amplitude spectra for the stations in the northern part of the array (Figs 3.5-3.7) support the view that the Z variations are mainly anomalous, and related to induction by X in a conductor south of the array, even at the northern stations. It is therefore reasonable to calculate transfer functions from components X_n and Y_n of the normal field to Z, where it is assumed that $Z_a = Z$. An estimate of the normal field in X and Y was made by taking for each spectral term of each event mean cosine and sine Fourier coefficients over all stations. The transfer functions z_X and z_Y were calculated using the relations given in eq. 2.27.

The transfer functions z_X and z_Y are complex quantities whose real parts give the in-phase responses of Z to X_n and Y_n while their imaginary parts give the quadrature-phase responses. The real parts of z_x and z_y at a specific station were combined to yield an in-phase induction vector which was as usual reversed to be in the same sense as a Parkinson arrow (Parkinson, 1959, 1962). The vector thus points toward a good conductor in which current flows in phase with the normal field. The imaginary parts of z_x and z_y were similarly combined to give a quadrature-phase induction vector which points away from a conductor in which current leads the normal field in phase.

In Section 2.5, on the calculation of transfer functions, it was pointed out that each cross- and autopower must be a mean value from a number of variation events with well distributed polarizations. Seven short events each of 120 minutes duration were therefore selected from the three disturbance sequences.

The in-phase and quadrature-phase induction vectors representing z_x and z_y derived from seven short events are shown in Fig. 3.11 at the fourteen stations which recorded all seven short events in three components. Four periods are represented. The in-phase vectors indicate the presence of a good conductor south-southwest of the array, and the parallel orientation of these vectors indicates an approximately straight current configuration. The large difference between the in-phase vectors at PAR and at the stations BEA and FRA indicates that PAR is close to the conductor.

In Section 3.3 it was remarked that the attenuation of short-period Z in the magnetograms at PAR suggested that this station was above the conductor, and the steep rise in X amplitude as PAR is approached from the north indicates that the current configuration is just south of PAR. These facts strongly suggest that a large conductive body lies under the Cape Folded Belt (Fig. 3.1). The continental edge is too far away to produce the steep anomalies

Figure 3.11 In-phase (solid) and quadrature phase (broken) induction vectors representing the transfer functions z_x and z_y at four periods, from seven 2-hour variation events.

T = 26 min

T = 43 min

T = 64 min

T = 128 min

UNIT ARROW

in Z and X indicated in Figs 3.8-3.11. Although, the in-phase induction vectors are not perpendicular to the continental edge (Figs 3.1 and 3.11) they are parallel to the Parkinson arrow for Hermanus (Fig. 3.1), a magnetic observatory on the coast some 100 km west of the southern tip of Africa (Parkinson, 1962).

An important point is the continued response of the conductive body as the period of the fields increases to 64 and 128 minutes. This frequency response is consistent with a deep conductor of large self-inductance, and so with an upper mantle structure. The in-phase response of Z to X indicated by Fig. 3.11 and Table 3.2 are consistent with a conductor in the upper mantle.

The southern corner of the array lies across the deep Karroo sedimentary basin. The effect of this will be discussed in Section 3.6. In Fig. 3.11 it can be seen that the quadrature-phase induction vectors at BEA, FRA and PAR show the effects of the sedimentary basin. At these stations the quadrature-phase vectors are large at short periods and are reduced to magnitudes like those elsewhere in the array at periods 64 and 128 minutes. At the shorter periods the quadrature-phase vectors tend to point away from the deep Karroo basin. No doubt the in-phase induction vectors at PAR are shortened, at the shorter periods, by the effect of the sediments to the north of this station.

3.5 Normalized anomalous fields

Anomalous fields cover most of the array. Northern stations, as far as possible from the southern anomaly, were arbitrarily designated as representing normal field components. For X and Y the mean amplitude from KUR, CHR and VRY was used to define the assumed inducing field over the array and, as residuals, the anomalous horizontal components X_a, Y_a at other stations. For Z the mean amplitude from VRY, CHR and VEN was deducted from Z at each other station to give an estimate of the anomalous vertical field Z_a. A profile was chosen approximately parallel to the in-phase induction vectors: it is shown in Fig. 3.1. From contour maps similar to Figs 3.8-3.10 and the normal field estimates just specified, normalized anomalous fields Z_a/H_n and H_a/H_n were estimated along the profile. Here H is the horizontal component along the profile. Normalized anomalous fields for six periods from three events are shown in Figs 3.12 and 3.13. Four other anomaly profiles, not shown, resemble those of Fig. 3.12, which shows the response to fields polarized nearly north-south. The more complicated and larger anomalies of Fig. 3.13 arise when the normal field polarization is close to north-west-south-east.

The normalized anomalous vertical fields Z_a/H_n associated with north-south polarized normal fields (Fig.

Figure 3.12 Normalized anomalous variation field components Z_a/H_n and H_a/H_n along the section line AB, Fig. 3.1, for periods 24 min (event of September 17, 1971), 51 min, 102 min and 293 min (event of September 26, 1971). The polarization indicated in Fig. 3.9 is representative (east of north).

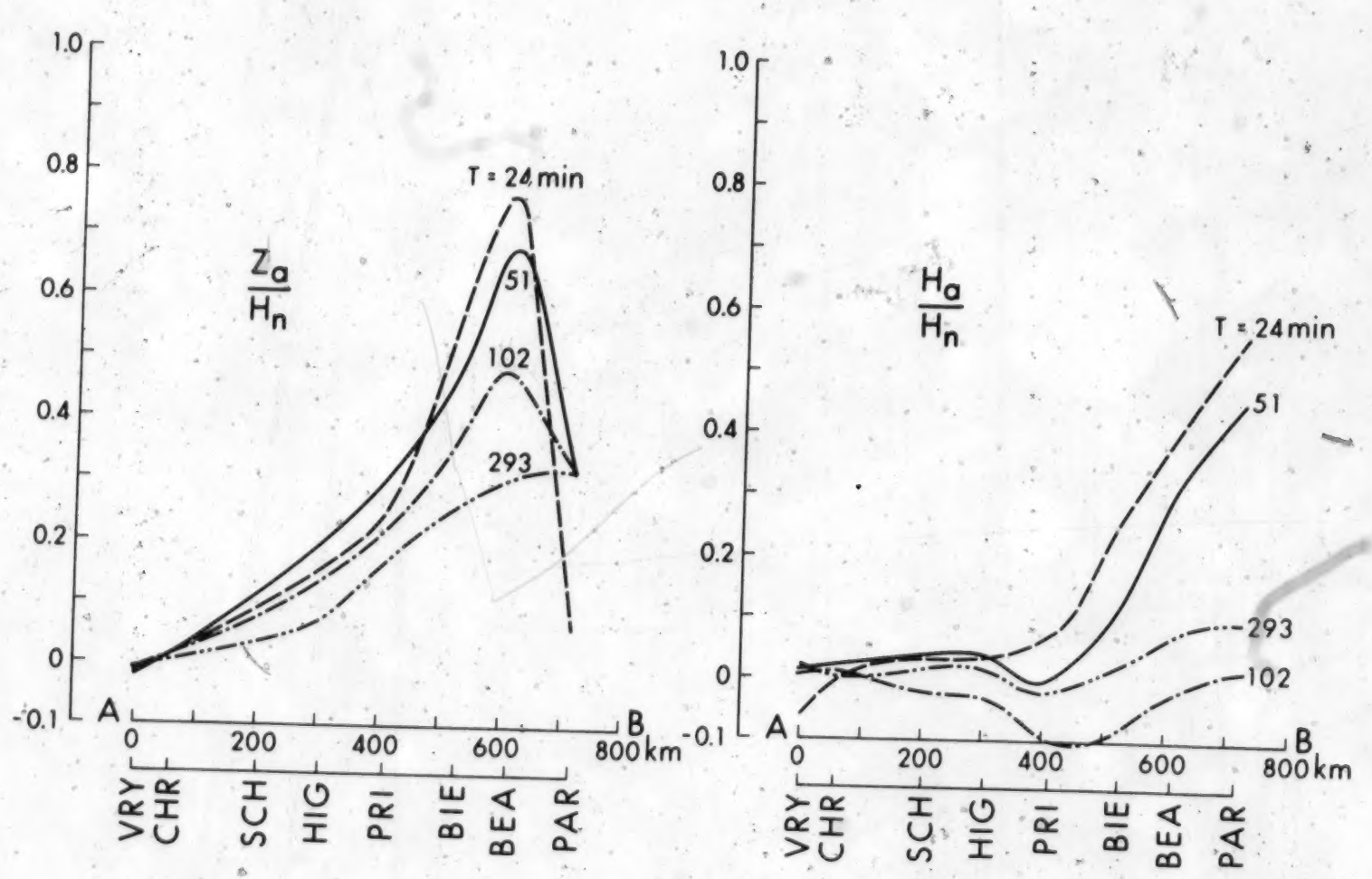
1.0
0.8
0.6
0.4
0.2
0
-0.1
$\frac{Z_a}{H_n}$
T = 24 min
51
102
293
A
B
0
200
400
600
800 km
VRY CHR
SCH
HIG
PRI
BIE
BEA
PAR
$\frac{H_a}{H_n}$
T = 24 min
51
293
102

Figure 3.13 Normalized anomalous components Z_a/H_n and H_a/H_n along AB (Fig. 3.1) at periods 24 min and 43 min in the event of August 31, 1971. The polarization in Fig. 3.8 is representative (west of north).

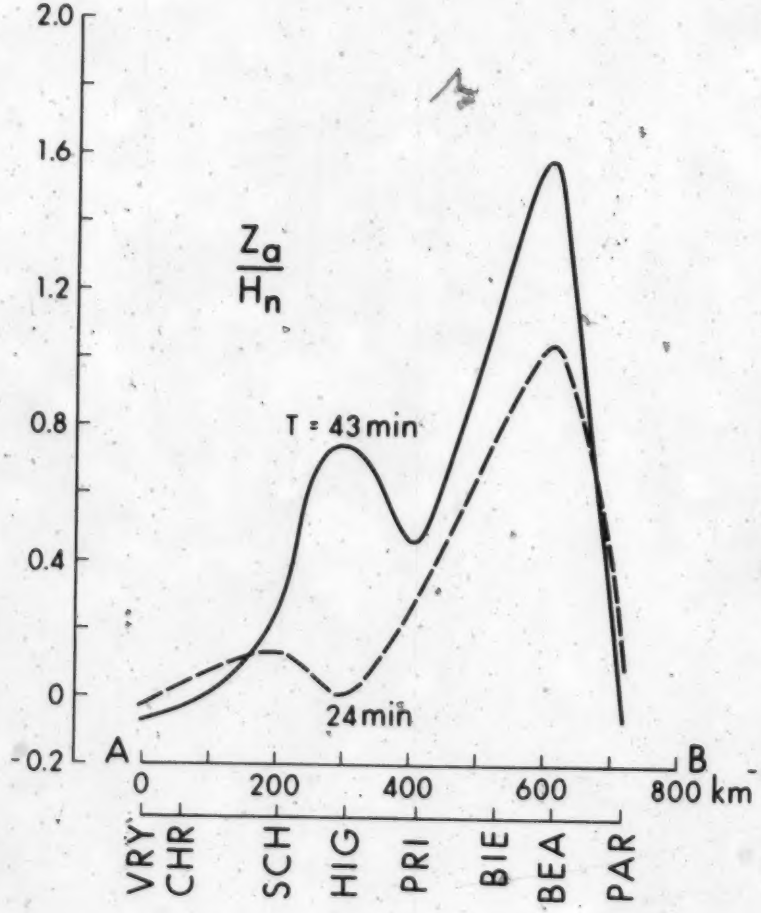
2.0
1.6
1.2
0.8
0.4
0
-0.2
$\frac{Z_a}{H_n}$
T = 43 min
24 min
A
B
0
200
400
600
800 km
VRY
CHR
SCH
HIG
PRI
BIE
BEA
PAR

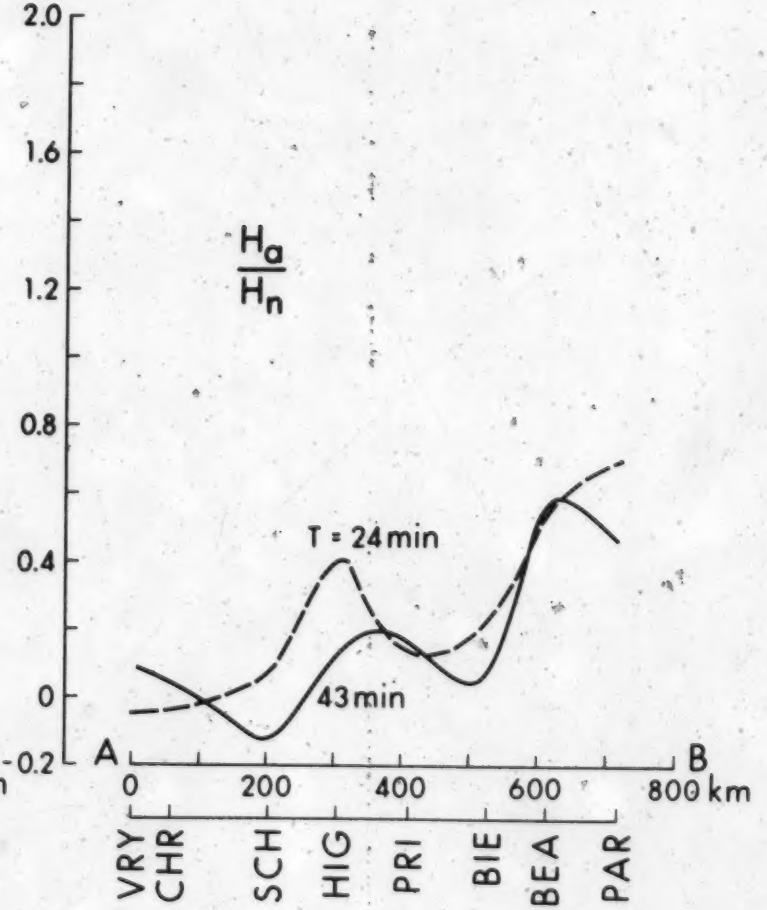
2.0
1.6
1.2
0.8
0.4
0
-0.2
$\frac{H_a}{H_n}$
T = 24 min
43 min
A
B
0
200
400
600
800 km
VRY
CHR
SCH
HIG
PRI
BIE
BEA
PAR

3.12) show maxima which decrease as the period increases. At PAR Z_a/H_n is small at T = 24 min and rises as T increases, suggesting a southward shift of the current system with increasing depth. The Karroo sedimentary basin may produce some or all of this effect. At short periods H_a/H_n rises steeply towards the southern corner of the array, but this anomaly flattens out at periods over 100 minutes. Qualitatively the horizontal component anomaly also suggests a southward shift of the current system with increase of T and of the depth of the induced currents.

When the normal field is polarized north-west-south-east (Fig. 3.13), both Z_a/H_n and H_z/H_n develop extra minima and become much larger than the corresponding anomalies with north-south normal fields. This feature of the response is not understood on the present limited information from an array which does not include the anomalous currents.

Both anomalies in Fig. 3.13 and those at T = 24 min and T = 51 min in Fig. 3.12 are too large to be compatible with induction in a conductor of two-dimensional geometry. The very large amplitudes must be associated with a three-dimensional configuration of conductors. The induction arrows of Fig. 3.11 lend no support to the presence of a curved conductor. One

possibility is that the anomaly is of the 'current concentration' type, with induction in a large region feeding a highly-conducting body. A second possibility is that constructive interference is present between the fields of two or more current systems. One could be in the Karroo basin and the other under the Cape Folded Belt.

Whatever the inductive mechanism, a maximum depth can usually be estimated from the half-width of an elongated anomaly, defined as the width of the H_a/H_n anomaly at half height. For a line current the half-width is twice the depth of the current, and the Z extrema are a half-width apart. Unfortunately the profiles of Figs 3.12 and 3.13 do not extend far enough to the south to allow the half-width to be estimated.

Normalized anomalies at periods 24 minutes and 102 minutes are repeated in Fig. 3.14 with a section showing the basement topography and the resistivity structure in the Karroo sedimentary basin. Average resistivities are shown as deduced from various deep structural electrical investigations whereas thickness information was obtained from deep drillings and seismic reflection work (Haughton, 1969; Fatti and Du Toit, 1970 and Winter and Venter, 1970).

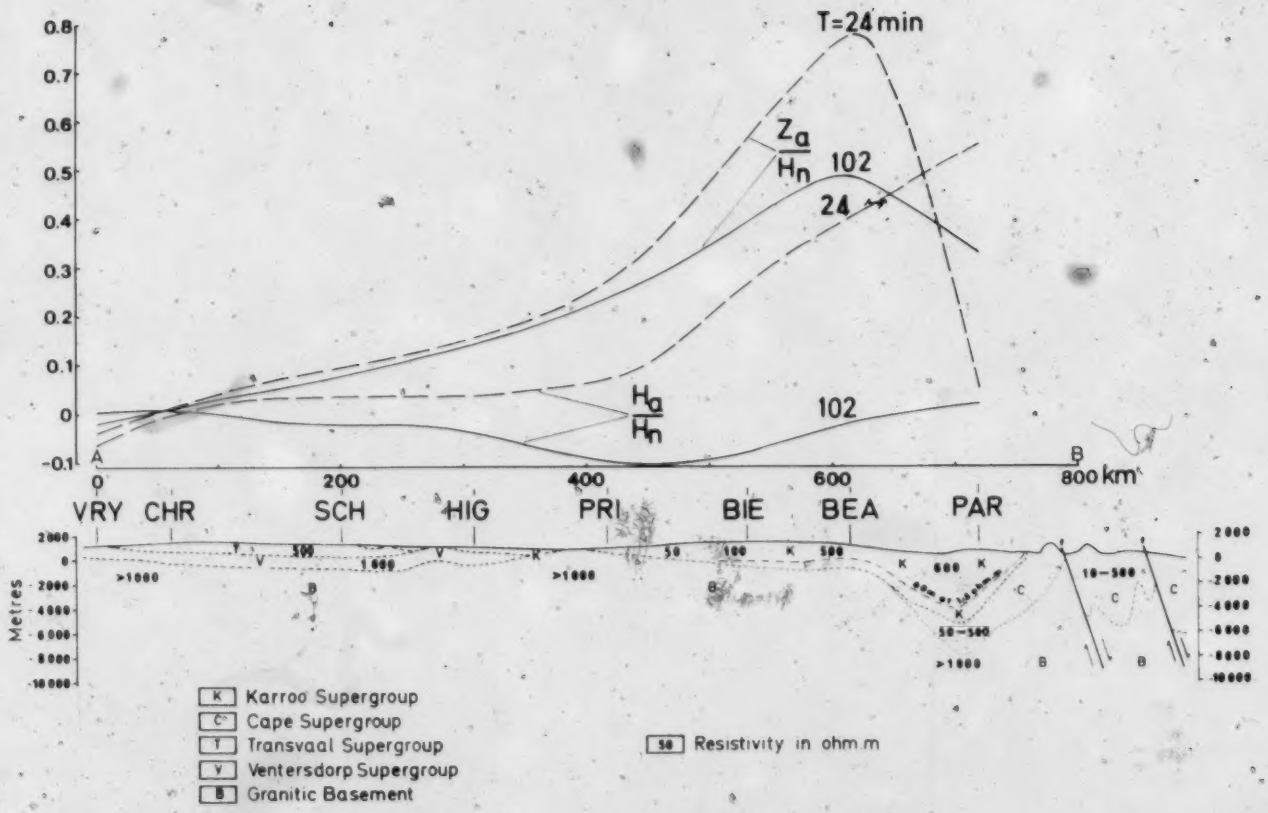

Figure 3.14 Normalized anomalous components Z_a/H_n and H_a/H_n along AB, Fig. 3.1, at periods of 24 min for the event of September 17, 1971 and 102 min for the event of September 26, 1971 with a geological section along AB showing resistivity structure.

3.6 Two-dimensional numerical modelling

Despite the fact that the array covered only about half the width of the anomaly, two-dimensional modelling was attempted to attain a better understanding of the anomaly. The two-dimensional model calculations have been made by means of the algorithm of Jones and Price (1970) as programmed by Jones and Pascoe (1971) and Pascoe and Jones (1972). This method has been described in Section 2.6. The models all include the near surface resistivity data shown in Fig. 3.14. Thirty-five different models were calculated. It was first established that the sedimentary basin alone could not be responsible for the anomaly, even when conductivities were scaled up by a factor of ten to allow for a possible current concentration effect. The computed anomalies were too far to the north and too narrow in relation to the observed profiles Z_a/H_n and H_a/H_n. Various conductors of rectangular and more complicated sections were added to the sedimentary model, at either crustal or upper mantle depths. Results for a crustal and a subcrustal conductive structure are respectively shown in Figs 3.15 and 3.16. The resistivity data for the "normal" crust away from the anomalous bodies correspond to that given by Van Zijl et al. (1970)

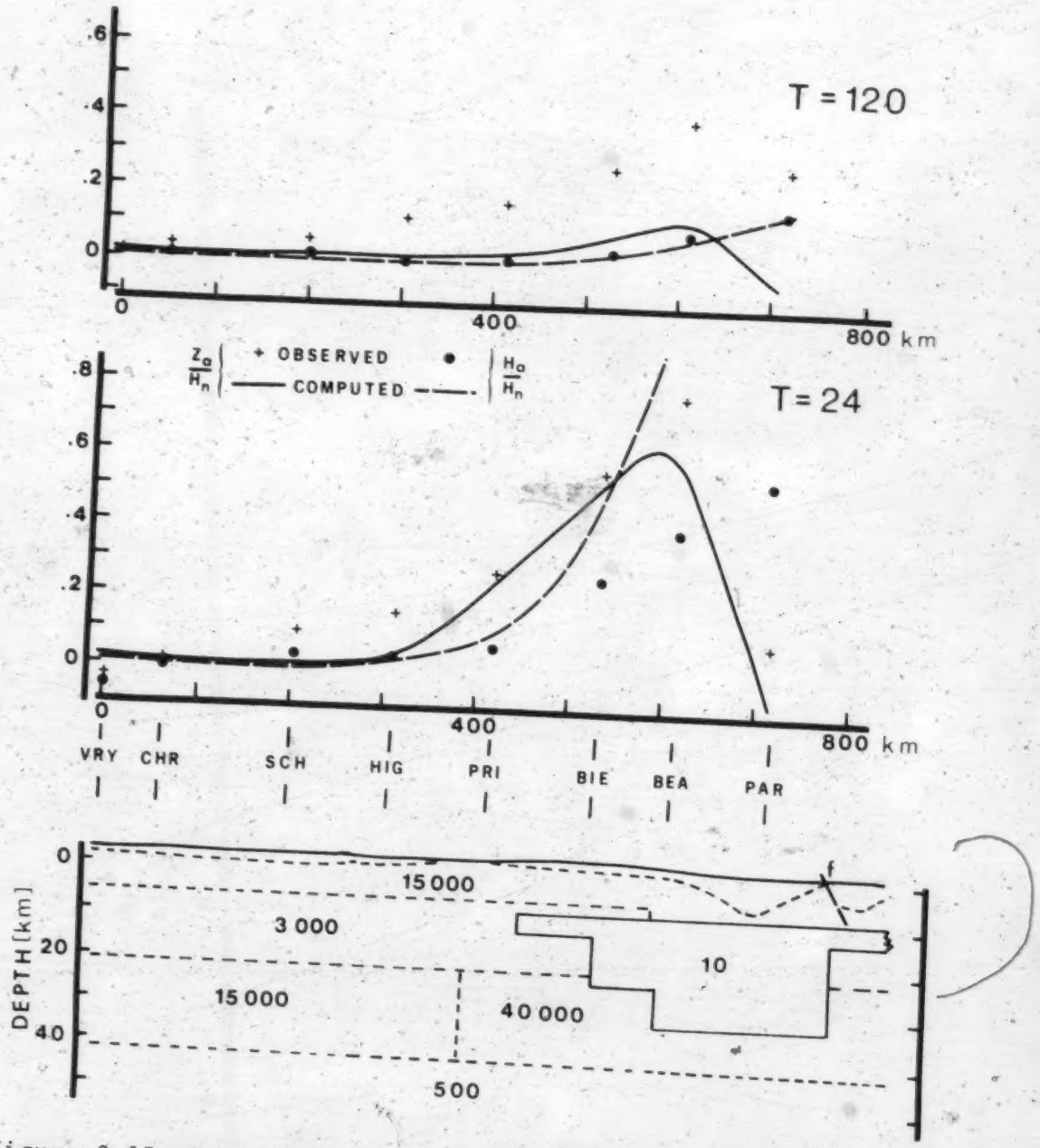

Figure 3.15 Results of two-dimensional model calculations for a complicated crustal structure with resistivity of 10 ohm.m. The normalized anomalous components Z_a/H_n and H_a/H_n along AB, Fig. 3.1, at period of 24 min are for the event of September 17, 1971 and at period 120 min for the event of August 31, 1971. The resistivities in the Karroo sediments are those indicated in Fig. 3.14.

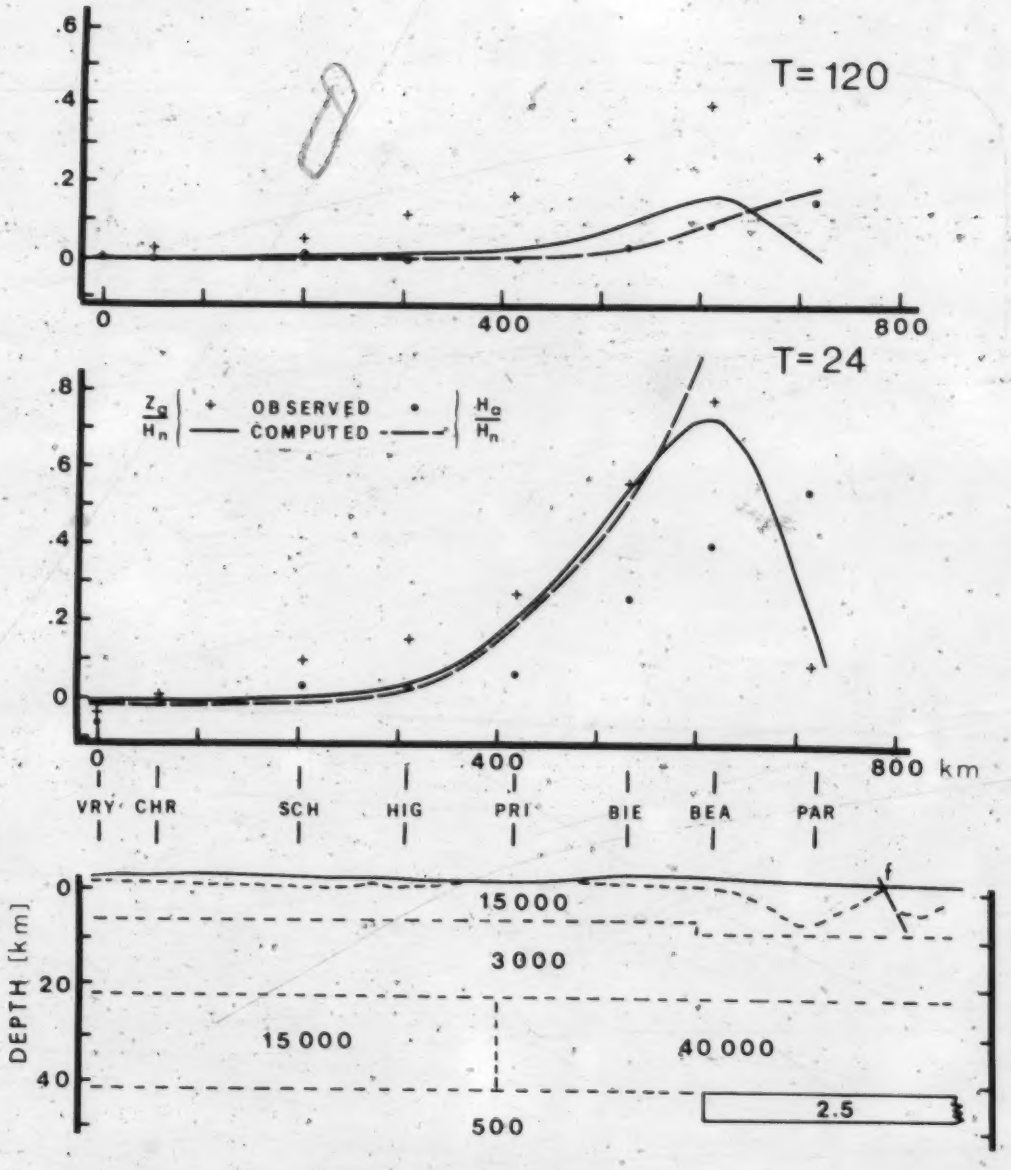

Figure 3.16 Results of two-dimensional model calculations for a simple subcrustal structure with resistivity of 2.5 ohm.m. The Z_a/H_n and H_a/H_n data are the same as those shown in Fig. 3.15. The resistivities in the Karroo sediments were decreased to 1/10 of the values shown in Fig. 3.14.

for the Kaapvaal craton and Namaqualand-Natal belt. These data differ slightly from those given by Van Zijl and Joubert (1975) as discussed in Section 1.4, but were the only available in 1972 when these calculations were made. Since the differences only involve the very resistive strata, they will have little or no effect on the results.

It proved possible to model either Z_a/H_n or H_a/H_n but not both, all models making $(H_a/H_n)/(Z_a/H_n)$ too large in relation to the observations. This problem is very well illustrated in Figs 3.15 and 3.16. From these figures it is clear that the frequency response also could not be matched by the model calculations. This was true for all models computed. In this respect Porath et al. (1971) encountered similar difficulty in trying to model the North American Central Plains anomaly, which is known to involve the current concentration effect. It was found that most models based on anomalous bodies in the crust, produce Z_a/H_n and H_a/H_n anomalies that are too narrow in relation to the observed profiles. Anomalous conductive structures in the mantle gave better results in this respect. The best results were obtained using models incorporating enhanced conductivities in the Karroo and Cape sediments, as well as mantle structures. As was remarked in the last section, the present anomaly is too

large to be produced by induction in a two-dimensional structure, so that two-dimensional model calculations can at best locate the structure on some assumption as to the amplifying effect of current concentration, constructive interference or some other cause.

3.7 Discussion

Although the attempts to model the magnetic induction anomaly were unsuccessful, it is clear that a major structure, involving conductivity contrasts of at least two orders of magnitude, underlies the Cape Fold belt and the deep part of the Karroo Basin. The Geophysics Division of the C.S.I.R. in Pretoria, South Africa is at present constructing an array of 26 Gough-Reitzel magnetometers. This array will be used to extend coverage towards the coast. Quantitative interpretation will be attempted when the anomaly is more completely known. The geology and other geophysical parameters in the array area will be discussed in Chapter 6.

The small anomaly near the stations OLI, PRI and PET for horizontal fields polarized NW-SE could be associated with the boundary between the craton and the mobile belt. This boundary seems to coincide with the Doornberg fault zone, a fault in the granite-gneiss basement which seems to be rejuvenated in the overlying

Karroo sediments (Olivier, 1972). The anomaly cannot, however, be due to local induction, because it only shows up for the horizontal field polarized almost parallel to the fault zone. This anomaly cannot be explained on the basis of this array study alone, but will be discussed in Chapter 6 in the light of information from the 1972 array study further north.

No indication has been found of any conductivity contrast between the Kaapvaal craton and the Namaqualand-Natal mobile belt. Any compositional effect on the conductivity of the crust or mantle in these tectonic units is too small to be detected by the present study.

CHAPTER IV

THE 1972 ARRAY STUDY IN SOUTH-WEST AFRICA BOTSWANA AND RHODESIA

4.1 Introduction

An array of 25 three-component magnetometers operated in South-West Africa, Botswana and north-western Rhodesia from December 13, 1971 to February 2, 1972. The location of the array is shown in Fig. 4.1. All the instruments but one were of a type described by Gough and Reitzel (1967). The instrument near Tsumeb (TSU) is a permanent recording station of the Magnetic Observatory of the C.S.I.R. and is of a type described by Scheepers (1973). Table 4.1 gives the names and coordinates of all stations in the array as well as the magnetic declination at each station.

The position of the array is shown in Fig. 4.2 in relation to the tectonic features and some earthquake epicentres in the area. Unconsolidated Kalahari sediments ranging in age from Tertiary to Recent cover most of Botswana and the eastern part of South-West Africa so that very little is known about the underlying solid rock geology and tectonic features. Faults of Karroo to Recent age in South-West Africa and Rhodesia are shown (Korn and Martin, 1951 and Provisional Geological Map of Rhodesia, 1971).

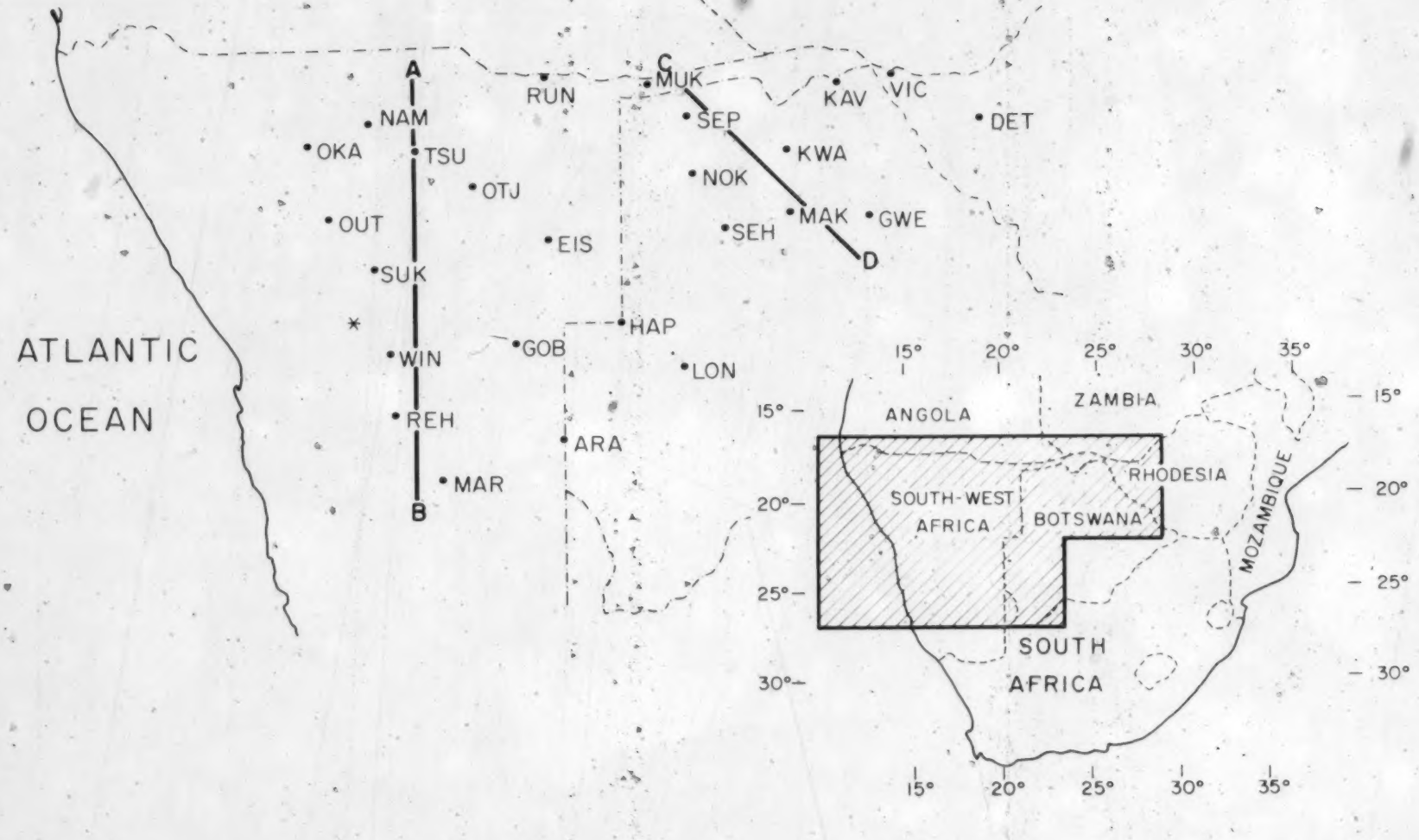

Figure 4.1 The location of the magnetometer array in South-West Africa, Botswana and Rhodesia (* indicates centre of deep electrical resistivity sounding).

Table 4.1

Coordinates and magnetic declination of stations in 1972 array

Station Name	Code	Latitude Degree and min South	Longitude Degree and min South	Magnetic Declination (Degrees)
Eiseb	EIS	20°38'	19°46'	-15.5
Otjituo	OTJ	19°42'	18°35'	-15.4
Rundu	RUN	17°55'	19°45'	-13.8
Namutoni	NAM	18°40'	16°54'	-15.4
Okaukuejo	OKA	19°00'	15°52'	-16.1
Gweta	GWE	20°14'	25°08'	-13.3
Aranos	ARA	23°55'	20°00'	-17.8
Makalamabedi	MAK	20°11'	23°52'	-13.6
Outjo	OUT	20°12'	16°09'	-16.8
Gobabis	GOB	22°21'	19°14'	-16.9
Happy Valley	HAP	22°00'	21°00'	-15.9
Lone Tree	LON	22°45'	22°00'	-16.3
Sukses	SUK	21°02'	16°54'	-16.9
Sehitwa	SEH	20°27'	22°42'	-14.2
Nokaneng	NOK	19°38'	22°10'	-13.8
Mariental	MAR	24°30'	17°56'	-18.9
Rehoboth	REH	23°25'	17°08'	-18.7
Dett	DET	18°37'	20°55'	-11.5
Windhoek	WIN	22°27'	17°06'	-17.9
Sepopa	SEP	18°44'	22°09'	-13.3
Mukwe	MUK	18°04'	21°27'	-13.3
Kwai River Lodge	KWA	19°09'	23°47'	-13.0
Kavimba	KAV	18°03'	24°36'	-12.0
Victoria Falls	VIC	17°57'	25°33'	-11.5
Tsumeb	TSU	19°02'	16°36'	-15.4

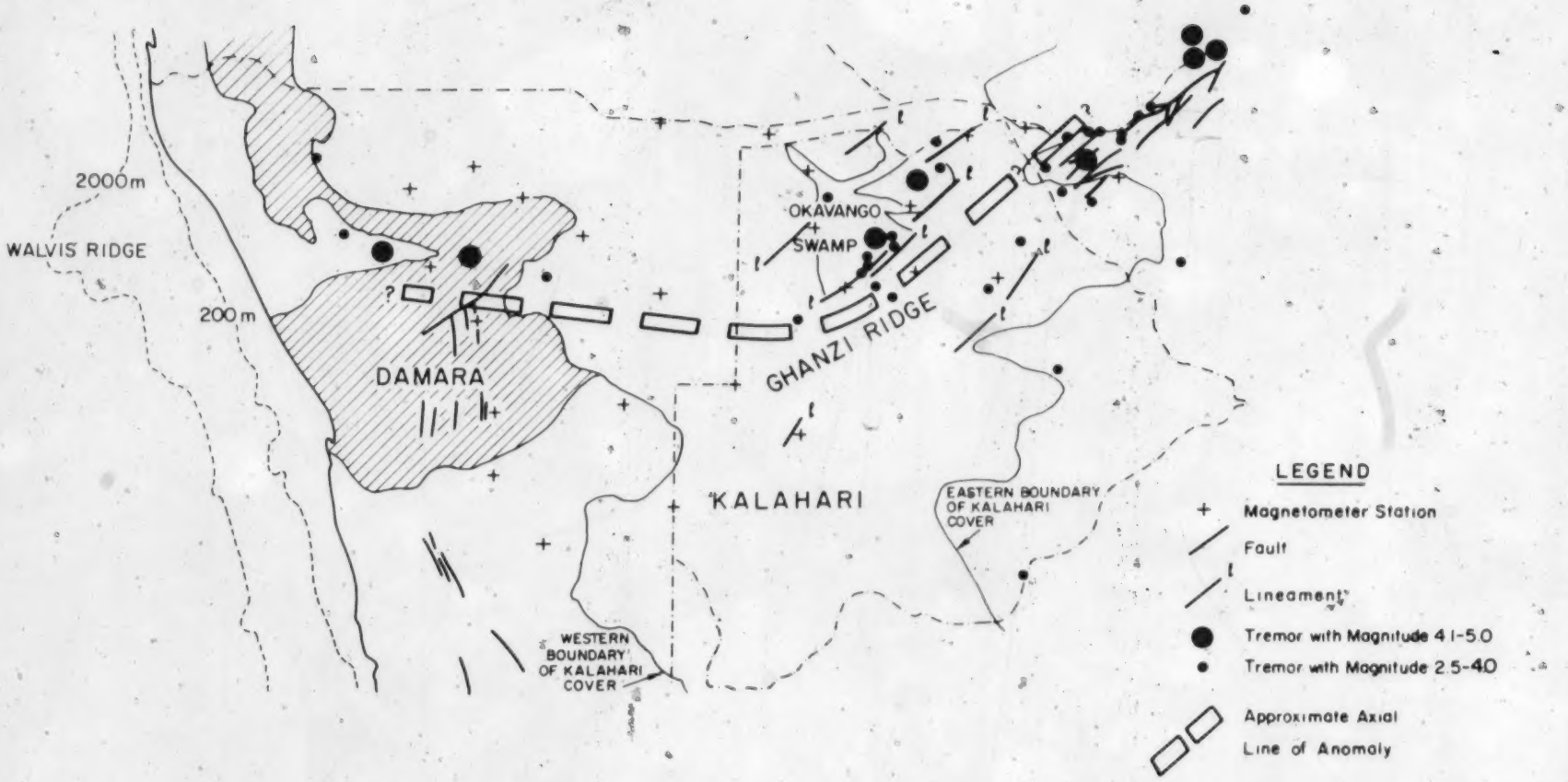

Figure 4.2 The array in relation to the main tectonic features in the study area. The Damara geosyncline striking NE-SW and the continental edge are also shown.

The major linear features in Botswana as outlined by Reeves (1972) are presented. Epicentres for earth tremors catalogued by Fernandez (1972) for 1971, Fernandez and Guzman (1973) for 1972 and Rhodesia Meteorological Services (1973) for 1973 are indicated. Reeves discussed the Botswana seismicity and concluded that the epicentres form two distinct spatial populations - that of the Okavango Delta and that of the Central Kalahari. These two seismically active areas Reeves believes to be separated by the Ghanzi Ridge, a broad upwarp of little explored Palaeozoic sediments isoclinally folded along a north-east trending axis. Outcrops of rocks in the Damara Geosyncline are also shown.

The array was located to look for possible contrasts in electrical conductivity of the crust and upper mantle associated with the Damara geosyncline and the seismicity in Botswana. A deep direct current electrical sounding (Schlumberger array) that was centred about halfway between SUK and WIN (Fig. 4.1) indicated that the resistive part of the crust in the Damara Geosyncline has a transverse resistance (thickness-resistivity product) an order of magnitude less than that of the crust in the Kaapvaal Craton and Namaqualand Metamorphic Complex (Van Zijl, Hugo and de Bellocq, 1970; Van Zijl and Joubert, 1975).

Since the magnetometers require film changes at three-weekly intervals the siting of the instruments was largely dictated by the few negotiable roads in the study area.

4.2 Magnetograms

From the geomagnetic data recorded over the nine weeks of operation, three periods of geomagnetic disturbance were selected for analysis. These periods were January 16, 14.00-23.00 G.M.T., January 21, 11.30-January 22, 04.30 G.M.T. and January 28, 14.30-22.30 G.M.T. Magnetograms for these events are presented in Figs 4.3-4.5. The H and D components (magnetic coordinates) were transformed to X and Y components (geographic coordinates) because of a 7.5° change in declination across the array. Stack 1 in Figs 4.3-4.5 portrays the data of the westernmost stations from OKA in the north to MAR in the south, Stack 2 the data of the adjacent 'line' of magnetometers from NAM in the north to ARA in the south, Stack 3 the data of the next 'line' from RUN to LON and Stack 4 the data of the group of six easternmost magnetometers.

The most prominent feature in these magnetograms is the reversal in the vertical variation field between OUT and SUK in Stack 1. The reversal in Z occurs in less

Figure 4.3 Magnetograms of a substorm 14.00-23.00 G.M.T., January 16, 1972. The stations are represented from north to south in each stack. Components are X northward, Y eastward and Z downward.

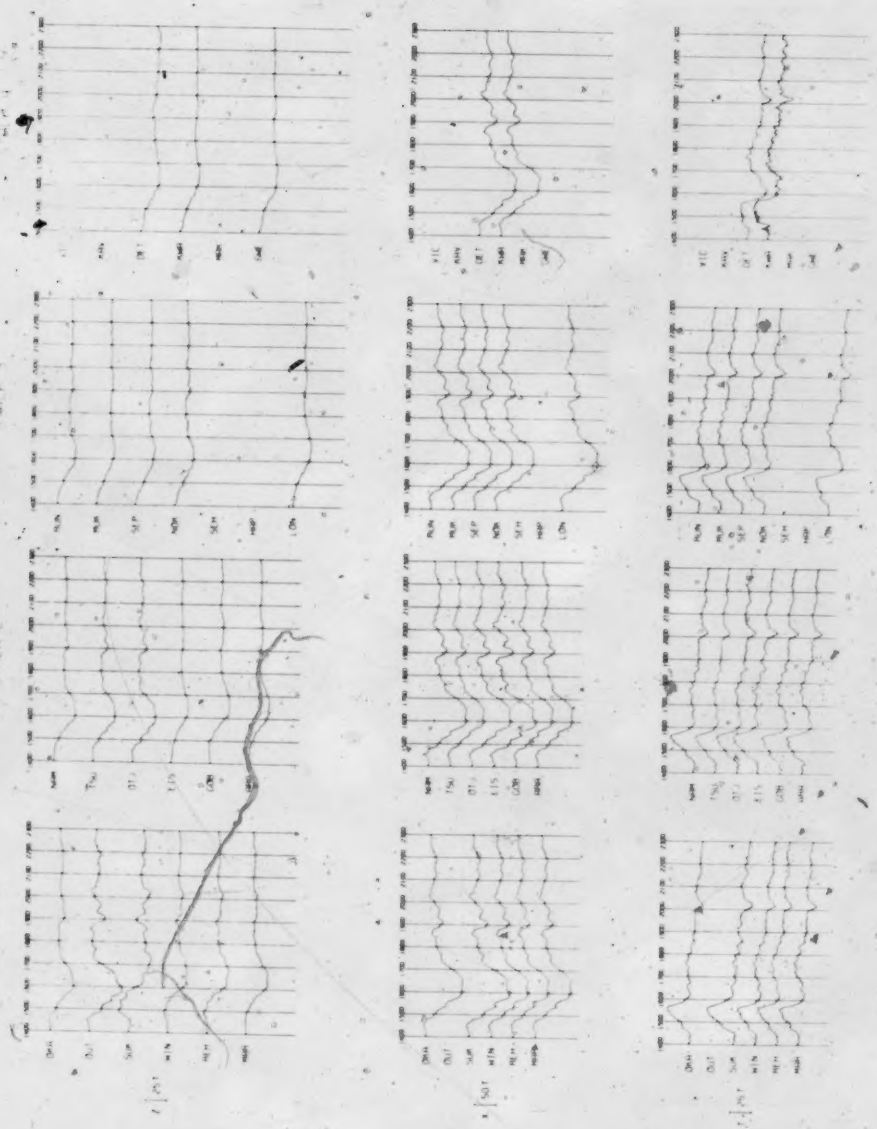
JANUARY 16, 1972

Figure 4.4a Magnetograms of an event January 21, 11.30-January 22, 04.30 G.M.T., Stack 1.

JANUARY 21 AND 22, 1972

STACK 1

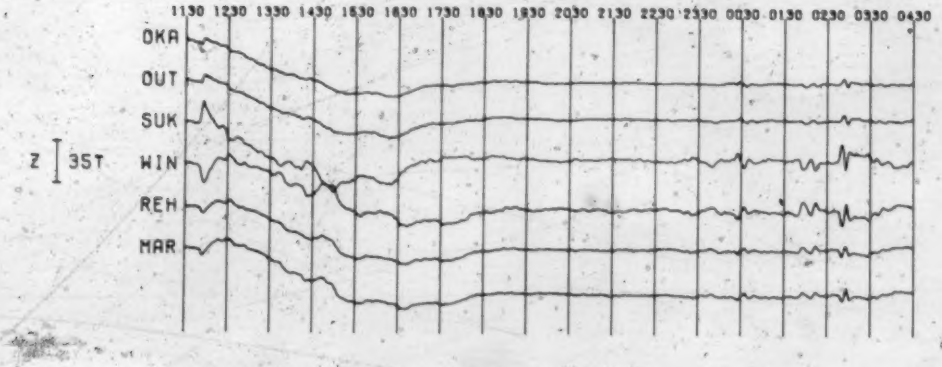

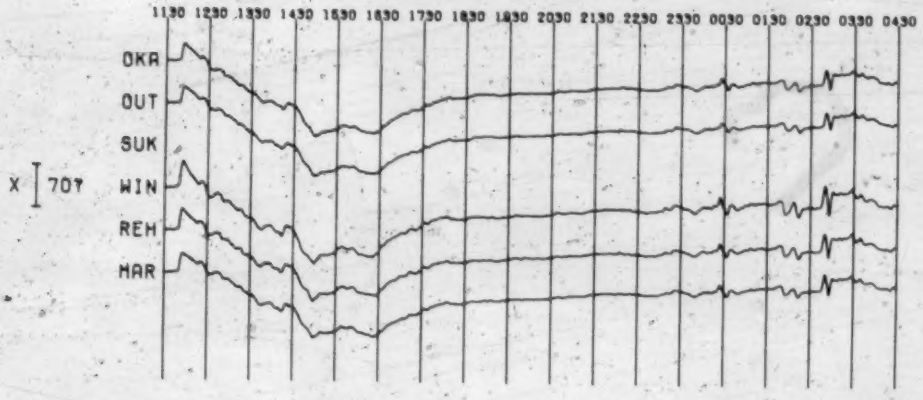

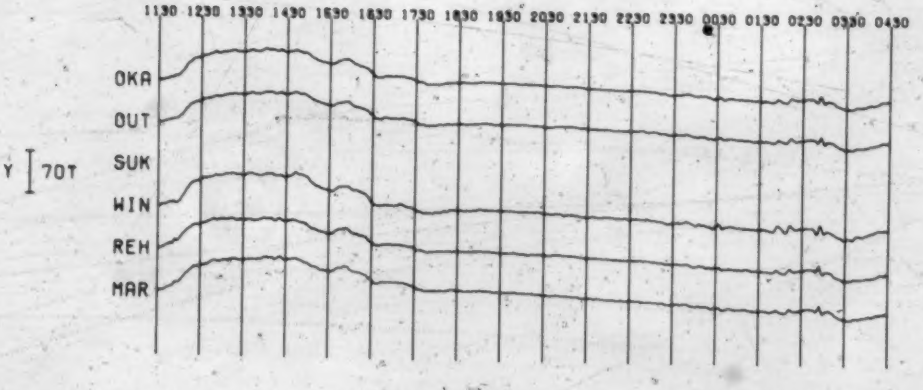

Figure 4.4b Magnetograms of an event January 21, 11.30-January 22, 04.30 G.M.T., Stack 2.

JANUARY 21 AND 22, 1972

STACK 2

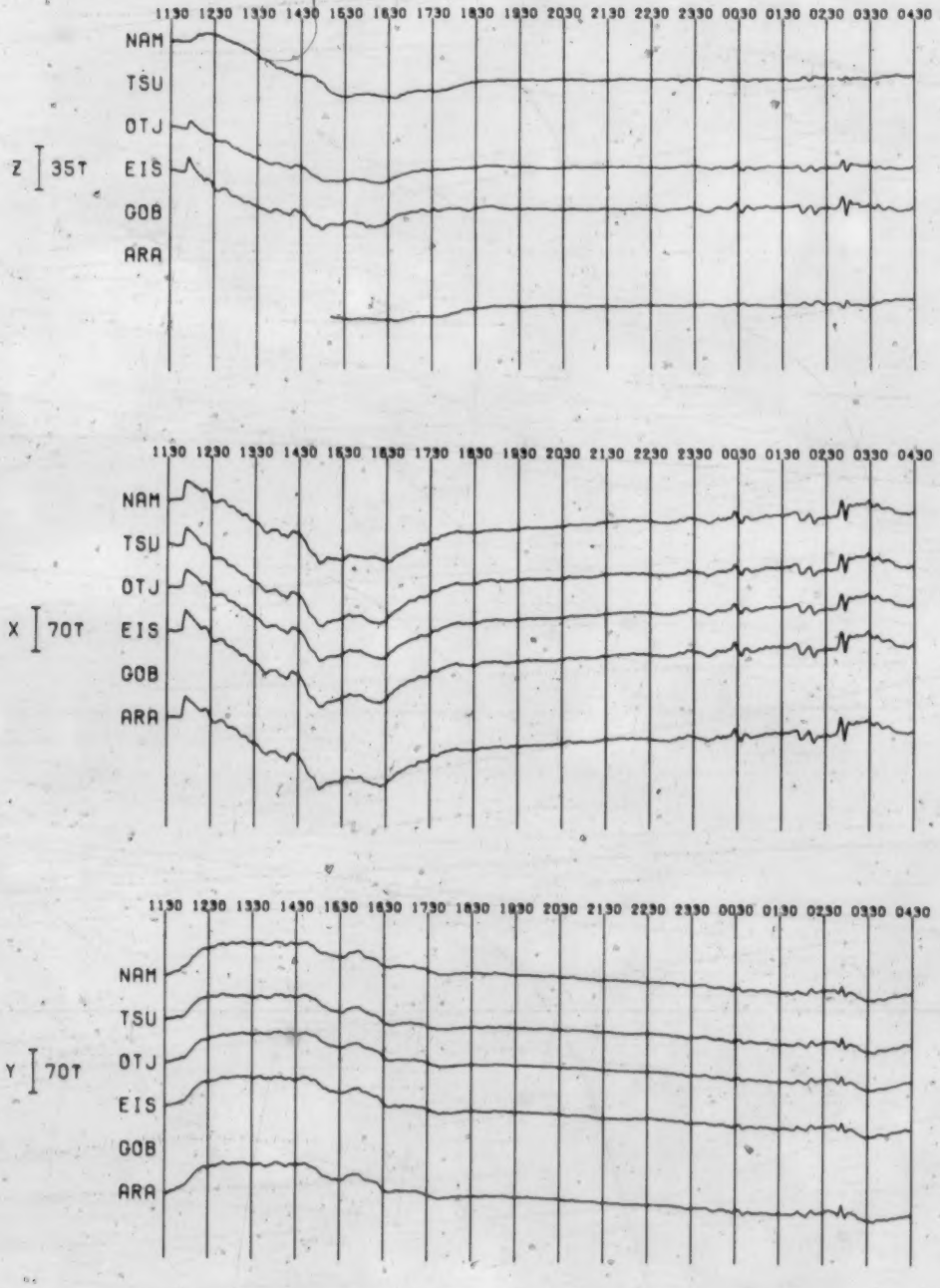

Figure 4.4c Magnetograms of an event, January 21, 11.30-January 22, 04.30 G.M.T., Stack 3.

JANUARY 21 AND 22, 1972

STACK 3

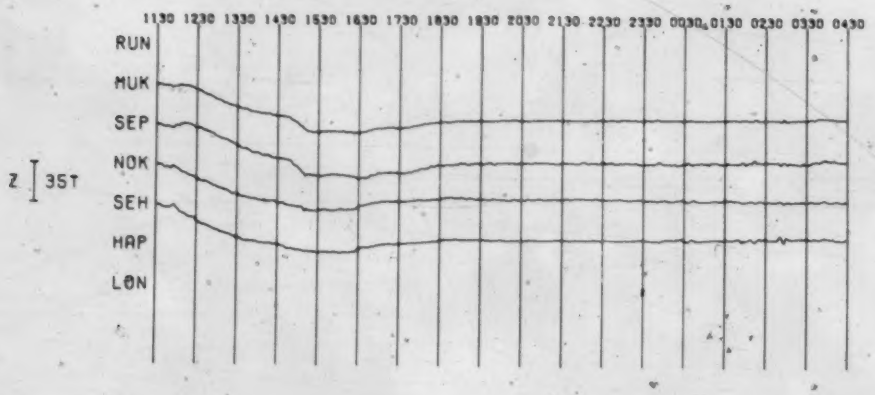

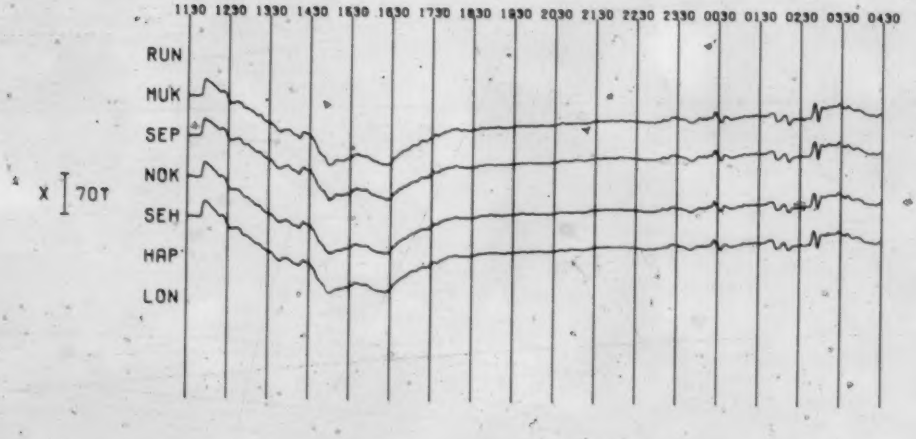

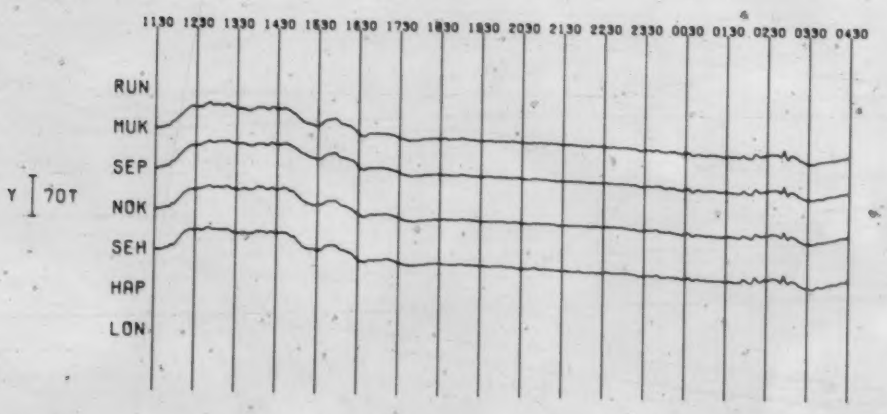

Figure 4.4d Magnetograms of an event January 21, 11.30-January 22, 04.30 G.M.T., Stack 4.

JANUARY 21 AND 22, 1972

STACK 4

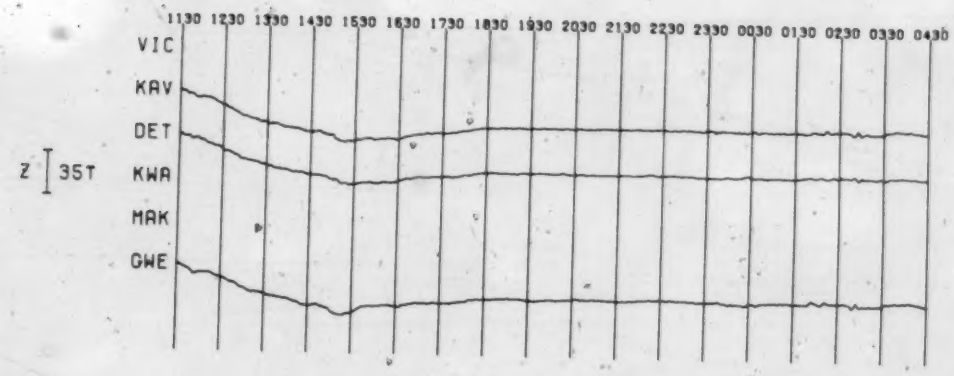

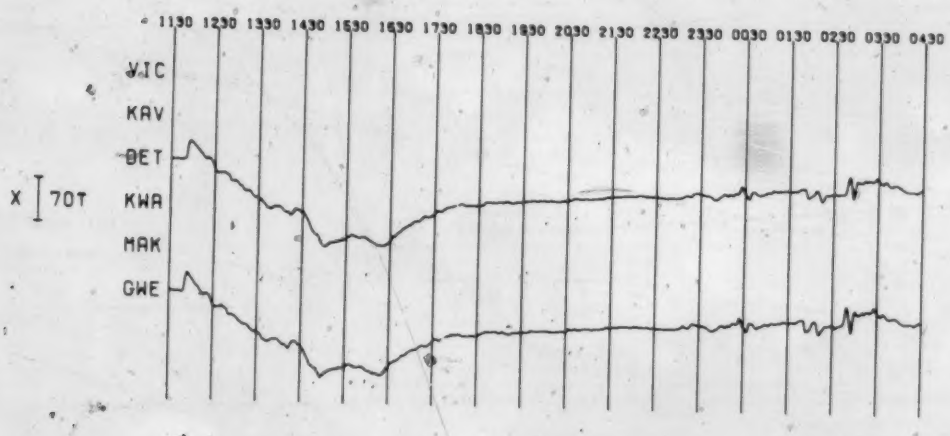

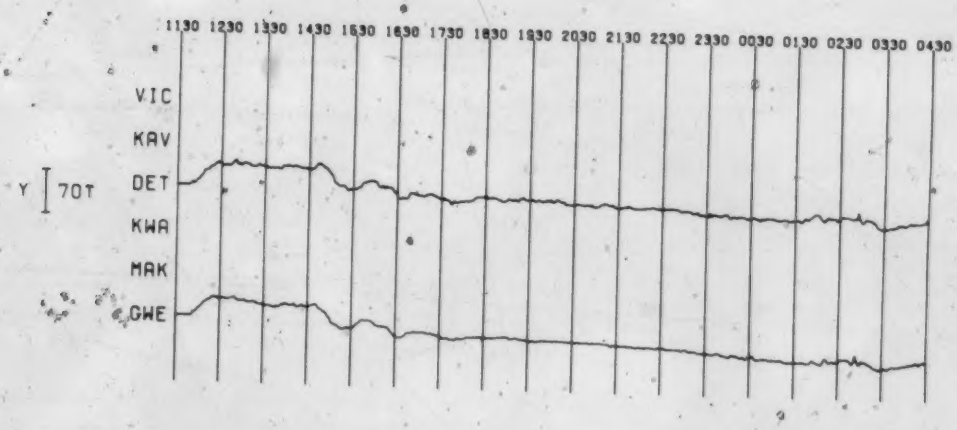

Figure 4.5 Magnetograms of a magnetic disturbance 14.30-22.30 G.M.T., January 28, 1972. This event was recorded with more than 90% efficiency.

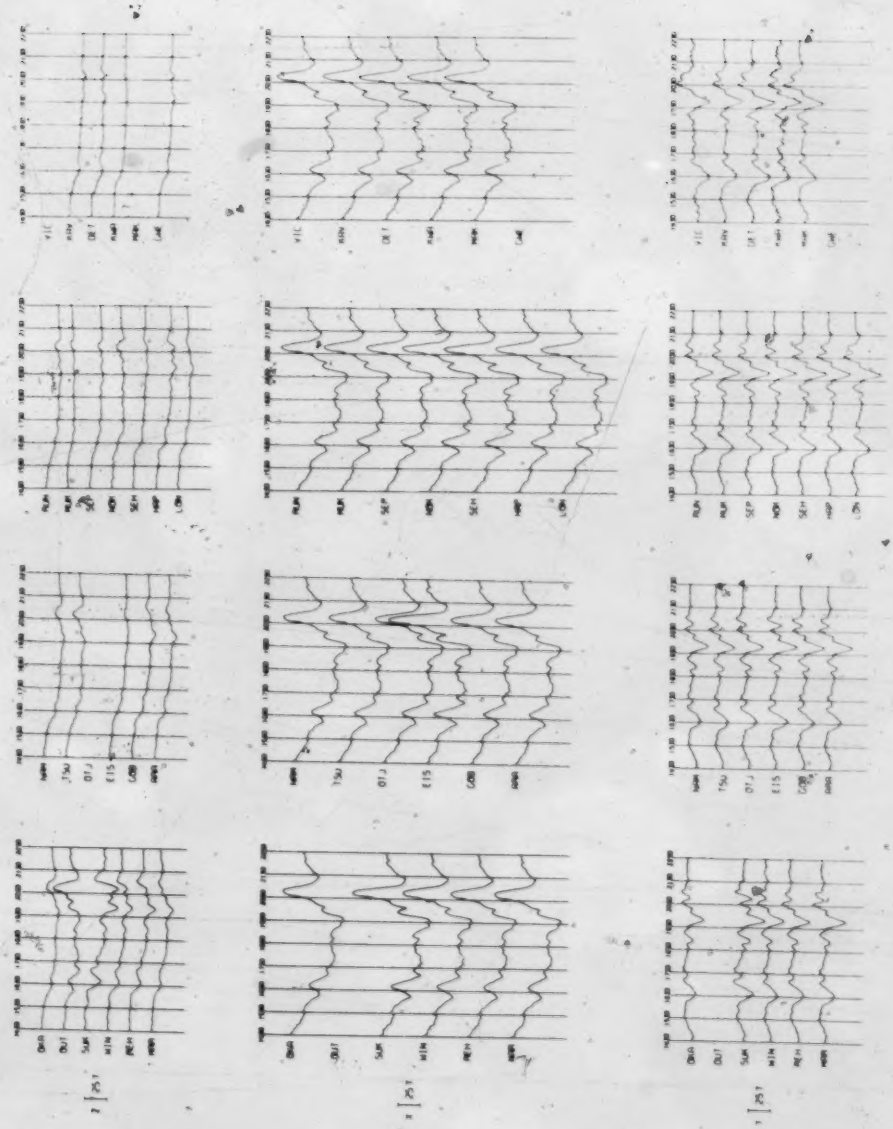
JANUARY 28, 1972
STACK 4
STACK 3
STACK 2
STACK 1

than 100 km. The waveform Z(t) at OUT bears a strong resemblance to X(t) while the short period variations at SUK seem to be 180° out of phase with those of OUT. The waveform Z(t) bears a strong resemblance to X(t) at the more western stations, and still resembles X(t) passed through a highcut filter even at the east of the array. This is particularly clear in Fig. 4.3. There is no resemblance of Z(t) to Y(t). The reversal in the vertical variation field in Z and the resemblance of its waveform to X suggest immediately that much of the Z variation field is an anomalous field resulting from induction in an east-west trending conductor between OUT and SUK.

Other features in the magnetograms are the enhancement of the X variation field at SUK and EIS indicating that the maximum concentration of induced current must be nearly beneath these stations, and the small amplitudes of the normal vertical force field in Botswana. Furthermore the high frequency variations in Z at EIS, LON, SEH and KWA show a marked attenuation which suggests that these stations are above conductive structures.

A reversal in Z is also observed between TSU and GOB, between NOK and HAP and between SEP and GWE. It is clear that reversals for short periods become phase

shifts of less than 180° for Z at larger periods, even between OUT and SUK. There is a definite phase shift between OTJ and EIS, but because the short period variations are suppressed southeast of EIS a clear reversal is not seen. In Stack 3 there is a phase shift between NOK and LON. This fact and a too large separation between magnetometer stations may be the major reasons why the conductor is less obvious in Stacks 2-4.

4.3 Maps of Fourier spectral components

Maps of Fourier transform amplitudes and phases were introduced in the first array study by the Alberta and Dallas groups (Gough, 1973) and serve two main purposes. Firstly they give a great deal of qualitative and some first order quantitative information, and secondly, they form the basis of any further quantitative interpretation.

Four sequences were selected for Fourier transformation from the three data sets. The event of January 16 was transformed over the time interval 14.00-18.00 G.M.T. and the event of January 21-22 over the interval 11.30-19.30 G.M.T. on January 21. The event of January 28, which was the one most successfully recorded, was transformed over the intervals 14.30-22.30 G.M.T. and 17.30-22.30 G.M.T. Figures 4.6 and 4.7 show amplitude

Figure 4.6 Fourier amplitude spectra in the period range 20-250 min for 14.00-18.00 G.M.T., January 16, 1972, for the stations OKA, EIS and DET.

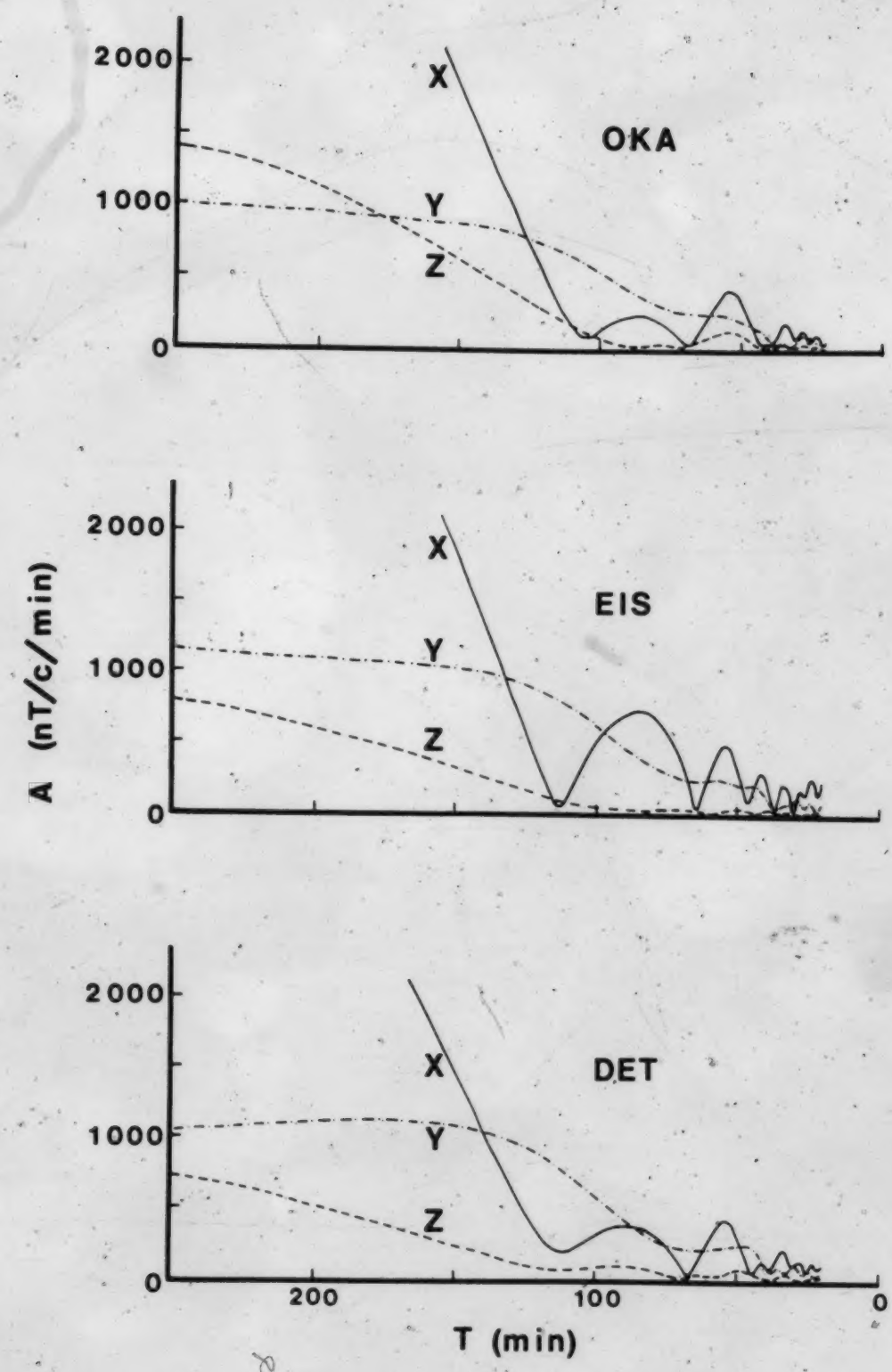
2000
1000
0
X
Y
Z
OKA
EIS
DET
A (nT/c/min)
200
100
0
T (min)

Figure 4.7 Fourier amplitude spectra in the period range 20-240 min for 17.30-22.30 G.M.T., January 28, 1972, for the stations OKA, DET and ARA.

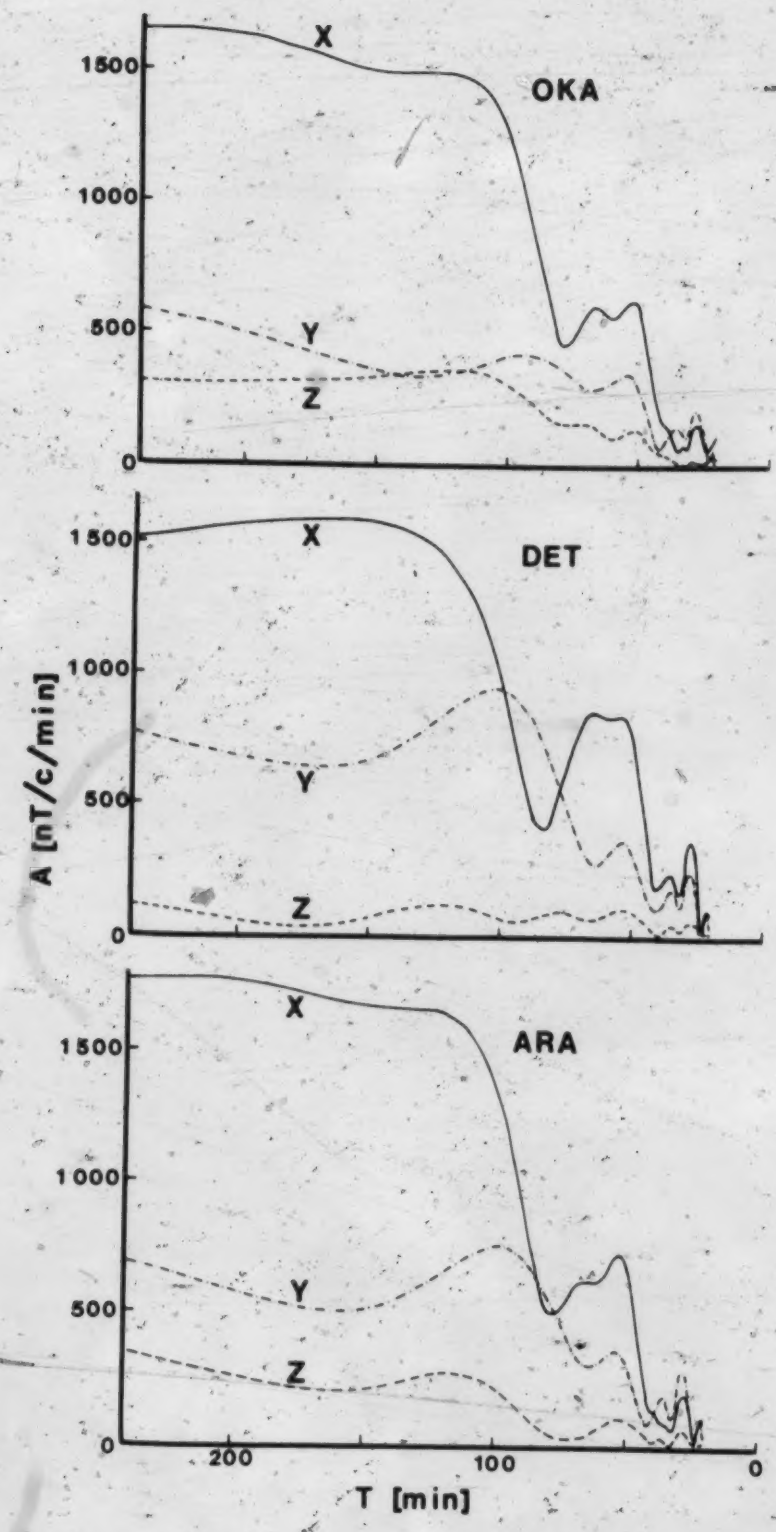
X
Y
Z
OKA
DET
ARA
1500
1000
500
0
A [nT/c/min]
200
100
0
T [min]

spectra for the time periods 14.00-18.00 G.M.T. January 16 and 14.30-22.30 G.M.T. January 28 for three stations.

Periods with spectral peaks for Z and an associated peak in either X or Y, but very often in both, were chosen and contour maps of amplitudes and phases at these periods were prepared according to techniques described by Reitzel et al. (1970) and Camfield et al. (1971) and also discussed in Section 2.2. Eleven sets of maps, each containing three amplitude and three phase maps, were drawn. The period range covered is 21-171 min. The polarization of the horizontal field was elliptical for the 11 periods mapped. The azimuth of the major axis ranged from N 60°W to N 17°E.

The sets of Fourier maps shown in Figs. 4.8-4.13 have been chosen as representative of the 11 sets of maps. These maps cover the period range 21-120 min and an azimuth range of N 60°W - N 13°E. Only maps transformed from the two sections of the January 28 event are presented because the stations in the eastern part of the array recorded this event most efficiently. In the western part of the array where the three events were equally well recorded, the contour maps show the same features in all 11 sets of maps, but in the east the maps for the January 28 event show more detail because of the availability of more data.

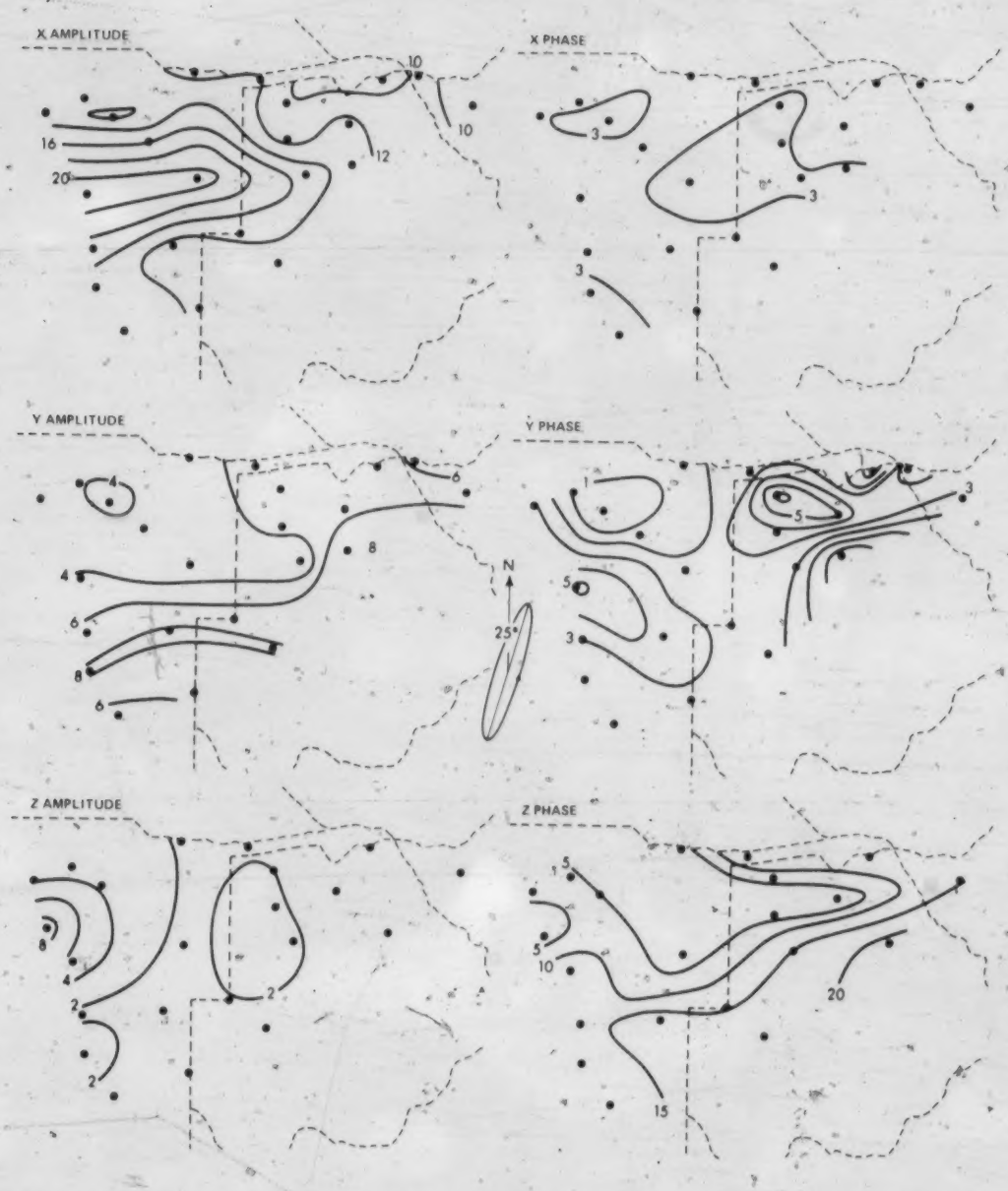

Figure 4.8 Fourier transform amplitudes (nT/c/min × 10) and phases (min) at period 21 min for 14.30-22.30 C.M.T., January 28, 1972. Estimates for the standard deviations in the X, Y and Z components are respectively 30, 30, 16 nT/c/min for the amplitudes and 1.5, 3.5 and 2.5 min for the phases. The polarization of the horizontal field is indicated.

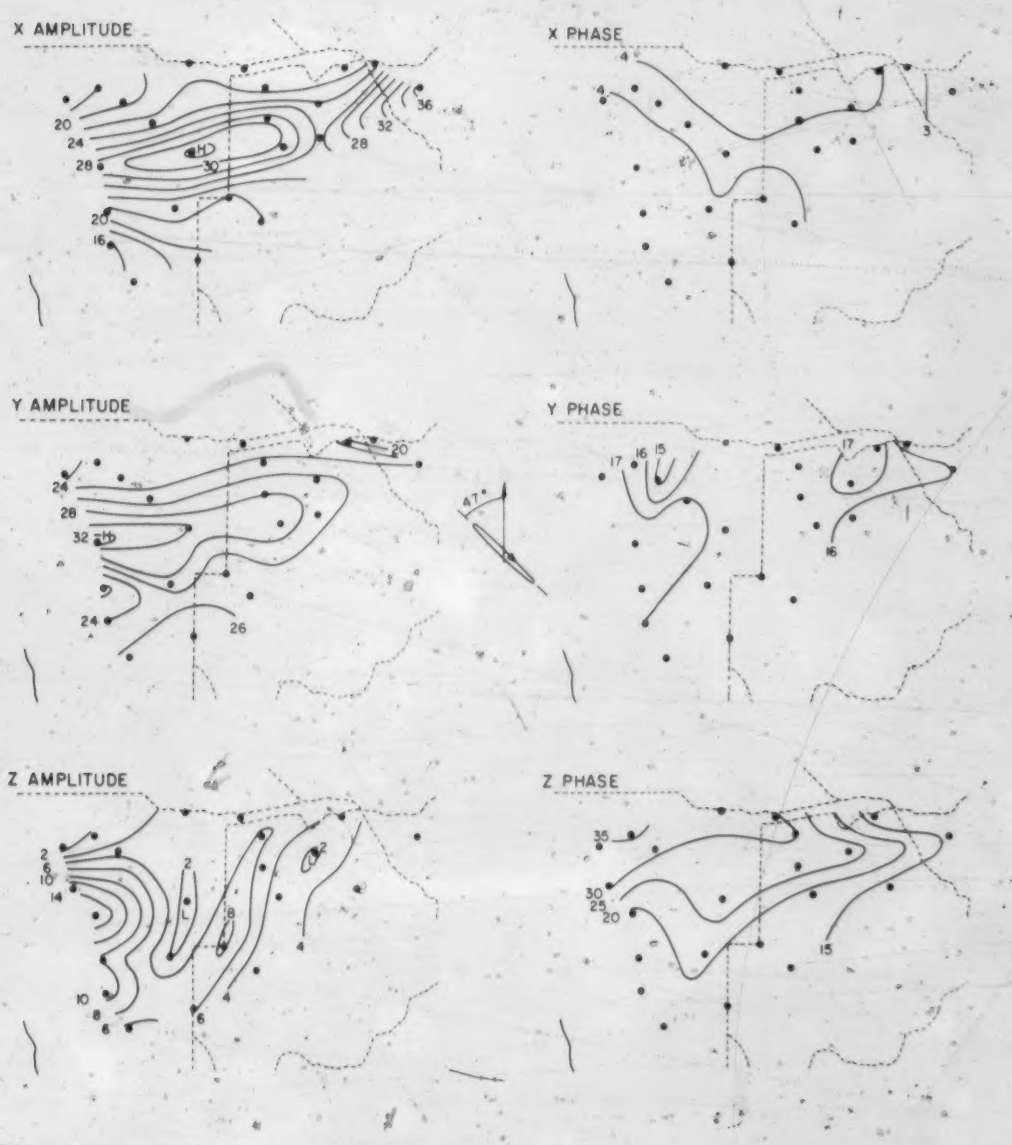

Figure 4.9 Fourier transform amplitudes (nT/c/min × 10) and phases (min) at period 28 min for 17.30-22.30 G.M.T., January 28, 1972. Estimates for the standard deviations in the X, Y and Z components are respectively 25, 29 and 13 nT/c/min for the amplitudes and 1.5, 1 and 2.5 min for the phases. The horizontal field polarization is indicated.

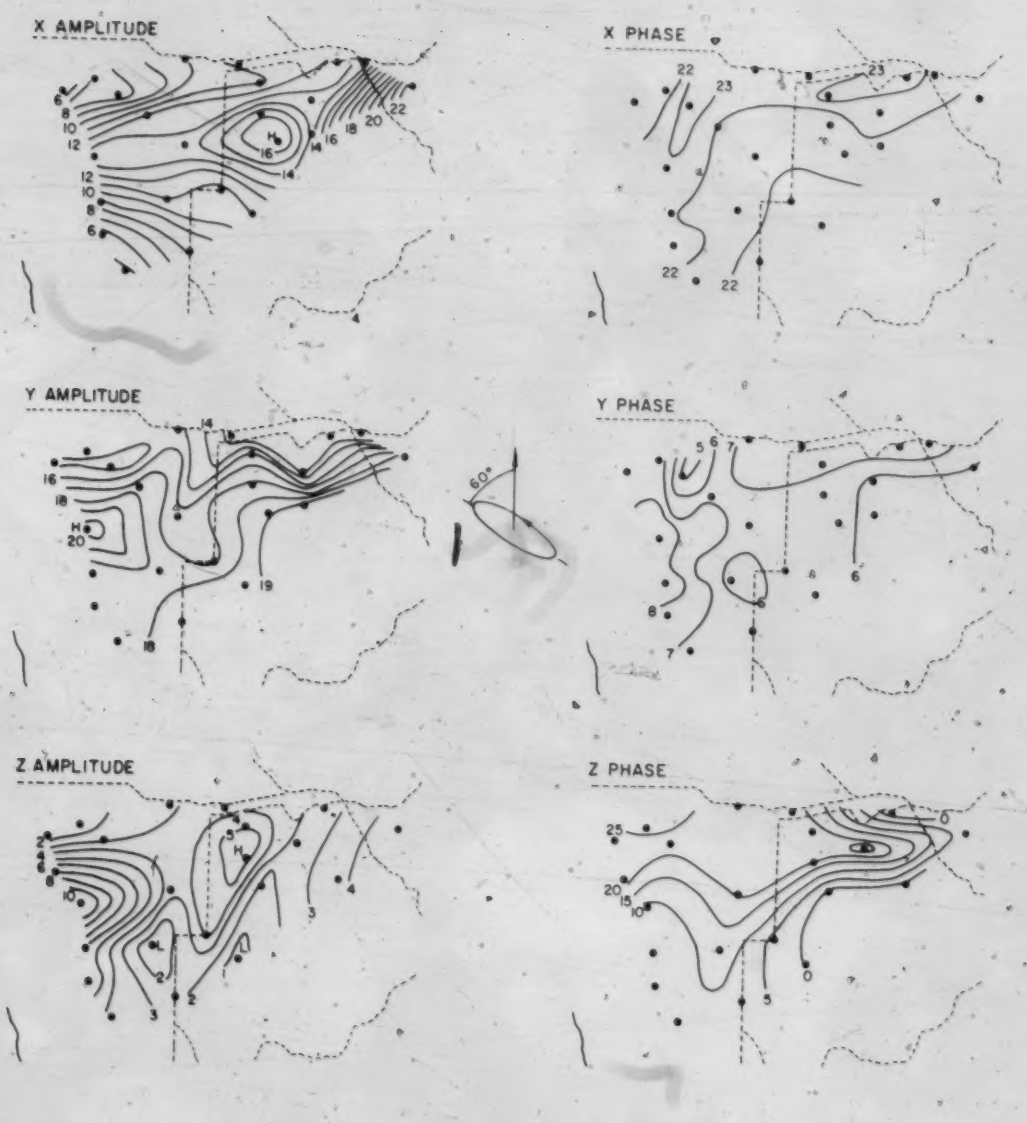

Figure 4.10 Fourier transform amplitudes (nT/c/min × 10) and phases (min) at period 35 min for 17.30-22.30 G.M.T., January 28, 1972. Estimates for the standard deviations in the X, Y and Z components are respectively 24, 24, 16 nT/c/min for the amplitudes and 3, 1.5 and 4 min for the phases. The horizontal field polarization is indicated.

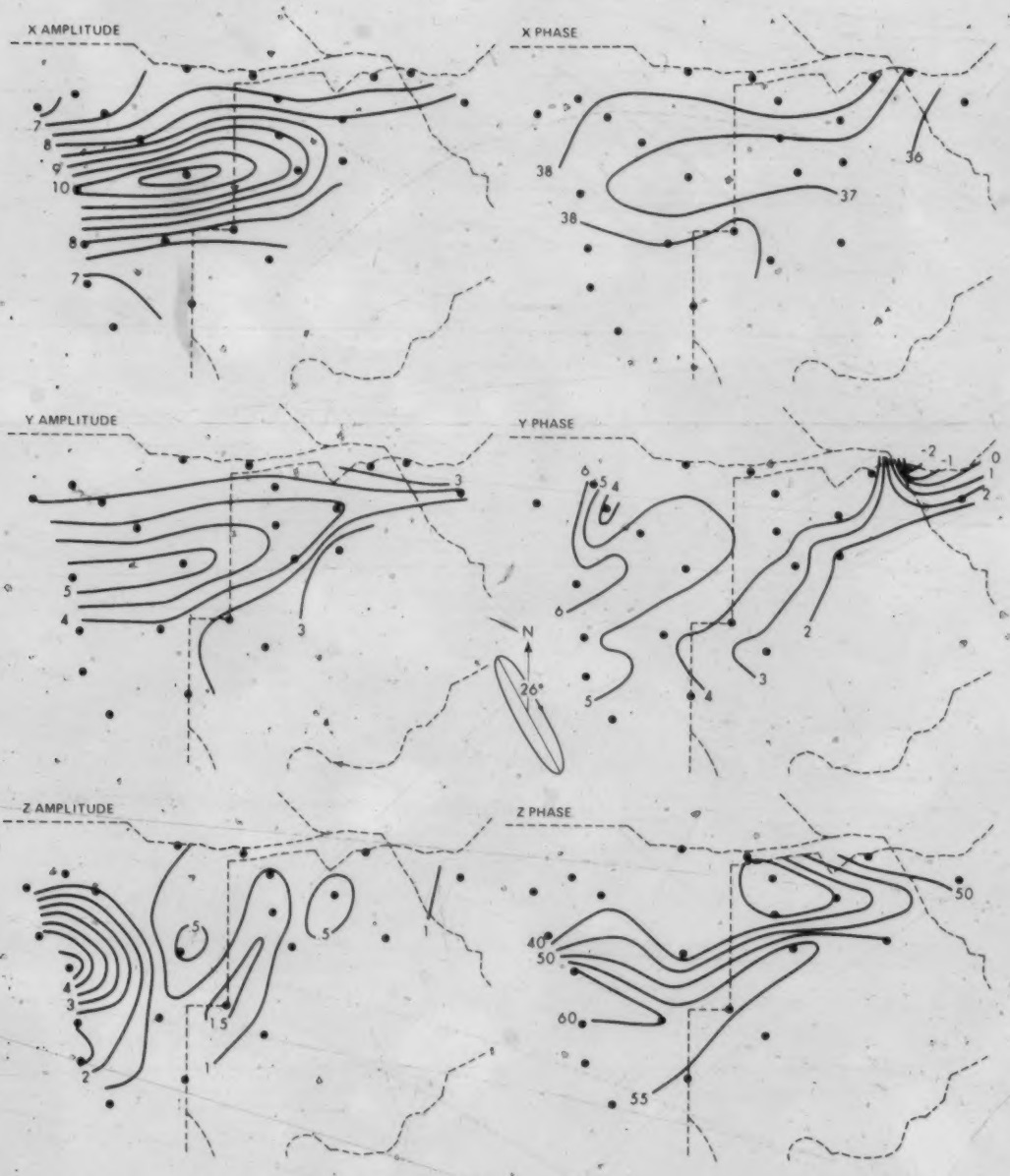

Figure 4.11 Fourier transform amplitudes (nT/c/min × 100) and phases (min) at period 54 min for 17.30-22.30 G.M.T., January 28, 1972. Estimates for the standard deviations in the X, Y and Z components are respectively 26, 30 and 14 nT/c/min for the amplitudes and 1, 1.5 and 1.5 min for the phases. The horizontal field polarization is indicated.

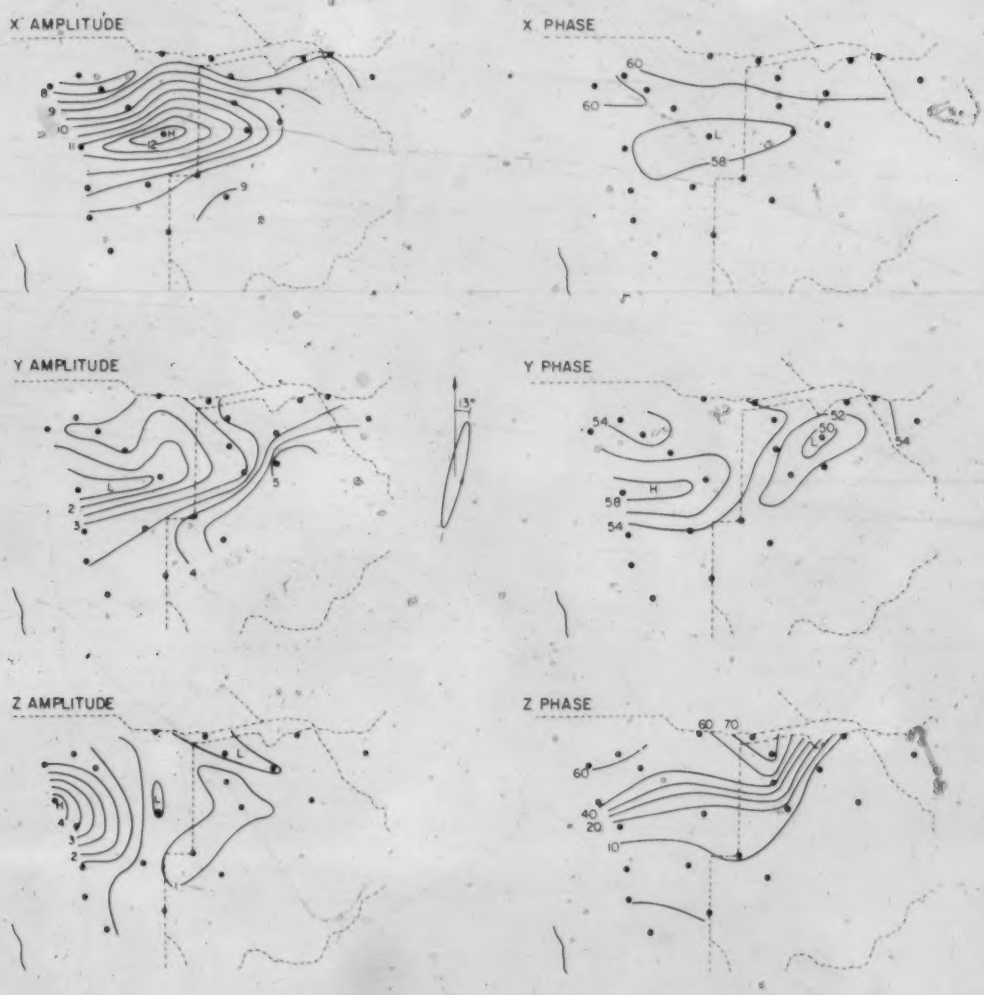

Figure 4.12 Fourier transform amplitudes (nT/c/min × 100) and phases (min) at period 79 min for 14.30-22.30 G.M.T., January 28, 1972. Estimates for the standard deviations in the X, Y and Z components are respectively 32, 37 and 20 nT/c/min for the amplitudes and 1, 2 and 2 min for the phases. The polarization of the horizontal field is indicated.

JANUARY 28, 1972. T=120 MIN.

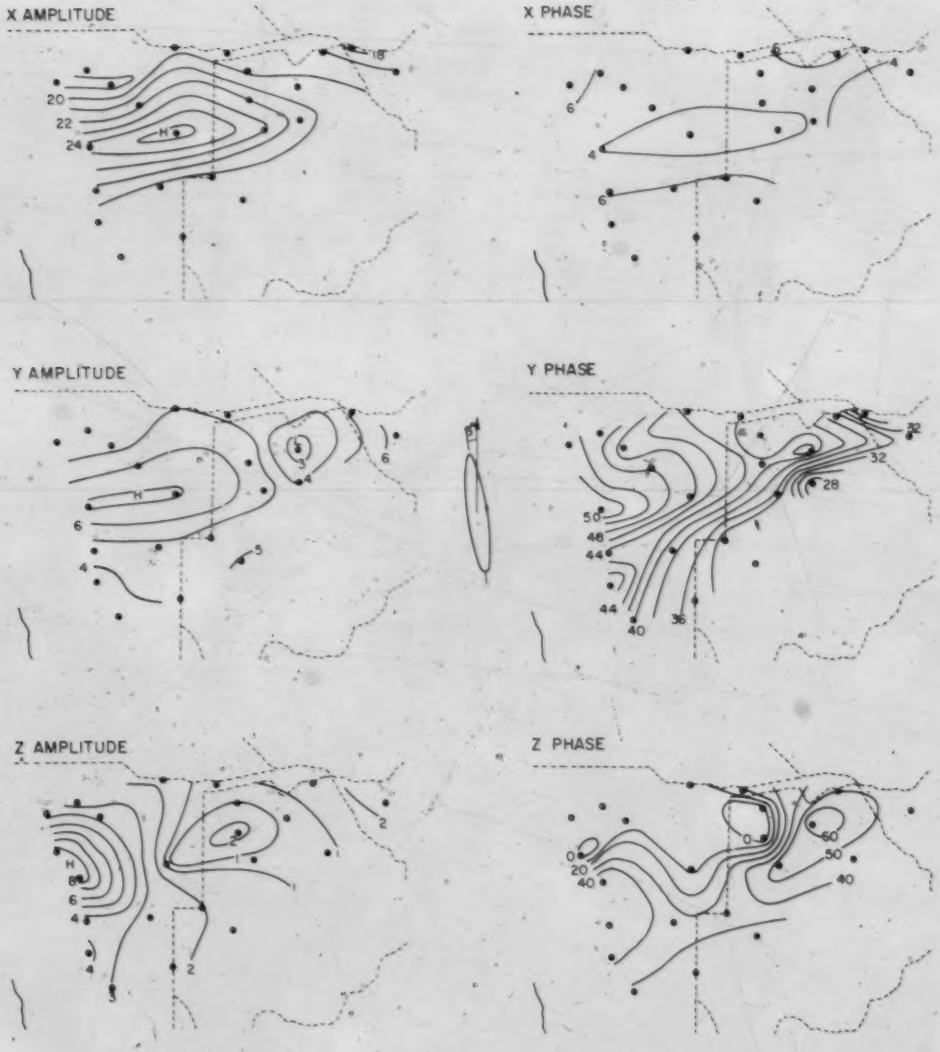

Figure 4.13 Fourier transform amplitudes (nT/c/min × 100) and phases (min) at period 120 min for 14.30-22.30 G.M.T., January 28, 1972. Estimates for the standard deviations in the X, Y and Z components are respectively 46, 36 and 25 nT/c/min for the amplitudes and 1.5, 2 and 2 min for the phases. The horizontal field polarization is indicated.

All the X amplitude contour maps show a prominent anomaly in X elongated in an east-west direction. The stations SUK, EIS and SEH are situated near the maximum of this component.

Seven of the Y component contour maps have a maximum at SUK and EIS coinciding with the maximum in X. The horizontal field was polarized north-west - south-east (Figs 4.9, 4.10, 4.11, 4.13) for most of these periods. This component increases to a local maximum at the south-eastern edge of the array (Figs 4.8, 4.9, 4.11 and 4.12) in five of the Y amplitude contour maps. For the two largest periods mapped, T = 120 and 171 min, the Y component amplitude maps show a minimum at KWA in the eastern part of the array (Fig. 4.13). Both these periods have the horizontal field polarized slightly west of north (Fig. 4.13). Maps for five other periods with a polarization east of north show a local maximum at KWA (Fig. 4.12) in the Y component.

The Z amplitude contour maps are more complicated than those for the X and Y components. A maximum in Z occurs at the stations SUK and OUT on the western edge of the array for all the Z amplitude contour maps compiled (Figs 4.8-13). A second smaller maximum in Z is present at REH near the south-western corner of the array.

The Z amplitudes in the eastern half of the array are invariably smaller than those in the western half. In the eastern half the Z amplitude anomalies are also polarization dependent. With the horizontal field polarized west of north SEP, NOK and HAP show a local maximum and SEH and KWA minima as in Figs 4.9-11 and 4.13. These anomalies become less prominent for the horizontal field polarized more towards the north-east as in Figs 4.8 and 4.12. The maximum at SEP and NOK for the horizontal field polarized north-west - south-east is in agreement with a curved conductor trending east-west in the western part of the array and curving north-east - south-westward in the eastern part of the array (Gough et al., 1972). Some features in the eastern part of the array may not be very well defined due to the instrument spacing.

The phase maps for the X and Y components appear to represent mainly the normal field and to be uninformative of internal structure. The Z phase maps are, however, of considerable interest. Although the Z phase values could have large errors in the eastern third of the array because the Z amplitudes are small there, all the Z phase maps and Table 4.2 show that there are large phase changes between the stations OUT and SUK, TSU and GOB, NOK and HAP, and between SEP and GWE. In

Table 4.2

Phase Differences for Z

	T min	OUT-SUK Δφ deg	TSU-GOB Δφ deg	NOK-HAP Δφ deg	SEP-GWE Δφ deg
January 16	23	+172	+144		+170
	51	-162	- 94		- 69
January 21	73	- 43	- 77		- 88
	114	-156	-123		-113
	171	-160	+ 17		+ 8
January 28	21	+169	+157	+215	+118
	28	+154	+139	+182	+232
	35	+144	+116	+169	+238
	54	-173	-150	-154	-113
	79	-159	-142	-172	- 46
	120	-159	- 98	-139	-139

terms of the simple assumption of a current flowing under the maximum gradient in Z phase and along the contours of the maps, Figs 4.8-13 and Table 4.2 suggest a current along a curved conductor passing between OUT and SUK near EIS, SEH and KWA, and thus substantiate the suggestions offered by the magnetograms and amplitude maps. Gough, Lilley and McElhinny (1972) pointed out that a curved conductor produces Z amplitude anomalies which are strongly dependent on the azimuth of the polarization. Since actual substorm fields are elliptically polarized, the phase difference between the X and Y components will enter into the problem (Bennett and Lilley, 1972; Gough, McElhinny and Lilley, 1974). Due to these complications it is necessary to work in terms of a parameter of Earth response to incident fields which preserves phase and amplitude information. Transfer functions between the components meet the need. Transfer functions as used by Schmucker (1964, 1970a) were thus computed in order to clarify the conductivity structure in the area.

4.4 Transfer functions

The array was situated at a magnetic latitude at which the normal Z component in substorm fields is relatively small. If it is assumed that the Z variation

fields are mainly anomalous, it is justifiable to calculate transfer functions from estimated normal horizontal components X_n and Y_n to Z. Although this method avoids inversion of the full transfer function matrix which relates each anomalous component to each normal component (a procedure which requires a full separation of normal and anomalous fields), it should be handled with care because a systematic Z-H correlation in the normal fields could affect the calculations adversely (Schmucker, 1964).

The transfer functions between the Z component (assumed anomalous) at a particular station and the estimated normal X component were calculated using the relations of eq. 2.27. As discussed in Section 2.5 the real part of the transfer functions z_x and z_y were combined to yield an in-phase 'induction vector'. This induction vector was as usual reversed to be in the same sense as a Parkinson arrow (Parkinson, 1959, 1962) so that it points towards a good conductor in which the current flows in phase with the normal field. Similarly the imaginary parts of z_x and z_y were combined to yield a quadrature-phase 'induction vector'. To be consistent with the in-phase induction vector, the sense of the quadrature-phase vectors were reversed as well to point towards conductors in which the current leads the normal fields in phase. In the 1971 array study the quadrature-

phase induction vectors as shown in Fig. 3.11 were not reversed.

Nine 120 min events which had been recorded in three components at 13 stations were selected from the three main events studied. These are listed in Table 4.3. Various combinations of six of the nine events had been recorded at 18 stations. Transfer functions computed from nine and six events recorded at the 13 stations yielded similar results. The induction vectors derived from all nine events, except at RUN, EIS, NOK and GOB where induction vectors are computed from the events of January 16 and 28 and at OTJ where they are computed from the events of January 16 and 21 are presented in Fig. 4.14. Four different periods are shown. For each spectral term of each event an estimate of the normal field in X and Y was made by taking the mean cosine and sine Fourier coefficients over all these stations.

The reversal in both the in-phase and quadrature-phase induction vectors clearly indicates a linear curved conductor underlying the array. The quadrature-phase induction vectors are generally smaller than the in-phase induction vectors. Along the western margin the quadrature-phase induction vectors for T = 43 min and T = 128 min tend to indicate the east-west conductive structure, while the in-phase induction vectors show a strong deflection

Table 4.3

Two-hour Events Used in Calculating Transfer Functions

Date	G.M.T.
January 16, 1972	14.00 - 16.00
	16.00 - 18.00
	18.30 - 20.30
January 21, 1972	11.30 - 13.30
	13.30 - 15.30
	01.30 - 03.30
January 28, 1972	15.30 - 17.30
	17.30 - 19.30
	19.30 - 21.30

Figure 4.14 In-phase (solid) and quadrature-phase (broken) induction vectors representing the transfer functions z_x and z_y at periods 14 min, 26 min, 43 min and 128 min.

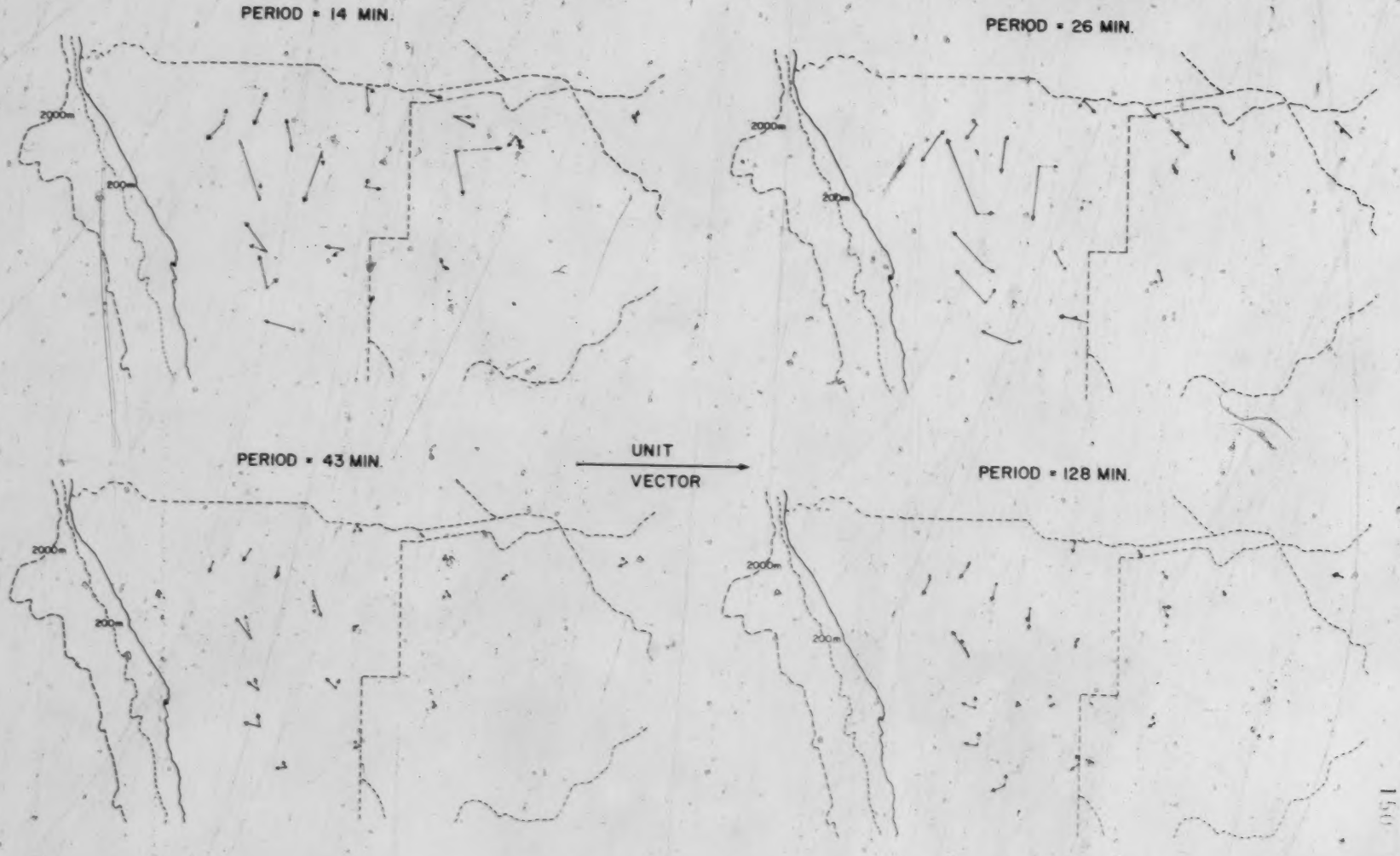
PERIOD = 14 MIN.
PERIOD = 26 MIN.
PERIOD = 43 MIN.
UNIT
VECTOR
PERIOD = 128 MIN.
2000m
200m

towards the coast. This deflection of the in-phase induction vectors is to a lesser degree also present for T = 14 min and T = 26 min, but the directions of the quadrature-phase induction vectors are more scattered for these periods.

This separation of the in-phase and quadrature-phase induction effects seems to indicate a structure with high reactance off the western edge of the array, while the east-west structure in the western half of the array has a low inductive reactance compared to its resistance.

4.5 Normalized anomalous fields

Profiles of normalized anomalous fields were constructed for the section A-B along the western margin of the array (Fig. 4.1) and the section C-D near the eastern edge of the array. Since anomalous fields cover most of the array, the stations OKA, NAM, MAR, ARA were arbitrarily designated as representing normal field components. The mean X amplitude from these stations was used to define the assumed inducing field along the profile AB and, as residuals, the anomalous horizontal components X_a at other stations along the section. For the profile CD the horizontal component 45° west of north of the same four stations was designated as

representing the "normal" or inducing field. This component is parallel to the induction vectors in the area. The mean Z amplitude at these stations was deducted from Z at every other station on the profiles to give an estimate of the anomalous vertical field Z_a. Under these assumptions Z_a/X_n and X_a/X_n were determined along the profile. Since the amplitudes of the anomalies showed a marked dependence on the polarization of the horizontal inducing field, Fig. 4.15 shows the profiles along AB for which the inducing field was polarized west of north and Fig. 4.16 shows those for which the inducing field was polarized east of north.

The most prominent feature in these profiles is the reversal in Z_a/X_n between OUT and SUK and the associated maximum of X_a/X_n (unfortunately the X component at OUT did not function).

It is clear that the anomaly has larger amplitudes especially in Z_a/X_n for the horizontal field polarized with an azimuth west of north, which is in agreement with a northward swing in the conductor further east. The ratio of X_a/X_n is not very different in the two diagrams, except for T = 35 min where X_a/X_n is very large. This is most probably because the azimuth of its horizontal field polarization is the furthest west.

Figure 4.15 Normalized anomalous variation field components Z_a/X_n and X_a/X_n along section AB (Fig. 4.1) for periods 54 min (event of January 16, 1972), 28, 35 and 120 (event of January 28, 1972). For all these periods the horizontal field polarization is west of north.

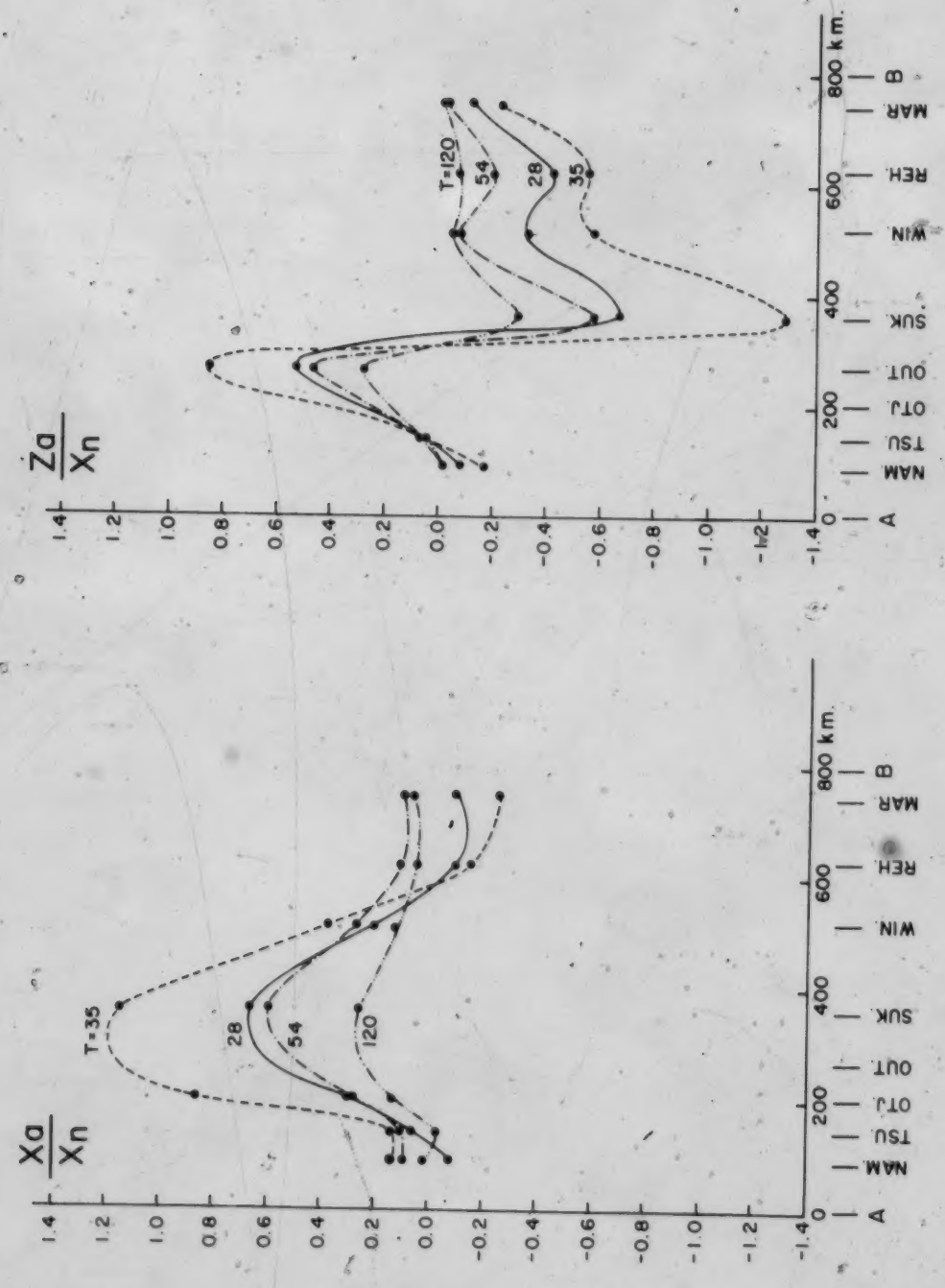
Za/Xn
T=120
54
28
35
A
NAM
TSU
OTJ
OUT
SUK
WIN
REH
MAR
B
800 km.
Xa/Xn
T=35
28
54
120

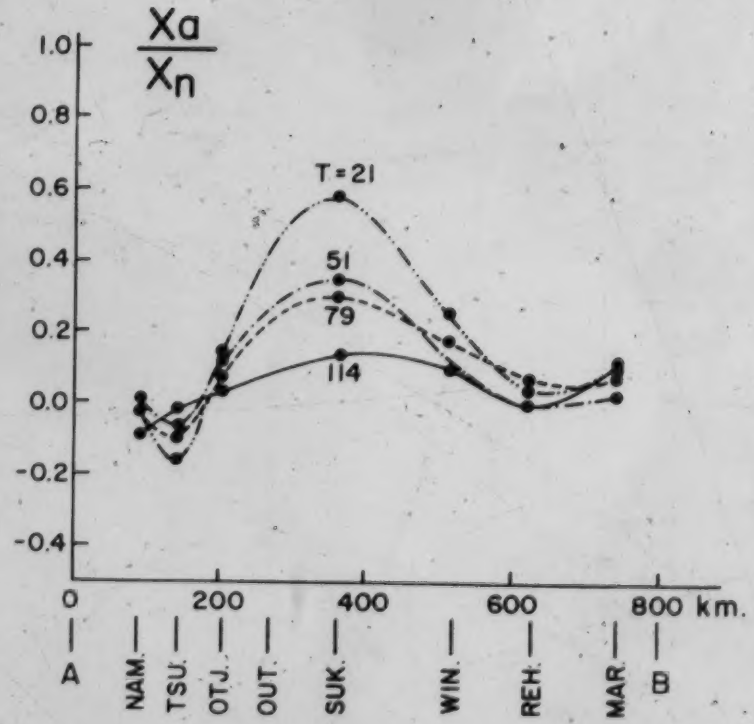

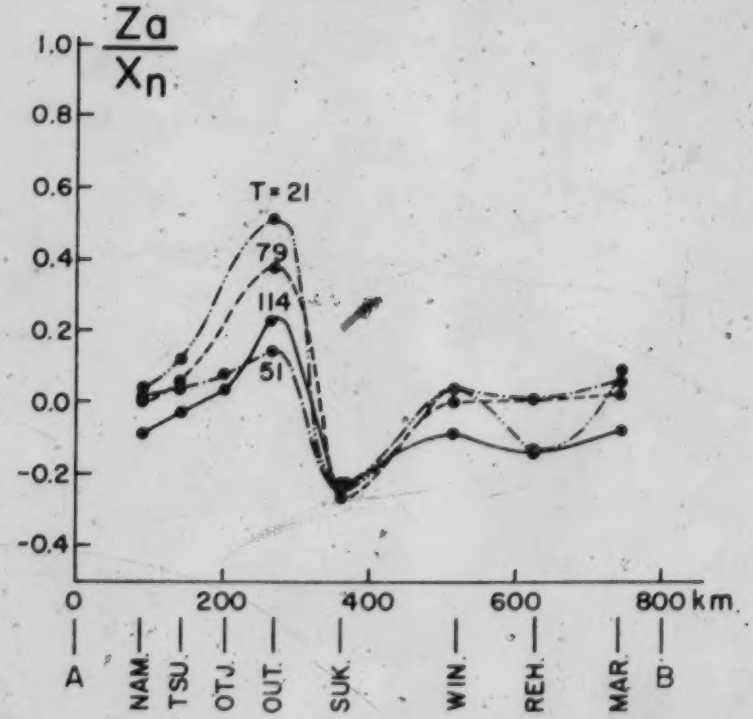

Figure 4.16 Normalized anomalous variation field components Z_a/X_n and X_a/X_n along section AB (Fig. 4.1) for periods 51 min (event January 16, 1972), 114 min (event January 21, 1972), 21 min and 79 min (event January 28, 1972). For all these periods the horizontal fields were polarized in a direction east of north.

The amplitudes of X_a/X_n and Z_a/X_n decrease with increasing period, with T = 35 min again an exception.

For the section CD the average horizontal field component in a direction 45° west of north for the stations OKA, NAM, MAR and ARA (the "normal" stations for profile AB) was designated as representing the "normal" or inducing field, H_n. This component of the horizontal field parallels the induction vectors along the section. The average vertical component at the above-mentioned stations represents the "normal" vertical component Z_n. These values of H_n and Z_n were subtracted from H (the horizontal component 45° west of north) and Z at every station along the profile to give estimates of H_a and Z_a. Figure 4.17 shows eight normalized anomalous profiles H_a/H_n and Z_a/H_n at eight different periods together with the average polarization of the horizontal field for that period. The profiles are arranged so that those that have polarizations west of north are on the left side of the diagram and those with polarizations east of north on the right.

All profiles show a maximum in Z_a/H_n at or near the station NOK, with a decrease in Z_a/H_n further south-eastward. Except for T = 54 min, all profiles indicate a maximum in H_a/H_n to the south-east of the

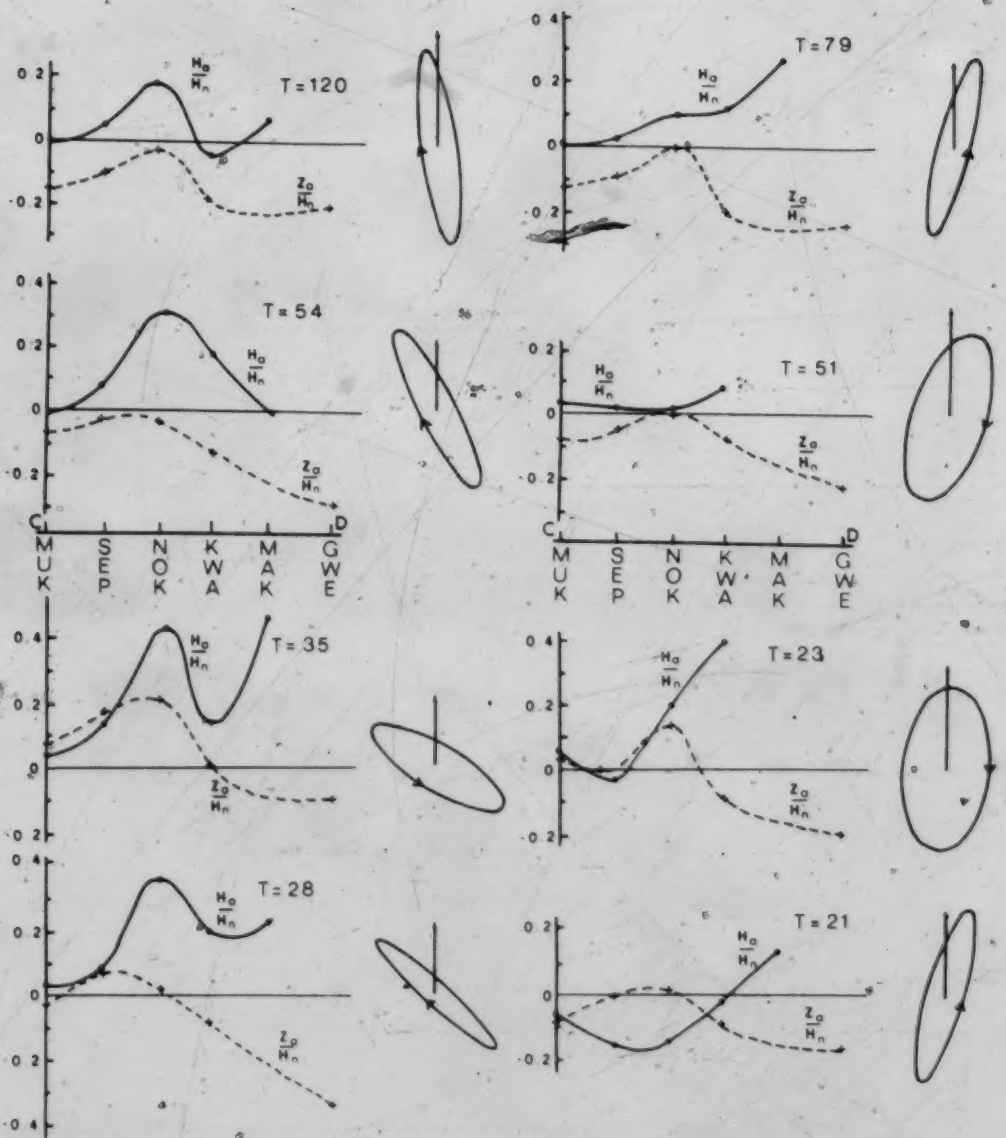

Figure 4.17 Normalized anomalous variation field components Z_a/H_n and H_z/H_n^* along the section CD (Fig. 4.1) at periods 23 min, 51 min (event of January 16, 1972), 21 min, 28 min, 35 min, 54 min, 79 min and 120 min (event of January 28, 1972). The polarization of the horizontal field is shown for each period.

station MAK. The main difference between the profiles of different horizontal field polarizations is the maximum in H_a/H_n at NOK for all profiles with polarizations west of north. At a period of 79 min with the horizontal field polarized NNE there is an indication of this feature, but for all other periods having inducing field polarized east of north, there is no maximum in H_a/H_n at NOK. This behaviour most probably indicates that the north-east trending branch of the conductor consists of more than one parallel conductor.

4.6 Discussion

The magnetograms, maps of Fourier spectral components, transfer functions and normalized anomalous fields all show a conductor with axial line approximately in the position indicated in Fig. 4.2. The position of the conductor is not very well defined near the eastern edge of the array. When the attenuation in Z at LON, the anomaly pattern along profile CD and the high Y amplitude values near the south-eastern margin of the array for certain periods and polarizations are considered it is quite possible that there are more than one conductor in the eastern half of the array. This can only be established by further studies in the area. The east-west trending conductor joins the NE-SW branch

which most probably continues as far south as LON, near SEH. Although the polarization sensitive behaviour of the anomaly precludes meaningful two-dimensional modelling a maximum depth can be estimated from the half-width of the anomaly defined as the width of the X_a/X_n anomaly at half-maximum value. A line current at depth d produces a X field of width 2d at the half-maximum value, and a Z field with extrema 2d apart. The actual current cannot be deeper than the line current best fitting the anomaly widths just defined (Gough, 1973b).

In this case the width at half-maximum value of X_a/X_n on profile AB is 250 km and the Z extrema are 100 km apart. This difference is due to the fact that the X component at OUT was not recorded. This reduced the definition of the X_a/X_n anomaly and the station spacing of the array was not designed to detect such narrow anomalous zones. These half-widths will indicate maximum depths of between 125 and 50 km. I am inclined to accept a maximum depth closer to the smaller depth especially if the separation of the in-phase and quadrature-phase induction vectors is considered. This separation of the induction effects seems to indicate that the east-west conductor is at a lithospheric depth. The conductive structure joins the African rift system at the eastern point of the array where it underlies the

Middle Zambezi Rift Valley containing Lake Kariba. This rift zone is the south-westward extension of the Luangwa Rift. Reeves (1972) found that the Kalahari seismic axis is indeed a well aligned extension of Zambia's Karroo-filled Luangwa Rift and the induction anomaly coincides with the seismic active areas. In Botswana the linear features in the Okavango lie parallel to the conductor, but in South-West Africa the conductive structure cuts obliquely across the general grain in the Damara Geosyncline. De Beer, Gough and Van Zijl (1975) reviewed the available geophysical and geological data in the area and concluded that the conductive zone marks an extension of the African Rift system along old weak zones in the lithosphere.

The deflection of the in-phase induction vectors towards the west could be due to the proximity of the continental edge and the Atlantic Ocean, but could also be caused by anomalous structures associated with the prominent north-south faults of Karroo to Recent age indicated in Fig. 4.2. Korn and Martin (1951) showed that most of these faults are still active. If the in-phase response is considered, however, it is clear that it is a structure with a high inductive reactance and is most probably a subcrustal conductor associated with the continental edge.

The work in this chapter has been the subject of a paper by De Beer et al. (in press).

The results of this array study will be discussed in more detail in Chapter 6.

CHAPTER V

A STUDY OF THE ELECTRIC CONDUCTIVITY STRUCTURE IN THE KAAPVAAL CRATON

5.1 Electromagnetic induction in a plane-layered Earth

The dimensions of magnetometer arrays in mid-latitudes are usually smaller than the spatial wavelengths of the inducing magnetic fields. When this is the case and there is no indication of major lateral inhomogeneities in the area under investigation, the Earth can be approximated by a plane-layered model and the problem becomes that of solving the normal equation (1.14) for plane layers. The solution of this problem is quite general and has been treated by Price (1950, 1962), by Wait (1953) and by Schmucker (1970a), among others.

In this induction problem the Earth is represented by a model with N-1 conductive layers above a conductive halfspace (Fig. 5.1). The model occupies the region $z \geq 0$ in a right-handed Cartesian coordinate system. The j-th layer ($j=1,2,\ldots,N-1,N$) of thickness $k_j = z_{j+1}-z_j$ has conductivity σ_j. The air above the surface is layer 0 and σ_0 is assumed zero. A periodic primary field with $\exp(i\omega t)$ time dependence is assumed.

Price (1962) showed that the solution of the diffusion equation (1.9) is of the form

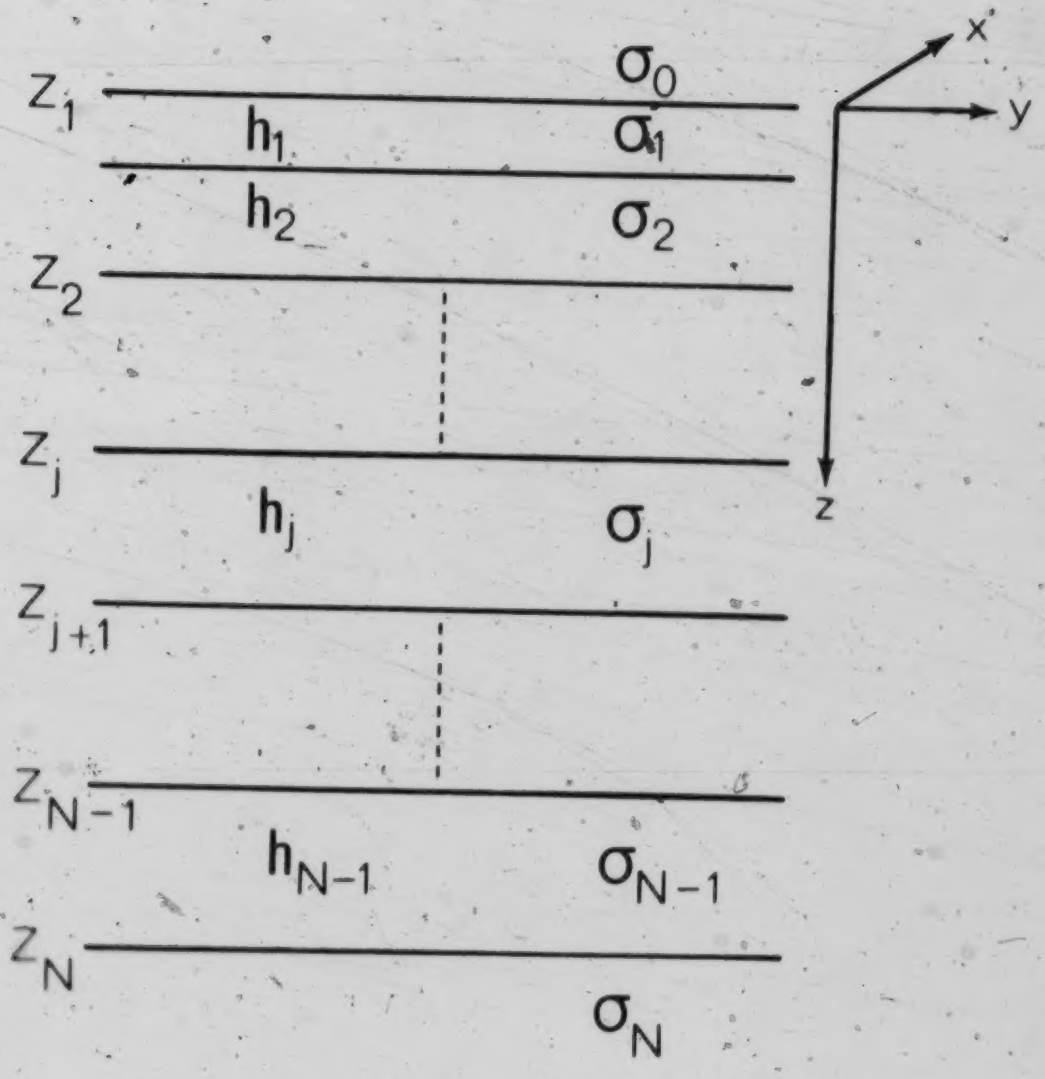

Figure 5.1 Earth model with N-1 conductive plane layers above a conductive halfspace.

$$\vec{E} = \exp(i\omega t) Z(z)\, \vec{F}(x,y) \tag{5.1}$$

where $$\vec{F}(x,y) = \left(\frac{\partial P}{\partial y}, -\frac{\partial P}{\partial x}, 0\right) \tag{5.2}$$

and $P(x,y)$ satisfies the equation

$$\frac{\partial^2 P}{\partial x^2} + \frac{\partial^2 P}{\partial y^2} + k^2 P = 0 \tag{5.3}$$

The parameter k is a measure of the non-uniformity of the primary field, and is given by $k = 2\pi/\lambda$ where λ is a linear dimension of the source field. Thus $k = 0$ implies a uniform source. The function of depth $Z(z)$ satisfies the equation

$$\frac{d^2 Z}{dz^2} = (k^2 + i\omega\mu_o\sigma) Z \tag{5.4}$$

or $$\frac{d^2 Z}{dz^2} = K^2 Z \tag{5.5}$$

with $$K^2 = k^2 + i\omega\mu_o\sigma \tag{5.6}$$

It is clear that eq. 5.3 has solutions for P of the form $\sin(kx)$, $\cos(kx)$, $\exp(ikx)$ and $\sin(k_x x + k_y y)$ where $k_x^2 + k_y^2 = k^2$. These solutions involve single values of k which may be regarded as individual modes of the source field.

The magnetic field is obtained from the equation

$$\nabla \times \vec{E} = - \frac{\partial \vec{B}}{\partial t} = - i\omega\mu_o \vec{H}$$

and is given by

$$i\omega\mu_o \vec{H} = - \{\frac{\partial Z}{\partial z}\frac{\partial P}{\partial x}, \frac{\partial Z}{\partial z}\frac{\partial P}{\partial y}, k^2 Z P\} \exp(i\omega t) \quad (5.7)$$

In the j-th layer the solution of eq. 5.5 is

$$Z_j(k,t,z) = A_j(k,t)\exp(-K_j z) + B_j(k,t)\exp(K_j z) \quad (5.8)$$

and $$\frac{dZ_j(k,t,z)}{dz} = - K_j\{A_j(k,t)\exp(-K_j z) - B_j\exp(K_j z)\} \quad (5.9)$$

so that $$Z_j = - \frac{g_j}{K_j}\frac{dZ_j}{dz}$$

where $$g_j(z) = \frac{A_j\exp(-K_j z) + B_j\exp(K_j z)}{A_j\exp(-K_j z) - B_j\exp(K_j z)} \quad (5.10)$$

In this case $g_j(z) \equiv \frac{1}{G_0(z)}$ of Schmucker (1970a, p. 63), $g_j(z) \equiv \theta_n Z_n(z)$ of Weaver (1973, p. 275) and $g_j(z) \equiv g_n$ as used by Schmucker (1971, p. 164).

At any interface the tangential magnetic and electric field intensities are continuous. This implies

$$z_j(z_{j+1}) = z_{j+1}(z_{j+1})$$

and $$\frac{dz_j(z_{j+1})}{dz} = \frac{dz_{j+1}(z_{j+1})}{dz} \qquad (5.11)$$

but also that

$$\frac{g_j(z_{j+1})}{K_j} = \frac{g_{j+1}(z_{j+1})}{K_{j+1}} \qquad (5.12)$$

From eq. 5.10 we have at the lower boundary of the j-th layer, i.e. interface j+1,

$$g_j(z_{j+1}) = \frac{A_j \exp(-K_j z_{j+1}) + B_j \exp(K_j z_{j+1})}{A_j \exp(-K_j z_{j+1}) - B_j \exp(K_j z_{j+1})} \qquad (5.13)$$

The coefficients A_j and B_j can thus be eliminated using eqs 5.10 and 5.13. The positive and negative arguments are combined to hyperbolic functions to yield

$$g_j(z) = \frac{g_j(z_{j+1}) + \tanh K_j(z_{j+1}-z)}{1 + g_j(z_{j+1}) \tanh K_j(z_{j+1}-z)} \qquad (5.14)$$

with $z_j \leq z \leq z_{j+1}$

Equation 5.14 corresponds to eq. 82 of Weaver (1973). Setting $z = z_j$ in this equation gives $g_j(z_j)$ in terms of $g_j(z_{j+1})$. Equation 5.12 is used to obtain

the basic recurrence formula for n-lane-layered conductors

$$g_j(z_j) = \frac{K_j g_{j+1}(z_{j+1}) + K_{j+1} \tanh K_j h_j}{K_{j+1} + K_j g_{j+1}(z_{j+1}) \tanh K_j h_j} \qquad (5.15)$$

with $h_j = z_{j+1} - z_j$ = the thickness of the j-th layer. The above equation is the same as the expression for g_n on p. 164 of Schmucker (1971).

The incident field disappears at great depth ($z \to +\infty$) so that the term B_N in the N-th layer (the halfspace) must be zero and

$$g_N(z_N) = 1 \qquad (5.16)$$

The value of $g_1(0)$ can thus be obtained by starting at the surface of the halfspace where $g_N(z_N) = 1$ and calculating successively the $g_j(z_j)$ by means of eq. 5.15.

Two limiting cases can be considered. Firstly when the skin-depth in the j-th layer is large in comparison to the wavelength of the source field, then

$$K_j \simeq k \qquad (5.17)$$

and the incident field penetrates through this layer as if it were nonconducting.

The second case arises when the wavelength of the incident field is large in comparison with the skin depth of, say, the j-th layer. From eq. 5.6

$$K_j \simeq \sqrt{i\omega\mu_o\sigma_j} = \frac{1+i}{\delta_j} \tag{5.18}$$

with δ the skin depth defined for the j-th layer as

$$\delta_j = \sqrt{\frac{2}{\omega\mu_o\sigma_j}} \tag{5.19}$$

the attenuation of the field in this layer is governed only by the skin depth and is independent of k.

In terms of eqs 5.1, 5.2 and 5.7-5.9

$$E_x = \exp(i\omega t)\{A_j\exp(-K_j z) + B_j\exp(K_j z)\}\frac{\partial P}{\partial y} \tag{5.20}$$

and

$$i\omega\mu_o H_y = \exp(i\omega t)\{A_j\exp(-K_j z) - B_j\exp(K_j z)\}\frac{\partial P}{\partial y} \tag{5.21}$$

so that the magnetotelluric impedance (eq. 1.24) at the earth's surface is given by

$$Z = \frac{E_x}{H_y} = \frac{i\omega\mu_o g_1(0)}{K_1} \tag{5.22}$$

and is independent of P.

From eq. 5.7 we have that at the earth's surface

$$\frac{H_z}{H_x} = -\frac{k^2}{K_1}\,a_1(0)\,\frac{P}{\partial P/dx} \tag{5.23}$$

but this relation is dependent on P.

Furthermore we have from eq. 5.3 that

$$\frac{\partial^2 P}{\partial x^2} + \frac{\partial^2 P}{\partial y^2} = -k^2 P \tag{5.24}$$

which means that from eq. 5.7

$$\frac{H_z}{\frac{\partial H_x}{\partial x} + \frac{\partial H_y}{\partial y}} = \frac{g_1(0)}{K_1} \tag{5.25}$$

again at the earth's surface. This equation gives a relation between the vertical variation field and the horizontal field gradient and is independent of P.

Schmucker (1970b, 1971) introduced the inductive scale length $C_j(\omega,k)$ - the response function used by Weidelt (1972) - and defined it as

$$C_j(\omega,k) = \frac{g_j(z)}{K_j} \tag{5.26}$$

Since we are working at the surface the subscript of C is dropped in the further discussion, but will imply C_1.

The magnetotelluric impedance (eq. 5.22) reduces to

$$Z = i\omega\mu_o C(\omega,k) \tag{5.27}$$

and eq. 5.25 can be written as

$$\frac{H_z}{\frac{\partial H_x}{\partial x} + \frac{\partial H_y}{\partial y}} = C(\omega,k) \qquad (5.28)$$

Schmucker (1970a) and Kuckes (1973a) independently introduced a simple inversion technique for one-dimensional problems. This method yields a first estimate of the conductivity at depth from the response function at the surface. These authors assume a uniform half-space of conductivity σ_2 underlies a layer with a low conductivity and thickness h. In this model the incident field will penetrate the top layer with negligible attenuation for frequencies of interest in array studies. The penetration depth in the half-space will be small compared to the spatial wavelength of the incident field.

From the limiting cases discussed in connection with eqs 5.17 and 5.18 we have for this case that

$$K_1 \approx k,\ kh << 1 \text{ and } K_2 = \frac{1+i}{\delta_2} \qquad (5.29)$$

where δ_2 is the skin depth in the second layer.

Equation 5.15 yields for a two-layer case

$$g_1(0) = \frac{K_1 g_2(z_2) + K_2 \tanh K_1 h}{K_2 + K_1 g_2(z_2) \tanh K_1 h} \qquad (5.30)$$

From eq. 5.16 $g_2(z_2) = 1$ and since $h << \delta_1 << 1/k$

$\tanh K_1 h \approx K_1 h$. Substituting these approximations and the limiting value for K_1 in eq. 5.30 yield

$$g_1(0) = \frac{k(1 + K_2 h)}{K_2} \tag{5.31}$$

and when the limiting value for K_2 is introduced

$$g_1(0) = kC \tag{5.32}$$

where $$C = h + \frac{\delta_2}{2} - i\frac{\delta_2}{2} \tag{5.33}$$

a complex length. Since $k = K_1$

$$C = \frac{g_1(0)}{K_1} = C(\omega,k) \tag{5.34}$$

the response function of eq. 5.26.

It is clear that

$$h = Re(C) + Im(C)$$

and $$\delta_2 = -2\ Im(C) \tag{5.35}$$

The general strategy of the inversion is to determine C at the surface by means of equations such as 5.27 and 5.28. The equations 5.35 are then used to get for each frequency component a depth and conductivity of a uniform "substitute conductor". This depth and conductivity are meaningful only when the argument of $C(\omega,k)$ for a specific

frequency lies between $-\frac{\pi}{4}$ and 0, yielding a positive depth h. For such a frequency a multi-layered structure is indistinguishable from and therefore replaceable by a uniform conductor at depth h. An underlying assumption is that $(h + \delta_2)$ is small compared to the wavelength of the source field.

$$\text{With} \qquad h^* = h + \frac{\delta_2}{2} \tag{5.36}$$

the depth of a perfect substitute conductor

$$h^* = \text{Re}(C) \tag{5.37}$$

and a modified apparent resistivity can be defined as

$$\rho^*(h^*) = 2\omega\mu_o\{\text{Im}(C)\}^2 \tag{5.38}$$

5.2 Considerations for interpreting observed data

The theory developed in Section 5.1 applies to specific source field configurations and specific geological conditions. In practice the investigator is faced by the problem that he seldom knows the source field configuration and actually studies the conductivity structure to learn more about the geology. Under certain conditions, assumptions can be made regarding these parameters to facilitate the computation of theoretical models.

Lilley (in press) considers the effect of different elementary P functions on eq. 5.23. For a travelling wave one can take P of the form

$$P(x) = \exp(ikx) \tag{5.39}$$

with k real. Then

$$\frac{P}{dP/dx} = \frac{1}{ik} \tag{5.40}$$

and eq. 5.23 reduces to

$$\frac{H_z}{H_x} = \frac{ikg_1}{K_1} = ikC(\omega;k) \tag{5.41}$$

This equation has been the basis of what Lilley terms traditional geomagnetic depth sounding, as developed for example by Price (1962), Whitham (1963), Caner et al. (1967), Cochrane and Hyndman (1970) and Caner (1971). Often the modulus of both sides of the equation is taken, thus losing the i and its significance. In this equation a specific knowledge of k is required. With P of the form 5.39

$$\frac{dH_x}{dx} = ikH_x \tag{5.42}$$

or for the general case with P a function of both x and y

$$\frac{\partial H_x}{\partial x} + \frac{\partial H_y}{\partial y} = ikF \tag{5.43}$$

with F the total horizontal field. This gives an estimate of k. The moduli of both sides of this equation are often taken, again losing the significance of the i-factor. For a travelling wave it is however valid to replace the ik factor in eq. 5.41 by $\frac{dH_x}{dx}/H_x$ to get.

$$\frac{H_z}{H_x} = \frac{dH_x}{dx} \cdot \frac{C(\omega,k)}{H_x} \qquad (5.44)$$

For standing waves one can take P of the form P = sin kx, when

$$\frac{P}{dP/dx} = \frac{\tan kx}{k} \qquad (5.45)$$

so that eq. 5.23 becomes

$$\frac{H_z}{H_x} = -kC(\omega,k) \tan kx \qquad (5.46)$$

This means that for standing waves eq. 5.23 is no longer independent of x. The use of eq. 5.23 to interpret observed H_z/H_x ratios is thus valid only for a single mode travelling-wave source field.

The magnetotelluric and array-gradient equations (5.22 and 5.25) seem not to depend on the question whether the source-field is of travelling-wave or standing-wave nature. In these cases one has to bear in mind that the relevant field components will vanish at nodal points.

The value of k does not enter in these equations in the same explicit way as in eq. 5.23, but does enter in the estimation of the K_j values. This point will be considered further on in the discussion.

Schmucker (1970b, 1973) discusses the general induction problem as seen from a particular surface point in terms of three relative scale lengths L_1, L_2 and L_3. The first scale length, L_1, refers to the spatial configuration of the source field and can be thought of as the spatial non-uniformity of the overhead source field. This can be for instance the height of an overhead line-current jet or the reciprocal of the wave number k for a sinusoidal field. The second scale length, L_2, is related to the degree of lateral uniformity of conducting matter beneath the surface. Schmucker (1973) assumes that the halfspace $z > 0$ is subdivided at vertical boundaries into different layered conductive structures. The length L_2 is defined as the distance between the point of observation and the nearest vertical boundary. Weidelt (1972) showed that in the special case of sufficiently uniform source fields the positive real part of the inductive scale $C(\omega,k)$ can be interpreted as the weighted mean depth of the induced currents in a stratified halfspace. The limiting value for $k \to 0$ is a convenient measure for the depth of penetration at a given frequency.

Schmucker (1973) thus defined its modulus for the relevant stratified section as the third scale length such that $L_3 = |C(\omega,0)|$. Obviously L_3 increases with increasing period.

If we assume a quasi-uniform source field, that the observation points are far removed from lateral boundaries and that the subsurface approximates a layered model, we have the case where $L_1, L_2 >> L_3$. This is a one-dimensional induction problem because, as Schmucker (1973) points out, for the area under consideration neither the exact configuration of the source field nor the conductivity in adjacent stratified sections matters. For this case one can set $k = 0$ to obtain the field relations for the so-called Cagniard case from eqs 5.22 and 5.27

$$\frac{E_x}{H_y} = i\omega\mu_o C(\omega,0) \qquad (5.47)$$

and

$$\frac{E_y}{H_x} = -i\omega\mu_o C(\omega,0) \qquad (5.48)$$

and from eq. 5.28

$$H_z = \left(\frac{\partial H_x}{\partial x} + \frac{\partial H_y}{\partial y}\right) C(\omega,0) \qquad (5.49)$$

Equation 5.49 can be used to obtain an estimate of $C(\omega,0)$ from the observed vertical field and horizontal field gra-

dients at a certain frequency. It is worth noting that from eq. 5.23 $\frac{H_z}{H_x} = 0$ when $k = 0$. To circumvent this problem Schmucker (1973) makes allowance for a small sinusoidal modulation of the source field with the constraint that

$$k \cdot |C(\omega,0)| = \frac{L_3}{L_1} << 1 \qquad (5.50)$$

Using this he then defines a locally effective "wave number" (personal communication between Schmucker and Lilley, 1972)

$$k_e = \left(\frac{\partial H_x}{\partial x} + \frac{\partial H_y}{\partial y}\right)/|F| \qquad (5.51)$$

where $$|F| = (H_x \cdot H_x^* + H_y \cdot H_y^*)^{1/2}$$

This converts eq. 5.49 into

$$\frac{H_z}{|F|} = k_e \, C(\omega,0) \qquad (5.52)$$

This means that both sides of eq. 5.49 are normalized with respect to $|F|$ and so differs from the use of eq. 5.41, where the observed H_z/H_x ratio is compared to the computed value of $ikC(\omega,k)$. Schmucker considers the reciprocal of k_e as a scale length for the overhead source.

A study of the properties of $C(\omega,0)$ as derived from eq. 5.49 can be helpful in examining the validity of the assumption of a plane layered earth with induction by a quasi-uniform source field. Firstly $C(\omega,0)$ has to vary smoothly with frequency and $\frac{\partial Re[C(\omega,0)]}{\partial \omega} < 0$ because the depth of induced currents changes smoothly with frequency, with the lower frequencies having larger penetration depths for a given conductivity distribution. From eq. 5.33 it is clear that $Re[C(\omega,0)] > 0$ and $Im[C(\omega,0)] < 0$. If $C(\omega,0)$ as determined from the observed data does not have these basic properties, some or all the assumptions regarding a one-dimensional model are violated. Another consequence of a departure from these properties will be that the Schmucker-Kuckes inversion technique cannot be applied.

5.3 Conductivity structure in the Kaapvaal craton as compared to a global model

The short period limits for studies of the radial distribution of electrical conductivity in the Earth and the resulting poor determination of the conductivity structure for depths less than 400 km have been discussed in Section 1.2.1. The northern part of the 1971 array was situated on the Kaapvaal craton and the magnetograms, maps of Fourier spectral components and induction arrows discussed in Chapter 3 indicate that,

of all the areas studied, this area seems to be the least affected by lateral inhomogeneities. It would thus seem that these array data offer an opportunity to determine a conductivity-depth profile for an Archean shield area. The results of the deep Schlumberger soundings in the area (Section 1.4) indicate that the geological structure does indeed approximate a plane-layered situation. It should, however, also be borne in mind that even at the north-east of the array $H_z(t)$ bears a strong resemblance to $H_x(t)$, suggesting that much of the H_z variation field is an anomalous field resulting from induction by H_x in the east-west conductor to the south of the array.

In principle the best approach to the problem of obtaining a conductivity model for the Kaapvaal craton should be a direct inversion technique such as those described by Bailey (1970) and Weidelt (1972). These two methods, however, require precise data over a broad frequency range, while in this case only data with a limited precision over a very limited frequency band are available. Weidelt himself advises: "it appears that the best way to handle geomagnetic induction data is still to interpret them by a set of homogeneous layers and to introduce, if necessary, further preconceived model assumptions" (Weidelt, 1972, p. 285). The modelling in this study was therefore performed with the aid of the

Figure 5.2 Conductivity models investigated in one-dimensional model studies. Model 1 is the "standard" model constructed from conductivity models by Banks (1972) and Van Zijl and Joubert (1975). Model 2 is derived from Model 1 by increasing layer thicknesses between 250 and 600 km by 50%. Model 3 is derived from Model 2 by decreasing conductivities between 225 and 900 km by a factor of 10.

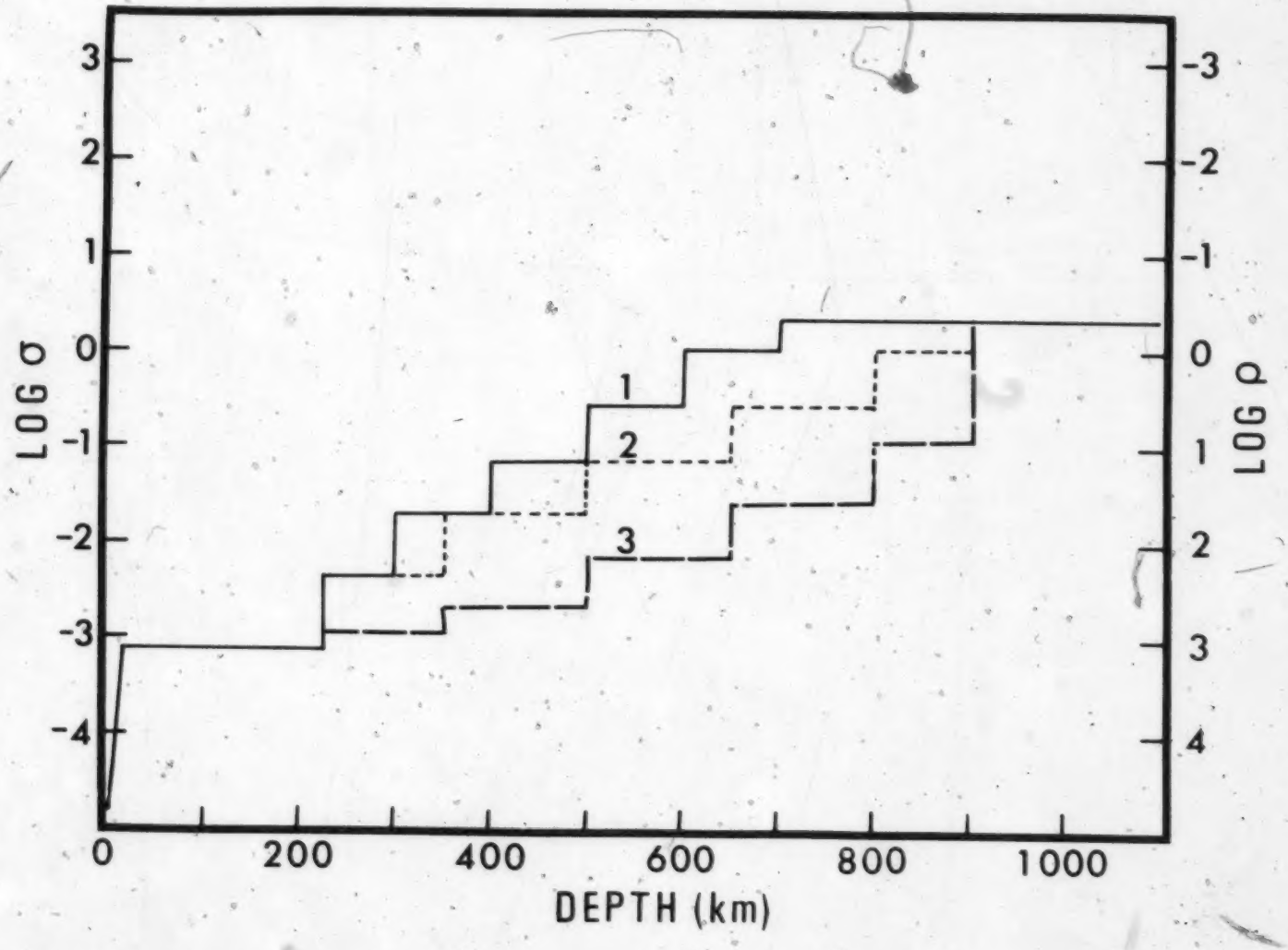
LOG σ
LOG ρ
DEPTH (km)
0
200
400
600
800
1000
3
2
1
0
-1
-2
-3
-4
-3
-2
-1
0
1
2
3
4
1
2
3

theory developed by Price (1962) and Schmucker (1970a) and discussed in Section 5.1.

Because of the effects of the Cape Fold Belt conductive structure on the data and the assumptions involved in the modelling techniques, it is clear that the present data allow, at best, a comparison with existing models and precludes any meaningful independent modelling. A good model for comparison is therefore required. Despite the limitations in the data of Banks (1969, 1972) discussed in Section 1.2.1, his models for the radial conductivity structure of the Earth are considered to be the best available. The conductivity models derived from deep Schlumberger soundings are the best available for the crust and uppermost mantle (depths < 200 km) in the craton (Figure 1.3), where lateral variations of conductivity can be reduced to acceptable limits. This model and that of Banks (1972) were therefore combined to form the "standard" model for comparison and is depicted as Model 1 in Figure 5.2.

The most severe problem in this type of modelling is to get an estimate of the spatial wavelength of the source field. Price (1962) estimated that for geophysical applications involving sources of natural origin the spatial wave number would lie in the range $1.57 \times 10^{-7} m^{-1}$ to $1.57 \times 10^{-5} m^{-1}$. Banks (1969) states that for mid-

latitude stations away from the auroral and equatorial electrojets generally $k < 2/R_E = 3.1 \times 10^{-7} m^{-1}$. For k in this range the approximation $C(\omega,k) \simeq C(\omega,0)$ holds (Larsen, 1973; Schmucker, 1973). This means that the first scale length $L_1 \rightarrow \infty$. With the station CHR (Fig. 3.1) as observation point, the nearest major lateral inhomogeneity observed in the array area (under the Cape Folded Belt) is about 600 km away. There may be, and most probably are, closer vertical boundaries outside the array. On the present data, however, L_2 is about 600 km.

The third scale length L_3 is defined as $\text{Mod}[C(\omega,0)]$. It will be shown that this quantity varies from about 400 km at a period of 20 minutes to about 1,000 km at a period of 300 minutes. This means that at best we have the situation that $L_1 >> L_2, L_3$ and do not actually have a one-dimensional case. It is however instructive to treat the problem as if $L_1, L_2 >> L_3$ and to observe the effects of the lateral inhomogeneities.

As a first study the classical geomagnetic depth sounding approach was investigated. The observed $|\frac{H_z}{F}|$ ratio was modelled using eq. 5.41 and the algorithm described in Section 5.1. The value of k in eq. 5.41 was determined by means of eq. 5.43 using only the moduli of H_x and H_y. This approach thus assumes a plane-wave source configuration. Straight lines were fitted by least squares

to the H_x values at the stations PET, KOF, DEA, SCH, CHR, VRY (Fig. 3.1) to determine $\frac{\partial H_x}{\partial x}$ and to the H_y values at OLI, KUR, CHR to determine $\frac{\partial H_y}{\partial y}$. The estimates of the standard errors of the slopes were combined with the errors in F to get the standard errors in k. A weighted average of the k estimates at 10 periods $(3.4 \pm .6) \times 10^{-7} m^{-1}$ was used in the calculations. This assumes that the k values for different periods belong to the same population and may not be a valid assumption, but certainly is better than guessing values. It will be noted that this value of k coincides with the Banks (1969) upper limit of $3.1 \times 10^{-7} m^{-1}$. All stations on the Kaapvaal shield as outlined in Fig. 3.1 were used to obtain an average $|\frac{H_z}{F}|$ ratio. From Fig. 5.3 it is clear that this quantity does not vary smoothly with period, an indication that the assumptions do not hold for all the data used. The figure also shows the $|\frac{H_z}{F}|$ values for the standard model (Model 1 in Fig. 5.2). At short periods the model approximates the observed ratios, but has too small a slope to match the observed ratios at the longer periods.

To determine the effects of perturbations to the model the thickness of the layers between 250 and 600 km depth in the standard model was changed to 150 km to obtain Model 2 (Fig. 5.2) and the calculation repeated.

Figure 5.3 Observed $|\frac{H_z}{F}|$ values for stations on the Kaapvaal shield in relation to computed values for Model 1 and Model 2. The values of k are for the one standard deviation limits.

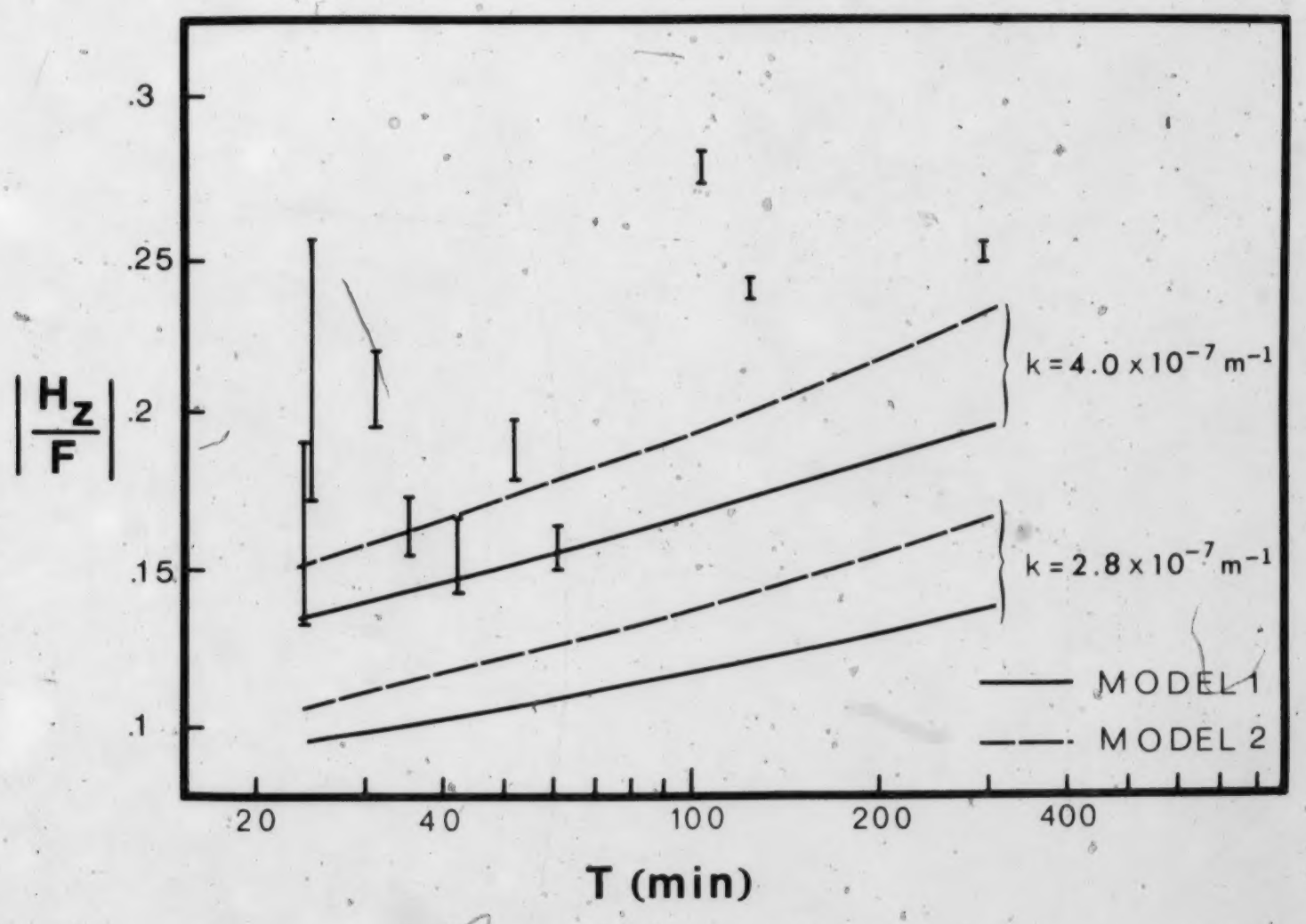
.3
.25
.2
.15
.1
$\left|\frac{H_z}{F}\right|$
k = 4.0 x 10⁻⁷ m⁻¹
k = 2.8 x 10⁻⁷ m⁻¹
MODEL 1
MODEL 2
20
40
100
200
400
T (min)

1186

The results are shown in Fig. 5.3. The slopes of the model curves are still too small. Model 3 in Fig. 5.2 was constructed by increasing the resistivities of the layers in the depth range 225 to 900 km a factor of 10 relative to Model 2. This model fits the data better than the standard model (Fig. 5.4).

The effect of the crustal model used was investigated by extending the lower crustal - upper mantle resistivity (1,300 ohm.m) right to the surface. The effect for $k = 3.4 \times 10^{-7} m^{-1}$ is shown by the broken line curve in Fig. 5.4 and it is obvious that near-surface conductive layers have only a slight effect at the shorter periods and none at the longer periods.

The normalized anomalous profiles in Figs 3.12 and 3.13 indicate that the fields at the southern stations on the shield (to the north-east of PRI) contain sizable anomalous parts due to the conductor to the south. The effect of including only the northernmost stations in the computation of an average $|\frac{H_z}{F}|$ was assessed by calculating this ratio for CHR and VRY. The result is shown in Fig. 5.5 in relation to theoretical values for the standard model and Model 2. Now the standard model fits the data for $T < 70$ min quite well and Model 2 fits all the data satisfactorily. It is interesting to note that in the range $T < 70$ min the approximation that

Figure 5.4 Observed $\left|\frac{H_z}{F}\right|$ values for stations on the Kaapvaal shield in relation to computed values for Model 3. The broken line curve indicates the effect of extending the lower crustal-upper mantle resistivity of 1,300 ohm.m to the surface of the Earth for $k = 3.4 \times 10^{-7} m^{-1}$.

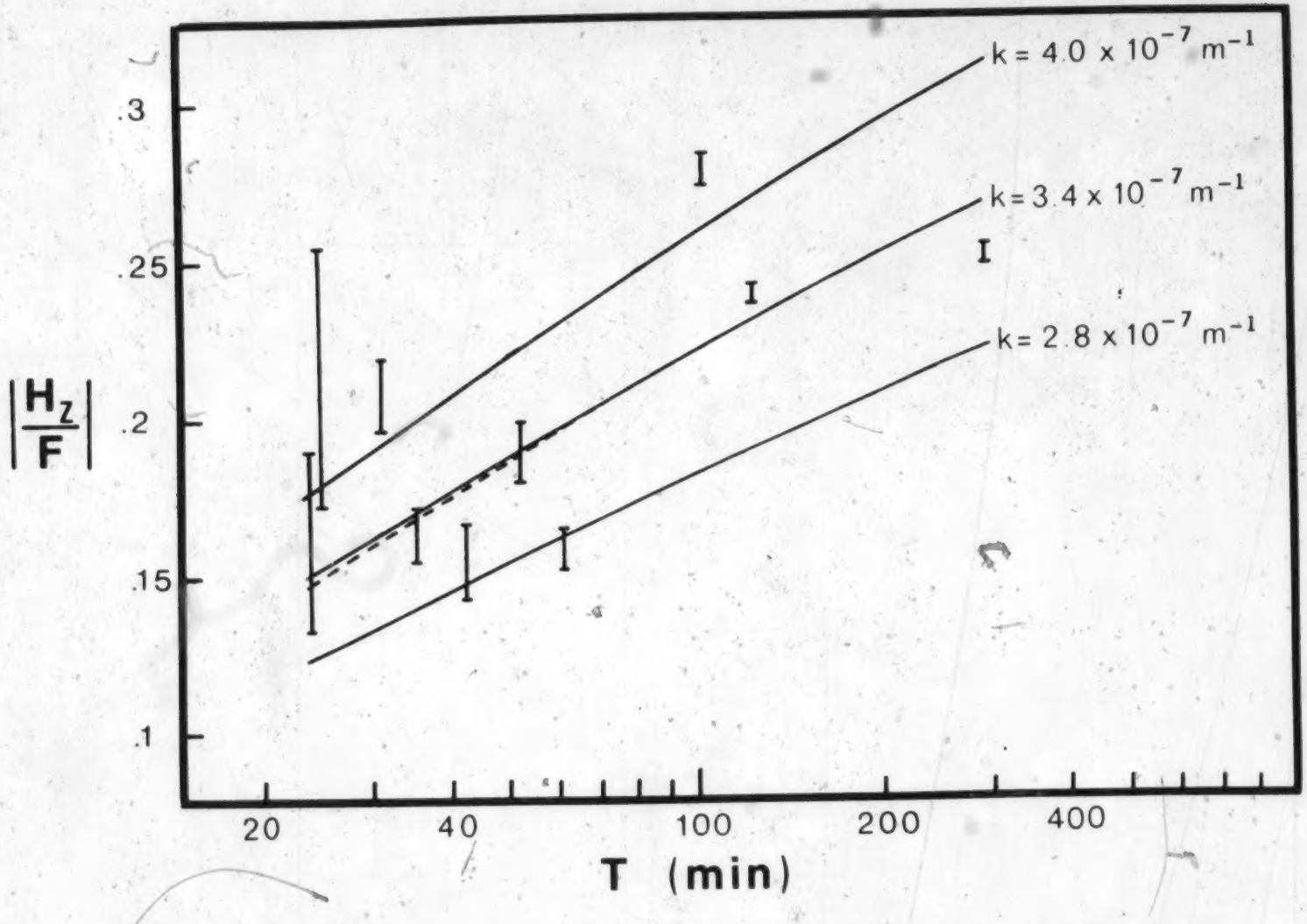
k = 4.0 x 10⁻⁷ m⁻¹
k = 3.4 x 10⁻⁷ m⁻¹
k = 2.8 x 10⁻⁷ m⁻¹
.3
.25
.2
.15
.1
|Hz/F|
20
40
100
200
400
T (min)

Figure 5.5 Observed $\left|\frac{H_z}{F}\right|$ ratios at the stations CHR and VRY in relation to computed values for Model 1 and Model 2.

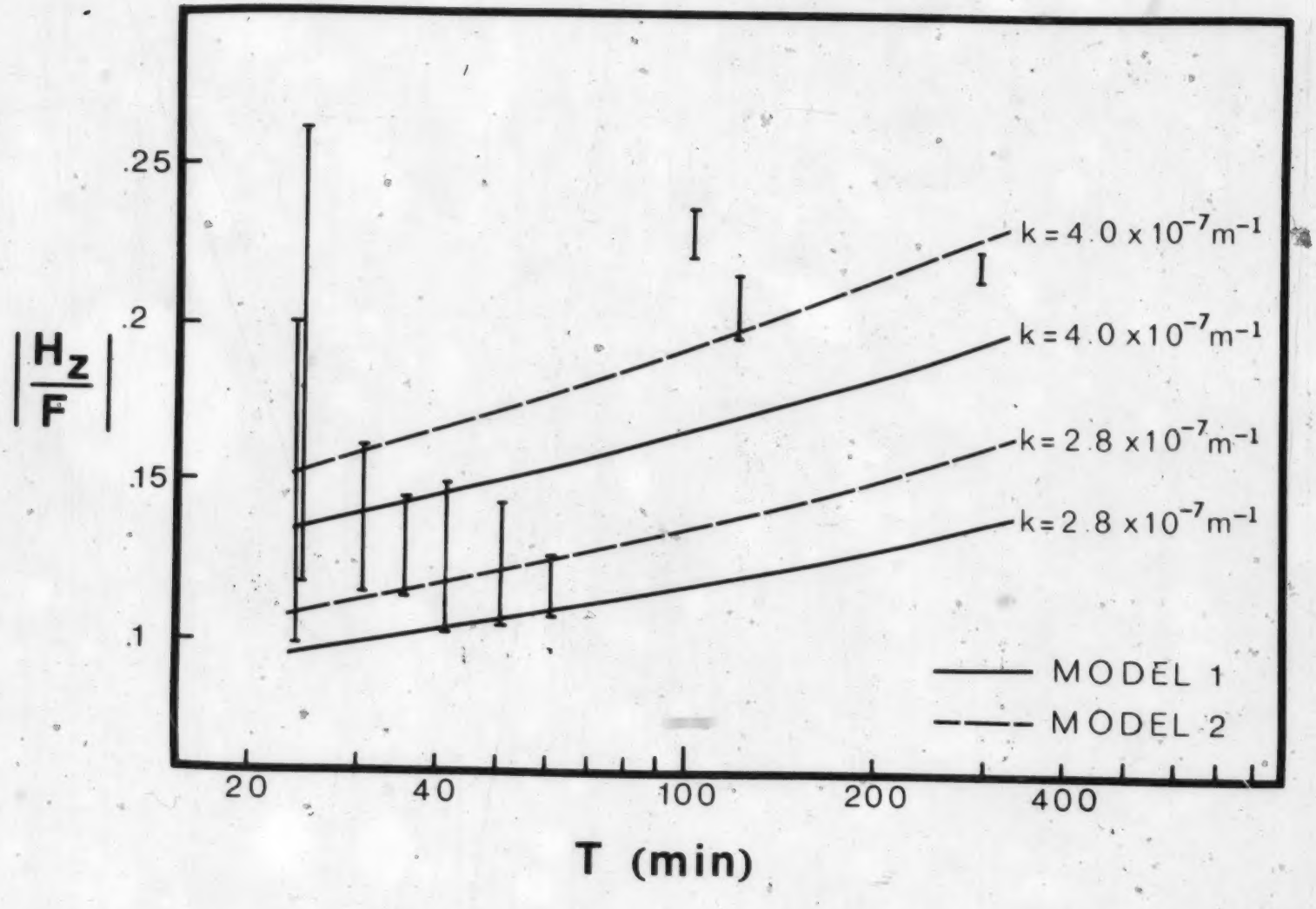
.25
.2
.15
.1
$\left|\frac{H_z}{F}\right|$
k = 4.0 x 10^{-7}m^{-1}
k = 4.0 x 10^{-7}m^{-1}
k = 2.8 x 10^{-7}m^{-1}
k = 2.8 x 10^{-7}m^{-1}
MODEL 1
MODEL 2
20
40
100
200
400
T (min)

$L_1, L_2 >> L_3$ is more appropriate than for longer periods, because L_3 increases with increasing period. The above calculations were repeated using the approximation of eq. 5.52, but with k as determined from the moduli of the field components. The results are almost identical to those discussed above. The biggest uncertainty in this type of analysis is the estimation of k. If for instance the largest k ($6.2 \times 10^{-7} m^{-1}$) obtained in the computation of the average k is used in the computation, the standard model gives a good fit to the data.

A method that avoids the estimation of k is therefore needed. The array gradient method is such a method. The observed response function was computed for different periods using eq. 5.49. In this case H_z, H_x and H_y were treated as complex quantities and $\frac{\partial H_x}{\partial x}$ was determined along a S-N line through KOF, DEA, SCH, CHR, and VRY (Fig. 3.1) and $\frac{\partial H_y}{\partial y}$ along an W-E line through OLI, KUR, CHR. The average H_z value at the stations VEN, VRY and CHR in the north-eastern corner of the array wasused in the computation of $C(\omega,0)$. The values as computed at single periods were found to contain large standard deviations, partly because of the small H_z values, but mostly because of the errors in the gradients. A frequency-band averaging technique was therefore devised to decrease the errors in $C(\omega,0)$. In this process response

functions were evaluated over a band containing up to 15 Fourier spectral estimates at periods near 20 min and two estimates at 300 min and then averaged over the band. This procedure is appropriate because the response function changes very slowly with frequency and the $C(\omega,0)$ within a limited frequency band can be considered to be an estimate of the same quantity. A similar technique is used in magnetotelluric studies in the estimation of the tensor impedance elements (Word et al., 1970; Hermance, 1973).

The bands were selected to include portions of the spectra with high energy in H_z, to increase the signal to noise ratio. The bands were also chosen over a period range where the polarization angle varied no more than about 30 degrees. Stability in the polarization direction was assumed to indicate stability in the source field. Changes in the polarization direction within a band may be valuable to eliminate the effects of local inhomogeneities, but for the present study stability in the source field was considered more important. A reason for this was that the $C(\omega,0)$ values varied a large amount within a band if the associated horizontal field polarization direction changed by a large amount. The Fourier coefficients represent averages over a time interval and changes in polarization with period may indicate contributions from more than one source.

The frequency-band averaged values of Mod[$C(\omega,0)$] are shown in Fig. 5.6. The response functions are plotted at the geometric mean period of each band. Only the moduli are plotted because in only one band were Re[$C(\omega,0)$] positive and Im[$C(\omega,0)$] negative as they should be (Weidelt, 1972). This agrees with the conclusion, from the earlier analysis in terms of scale lengths, that the structure is not in fact one-dimensional. The penetration depth increases with increasing period as it should. The theoretical response functions for Model 1 and Model 3 of Fig. 5.2 are superposed on the data and the latter clearly fits the data better. This is consistent with the results from the study of $|\frac{H_z}{F}|$.

In some of the bands investigated but not shown in Fig. 5.5 the values of $C(\omega,0)$ were unstable because slopes with about equal magnitudes, but opposite signs were added in the denominator of eq. 5.49. This problem can be avoided by rotating the time domain data to components parallel and perpendicular to the long axis of the polarization ellipse. This will mean that the data have to be Fourier analysed to obtain the polarization parameters before the rotation can be done. The rotated time domain data are then Fourier analysed and the gradients obtained in the new reference frame. In the case of a linear or near-linear polarization only

Figure 5.6 Frequency-band averaged values of Mod[$C(\omega,0)$] in relation to computed values for Model 1 and Model 3. The vertical bars indicate the standard errors and the horizontal bars indicate the width of the frequency bands.

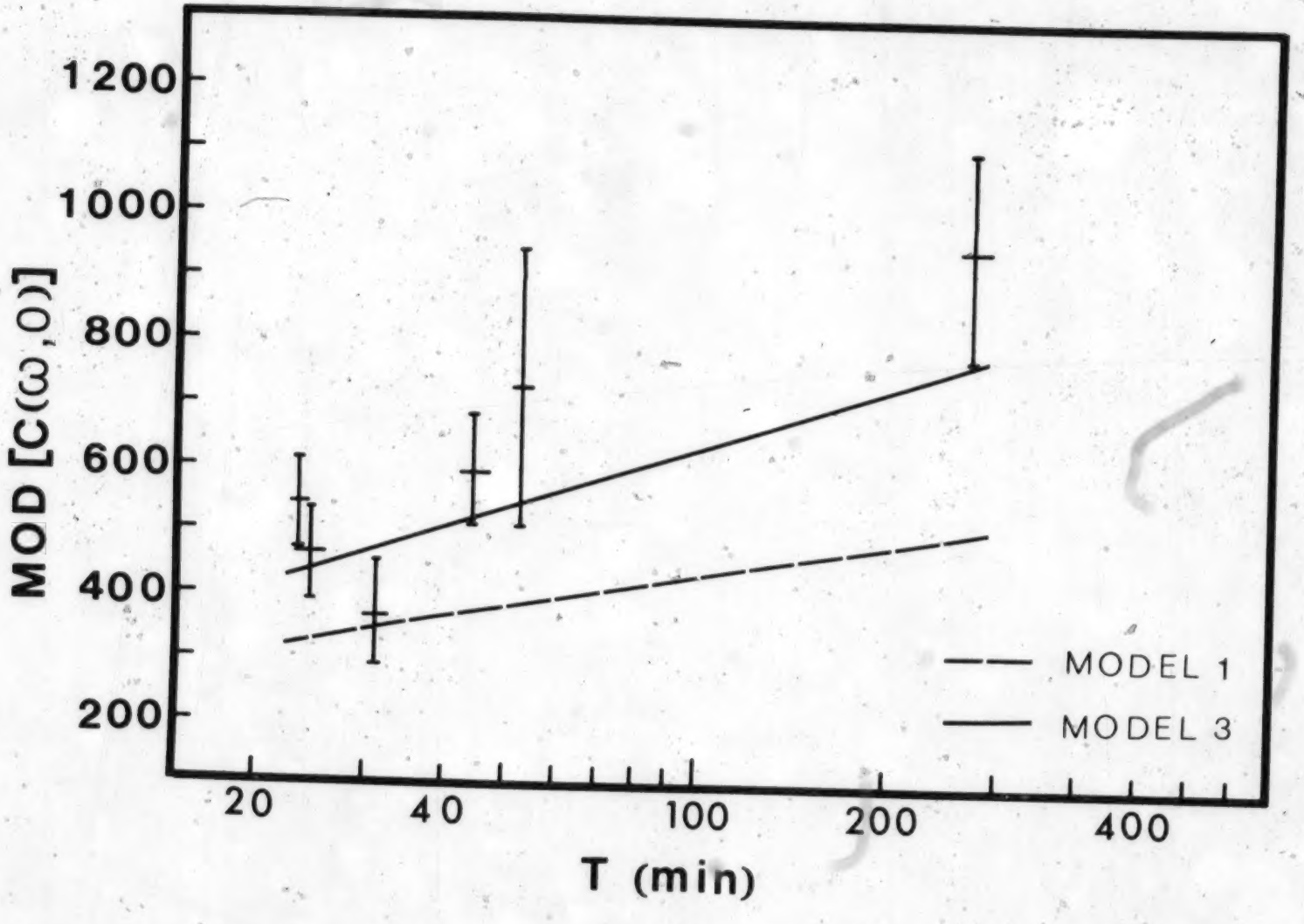
1200
1000
800
600
400
200
MOD [C(ω,0)]
20
40
100
200
400
T (min)
MODEL 1
MODEL 3

196

one derivative has to be taken which will enhance the accuracy of $C(\omega,0)$. In this study there are too few stations in the study area to carry out this process.

Although the data used in this analysis have some properties that indicate a deviation from a one-dimensional structure, the results suggest that the conductivity profile in the approximate depth range 200-800 km under the Kaapvaal shield differs from that of the Banks model. The observed fields require a slower rise in conductivity with depth. Magnetometer array studies are well suited for studies in this depth range which is deeper than that for Schlumberger and magnetotelluric studies and is near the short period limit of radial conductivity studies. A magnetometer array located on the Kaapvaal and Rhodesian shields might help to establish an electric conductivity profile for this shield region.

With more stations removed from major induction anomalies, a trend surface could be fitted to the horizontal field components which would lead to better estimates of the gradients and also $C(\omega,0)$. A serious attempt should also be made to develop a Backus and Gilbert type inversion technique for this type of problem.

CHAPTER VI

THE CONDUCTIVITY ANOMALIES IN SOUTHERN AFRICA IN RELATION TO LOCAL GEOLOGY AND GEOPHYSICAL PARAMETERS AND THEIR POSSIBLE CAUSES

6.1 The Southern Cape induction anomaly

The principal result of the 1971 array study discussed in Chapter 3 was the discovery of the east-west trending conductor under the west central Cape Fold Belt and deep part of the Karroo basin (Fig. 3.14). This conductive structure was so far from being expected that most of it passes to the south of the southern corner of the triangular array. Nevertheless it is clear that a large highly-conductive structure elongated east-west underlies the deep Karroo basin and the Cape Fold Belt. The phase relations and frequency response of transfer functions discussed in Chapter 3 indicate that the conductor is most likely in the lower lithosphere or asthenosphere. The relations of this conductivity anomaly to other geophysical parameters in the area and to the local geology are very interesting and warrant a short discussion.

6.1.1 Heat flow data

Conductivity anomalies in the crust and uppermost mantle can be related to temperature, as in the western

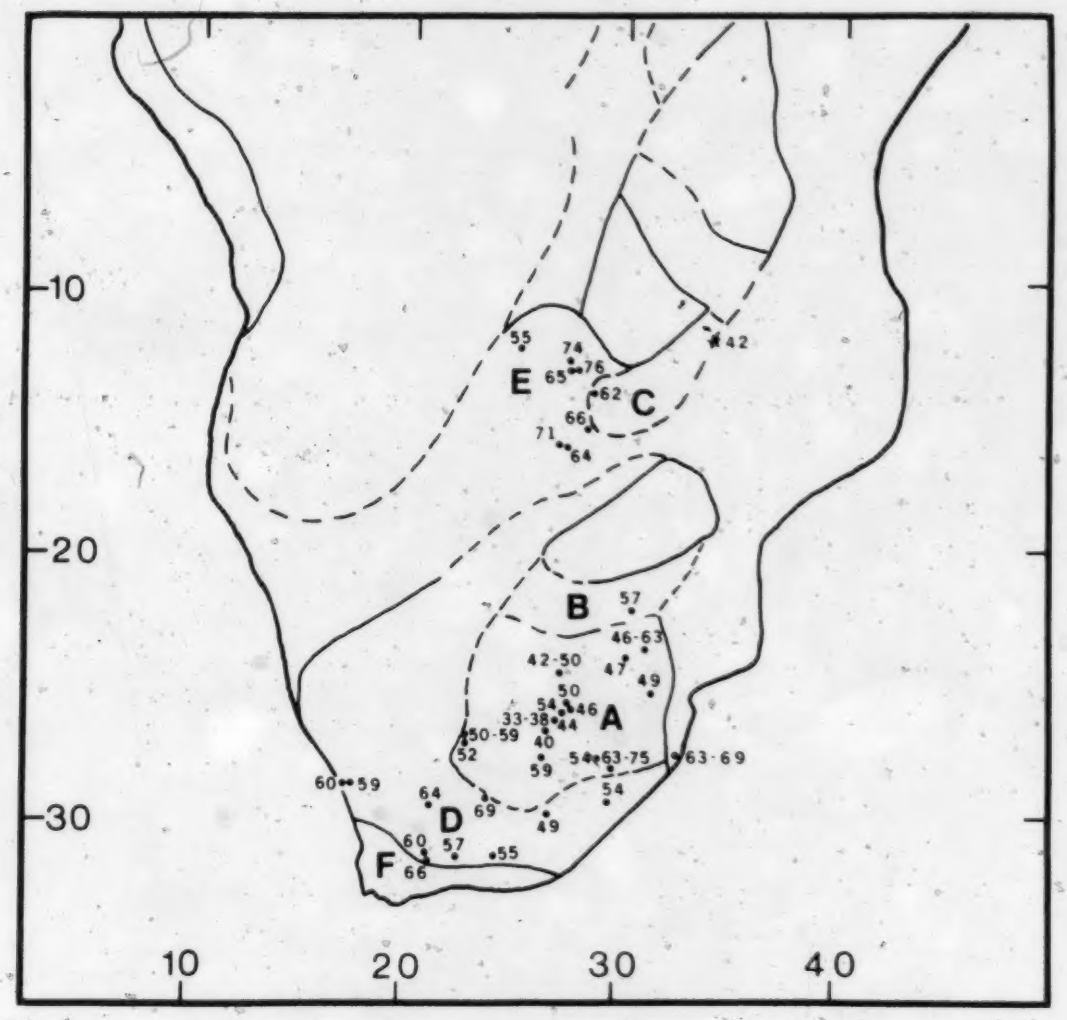

Figure 6.1 Published heat flow data (Gough, 1963; Carte and Van Rooyen, 1969; Chapman and Pollack, 1975; Von Herzen and Vacquier, 1967) for southern Africa in relation to tectonic provinces of Fig. 1.2. The labelled tectonic provinces are in chronological order: A the Kaapvaal shield, B the Limpopo Belt, C the Irumide Fold Belt, D the Namaqualand-Natal Belt, E Damaran-Katangan age province and F the Cape Fold Belt. The star indicates an average of 20 heat flow measurements in Lake Malawi (Von Herzen and Vacquier, 1967) and the other eight values north of 20°S are the recently reported values for Zambia (Chapman and Pollack, 1975).

U.S.A. (Gough, 1974), or to composition (Garland, 1975). Figure 6.1 shows some published heat flow data (Gough, 1963; Carte and Van Rooyen, 1969; Chapman and Pollack, 1975; Von Herzen and Vacquier, 1967) for southern Africa superimposed on the tectonic provinces of Fig. 1.2. There are no heat flow data from the Cape Fold Belt, but at least three heat flow measurements on the conductivity anomaly just to the north of the fold belt and one further east just to the north of the folding (Gough, 1963). These four heat flow values have a mean of 60 mWm^{-2} (1 HFU = 1u cal $cm^{-2}s^{-1}$ = 41.8 mWm^{-2}) which is 1 mWm^{-2} more than that for the other six values on the Namaqualand-Natal Belt. There seems to be no higher heat flow over the anomaly.

6.1.2 Gravity data

A large negative isostatic gravity anomaly exists in south-eastern South Africa at the eastern end of the Cape Fold Belt (Fig. 6.2). It reaches a minimum of -800 g.u. (1 g.u. = 1×10^{-6} ms^{-2} = 0.1 mgal) of which about 200 g.u. can be ascribed to Cretaceous sediments (De Beer et al., 1974). This anomaly is elongated along an east-west axis. In reporting this anomaly Hales and Gough (1960, 1961) explained it as being caused by a relict root or thickening of the crust which had provided Airy type compensation for

Figure 6.2 Magnetic, gravity and conductivity anomalies in southernmost Africa in relation to the Cape Fold Belt. The maximum and minima of the Beattie magnetic anomalies shown in Fig. 6.3 are indicated. The gravity anomalies are departures from an Airy model of isostatic compensation with crustal thickness 30 km. The inset map is adapted from Hales and Gough (1960) and the gravity units are in mgal (1 mgal = 10 g.u.). The arrows represent the negative of the in-phase induction vectors for a period of 128 min for the five stations nearest to the anomaly. The approximate axial line of the conductive structure is indicated.

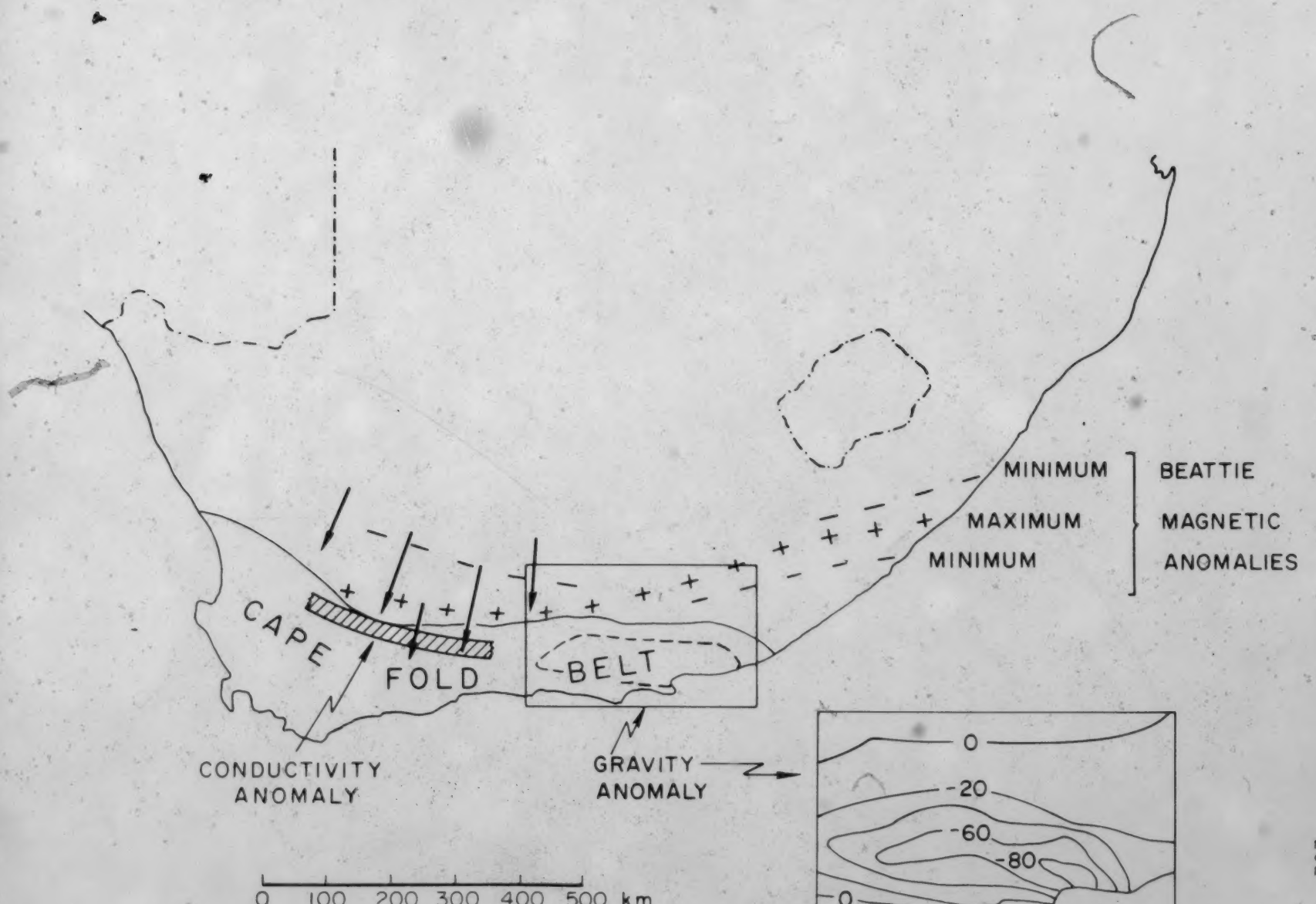
MINIMUM
MAXIMUM
MINIMUM
BEATTIE
MAGNETIC
ANOMALIES
CAPE
FOLD
BELT
CONDUCTIVITY
ANOMALY
GRAVITY
ANOMALY
0
-20
-60
-80
0
0 100 200 300 400 500 km

a mountain range since eroded away. It was pointed out that a mountain range which would just be supported by the root would be 30 km wide and 1.4 km high. Since large stresses are necessarily associated with isostatic anomalies of this large magnitude and area, a sequence of failures was predicted by Hales and Gough (1960) leading finally to uplift near the anomaly axis and reduction of the isostatic anomaly and the stresses. There are no large scale isostatic anomalies in the western half of the Cape Fold Belt which could be explained by postulating that the process of uplift is more advanced there than in the east. Söhnge (1935) showed that large vertical movement had in fact occurred in the western region.

6.1.3 Aeromagnetic data

The most prominent linear geophysical feature in South Africa is the Beattie Ridge magnetic anomaly (Beattie, 1909) which lies to the north of and, for most of its 900 km length, parallel to the Cape Fold Belt (Figs 6.2 and 6.3). The main anomaly consists of a maximum with amplitude ranging from about 100 to 500 nT (total intensity) flanked over large distances by long linear minima. Inspection of the 1:1,000,000 Bouguer anomaly map of South Africa (Smit, Hales and Gough, 1962) reveals no associated gravity anomaly. Deep Schlumberger

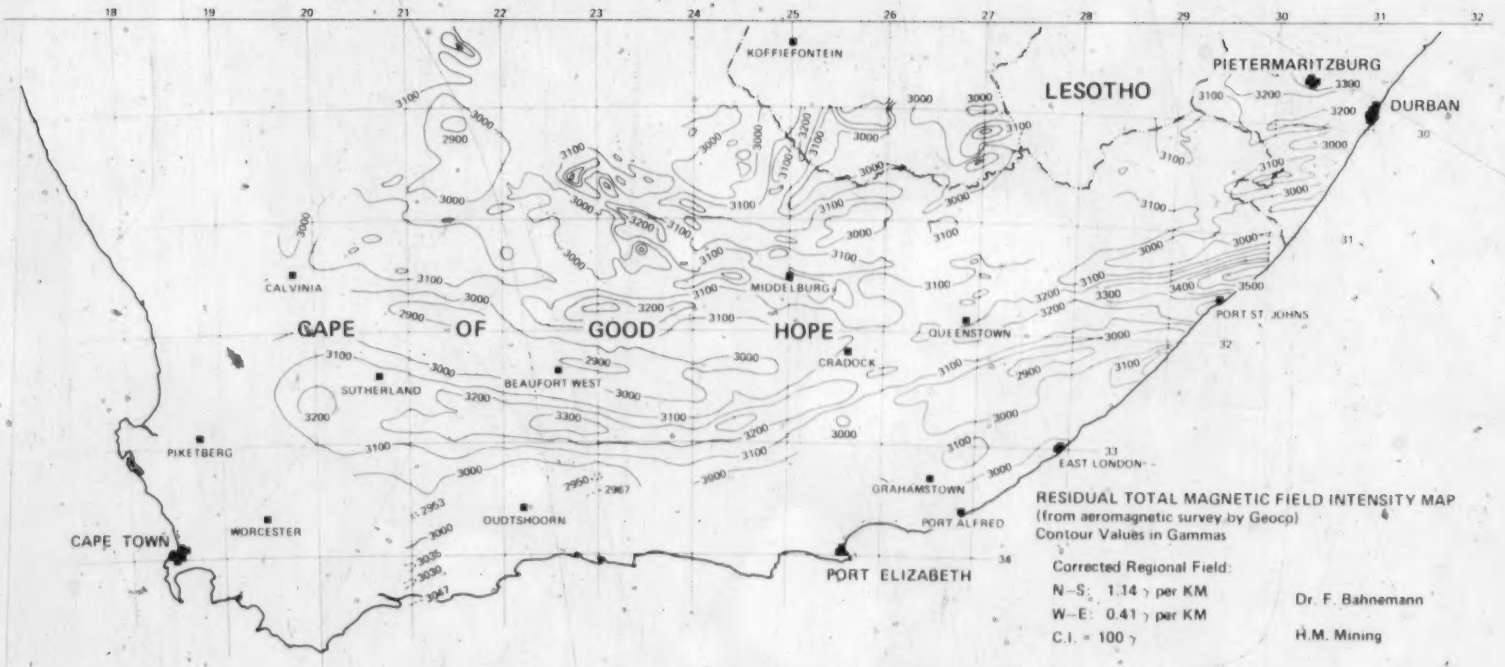

Figure 6.3 Residual aeromagnetic map of central and south-eastern Cape Province, South Africa, constructed from the SOEKOR aeromagnetic map of the area by Dr. F. K. Bahnemann, from H. M. Mining. (Dr. Bahnemann's permission to reproduce this diagram is acknowledged with thanks.)

soundings across the anomalous magnetic structure (Van Zijl, Bahnemann and De Beer, unpublished observations) suggest that the causative body is in the basement beneath the Karroo sediments. Model studies by F. Bahnemann (personal communication) indicate that the anomalous magnetic structure is most likely in the middle or lower crust. Du Plessis and Simpson (1974) found that at their eastern extremeties the linear east-west trending Beattie anomalies are truncated by the continental slope. These authors showed from simple depth calculations that on the continental shelf the bodies causing the anomalies lie at depths varying between 0.6 km and 3.0 km. In this depth range seismic refraction studies have been interpreted as indicating Cape-Karroo rocks (Ludwig et al., 1968). This is not consistent with the results from the deep Schlumberger soundings further west. Du Plessis and Simpson (1974) believe that the causative bodies are late-Karroo dolerite intrusions rather than Precambrian intrusives and metamorphics. This explanation is not consistent with the situation further west in the array area, because there the Beattie Ridge anomaly lies well south of the southern Karroo dolerite occurrence. There are no Karroo dolerites intruded into the western part of the fold belt and the whole fold belt actually shows a total absence of any significant igneous or regional metamorphic activity. From

Figs 6.2 and 6.3 it is clear that the Beattie anomalies do not continue under the fold belt.

6.1.4 The Cape Fold Belt and its origin

The Cape Fold Belt consists of two folded chains, a smaller north-south belt along the western edge of the fold mountains and the principal east-west chain along the Cape Fold Belt marked in Fig. 6.2. The folded sediments range in age from Late Ordovician (Cocks et al., 1970; Cramer et al., 1974) to late Permian (Haughton, 1969) but the main phase of folding was in the Triassic (Haughton, 1969) and involved the east-west chain. The less severe north-south trending Cedarberg folding occurred in pre-Dwyka times (i.e. before the Middle-Carboniferous). The lithology and palaeontology of the Table Mountain and Bokkeveld Groups (the two lower stratigraphic units in the Cape-Karroo sedimentary sequence) argue for deposition on a continental slope with marine conditions to the south (Rust, 1973). The first signs of a southern land mass (Ryan, 1967) and pre-Dwyka folding in the east-west fold belt (Haughton, 1969) are observable in Witteberg (Lower Carboniferous) strata. There is now good evidence that this southern land mass was not simply an uplifted part of the continental craton as was widely accepted (e.g. Haughton, 1969; Newton, 1973), but an island

arc type of orogenic welt possibly related to a subduction zone with associated trench south of the present coastline. Near the southern edge of the Karroo basin graywackes rich in volcanic fragments and tuff layers are found in sediments that were transported from the south (Martini, 1974; Elliot and Watts, 1974). Since there was no volcanic activity in the Cape Fold Belt, the volcanoes must have been situated seaward of the present south coast, in Gondwanaland of Permian times.

The origin of the folding in the Cape Fold Belt is still a matter of controversy. Some geologists (e.g. Newton, 1973, 1974a,b) argue that the fold belt does not resemble a typical "Plate Tectonics" orogen in respect of structural style, sedimentation or igneous and metamorphic activity. Newton (1973) therefore proposed a gravity-folding model controlled by the structure of the pre-Cape rocks.

Other geologists (e.g. De Swardt et al., 1974) suggest that the Cape orogeny is of Alpine type generally ascribed to gravity sliding away from a median zone of excessive uplift, with movement of the cover over a more rigid basement, which is accompanied by folding and thrusting. It is further pointed out by these authors that the best explanation for orogenies of Alpine type is that of collision of continental lithospheric plates.

An important factor in the assessment of the two proposals is the relative position of southernmost Africa in the pre-drift Gondwanaland. Geophysical evidence concerning the south-eastern continental margin of South Africa (Francheteau and Le Pichon, 1972; Scrutton and Du Plessis, 1973; Scrutton, 1973a,b; Du Plessis and Simpson, 1974) as well as drilling results from the Falkland Plateau (preliminary reports from Scientists aboard Glomar Challenger for Leg 36 of DSDP, 1974) strongly suggest an Upper Triassic-Lower Jurassic Gondwana model in which the Falkland Plateau as part of the South American plate bordered the African plate and extended as far as Durban along the present coast (Scrutton, 1973a). The Gondwana reconstruction would then be like that of Smith and Hallam (1970) with the Antarctic Peninsula perhaps positioned further south. Patagonia and the Antarctic Peninsula would be situated to the south of Africa, taking directions with reference to present-day Africa. In his book "Our Wandering Continents" Du Toit (1937) described this fold belt crossing southern Gondwanaland, and it is clear that the Cape Fold Belt represents only the northern edge of this Gondwanide Orogen.

The available evidence seems to support the hypothesis that during late Palaeozoic-early Mesozoic times an oceanic plate underthrust Gondwanaland along its

then southern boundary. Finally a continent-continent or more likely continent-island arc collision occurred producing mountain building which lasted from the Permian to middle Triassic. In South Africa the most obvious result of this collision is the Cape fold mountains. Over-folding to the north is a prominent feature in these mountains indicating that the pressure was directed mainly from the south.

The absence of volcanic activity in the Cape Fold Belt is consistent with a subduction zone with trench off the present southern coastline of Africa. The geology and palaeontology of the Falkland Islands and results of deep sea drilling on the Falkland Plateau (preliminary report from the Scientists aboard the Glomar Challenger for Leg 36 of DSDP, 1974) indicate that the islands were also to the north of such a subduction zone.

Padula et al. (1967) presented geological evidence for a subduction zone (they refer to an eugeosyncline) that bordered the western rim of present-day Patagonia, possibly from Devonian to Triassic times. The likelihood of this subduction is well supported by the presence of a paired metamorphic belt extending along the Pacific coast of South America from Santiago de Chile to Tierra del Fuego. The high-pressure metamorphic zone is situated on the western side of this belt and the age of the metamorphism is

Permian (Gonzalez-Bonorino et al., 1970). In Patagonia late Palaeozoic to earliest Mesozoic magmatic activity, both intrusive and extrusive, has been demonstrated for the North Patagonian Massif and southward to the Deseado Massif (Halpern, 1968; Halpern et al., 1972). Rubidium-strontium whole-rock isochrons and mineral dates indicate igneous activity from Carboniferous to earliest Triassic for the South American sector Gondwanide Orogen.

In West Antarctica there exists similar evidence for subduction. The deformation is of early Mesozoic age in the Ellsworth Mountains and through West Antarctica there are late Palaeozoic and early Mesozoic intrusions, which suggest that the Gondwanide Orogen crossed this part of the continent (Halpern, 1968; Dalziel and Elliot, 1973). The upward increase in air-fall tuff beds in Triassic strata of the Beardmore region suggests that the centres of volcanism were becoming more vigorous or slowly encroaching on the Beardmore area (Elliot and Watts, 1974). A subduction to the south of Permo-Triassic Gondwanaland is thus firmly established.

A folding model based on continental (or continent-island-arc) collision offers an explanation for the negative isostatic anomaly associated with the Cape Fold Belt, because the roots of collision mountain belts will be sialic.

This model, however, does not offer a direct explanation to the presence of the Beattie magnetic anomalies or the induction anomaly which is actually of primary importance in this discussion.

6.1.5 Proposed causes of induction anomaly

Gough (1973c) suggested that it is possible that the high conductivity zone is associated with anomalously high temperatures and partial melting and that the conductive body could in fact be a linear region of ascending mantle material - a ridge-like structure on the more conductive zone in the mantle. The isostatic anomaly may then be the gravitational signature of this same east-west trending region of high temperature in the upper mantle. If this is the case further work should indicate that the isostatic and induction anomalies coincide in the eastern part of the Cape Fold Belt. The heat flow data in Fig. 6.1 neither support nor deny this suggestion. In the earlier discussion it was noted that the main phase of folding occurred during Triassic times. The folding itself therefore will be unrelated to any possible thermal anomaly in the mantle because it is hardly possible that such an anomaly would persist for a time of order 10^8 yr. Recent uplift in the region, however, could be related to a present thermal structure.

Despite this Newton (1974a) suggested that Gough's proposal supported his model for the formation of the fold belt. Newton proposed that such linear mantle bulges would offer a driving force for the vertical movements of the fault-defined blocks which his model requires. He also suggested that the conductivity anomaly should lie to the north of the isostatic anomaly because the isostatic anomaly lies on the depressed southern side of the major fault bounding the Cretaceous-filled Algoa basin. This is in contradiction to Gough's explanation of the isostatic anomaly and would also imply that the thermal anomaly persisted for about 10^8 yr.

A set of data that has not been used in this discussion is the radiometric ages for the basement rocks. Nicolaysen and Burger (1965) pointed out that a south-westerly traverse starting on the Kaapvaal craton would pass from granitic gneisses older than 2,600 Myr old gneisses of the Namaqualand-Natal Belt and then through the Malmesbury geosyncline intruded by 600 Myr old granites and capped by the Palaeozoic-Mesozoic Cape Fold Belt. In this extensive age study of the Namaqualand-Natal Belt they suggested that the thermal event that caused the metamorphism could have been a linear incursion of heated mantle below the Namaqualand-Natal metamorphic

zone. They further suggested that the continent grew by the accretion of younger mobile belts like the Malmesbury geosyncline. Put into modern plate tectonic language this could mean that a plate was underthrust beneath the Gondwanaland of about 1,000 Myr ago along its southern boundary to produce the high temperature belt that caused the 1,000 Myr old metamorphism. This process also accreted material onto the continent to extend the continent southward and in this process formed the Malmesbury geosynclinal sequence into which the 600 Myr old Cape Granites are intruded. A similar, but much more extensive process has been suggested for the formation of most of Western Canada west of the Rocky Mountains (Monger et al., 1972).

The Beattie magnetic anomalies are in agreement with such a linear accreting process. From Figs 6.1 and 6.3 it is clear that these anomalies roughly parallel the southern boundary of the Kaapvaal craton. The aeromagnetic maps of British Columbia also show linear anomalies of comparable amplitude parallel to the coast (Haines et al., 1971; Stacey, 1973). The conductivity anomaly therefore could be caused by the transition from the highly metamorphic crust and associated uppermost mantle to the much younger (at least, 1,600 Myr younger) crust and uppermost mantle of the Malmesbury geosyncline. In its exposures to the south

of the fold mountains the Malmesbury rocks consists of grits, shales, graywackes, limestones, basic lavas and tuffs, quartzites, phyllites, schists and with higher grade metamorphic rocks in the areas intruded by granites. In general the metamorphism was low-grade (Haughton, 1969). Highly magnetic peridotite incorporated into the crust could give rise to the Beattie magnetic anomalies. This model would explain the association of the induction anomaly and the static magnetic anomaly. From Fig. 3.14 it is clear that the Karroo sediments are thin to the north of the station BEA (Beaufort-West) which is on the northern edge of the induction anomaly, while to the south of it the Karroo basin deepens dramatically and the folding begins. This is most probably due to the difference in mechanical properties between the older lithosphere north and the younger lithosphere south of Beaufort-West. In this case the northern edge of the conductor would mark the southern boundary of the Kalahari craton (Clifford, 1967).

6.1.6 Conclusion

This discussion is necessarily speculative because some of the crucial data to determine which of these hypotheses, if any, is the correct one are still lacking. The required data will include an extension of

the array coverage further east, heat-flow studies in the Cape Fold Belt and seismic crustal studies to determine if such a drastic transition from the Namaqualand-Natal Belt to the Malmesbury geosyncline do exist. Geological investigation of the problem is severely hampered by the thick cover of Palaeozoic-Mesozoic sediments in the important areas. The problems concerning the Cape Fold Belt and its relation to the basement geology and geophysical parameters in the area form part of the South African contribution to the Geodynamics Project.

On the present data, which are in many respects incomplete, the writer prefers the hypothesis that the induction anomaly is due to a compositional difference between the lithosphere in the Kalahari craton and the younger lithosphere further south. This hypothesis seems to me more consistent with the available data than the proposal of Gough (1973c), but a decision is impossible at this stage.

In Chapter 3 a NW-SE trending anomaly was described, seen at the stations OLI, PRI and PET for horizontal fields with north-westerly polarizations. This anomaly coincides with the Doornberg-Brakbos fault system which marks the boundary between the Kaapvaal craton and the Namaqualand Belt (Viljoen, 1975) and which ends in the North Cape Fold Belt. This fold Belt shows up in the gravity

maps for South Africa (Smit, Hales and Gough, 1962) and Botswana (Reeves and Hutchins, 1975) and runs north from the stations UPI and OLI in Fig. 3.1 to just south of the Okavango Delta in Botswana (Fig. 6.4). In Chapter 4 evidence was given for a conductor running east-west through South-West Africa and turning northeast in Botswana to enter the mid-Zambezi valley. It was shown that induced currents were larger for NW-SE polarization of the horizontal field than for NE-SW polarization. The North Cape Fold Belt may link this conductive zone to the Doornberg-Brakbos fault zone, in a structure generally consistent with the observed polarization dependence of the induction anomaly.

6.2 The conductive zone in South-West Africa and Botswana

The most significant result of the 1972 array study in South-West Africa, Botswana and western Rhodesia is the discovery of a zone of concentrated induced electric currents indicated in Figs 6.4 and 6.5. The station spacing defines the boundaries of the conductive zone within about half a degree, except at its western extremity where they are determined within a quarter degree.

The work in this section has been reported on by De Beer, Gough and Van Zijl (1975).

Figure 6.4 The conductor in relation to seismicity and tectonics of southern central Africa. Small dots, $2 \leq m \leq 4$; large dots, $m > 4$. Small squares intensities ≤ 3; large squares > 3. Faults (bold lines) are from Geological Map of Botswana (1973), Gough and Gough (1970), Geological Map of South West Africa (1963), Provisional Geological Map of Rhodesia (1971) and International Tectonic Map of Africa (1968). Geological boundaries are from the geological maps of Botswana and South-West Africa and Haughton (1969). The bathymetric depths are in metres.

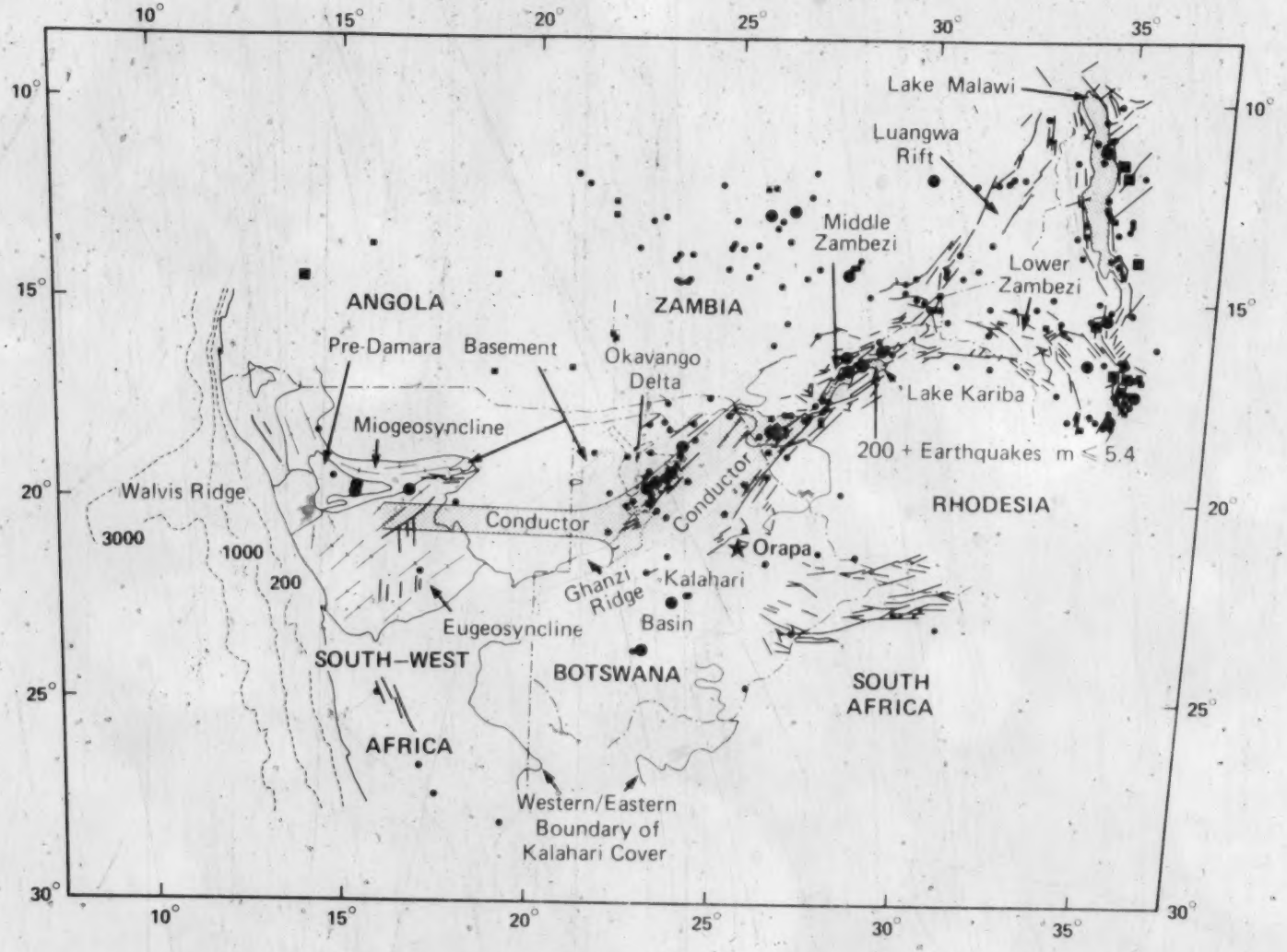
10°
15°
20°
25°
30°
35°
Lake Malawi
Luangwa Rift
Middle Zambezi
Lower Zambezi
ANGOLA
ZAMBIA
Pre-Damara
Basement
Okavango Delta
Lake Kariba
Miogeosyncline
200 + Earthquakes m ≤ 5.4
Walvis Ridge
3000
1000
200
Conductor
Conductor
RHODESIA
Orapa
Ghanzi Ridge
Kalahari Basin
Eugeosyncline
SOUTH–WEST AFRICA
BOTSWANA
SOUTH AFRICA
Western/Eastern Boundary of Kalahari Cover

Figure 6.5 African rifts and shields in relation to the conductivity anomaly (compiled from a map by McConnell (1972) and other sources).

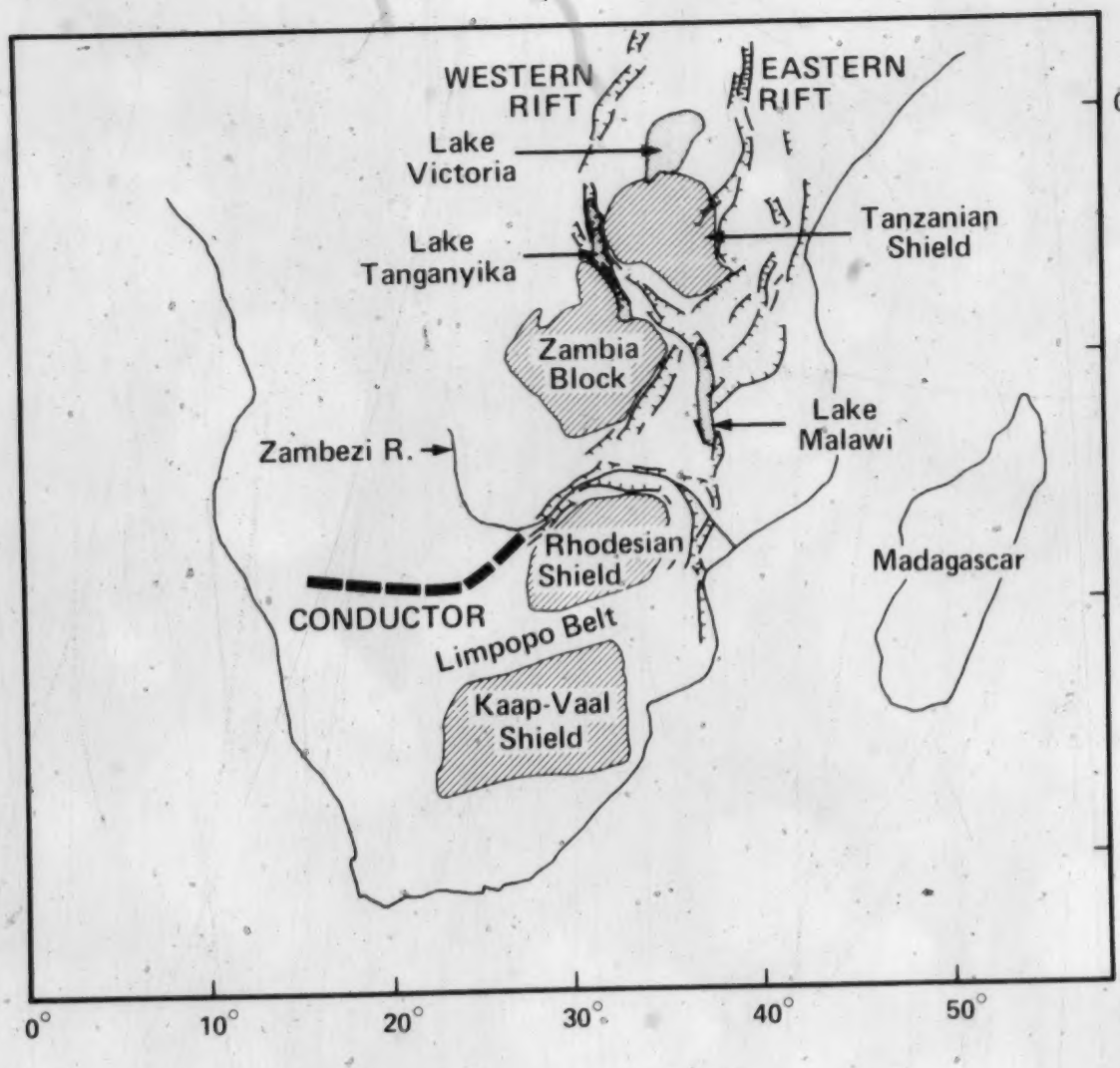
WESTERN RIFT
EASTERN RIFT
Lake Victoria
Lake Tanganyika
Tanzanian Shield
Zambia Block
Lake Malawi
Zambezi R.
Rhodesian Shield
Madagascar
CONDUCTOR
Limpopo Belt
Kaap-Vaal Shield
0°
10°
20°
30°
40°
50°

The half-widths of normalised anomalous fields and the induction vectors indicate that the conductor is at crustal depth. From east to west the conductive zone continues the south-westward line of the Luangwa-middle Zambezi Rift (Fig. 6.5) and bends south of the Okavango Delta to run nearly westward across South-West Africa. In the north-eastern part of South-West Africa and all of Botswana the Kalahari sands of Tertiary or younger age cover the solid rock and hide almost all tectonic features. The Kalahari basin was formed in Tertiary times when large parts of southern Africa went through phases of intermittent and differential uplift intercalated with periods of peneplanation or pediplanation (Haughton, 1969). Boreholes reveal Mesozoic Karroo sediments or volcanics under much of the Kalahari basin indicated in Fig. 6.4 (Reeves, 1972; Reeves and Hutchins, 1975) but have not so far penetrated the Kalahari sediments in the Okavango Delta (D. Hutchins, personal communication). Major linear features with a north-east trend are found near the Okavango and have been interpreted as faults (Reeves, 1972; Geological Map of Botswana, 1973; Scholz et al., in press). These lineaments continue the line of the middle Zambezi-Luangwa Rift, an important linear structural element in the tectonic framework of central southern Africa. The middle Zambezi valley containing Lake Kariba, is an

asymmetric rift preserving Karroo rocks downfaulted along about Middle Jurassic faults (G. Bond, personal communication) between Precambrian shield rocks. Although the fault pattern is reasonably well known (Cox, 1970; Gough and Gough, 1970) little is known about the mineralization and water bearing qualities of the faults (G. Bond, personal communication). In the Luangwa Rift we also have Upper Karroo sediments and volcanics downfaulted against basement rocks, with the age of faulting generally the same (Drysdall et al., 1972). Several igneous centres are known along the Luangwa Rift (Cox, 1970), including Cretaceous carbonatite volcanoes (Vail, 1968; Bailey, 1961). There are also carbonatites and kimberlites in the middle Zambezi (Lee, 1974) and a cluster of diamond-bearing kimberlites near Orapa in Botswana (Fig. 6.4). As early as 1921 Gregory considered the Luangwa-middle Zambezi Rift as an extension of the East African rift system better developed and known in Kenya and Ethiopia. Others, like Du Toit (1954) and Bailey (1961) used geological arguments to propose south-westward continuation of the Luangwa-middle Zambezi Rift into Botswana.

To test the hypothesis that the conductive zone indicates a continuation of the known rift system of Africa other geophysical parameters in the better studied rifts further north are compared to the same parameters in the study area.

6.2.1 Seismological evidence

The two northern branches of the East African Rift system (Fig. 6.5) are characterized by continuous belts of normal faulting and graben structures and the occurrence of shallow earthquakes (e.g. Baker et al, 1972; Wohlenberg, 1975). The Eastern and Western Rifts, however, differ from each other in several other respects (Maasha and Molnar, 1972). The seismic activity of the Eastern Rift is much less than that of the Western Rift (Gouin, 1970; Fairhead and Girdler, 1971) and increases to the south. Molnar et al (1970) suggested that much of the deformation in the Eastern Rift occurs aseismically. In contrast to mid-oceanic ridges and rift structures seismic activity extends to some 100 km beyond the main rift flanks (Wohlenberg, 1975; Bath, 1975).

Considerable seismic activity with magnitudes up to 6.7 occurred in the Okavango Delta region in the period 1949-1955 with 90% of the events in late 1952-early 1953 (Gane and Oliver, 1953; Oliver, 1956). Reeves (1972) mapped 50 earthquakes in Botswana over the period 1965-1971 and found a concentration of epicentres in the Okavango Delta and scattered events in the central Kalahari. Reeves believes the broad Ghanzi Ridge of post-Damara sediments separates the two seismic regions. In the Lake Kariba region a low initial level of seismicity rose several orders

of magnitude as the lake filled, culminating in three events of magnitudes near 6 in 1963 just after the lake level peaked. Triggering of renewed activity on the existing faults, by incremental solid stress rather than water pressure, was suggested by Gough and Gough (1970). Since 1963 activity has continued with very slow, if any, decline, in a manner consistent with the hypothesis that the region is now seismic in a steady state. Mechanisms for two of the large events show normal faulting with one nodal plane striking N 25°E parallel to regional faults (Sykes, 1967; Fairhead and Girdler, 1971). These and other fault plane solutions for earthquakes in eastern and southern Africa (Banghar and Sykes, 1969; Fairhead and Girdler, 1971; Maasha and Molnar, 1972) suggest tensile deviatoric stress in a WNW-ESE direction. Fairhead and Girdler (1971) showed that in the period 1963-1970 earthquakes in southern central Africa were located in a broad seismic zone running southward from Lake Tanganyika to a point just west of Lake Kariba. Except in the Lake Kariba area the middle Zambezi-Luangwa Rift was virtually aseismic through 1963-1970.

Epicentres from several sources (Fernandez, 1972; Fernandez and Guzman, 1973; Rhodesia Meteorological Services, 1973; L. M. Fernandez and J. A. Guzman, unpublished) for the period 1965-1973 have been plotted in Fig. 6.4. Their

distribution supports the hypothesis that the Luangwa-middle Zambezi Rift continues to the south-west into Botswana. The focal depths of the earthquakes range down to 50 km (Fernandez, 1972; Fernandez and Guzman, 1973).

A micro-earthquake study was done in the Okavango region from mid-September to mid-December, 1974 (Scholz et al., in press). The activity was largely confined to a narrow band running northeast along the southeastern edge of the Okavango Delta and further north-east towards the Zambian border. The rate of seismicity was found to be about the same as that in the main rift valleys of East Africa. A composite focal mechanism for well located events near the southeastern boundary of the delta indicates normal faulting on north-east striking planes. One nodal plane dipping 60° to the northwest strikes parallel to the faults in the area. Scholz et al. (in press) suggest that the delta is at the tip of a zone of incipient rifting that follows the older Mid-Zambezi Luangwa Rift.

West of the Okavango the conductive zone runs a few degrees north of due west to the exposed part of the Damara Geosyncline in South-West Africa (Fig. 6.4). The zone of high conductivity cuts obliquely across the WSW-ENE grain (Haughton, 1969; Clifford, 1967) of the high-grade metamorphic rocks of the eugeosynclinal Swakop

Facies of Upper Proterozoic-Lower Palaeozoic ages (Clifford, 1967). The miogeosynclinal Outjo Facies to the north has generally E-W strikes in its eastern exposures and gradually assumes a more northerly strike westward. The conductor runs roughly parallel to the folding in the eastern outcrops of Outjo Facies rocks and the boundary between the eugeosyncline and the miogiosyncline. It also parallels the northern limit of the Damara regional metamorphism (Clifford, 1967). No recent major faults are known to run parallel to it. At least four earthquake epicentres were located close to the northern edge of the conductor for the period 1965-1973 (Fig. 6.4). An association of the conductor with the boundary between two stable crustal blocks seems possible.

Seismological evidence for the mantle under the East African rifts shows low P velocities and attenuation of S_n north of a discontinuity near latitude 4°S (Fairhead and Girdler, 1971; Maasha and Molnar, 1972; Baker et al., 1972; Wohlenberg, 1975). For a path Addis Ababa-Nairobi, Rayleigh wave phase velocities are low for a continental path (Knopoff and Schlue, 1972) and resemble those in the Basin and Range province of western North America. Elsewhere in Africa phase and group velocities of surface waves and travel times of P_n, S_n

and L_g indicate that the structure beneath most of Africa is typical of stable continental regions (Bloch et al., 1969; Gumper and Pomeroy, 1970).

Bloch, Hales and Landisman (1969) studied Rayleigh-wave phase velocities in southern Africa and found lower phase velocities west of a line through Pretoria and Bulawayo than along that line and east of it. In the western region which includes the magnetometer array area the Rayleigh-wave phase velocities are very similar to those in the central United States and eastern Australia, which are both non-shield continental regions. This is consistent with the tectonic pattern of southern Africa as discussed in Section 1.3 and portrayed in Fig. 1.2.

6.2.2 Gravity data

Both the Western and Eastern Rifts north of about 4°S show broad (200-500 km wide) negative gravity anomalies. To the south of 4°S these negative anomalies disappear, but along the Western Rift there are localised positive anomalies (Wohlenberg, 1975). The gravity data in this region are however very sparse. North of 2°S the Eastern Rift has a central positive anomaly superimposed on the broad negative anomaly, usually interpreted as evidence of intrusion of mantle-derived material (Girdler and Sowerbutts, 1970: Searle, 1970; Baker and Wohlenberg,

1971; Darracott et al., 1972: Wohlenberg, 1975). There is no central positive anomaly and thus no evidence of a central intrusion under the Western Rift (Wohlenberg, 1975). For no rift is there geophysical evidence of partial melting in the mantle south of 4°S, at which latitude the fracture pattern in the eastern rift changes from grid faulting in the north to block faulting in the south (Fairhead and Girdler, 1972). Girdler (1975) drew attention to a large negative anomaly on the Bouguer anomaly map of Africa (Slettene et al., 1973) as shown in simplified form in Fig. 6.6a. Girdler pointed out that north of 10°S the anomaly can be associated with rifting, but he could not offer an explanation for the westward extension. Figure 6.6b shows a simplified relief map of Africa and it is clear that the negative anomaly pattern correlates with the uplifted regions of the continent. This means no more than that the uplifted topography is isostatically compensated. The east-west arm of this negative Bouguer anomaly lies about eight degrees north of the induction anomaly.

Figure 6.7 shows the outline of the conductive zone superimposed on a simplified compilation of the Bouguer anomaly maps of South-West Africa (Geological Map of South-West Africa (showing mineral occurrences and gravity contours), 1963; Kleywegt, 1967), Botswana

Figure 6.6a Simplified Bouguer anomaly map of Africa (Girdler, 1975).

Figure 6.6b Simplified relief map of Africa (Bailey, 1972).

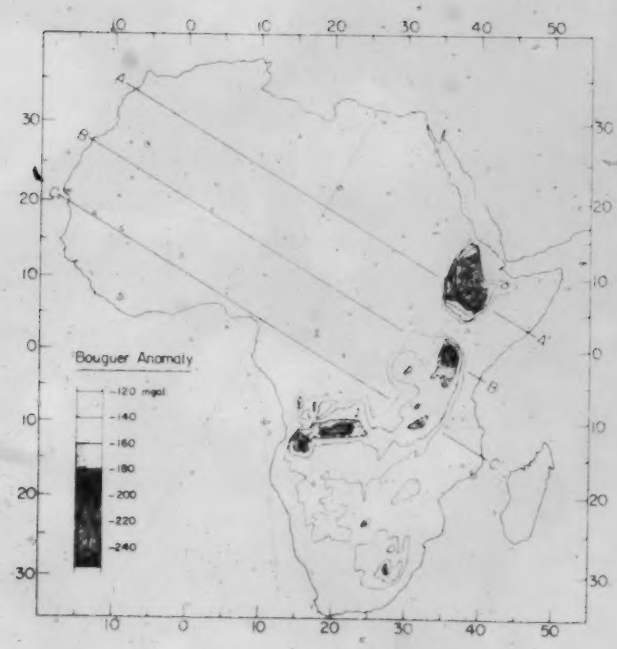
Bouguer Anomaly
-120 mgal
-140
-160
-180
-200
-220
-240
A
B
C
A'
B'
C'

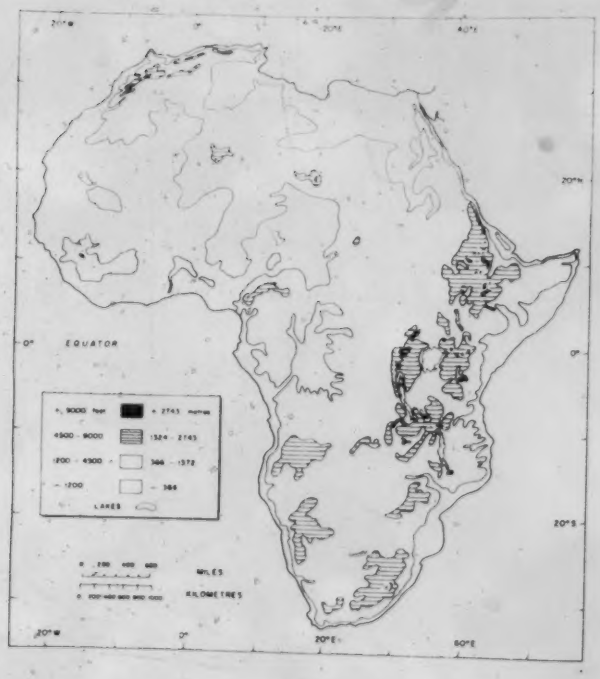
EQUATOR
LAKES
MILES
KILOMETRES

Figure 6.7 Simplified Bouguer anomaly map of South-West Africa, Botswana and Zambia (Geological Map of South-West Africa, 1963; Bouguer Anomaly Map of Botswana, 1974; Provisional Gravity Map of the Republic of Zambia, 1974).

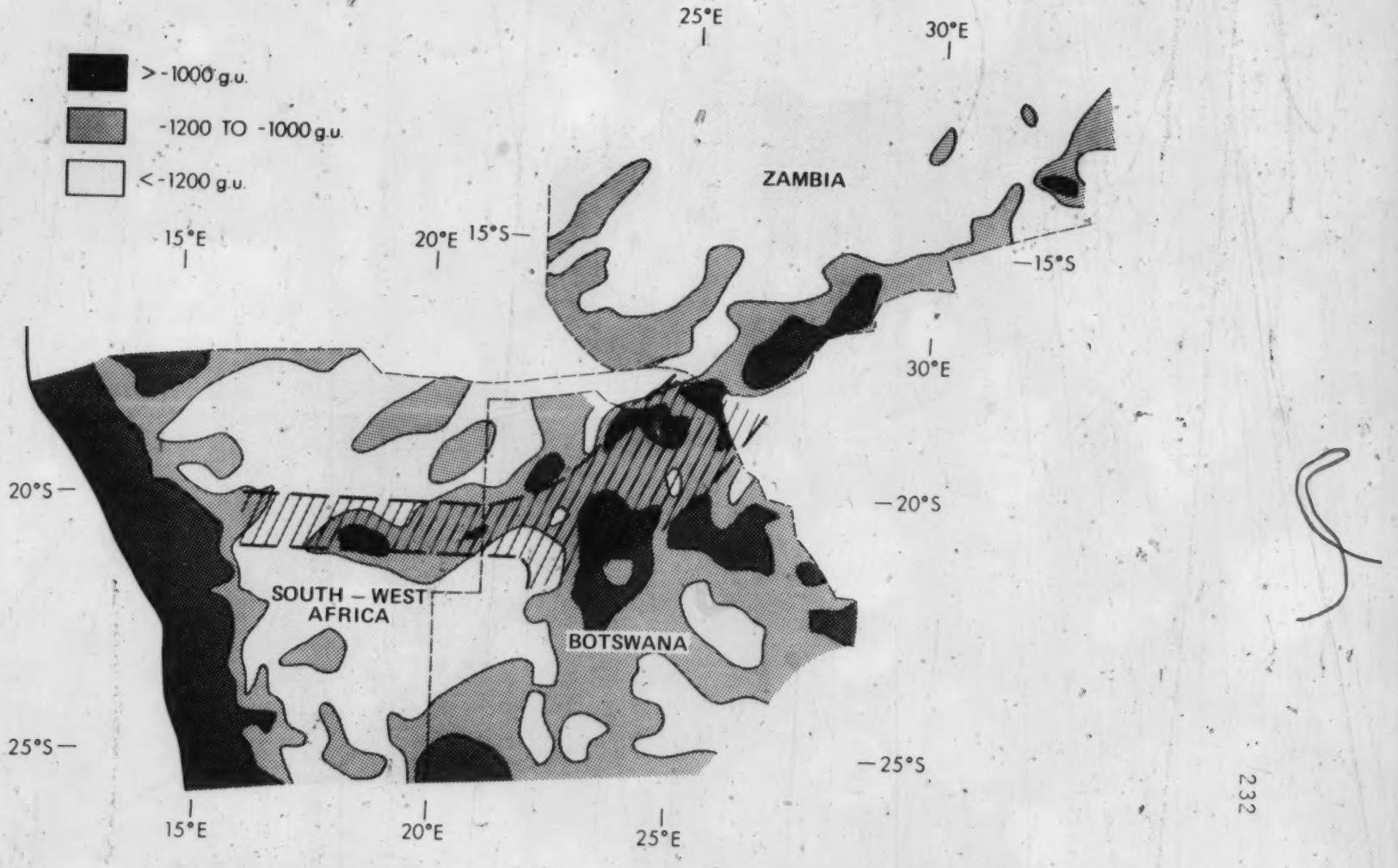
> -1000 g.u.
-1200 TO -1000 g.u.
< -1200 g.u.
25°E
30°E
ZAMBIA
15°E
20°E
15°S
15°S
30°E
20°S
20°S
SOUTH – WEST AFRICA
BOTSWANA
25°S
25°S
15°E
20°E
25°E

(Bouguer Anomaly Map of Botswana, 1974; Reeves and Hutchins, 1975) and Zambia (Provisional Gravity Map of the Republic of Zambia, 1974). The conductive structure and the positive gravity anomalies in the area shows a remarkable correlation. Most of Botswana shows a positive anomaly pattern compared with Zambia and South-West Africa with the exception of the coastal strip. Since Tertiary times most of Botswana has been going through a phase of depression with respect to the neighbouring areas which has gone through several phases of uplift (Haughton, 1969). The changes in relief are thus in accordance with the general gravity pattern. Where the solid rock is exposed in Botswana, as for instance to the south of the south-eastern limit of the conductor, some of the gravity highs are produced by Archean greenstone belts. Reeves and Hutchins (1975) pointed out that a change in the "texture" of the anomalies at a SW-NE striking line coinciding in the east with the south-eastern limit of the conductive zone divides the gravity map of Botswana into two distinct areas. The authors speculated that this change may be associated with an abrupt change in crustal thickness or density or that it may represent the edge of the foreland to the Damaran orogenic belt. Anomalous density distribution resulting from folding and intrusion during the Damara tectono-thermal event could account for some of the

gravity anomalies to the north of this boundary. Kleyweqt (1967) found that the north-easterly trend in the gravity anomalies in South-West Africa is indeed related to folding in the Damara eugeosyncline. In South-West Africa the gravity trend associated with the conductor cuts across the NE-SW trend of the anomalies related to the Damaran orogeny. Figure 6.8 shows a simplified isostatic anomaly map for South-West Africa as computed by Kleyweqt (1967) for an Airy-Heiskanen model with a sea-level crustal thickness of 30 km. The conductive zone coincides with the largest isostatic anomaly in the area. This anomaly reaches a maximum of + 660 g.u. For most of its length in South-West Africa the conductor coincides with an area undergoing subsidence related to the subsidence in the Okavango Delta and Kalahari basin.

The reason for this correlation between an induction anomaly and positive gravity anomalies is not clear. The positive gravity anomalies could be related to anomalous densities and/or crustal thinning. In Chapter 4 it was pointed out that the amplitudes of magnetic variation fields were found to be smaller in Botswana than further west. This reduction in amplitude could be related to a thinner crust or lithosphere in northern Botswana, and some or all of the positive gravity anomalies may be due to thinning. It is worth noting that

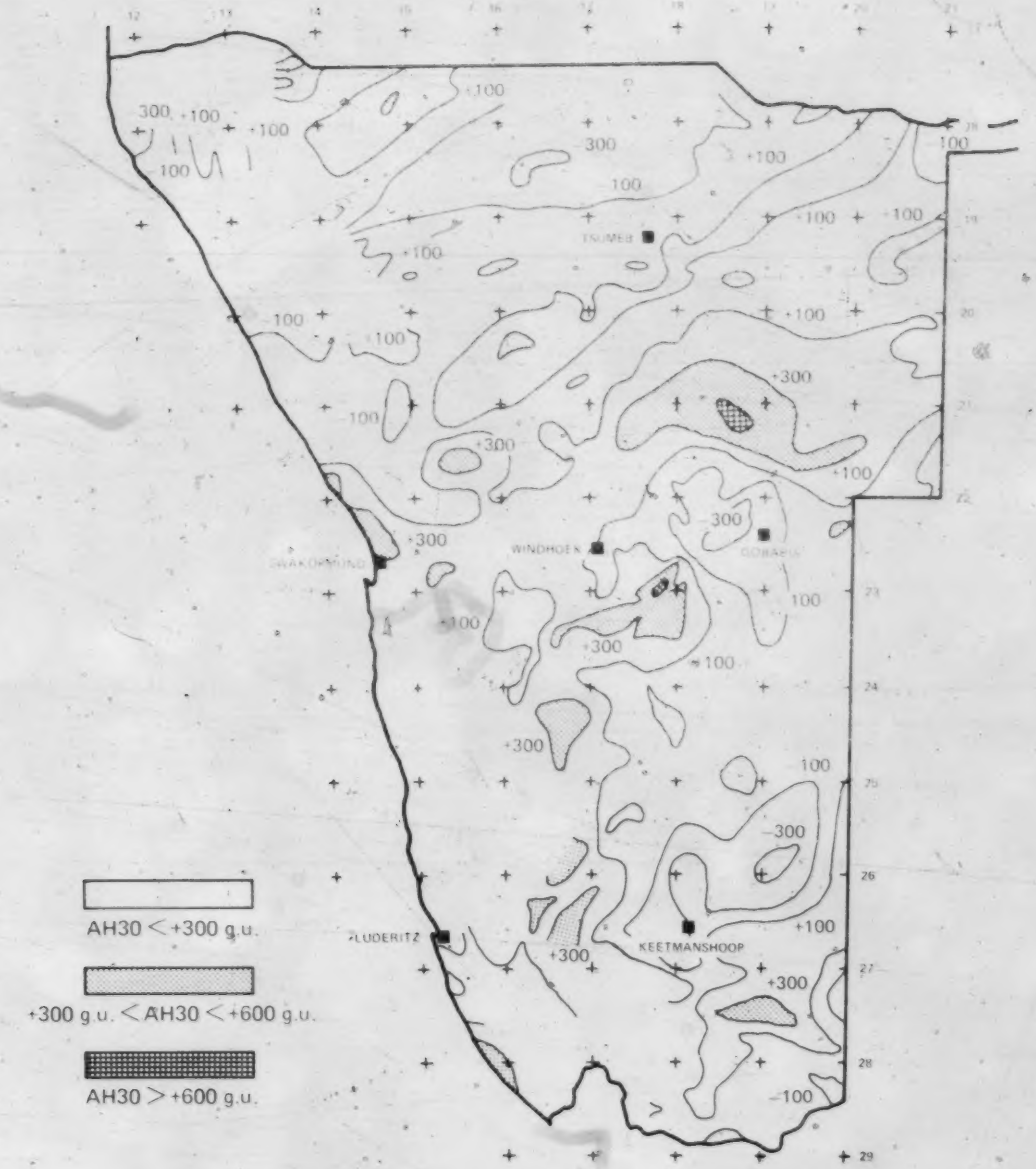

Figure 6.8 Simplified isostatic anomaly map for South-West Africa as computed for an Airy-Heiskanen model with a sea-level crustal thickness of 30 km (Kleywegt, 1967).

the Limpopo Belt between the Kaapvaal and Rhodesian cratons is associated with a positive Bouguer anomaly (Smit, Hales and Gough, 1962). The coincident gravity and induction anomalies may thus mark a similar weak zone between two old stable regions. In the eastern part they coincide with the northern boundary of the Kalahari craton of Clifford (1967).

6.2.3 Geomagnetic depth sounding and heat flow

Geomagnetic depth sounding across the Eastern Rift at the Equator (Banks and Ottey, 1974) revealed anomalies accountable in terms of a conductive region 20 km below the rift floor and another 50 km deep 100 km east of the Rift. Soundings south of 5°S might give different results, in view of the seismological evidence of a change in asthenosphere properties near 2°S.

Recently eight new heat flow values ranging from 55-76 mWm^{-2} were reported from Zambia (Chapman and Pollack, 1975). The authors compared these values (shown in Fig. 6.1) with the mean for Precambrian provinces elsewhere (Polyak and Smirnov, 1968) and found the Zambian values high by about 50%. This led them to conclude that these results support the hypothesis of an incipient arm of the East African rift system (a zone of crustal thinning) running southward from Lake Tanganyika to a point just west of Lake Kariba as proposed by Fairhead and

Girdler (1969). The writer believes this comparison is not fully justified. The heat flow results for South Africa as summarized by Carte and Van Rooyen (1969) give means for the 2,600 Myr old Kaapvaal shield of 50 mWm^{-2} and the 1,000 Myr old Namaqualand-Natal Belt of 60 mWm^{-2}. The seven Zambian sites affected by the Damaran-Katangan tectono-thermal event between 500 and 750 Myr ago give a mean of 67 mWm^{-2}, which is not abnormally high compared to that of the Kaapvaal shield and Namaqualand-Natal Mobile Belt.

6.2.4 Origin of the conductive zone

Regions of high conductivity which produce geomagnetic induction anomalies may be related to high temperatures and partial melting in the upper mantle, as in the western U.S.A. (Gough, 1974), or to compositional conductors such as graphite or saline water which are often concentrated in fracture zones (Gough and Camfield, 1972; Garland, 1975). If the conductive zone under discussion is associated with the African rift system its conductivity could be associated with anomalously high temperature in the upper mantle, or with a fracture zone in the lithosphere, or with both. No definitive decision is possible, but a fracture zone seems the likeliest explanation. From Kariba to the Okavango the conductor can reasonably be

associated with the known fractures, whose activity resembles that of the Western, Lake Tanganyika, Rift. The absence of known fractures along the westward arm of the conductor does not preclude their existence because of the Kalahari cover, and seismic activity is present. The westward arm is in line with the eastern-most part of the Walvis Ridge (Fig. 6.4), which may, on recent geophysical evidence, have a fracture-zone origin, either a pure transform fault or some type of tectonic process following an older line of weakness (Goslin et al., 1974; preliminary report from Scientists aboard Glomar Challenger for Leg 40 of DSDP, 1975). The conductivity anomaly could lie on the original line of weakness within the continent, along the boundary in pre-Damara basement rocks between the eugeosyncline and the miogeosyncline. It is a well-established fact that pre-existing cratons and orogenic belts in southern Africa have often controlled later tectonics (Cox, 1970; McConnell, 1972; Bailey, 1972; Fyfe and Leonardos, 1973; Thorpe and Smith, 1974). The seismicity may thus trace contemporary failure, under a general WNW-ESE tensile stress field, on pre-existing fractures. In addition the gravity data indicate the crust may be thinner along the conductor. The first down-faulting in the middle Zambezi probably occurred during early Mesozoic times (Cox, 1970; Gough and

Gough, 1970) along fractures in the Upper Proterozoic-Lower Palaeozoic mobile zone related to the tectono-thermal Katangan and Damaran Episodes (Clifford, 1967). The conductor could mark this zone of weakness in the lithosphere (Watterson, 1975) along which intermittent movement has occurred since the Upper Proterozoic.

The possibility of a thinner crust associated with the conductor raises the possibility that some of the anomalous conductivity could be due to heat. Another point that has to be borne in mind is that Cainozoic volcanism in Africa has been limited almost exclusively to areas affected by the Damaran-Katangan tectono-thermal event (Thorpe and Smith, 1974). This affinity of volcanism for intercratonic areas is consistent with the higher heat flux of such areas in relation to the cratons (Fig. 6.1) and may reflect variations in other properties of the lithospheric mantle such as variation in chemical and/or mineralogic components which favour formation and segregation of basaltic magma (Kesson, 1973).

The absence of evidence for opening of rifts in southern Africa can be related to global tectonics in two alternative ways. In terms of classical plate tectonics the pole of opening for the East African rift system is in southern Africa (Fairhead and Girdler, 1971; Baker et al., 1972) where opening will therefore be small. On the

membrane stress hypothesis of Oxburgh and Turcotte (1974) the rifts are caused by northward movement of the continent over the equatorial bulge. Again propagating fractures with small displacements would be found in southern Africa.

6.3 Concluding remarks

The two magnetometer array studies discussed in this thesis served as reconnaissance surveys to determine the suitability of this method for resistivity surveys of the old shields and mobile belts in southern Africa. The results were different than expected, and perhaps raised more questions than they answered. From the discussion in this chapter and the previous one it is clear that these surveys set the stage for several experiments, in diverse geophysical disciplines, that could lead to a much better understanding of the deeper structural differences between the various tectonic units in the area as well as the resistivity structure within each unit.

REFERENCES

Alabi, A. O., 1974. A study of the North American Central Plains conductivity anomaly, Unpublished Ph.D. thesis, Dept. of Physics, University of Alberta, Edmonton, Canada.

Alabi, A. O., Camfield, P. A. and Gough, D. I., 1975. The North American Central Plains conductivity anomaly. Geophys. J. R. astr. Soc. 43, 815-833.

Allsopp, H. L., Davies, R. D., De Gasparis, A. A. A. and Nicolaysen, L. O., 1969. Review of Rb-Sr age measurements from the early Precambrian terrain in the south-eastern Transvaal and Swaziland. Geol. Soc. S. Afr. Spec. Publ. 2, 433-444.

Al'pin, L. M., Berdichevsky, M. N., Vedrintsev, G. A. and Zagarmistr, A. M., 1966. Dipole methods for measuring earth conductivity. Consultants Bureau, New York.

Anderson, C. W., 1970. Geomagnetic depth sounding and the upper mantle in the Western United States. Unpublished Ph.D. thesis, Dept. of Physics, University of Alberta, Edmonton, Canada.

Anhaeusser, C. R., 1973. Evolution of the early Precambrian crust of Southern Africa. Phil. Trans. R. Soc. London A273, 359-388.

Anhaeusser, C. R., Mason, R., Viljoen, M. and Viljoen, R. P., 1969. A reappraisal of some aspects of Precambrian shield geology. Geol. Soc. Am. Bull. 80, 2175-2200.

Backus, G. and Gilbert, F., 1967. Numerical applications of a formalism for geophysical inverse problems. Geophys. J. R. astr. Soc. 13, 247-276.

Backus, G. and Gilbert, F., 1968. The resolving power of gross earth data. Geophys. J. R. astr. Soc. 16, 169-205.

Bailey, D. K., 1961. The mid-Zambezi-Luangwa Rift and related carbonatite activity. Geol. Mag. 98, 277-284.

Bailey, D. K., 1972. Uplift, rifting and magmatism in continental plates. J. Earth Sci. 8, 225-239.

Bailey, R. C., 1970. Inversion of the geomagnetic induction problem. Proc. R. Soc. (London) 315, 185-194.

Baker, B. H., Mohr, P. A. and Williams, L. A. J., 1972. Geology of the Eastern Rift System of Africa. Geol. Soc. Am. Spec. Paper 136.

Baker, B. H. and Wohlenberg, J., 1971. Structure and evolution of the Kenya Rift Valley. Nature 229, 538-542.

Banghar, A. R. and Sykes, L. R., 1969. Focal mechanisms of earthquakes in the Indian Ocean and surrounding areas. J. Geophys. Res. 74, 632-649.

Banks, R. J., 1969. Geomagnetic variations and the electrical conductivity of the upper mantle. Geophys. J. R. astr. Soc. 17, 457-487.

Banks, R. J., 1972. The overall conductivity distribution of the earth. J. Geomag. Geoelectr. 24, 337-351.

Banks, R. J. and Beamish, D., 1974. A magnetometer array study of the Kenya Rift Valley. Abstract in proceedings of Second Workshop on Electromagnetic Induction in the Earth, Ottawa (unpublished).

Banks, R. J. and Ottey, P., 1974. Geomagnetic deep sounding in and around the Kenya Rift Valley. Geophys. J. R. astr. Soc. 36, 321-335.

Bath, M., 1975. Seismicity of the Tanzania region. Tectonophysics 27, 353-379.

Beattie, J. C., 1909. Report of a magnetic survey of South Africa. R. Soc. Lond. publ., Cambridge University Press.

Bennett, D. J., 1972. Geomagnetic deep sounding studies in south-eastern Australia. Unpublished Ph.D. thesis, Australian National University, Canberra, Australia.

Bennett, D. J. and Lilley, F. E. M., 1972. Horizontal polarization in array studies of anomalous geomagnetic variations. Nature Phys. Sci. 237, 8-9.

Bennett, D. J. and Lilley, F. E. M., 1973. An array study of daily magnetic variations in south-east Australia. J. Geomag. Geoelectr. 25, 39-62.

Berktold, A., Bennett, D.J., Angenheister, G., Dziewonski, A., Gouin, P., Haak, V. and Porath, H., 1974. The distribution of the electrical conductivity in eastern Ethiopia (Afar depression and the main rift). Abstract in proceedings of the Second Workshop on Electromagnetic Induction in the Earth, Ottawa (unpublished).

Bevington, P. R., 1969. Data reduction and error analysis for the physical sciences. McGraw-Hill Book Co., New York.

Bloch, S., Hales, A. L. and Landisman, M., 1969. Velocities in the crust and upper mantle of southern Africa from multimode surface wave dispersion. Bull. Seismol. Soc. Am. 59, 1599-1629.

Born, M. and Wolf, E., 1959. Principles of optics. Pergamon Press Ltd., London.

Bouguer Anomaly Map of Botswana (Provisional), 1974. Scale 1:1,000,000. Geological Survey Department, Lobatse, Botswana.

Cagniard, L., 1953. Basic theory of the magneto-telluric method of geophysical prospecting. Geophysics 18, 605-635.

Cahen, L., 1961. The geochronological knowledge in middle and northern Africa. New York Acad. Sci. Annals 91, 535-567.

Cahen, L. and Snelling, N. J., 1966. The geochronology of equatorial Africa. Amsterdam, North-Holland Publ. Co.

Camfield, A., 1973. Studies with a two-dimensional magnetometer array in north-western United States and south-western Canada. Unpublished Ph.D. thesis, Dept. of Physics, University of Alberta, Edmonton, Canada.

Camfield, P. A. and Gough, D. I., 1975. Anomalies in daily variation magnetic fields and structure under north-western United States and south-western Canada. Geophys. J. R. astr. Soc. 41, 193-218.

Camfield, P. A., Gough, D. I. and Porath, H., 1971. Magnetometer array studies in the northwestern United States and southwestern Canada. Geophys. J. R. astr. Soc. 22, 201-221.

Caner, B., 1971. Quantitative interpretation of geomagnetic depth-sounding in Western Canada. J. Geophys. Res. 76, 7202-7216.

Caner, B., Cannon, W. H., Livingstone, C. E., 1967. Geomagnetic depth sounding and upper mantle structure in the Cordillera region of western North America. J. Geophys. Res. 72, 6335-6351.

Carte, A. E. and Van Rooyen, A. I. M., 1969. Further measurements of heat flow in South Africa. Upper Mantle Project. Geol. Soc. S. Afr., Spec. Publ. 2, 445-448.

Chapman, D. S. and Pollack, H. N., 1975. Heat flow and incipient rifting in the Central African Plateau. Nature 256, 28-30.

Clifford, T. N., 1967. The Damaran Episode in the Upper Proterozoic-Lower Paleozoic structural history of Southern Africa. Geol. Soc. Am. Spec. Paper 92.

Clifford, T. N., 1968. Radiometric dating and the pre-Silurian geology of Africa, in: Hamilton, E. I. and Farquhar, R. M., eds., Radiometric dating for geologists. New York, Interscience Publs., 299-416.

Clifford, T. N., 1972. The evolution of the African crust. Maroc Service Géol. Notes et Mém. 236, 29-39.

Clifford, T. N., 1974. Review of African granulites and related rocks. Spec. Pap. Geol. Soc. Am. 156.

Clifford, T. N., Gronow, J., Rex, D. C. and Burger, A. J., 1975. Geochronological and petrogenetic studies of high-grade metamorphic rocks and intrusives in Namaqualand, South Africa. J. Petrology 16, 154-188.

Cochrane, N. A. and Hyndman, R. D., 1970. A new analysis of geomagnetic depth-sounding data from western Canada. Can. J. Earth Sci. 7, 1208-1218.

Cocks, L. R. M., Brunton, C. H. C., Rowell, A. J. and Rust, I. C., 1969. The first lower Palaeozoic fauna proved from South Africa. Quart. J. Geol. Soc. 125, 583-603.

Coggon, J. H., 1971. Electromagnetic and electrical modelling by finite element method. Geophysics 36, 132-155.

Cooley, J. W. and Tukey, S. W., 1965. An algorithm for the machine calculation of complex Fourier series. Maths Comp. 19, 297-301.

Cox, K. G., 1970. Tectonics and vulcanism of the Karroo period and their bearing on the postulated fragmentation of Gondwanaland, in: Clifford, T. N. and Gass, I. G., eds., African Magmatism and Tectonics, Oliver and Boyd, Edinburgh, 211-235.

Cramer, F. H., Rust, I. C. and Diez de Cramer, M. D. C. R., 1974. Upper Ordovician Chitonozoans from the Cedarberg Formation of South Africa. Preliminary Note. Geol. Rdsch. 63, 340-345.

Currie, R. G., 1968. Geomagnetic spectrum of internal origin and lower mantle conductivity. J. Geophys. Res. 73, 2779-2786.

Dalziel, W. D. and Elliot, D. H., 1973. The Scotia Arc and Antarctic margin, in: Nairn, A. E. M. and Stehli, F. G., eds., The Ocean Basins and Margins, V. 1, The South Atlantic. Plenum Press, New York, 171-234.

Darracott, B. W., Fairhead, J. D. and Girdler, R. W., 1972. Gravity and magnetic surveys in northern Tanzania and southern Kenya, in: Girdler, R. W., ed., East African Rifts. Tectonophysics 15(1), 131-141.

De Beer, J. H., Gough, D. I. and Van Zijl, J. S. V., 1975. An electrical conductivity anomaly and rifting in southern Africa. Nature 225, 678-680.

De Beer, J. H., Van Zijl, J. S. V. and Bahnemann, F. K., 1974. Plate tectonic origin for the Cape Fold Belt? Nature 252, 675-676.

De Beer, J. H., Van Zijl, J. S. V., Huyssen, R. M. J., Hugo, P. L. V., Joubert, S. J. and Meyer, R., (in press). A magnetometer array study in South-West Africa, Botswana and Rhodesia. Geophys. J. R. astr. Soc.

d'Erceville, I. and Kunetz, G., 1962. The effect of a dyke fault on the earth's natural electromagnetic field. Geophysics 27, 651-665.

De Swardt, A. M. J., Fletcher, O. and Toschek, P., 1974. Note on orogenic style in the Cape Fold-Belt. Trans. Geol. Soc. S. Afr. 77, 53-58.

Dosso, H. W., 1966. Analogue model measurements for electromagnetic variations near vertical faults and dykes. Can. J. Earth Sci. 3, 287-303.

Dosso, H. W. and Jacobs, J. A., 1968. Analogue model measurement of electromagnetic variations in the near field of an oscillating line current. Can. J. Earth Sci. 5, 23-29.

Drysdall, A. R., Johnson, R. L., Moore, T. A. and Thieme, J. G., 1972. Outline of the geology of Zambia. Geologie en Mijnbouw 51, 265-276.

Du Plessis, A. and Simpson, E. S. W., 1974. Magnetic anomalies associated with the south-eastern continental margin of South Africa. Mar. Geophys. Res. 2, 99-119.

Du Toit, A. L., 1937. Our Wandering Continents. Oliver and Boyd, Edinburgh.

Du Toit, A. L., 1954. Geology of South Africa. 3rd ed., Oliver and Boyd, Edinburgh.

Dvořák, Z., 1975. Electrical conductivity models of the crust. Can. J. Earth Sci. 12, 962-970.

Eckhardt, D., 1968. Theory and interpretation of the electromagnetic impedance of the Earth. J. Geophys. Res. 73, 5317-5326.

Elliot, D. H. and Watts, D. R., 1974. The nature and origin of volcaniclastic material in some Karroo and Beacon rocks. Trans. Geol. Soc. S. Afr. 77, 109-112.

Everett, J. E. and Hyndman, R. D., 1967. Geomagnetic variations and electrical conductivity structures in southwestern Australia. Phys. Earth Planet. Int. 1, 24-34.

Fairhead, J. D. and Girdler, R. W., 1971. The seismicity of Africa. Geophys. J. R. astr. Soc. 21, 271-301.

Fairhead, J. D. and Girdler, R. W., 1972. The seismicity of the East African Rift System, in: Girdler, R. W., ed., East African Rifts. Tectonophysics 15(½), 115-222.

Fatti, J. L. and Du Toit, J. J. L., 1970. A regional reflection-seismic line in the Karroo Basin near Beaufort West. Trans. Geol. Soc. S. Afr. 73, 17-28.

Fernandez, L. M., 1972. Catalogue of earth tremors in Southern Africa and surrounding oceans for 1971. Seism. Ser. Geol. Surv. S. Afr. 1, 1-17.

Fernandez, L. M. and Guzman, J. A., 1973. Catalogue of earth tremors in Southern Africa and surrounding oceans for 1972. Seism. Ser. Geol. Surv. S. Afr. 3, 1-20.

Francheteau, J. and Le Pichon, X., 1972. Marginal fracture zones as structural framework of continental margins in South Atlantic Ocean. Am. Ass. Petr. Geol. Bull. 56, 991-1007.

Frazer, M. C., 1974. Geomagnetic deep sounding with arrays of magnetometers. Rev. Geophys. Space Phys. 12, 401-420.

Fyfe, W. S. and Leonardos, O. H., 1973. Ancient metamorphic-migmatite belts of the Brazilian African Coasts. Nature 244, 501-502.

Gane, P. G. and Oliver, H. O., 1953. South African earthquakes - 1949 to December, 1952. Trans. Geol. Soc. S. Afr. 56, 21-33.

Garland, G. D., 1975. Correlation between electrical conductivity and other geophysical parameters. Phys. Earth Planet. Int. 10, 220-230.

Gentleman, W. M. and Sande, G., 1966. Fast Fourier transforms - for fun and profit. AFIPS proc., Fall Joint Computer Conf. 29, 563-578.

Geological Map of Botswana, 1973. Scale 1:1,000,000. Geological Survey and Mines Department, Lobatse, Botswana.

Geological Map of South-West Africa, 1963. Scale 1:1,000,000. Shows mineral occurrences and gravity contours. Government Printer, Pretoria, South Africa.

Girdler, R. W., 1975. The great negative Bouguer Gravity anomaly over Africa. Trans. Am. Geophys. Un. 56, 516-519.

Girdler, R. W. and Sowerbutts, W. T. C., 1970. Some recent geophysical studies of the rift system in East Africa. J. Geophys. Geoelectr. 22, 153-163.

Gonzales-Bonorino, F. and Aguirre, L., 1970. Metamorphic facies series of the crystalline basement of Chile. Geol. Rdsch. 59, 979-994.

Goslin, J., Mascle, J., Sibuet, J. C. and Hoskins, H., 1974. Geophysical study of the easternmost Walvis Ridge, South Atlantic: Morphology and shallow structure. Geol. Soc. Am. Bull. 85, 619-632.

Gough, D. I., 1963. Heat flow in the Southern Karroo. Proc. Roy. Soc. A272, 207-230.

Gough, D. I., 1973a. The geophysical significance of geomagnetic variation anomalies. Phys. Earth Planet. Int. 7, 379-388.

Gough, D. I., 1973b. The interpretation of magnetometer array studies. Geophys. J. R. astr. Soc. 35, 83-98.

Gough, D. I., 1973c. Possible linear plume under Southernmost Africa. Nature 245, 93-94.

Gough, D. I., 1974. Electrical conductivity under western North America in relation to heat flow, seismology and structure. J. Geomag. Geoelectr. 26, 105-123.

Gough, D. I. and Camfield, P. A., 1972. Convergent geophysical evidence of a metamorphic belt through the Black Hills of South Dakota. J. Geophys. Res. 77, 3168-3170.

Gough, D. I., De Beer, J. H. and Van Zijl, J. S. V., 1973. A magnetometer array study in southern Africa. Geophys. J. R. astr. Soc. 34, 421-433.

Gough, D. I. and Gough, W. I., 1970. Earthquakes induced by hydrostatic loading on Kariba Dam. Geophys. J. R. astr. Soc. 21, 79-101.

Gough, D. I., Lilley, F. E. M. and McElhinny, M. W., 1972. A polarization-sensitive magnetic variation anomaly in South Australia. Nature Phys. Sci. 239, 88-91.

Gough, D. I., McElhinny, M. W. and Lilley, F. E. M., 1974. A magnetometer array study in southern Australia. Geophys. J. R. astr. Soc. 36, 345-362.

Gough, D. I. and Reitzel, J. S., 1967. A portable three-component magnetic variometer. J. Geomag. Geoelectr. 19, 203-215.

Gouin, P., 1970. Seismic and gravity data from Afar in relation to surrounding areas. Phil. Trans. Roy. Soc. London A267, 339-358.

Gumper, F. and Pomeroy, P. W., 1970. Seismic wave velocities and earth structure on the African continent. Seism. Soc. Am. Bull. 60, 651-668.

Haines, G. V., Hannaford, W. and Riddihough, R. R., 1971. Magnetic anomalies over British Columbia and the adjacent Pacific Ocean. Can. J. Earth Sci. 8, 387-391.

Hales, A. and Gough, D. I., 1960. Isostatic anomalies and crustal structure in the southern Cape. Geophys. J. R. astr. Soc. 3, 225-236.

Hales, A. and Gough, D. I., 1961. Correction to paper: Isostatic anomalies and crustal structure in the southern Cape. Geophys. J. R. astr. Soc. 5, 263.

Halpern, M., 1968. Ages of Antarctic and Argentine rocks bearing on continental drift. Earth Planet. Sci. Letters 5, 159-167.

Halpern, M., Urquhart, M. U. and Linares, E., 1972. Radiometric ages of crystalline rocks from southern South America as related to Gondwana and Andean geologic provinces, 345-356, Int. Upper Mantle Project. Conf. on solid earth problems, V. II, Symp. on results of Upper Mantle investigations with emphasis on Latin America, Buenos Aires, Argentina.

Haughton, S. H., 1969. Geological history of Southern Africa. Geological Society of South Africa, Johannesburg.

Hermance, J. F., 1968. Model studies of the coast effects on geomagnetic variations. Can. J. Earth Sci. 5, 515-522.

Hermance, J. F., 1972. Discussion on a paper by F. W. Jones and A. T. Price. Geophysics 37, 540-541.

Hermance, J. F., 1973. Processing of magnetotelluric data. Phys. Earth Planet. Int. 7, 349-364.

Hobbs, B. A., 1975. Analytic solutions to global and local problems of electromagnetic induction in the earth. Phys. Earth Planet. Int. 10, 250-261.

Holmes, A., 1951. The sequence of Pre-Cambrian orogenic belts in south and central Africa. 18th Inter. Geol. Congr., Great Britain, 1948, pt. 14, 254-269.

Inman, J. R., Ryu, J. and Ward, S. H., 1973. Resistivity inversion. Geophysics 38, 1088-1108.

International Tectonic Map of Africa, 1968. Scale 1:5,000,000. Unesco.

Jady, R. J., 1974a. The conductivity of spherically symmetric layered Earth models determined by Sq and longer period variations. Geophys. J. R. astr. Soc. 36, 399-410.

Jady, R. J., 1974b. Conductivity models and Banks' data. Geophys. J. R. astr. Soc. 37, 447-452.

Jenkins, G. M. and Watts, D. G., 1968. Spectral analysis and its applications. Holden-Day, San Francisco.

Jones, F. W. and Pascoe, L. J., 1971. A general computer program to determine the perturbation of alternating electric current in a two-dimensional model of a region of uniform conductivity with an embedded inhomogeneity. Geophys. J. R. astr. Soc. 24, 3-30.

Jones, F. W. and Price, A. T., 1970. The perturbation of alternating geomagnetic fields by conductivity anomalies. Geophys. J. R. astr. Soc. 20, 317-334.

Jones, F. W. and Price, A. T., 1971. The geomagnetic effect of two-dimensional conductivity inhomogeneities at different depths. Geophys. J. R. astr. Soc. 22, 333-345.

Keller, G. V., 1971. Electrical studies of the crust and upper mantle, in: Heacock, J. G., ed., The structure and physical properties of the earth's crust. AGU Monograph 14, Washington, D.C., 107-126.

Keller, G. V., Anderson, L. A. and Pritchard, J. I., 1966. Geological Survey investigations of the electrical properties of the crust and upper mantle. Geophysics 31, 1078-1087.

Keller, G. V. and Frischknecht, F. C., 1966. Electrical methods in geophysical prospecting. Pergamon, New York, N.Y.

Kennedy, W. A., 1965. Influence of basement structure on the evolution of the coastal (Mesozoic and Tertiary) basins of Africa, in: Salt Basins Around Africa, Inst. Petroleum, London, 7-16.

Kesson, S. E., 1973. The primary geochemistry of the Monaro alkaline volcanics, south-eastern Australia - Evidence for upper mantle heterogeneity. Contr. Mineral. Petrol. 32, 93.

Kleywegt, R. J., 1967. The gravity survey of South-West Africa. Unpublished Ph.D. thesis, Univ. of Natal, Pietermaritzburg, South Africa.

Knopoff, L. and Schlue, J. W., 1972. Raleigh wave phase velocities for the path Addis Ababa-Nairobi, in: Girdler, R. W., ed., East African Rifts. Tectonophysics 15(½), 157-163.

Korn, H. and Martin, H., 1951. The seismicity of South-West Africa. Trans. Geol. Soc. S. Afr. 54, 85-88.

Kuckes, A. F., 1973a. Relations between electrical conductivity of a mantle and fluctuating magnetic fields. Geophys. J. R. astr. Soc. 32, 119-131.

Kuckes, A. F., 1973b. Correspondence between the magnetotelluric and field penetration depth analyses for measuring electrical conductivity. Geophys. J. R. astr. Soc. 32, 381-385.

Kunetz, G., 1966. Principles of direct current resistivity prospecting. Gebrüder Borntraeger, Berlin.

Kunetz, G. and Rocroi, J. P., 1970. Traitement automatique des sondages électriques (Automatic processing of electrical soundings). Geophys. Pros. 18, 157-198.

Lahiri, B. N. and Price, A. T., 1939. Electromagnetic induction in non-uniform conductors and the determination of the conductivity of the earth from terrestrial magnetic variations. Phil. Trans. Roy. Soc. A237, 509-540.

Larsen, J. C., 1973. An introduction to electromagnetic induction in the ocean. Phys. Earth Planet. Int. 7, 389-398.

Lee, C. A., 1974. The geology of the Katete carbonatite, Rhodesia. Geol. Mag. 3, 133-142.

Lilley, F. E. M., 1975. Magnetometer array studies: a review of the interpretation of observed fields. Phys. Earth Planet. Int. 10, 231-240.

Lilley, F. E. M., (in press). Running waves and standing waves in geomagnetic depth sounding.

Lilley, F. E. M. and Bennett, D. J., 1972. An array experiment with magnetic variometers near the coast of south-east Australia. Geophys. J. R. astr. Soc. 29, 49-64.

Ludwig, W. J., Nafe, J. E. and Simpson, E. S. W., 1971. Geophysical reconnaissance on African Shelf: 1. Cape Town to East London. Am. Assoc. Petr. Geol. Bull. 55, 651-657.

Maasha, M. and Molnar, P., 1972. Earthquake fault parameters and tectonics in Africa. J. Geophys. Res. 77, 5731-5743.

Madden, T. R., 1971. The resolving power of geoelectric measurements for delineating resistance in the crust, in: Heacock, J. G., ed., The structure and physical properties of the earth's crust. AGU Monograph 14, Washington, D.C., 95-105.

Madden, T. R. and Swift, C. M., 1969. Magnetotelluric studies of the electrical conductivity structure of the crust and upper mantle, in: Hart, P. J., ed., The Earth crust and Upper Mantle, AGU Monograph 13, Washington, D. C., 469-479.

Martin, H., 1969. Problems of age relations and structure in some metamorphic belts of southern Africa. Spec. Pap. Geol. Ass. Canada 5, 17-26.

Martini, J. E. J., 1974. The presence of ash beds and volcanic fragments in the greywackes of the Karroo System in the southern Cape Province (South Africa). Trans. Geol. Soc. S. Afr. 77, 113-116.

Mason, R., 1973. The Limpopo mobile belt - southern Africa. Phil. Trans. R. Soc. London A273, 463-485.

McConnell, R. B., 1972. Geological development of the rift system of eastern Africa. Geol. Soc. Am. Bull. 83, 2549-2572.

McDonald, K. L., 1957. Penetration of the geomagnetic secular field through a mantle with variable conductivity. J. Geophys. Res. 62, 117-141.

Molnar, P. T., Fitch, J. and Asfaw, L. M., 1970. A microearthquake survey in the Ethiopian rift. Earthquake Notes 41, 37.

Monger, J. W. H., Souther, J. G. and Gabrielse, H., 1972. Evolution of the Canadian Cordillera: a plate-tectonic model. Am. J. Sci. 272, 577-602.

Newton, A. R., 1973. A gravity-folding model of the Cape Fold-Belt. Trans. Geol. Soc. S. Afr. 76, 145-152.

Newton, A. R., 1974a. Nature of South Africa's Cape Fold Belt. Nature 248, 499-500.

Newton, A. R., 1974b. Reply to discussion by R. C. Rhodes of: A gravity-folding model of the Cape Fold-Belt. Trans. Geol. Soc. S. Afr. 77, 208-209.

Nicolaysen, L. O., 1962. Stratigraphic interpretation of age measurements in southern Africa, in: Engel, A. E., James, H. L. and Leonard, B. F., eds., Petrologic studies. Geol. Soc. Am., Buddington Volume, 569-598.

Nicolaysen, L. O. and Burger, A. J., 1965. Note on an extensive zone of 1000 million-year old metamorphic and igneous rocks in Southern Africa. Sci. de la Terre 10, 497-516.

Oldenburg, D. W., 1969. Separation of magnetic substorm fields for mantle conductivity studies in the western United States. Unpublished M.Sc. thesis, Department of Physics, University of Alberta, Edmonton, Canada.

Oliver, H. O., 1956. South African Earthquakes - January 1963 to December 1955. Trans. Geol. Soc. S. Afr. 59, 123-129.

Olivier, H. J., 1972. Geohydrological investigation of the flooding at Shaft 2, Orange-Fish tunnel, north-eastern Cape Province. Trans. Geol. Soc. S. Afr. 75, 195-219.

Orellana, E. and Mooney, H. M., 1966. Master tables and curves for vertical electrical sounding over layered structures. Intersciencia, Madrid.

Otnes, R. K. and Enochson, L., 1972. Digital time series analysis. John Wiley and Sons, New York.

Oxburgh, E. R. and Turcotte, D. L., 1974. Membrane tectonics and the East African rift. Earth Planet. Sci. Letters 22, 133-140.

Padula, E. L., Rolleri, E. O., Mingramm, A. R. G., Roque, P. C., Flores, M. A. and Baldis, B. A., 1967. Devonian of Argentina. Int. Symp. on the Devonian System, V. 2, Oswald, D. H., ed., Alberta Soc. Petrol. Geol., Calgary, 165-199.

Parker, R. L., 1970. The inverse problem of electrical conductivity in the mantle. Geophys. J. R. astr. Soc. 22, 121-138.

Parker, R. L., 1972. Inverse theory with grossly inadequate data. Geophys. J. R. astr. Soc. 29, 123-138.

Parkinson, W. D., 1959. Directions of rapid geomagnetic fluctuations. Geophys. J. R. astr. Soc. 2, 1-14.

Parkinson, W. D., 1962. The influence of continents and oceans on geomagnetic variations. Geophys. J. R. astr. Soc. 6, 441-449.

Pascoe, L. J. and Jones, F. W., 1972. Boundary conditions and calculation of surface values for the general two-dimensional electromagnetic induction problem. Geophys. J. R. astr. Soc. 27, 179-193.

Polyak, B. G. and Smirnov, Ya. B., 1968. Relationship between terrestrial heat flow and the tectonics of continents. Geotectonics 4, 205-213.

Porath, H., 1971. A review of the evidence on low-resistivity layers in the Earth's crust, in: Heacock, J. G., ed., The structure and physical properties of the earth's crust. AGU Monograph 14, Washington, D.C., 127-144.

Porath, H. and Dziewonski, A., 1971a. Crustal electrical conductivity anomalies in the Great Plains province of the United States. Geophysics 36, 385-395.

Porath, H. and Dziewonski, A., 1971b. Crustal resistivity anomalies from geomagnetic deep sounding studies. Rev. Geophys. Space Phys. 9, 891-915.

Porath, H. and Gough, D. I., 1971. Mantle conductive structures in the western United States from magnetometer array studies. Geophys. J. R. astr. Soc. 22, 261-275.

Porath, H., Gough, D. I. and Camfield, P. A., 1971. Conductive structures in the northwestern United States and southwest Canada. Geophys. J. R. astr. Soc. 23, 387-398.

Porath, H., Oldenburg, D. W. and Gough, D. I., 1970. Separation of magnetic variation fields and conductive structures in the western United States. Geophys. J. R. astr. Soc. 19, 237-260.

Price, A. T., 1950. Electromagnetic induction in a semi-infinite conductor with a plane boundary. Quart. J. Mech. Appl. Math. 3, 385-410.

Price, A. T., 1962. The theory of magnetotelluric fields when the source field is considered. J. Geophys. Res. 67, 1907-1918.

Price, A. T., 1967. Electromagnetic induction within the earth, in: Matsushita, S. and Campbell, W. H., eds., Physics of Geomagnetic Phenomena. Academic Press, New York, 235-295.

Price, A. T. and Jones, F. W., 1972. Reply by authors to discussion by J. F. Hermance. Geophysics 37, 541-542.

Provisional Geological Map of Rhodesia, 1971. Scale 1:1,000,000. Rhodesia Geological Survey, Salisbury, Rhodesia.

Provisional Gravity Map of the Republic of Zambia, 1974. Scale 1:1,500,000. Geological Survey of Zambia, Lusaka, Zambia.

Rankin, D., 1962. The magnetotelluric effect on a dike. Geophysics 27, 666-676.

Rastogi, R. G., 1962. The effect of geomagnetic activity on the F_2 region over Central Africa. J. Geophys. Res. 67, 1367-1374.

Reddy, I. K. and Rankin, D., 1973. Magnetotelluric response of a two-dimensional sloping contact by the finite element method. Pure Appl. Geophys. 105, 847-857.

Reeves, C. V., 1972. Rifting in the Kalahari? Nature 237, 95-96.

Reeves, C. V. and Hutchins, D. G., 1975. Crustal structures in central southern Africa. Nature 254, 408-410.

Reitzel, J. S., Gough, D. I., Porath, H. and Anderson, C. W., 1970. Geomagnetic deep sounding and upper mantle structure in the western United States. Geophys. J. R. astr. Soc. 19, 213-235.

Rhodes, R. C., 1974. Discussion of: A gravity-folding model of the Cape Fold-Belt. Trans. Geol. Soc. S. Afr. 77, 207-209.

Rhodesia Meteorological Services, 1965-1973. Monthly Seismological Bulletins. Salisbury, Rhodesia.

Rikitake, T., 1966. Electromagnetism and the earth's interior. Developments in Solid Earth Geophysics 2, Elsevier Publishing Co., New York.

Rikitake, T., 1973. Global electrical conductivity of the earth. Phys. Earth Planet. Int. 7, 245-250.

Rikitake, T. and Honkura, Y., 1973. Recent Japanese studies on conductivity anomalies. Phys. Earth Planet. Int. 7, 203-213.

Rostoker, G., 1972. Polar magnetic substorms. Rev. Geophys. Space Phys. 10, 157-211.

Rust, I. C., 1973. The evolution of the Paleozoic Cape Basin, southern margin of Africa, in: Nairn, A. E. M. and Stehli, F. G., eds., The ocean basins and margins, V. 1, The South Atlantic, Plenum Press, New York, 247-275.

Ryan, P. J., 1967. Stratigraphy of the Ecca Series and lowermost Beaufort Beds (Permian) in the Great Karroo basin of South Africa. Int. Un. Geol. Sci. Symp. on Gondwana Stratigraphy, Buenos Aires, 945-965.

Scheepers, G. L. M., 1973. The MOCSIR variometer system. Symposium on modern magnetic observation techniques. IAGA Assembly, Kyoto, Japan.

Schmucker, U., 1964. Anomalies of geomagnetic variations in the southwestern United States. J. Geomag. Geoelectr. 15, 193-221.

Schmucker, U., 1970a. Anomalies of geomagnetic variations in the southwestern United States. Bulletin of the Scripps Institution of Oceanography. Univ. of California, San Diego, La Jolla, California, V. 13, Univ. of California Press.

Schmucker, U., 1970b. An introduction to induction anomalies. J. Geomag. Geoelectr. 22, 9-33.

Schmucker, U., 1971. Interpretation of induction anomalies above nonuniform surface layers. Geophysics 36, 156-165.

Schmucker, U., 1973. Regional induction studies: a review of methods and results. Phys. Earth Planet. Int. 7, 365-378.

Schmucker, U., Forbush, S. E., Hartmann, O., Giesecke, A. A., Casaverde, M., Castillo, J., Salgueiro, R. and Del Pozo, S., 1967. Electrical conductivity anomaly under the Andes. Annual report, Dept. Terrestrial Magn., Carnegie Inst. of Washington, 11-28.

Scholz, C. H., Koczynski, T. A. and Hutchins, D. G., (in press). Evidence for incipient rifting in Southern Africa. Geophys. J. R. astr. Soc.

Scientists aboard the Glomar Challenger for Leg 36 of the Deep Sea Drilling Project, 1974. Southwestern Atlantic Leg 36. Geotimes 19(11), 16-18.

Scientists aboard Glomar Challenger for Leg 40 of DSDP, 1975. Basins and margins of the eastern South Atlantic. Geotimes 20(6), 22-24.

Scrutton, R. A., 1973a. Structure and evolution of the sea floor south of South Africa. Earth Planet. Sci. Letters 19, 250-256.

Scrutton, R. A., 1973b. Gravity results from the continental margin of south-western Africa. Marine Geophys. Res. 2, 11-21.

Scrutton, R. A. and Du Plessis, A., 1973. Possible marginal fracture ridge south of South Africa. Nature 242, 180-182.

Searle, R. C., 1970a. Evidence from gravity anomalies for thinning of the lithosphere beneath the rift valley in Kenya. Geophys. J. R. astr. Soc. 21, 13-31.

Shackleton, R. M., 1973. Problems of the evolution of the continental crust. Phil. Trans. R. Soc. Lond. A273, 317-320.

Sik, J. M., Hutton, V. R. S., Jones, A. G. and Alabi, A. O., 1974. Geomagnetic deep sounding in Scotland. Abstract in proceedings of Second Workshop on Electromagnetic Induction in the Earth, Ottawa (unpublished).

Slettene, R. L., Wilcox, L. E., Blouse, R. S. and Sanders, J. R., 1973. A Bouguer gravity anomaly map of Africa. DMAAC Technical Paper No. 73-003.

Smit, P. J., Hales, A. and Gough, D. I., 1962. The gravity survey of the Republic of South Africa, Handbook 3. Government Printer, Pretoria, South Africa.

Smith, A. G. and Hallam, A., 1970. The fit of the southern continents. Nature 225, 139-144.

Smylie, D. E., 1965. Magnetic diffusion in a spherically-symmetric mantle. Geophys. J. R. astr. Soc. 9, 169-184.

Söhnge, P. G., 1935. The Worcester fault. Trans. Geol. Soc. S. Afr. 37, 253-278.

Stacey, R. A., 1973. The Canadian Cordillera. Geofisica Internacional 13, 243-266.

Swift, C. M., 1971. Theoretical magnetotelluric and Turam response from two-dimensional inhomogeneities. Geophysics 36, 38-52.

Sykes, L. R., 1967. Mechanism of earthquakes and nature of faulting on the mid-ocean ridges. J. Geophys. Res. 72, 2131-2153.

Thorpe, R. S. and Smith, K., 1974. Distribution of Cenozoic volcanism in Africa. Earth Planet. Sci. Letters 22, 91-95.

Tozer, D. C., 1959. The electrical properties of the earth's interior, in: Rankama, K. and Runcorn, S. K., eds., Physics and Chemistry of the Earth, V. 3, Pergamon Press, New York, 414-435.

Vail, J. R., 1965. An outline of the geochronology of the late Precambrian formations of east central Africa. Proc. Roy. Soc. (London) A284, 354-369.

Vail, J. R., 1968. Significance of the tectonic pattern of Southern Africa. Tectonophysics 6, 403-411.

Vail, J. R. and Dodson, M. H., 1969. Geochronology of Rhodesia. Trans. and Proc. Geol. Soc. S. Afr. 72, 79-113.

Vail, J. R. and Snelling, N. J., 1971. Isotope age measurements for the Zambezi orogenic belt and the Urungwe Klippe, Rhodesia. Geol. Rdsch. 60, 619-630.

Vail, J. R., Snelling, N. J. and Rex, D. C., 1968. Pre-Katangan geochronology of Zambia and adjacent parts of Central Africa. Can. J. Earth Sci. 5, 621-632.

Van Breemen, O. and Dodson, M. H., 1972. Metamorphic chronology of the Limpopo Belt, Southern Africa. Geol. Soc. Am. Bull. 8, 2005-2018.

Van Niekerk, C. B. and Burger, A. J., 1969. A note on the minimum age of the acid lava of the Onverwacht Series of the Swaziland System. Trans. Geol. Soc. S. Afr. 72, 9-21.

Van Zijl, J. S. V., 1969. A deep Schlumberger sounding to investigate the electrical structure of the crust and upper mantle in South Africa. Geophysics 34, 450-462.

Van Zijl, J. S. V., Hugo, P. L. V. and De Bellocq, J. H., 1970. Ultra deep Schlumberger sounding and crustal conductivity structure in South Africa. Geophys. Prosp. 18, 615-634.

Van Zijl, J. S. V. and Joubert, S. J., 1975. A crustal geoelectrical model for South African Precambrian granitic terrains based on deep Schlumberger soundings. Geophysics 40, 657-663.

Viljoen, R., 1975. The use of ERTS imagery in problems of regional geology and mineral exploration in the North West Cape. Abstract in proceedings of Geokongres 75, Stellenbosch, South Africa (unpublished).

Von Herzen, R. P. and Vacquier, V., 1967. Terrestrial heat flow in Lake Malawi, Africa. J. Geophys. Res. 72, 4221-4226.

Wait, J. R., 1953. Propagation of radio waves over a stratified ground. Geophysics 18, 416-422.

Watterson, J., 1975. Mechanism for the persistence of tectonic lineaments. Nature 253, 520-522.

Weaver, J. T., 1963. The electromagnetic field within a discontinuous conductor with reference to geomagnetic micropulsations near a coastline. Can. J. Phys. 41, 484-495.

Weaver, J. T., 1973. Induction in a layered plane earth by uniform and non-uniform source fields. Phys. Earth Planet. Int. 7, 266-281.

Weaver, J. T. and Thomson, D. J., 1972. Induction in a non-uniform conducting half-space by an external line current. Geophys. J. R. astr. Soc. 28, 163-185.

Weidelt, P., 1972. The inverse problem of geomagnetic induction. Zeitschrift für Geophysik 38, 257-289.

Whitham, K., 1963. An anomaly in geomagnetic variations at Mould Bay in the arctic archipelago of Canada. Geophys. J. R. astr. Soc. 8, 26-43.

Wiese, H., 1962. Geomagnetische Tiefentellurik Teil II: Die Streichrichtung der Untergrundsstrukturen des elecktrischen Widerstandes, erschlossen aus geomagnetischen Variationen. Geofis. Pura Appl. 52, 83-103.

Wilson, J. F. and Harrison, N. M., 1973. Recent K-Ar age determinations on some Rhodesian granites. Geol. Soc. South Africa Spec. Publ. 3, 69-78.

Winter, H. de la R. and Venter, J. J., 1970. Lithostratigraphic correlation of recent deep boreholes in the Karroo-Cape sequence. Proc. 2nd Gondwana Symposium, I.U.G.S. Comm. on Stratigraphy, 395-408.

Wohlenberg, J., 1975. Geophysikalische Aspekte der ostafrikanischen Grabenzonen. Geologisches Jahrbuch, Reihe E, Heft. 4.

Word, D. R., Smith, H. W. and Bostick, F. X., 1970. An investigation of the magnetotelluric tensor impedance method. Technical Report No. 82, Electrical Geophysics Research Laboratory, Electronics Research Center, Univ. of Texas at Austin, Austin, Texas.

Word, D. R., Smith, H. W. and Bostick, F. X., 1971. Crustal investigations by the magnetotelluric tensor impedance method, in: Heacock, J. G., ed., The structure and physical properties of the earth's crust. AGU Monograph 14, Washington, D.C., 145-167.

Wright, J. A., 1969. The magnetotelluric and geomagnetic response of two-dimensional structures. Gamma 7, Inst. of Geophys. and Meteorol., Tech. Univ. of Braunschweig, Braunschweig, Germany.